Biomimetic and multifunctional poly(glycerol sebacate)-based elastomeric hydrogels for soft tissue healthcare

By Sungkwon Yoon

A thesis submitted in partial fulfilment of the requirements for the degree of
Doctor of Philosophy

The University of Sheffield

Faculty of Engineering

Department of Materials Science and Engineering

September 2019

Declaration

I hereby declare that this thesis is my own work and effort, and that this thesis has not been submitted to another university in full or in part for another degree or qualification. Where other sources of information have been used, they have been acknowledged. Permission has been granted from copyright holders to replicate figures or data within this thesis.

Sungkwon Yoon

September 2019

Abstract

A critical aspect in designing biomaterials with the advanced healthcare functionalities is their interaction with biology. In this regard, elastomers capable of responding to the various physiological dynamics *in vivo* are of significant interest in advanced soft tissue healthcare applications. In this thesis, new multifunctional biocompatible elastomers with bioactive and biomimetic behaviours were developed and characterised based on poly(glycerol sebacate) (PGS), for their potential soft tissue healthcare applications such as soft tissue engineering, wound healing, and drug delivery.

The direct crosslinking and copolymerisation of the PGS pre-polymer and gelatin was studied by varying the ratio between PGS and gelatin. The biomimetic mechanical properties as well as an architecture of porous tissue scaffold illustrate their potential in soft tissue engineering. The pH-responsive water swelling property given by gelatin was further investigated in pH-responsive drug delivery applications.

PGS-based polyurethane-clay nanocomposites with varying amounts of an organically modified clay were successfully synthesised on the modulation of physical properties of PGS. The synthesis was performed in a combined approach of the solvent method and *in situ* polymerisation. Hydration, mechanical, and degradable properties were improved with the addition of clay, illustrating its potential in soft tissue engineering. The selective drug loading and absorption behaviour was studied for controlled drug delivery application.

Polyester-clay nanocomposites with different clay contents were developed. The hydration, hydrophilicity, and water vapour permeability were engineered with the addition of clay. Novel pro-angiogenic and malodourous diamine-controlling properties were also studied. Together with the porous foam structure, the potential of these new nanocomposites in the wound healing and soft tissue engineering applications was discussed.

Overall, the new elastomers developed in this thesis based on PGS, exhibit great potentials in soft tissue healthcare applications with finely engineered or newly created properties on PGS.

I would like to dedicate this thesis to my family, friends, and the most beloved one.

Acknowledgments

First and foremost, I express my sincerest gratitude to my supervisor, Prof. Biqiong Chen, for her insightful guidance, inspiring discussion, and being a great role model not only as a scholar but also as a person.

I am also thankful to the University of Sheffield, for providing me with financial support through the University Prize Scholarship. I also express my thanks to Prof Sheila McNeil and Serkan Dikici for their collaborative work on the CAM assay.

My gratitude also goes to the fellow researchers and staff members at the University of Sheffield. I am thankful to Dr Xiangbing Zeng, Dr Gabriella Kakonyi, Dr Martin Frydrych, Ben Palmer, Heather Grievson, and Dawn Bussey, for their kind and professional academic and technical supports in the early half of my PhD study.

I would like to thank the technical support staff members and fellow researchers at the Queen's University Belfast. I thank Troy Patterson, Brian McLaughlin, Jonathan Stewart, Dr Efrosyni Themistou, Mark Russel, and Mari Finnegan, for their help on my experimental work. My thanks also go to Dr Paula Douglas, Dr Bronagh Millar, and Dr Paul Hanna in PPRC for their kind help on the polymer analysis.

I am thankful to Prof. William Nichols of the Department of Materials Science and Engineering at the Hanyang University, for his advice and guidance before my PhD study.

My thanks go further to my colleagues and friends, Andreas Samourides, Vicky Guo, Belinda Joseph, and Georg Graninger. They are the best friends as well as the craziest young researchers.

Finally, I express my deepest gratitude to my family. Even from the distance, their heartful and endless support have always been fuelling myself to go through my study.

Table of Contents

Nomenclature

3D	Three-dimensional
ADSC	Adipose-derived stem cells
AFM	Atomic force microscopy
ATR-FTIR	Attenuated total reflectance Fourier transform infrared spectroscopy
CAM	Chick chorioallantoic membrane
CD	Cyclodextrin
CNT	Carbon nanotube
°C	Degree Celcius
σ_{tmax}	Ultimate tensile strength
DMEM	Dulbecco’s modified Eagle’s medium
DMF	Dimethylformamide
DMSO	Dimethyl sulfoxide
DOX	Doxycycline hyclate
DPBS	Dulbecco’s phosphate buffered saline
DSC	Differential Scanning Calorimetry
E2	17β-estradiol
ECM	Extracellular matrix

ELP	Elastin-like peptides
ε_{tb}	Strain to failure
E_t	Young’s modulus
eqn	Equation
EWC	Equilibrium water content
FDA	US Food and Drug Administration
g	Gram, often prefixed with μ (micro-), m (milli-), or k (kilo)
Gly	Glycine
h	Hour in time
ISO	International standard organization
HDI	Hexamethylene diisocyanate
HEPES	4-(2-hydroxyethyl)-1-piperazineethanesulfonic acid
l	Litre, often prefixed with μ (micro-), or m (milli-)
m	Metre, often prefixed with n (nano-), μ (micro-), c (centi-), or m (milli-)
min	Minute in time
MMT	Montmorillonite
mol	Mole
N	Newton

NEAA	Non-essential amino acid solution
NMR	Nuclear magnetic resonance
P4HB	poly(4-hydroxybutyrate)
Pa	Pascal, often prefixed with k (kilo-), M (mega-), or G (giga)
PANi	Polyaniline
PBA	Poly(butyl acrylate)
PBS	Phosphate-buffered saline
PCL	Poly(ε-caprolactone)
PCNC	Polymer-clay nanocomposite
PDLA	Poly(D-lactic acid)
PDLLA	Poly(D,L-lactic acid)
PDOPA	Poly(diol polybasic acid)
PEG	Poly(ethylene glycol)
PEGDA	Poly(ethylene glycol diacrylate)
PEU	Polyester-based polyurethane
PEUC	Polyester-based polyurethane-clay nanocomposites
PGS	Poly(glycerol sebacate)
PGSG	Poly(glycerol sebacate)-gelatin copolymers

PGA	Poly(glycolic acid)
PHA	poly(hydroxyalkanoate)
PHBV	Poly(3-hydroxybutyrate-co-3-hydroxyvalerate)
PLA	Poly(lactic acid)
PLGA	Poly(lactic-*co*-glycolic acid)
PDLLA	Poly(D,L-lactic acid)
PMAA	Poly(methacrylic acid)
PNIPAAm	Poly(*N*-isopropylacrylamide)
POM	Polarised optical microscopy
PPODA	Poly(polyol dicarboxylic acid)
PTFE	Polytetrafluoroethylene
PU	Polyurethane
RGD	A peptide with arginine-glycine-aspartic acid sequence
rpm	Revolutions per minute
SAXS	Small angle X-ray scattering
sec	Second in time
SELP	Silk elastin-like protein
SEM	Scanning electron microscopy

STE	Soft tissue engineering
t	Time
TGA	Thermogravimetric Analysis
TCP	Tissue culture plastic
TEM	Transmission electron microscopy
THF	Tetrahydrofuran
tin(II)	Tin(II) 2-ethylhexanoate
UTS	Ultimate tensile strength
V	Volt
VEGF	Vascular endothelial growth factor
v/v %	Volume/volume percentage
WAXS	Wide angle X-ray scattering
WVTR	Water vapour transmission rate
wt%	Weight percentage
w/v %	Weight/volume percentage
XRD	X-ray diffraction

List of Figures

List of Tables

Chapter 1 Introduction

The subject of biomaterials is biomimetics in its nature, as it includes the material interactions with the complex physicochemical dynamics *in vivo*. In this regard, elastomeric hydrogels are an attractive class of biomaterials for soft tissue healthcare. Their flexible and stretchable mechanical behaviours are valuable assets to provide the biomimetic and synchronous movements responding to the extreme mechanical dynamics in soft tissues.[1] Their biomimetic water content allows the transportation of desired chemical species, not only to help the cellular communications, but also to administrate the medicinal substances.[2–6]

Furthermore, the recent progress in biotechnology increasingly demands the multifunctionalities in biomaterials which are capable of responding to various *in vivo* stimuli and/or play multiple clinical roles in a single application such as tissue engineering, wound healing, drug delivery. For instance, the incorporation of drugs into tissue engineering scaffolds may be required to prevent infection after applications and induce bioactivity to engineer the cell biology and optimise the tissue regeneration.[7] The multifunctionalities can be achieved by pursuing synergy among different types of materials as well as choosing appropriate material structures.[8]

Poly(glycerol sebacate) (PGS) is a synthetic elastomer. PGS has attracted a significant attention in soft tissue applications for its flexibility and stretchability which resemble the mechanical behaviours of soft tissues.[9] Furthermore, PGS exhibits a surface erodible nature with a linear mass loss and good strength retention, which would be beneficial for its stable performance *in vivo*.[9–11] A number of *in vivo* and *in vitro* studies demonstrated that the polymer has good biocompatibility with minimal inflammatory responses.[9–11] As a consequence, PGS has been reviewed in the soft tissue healthcare sector mainly in the soft tissue engineering.[12–19] However, the limitations exist in PGS in terms of the material properties and architectures. Although the mechanical properties of PGS can be altered in some extent with the synthesis condition,[20–25] it relies only on the crosslinking density of the polymer. Therefore, the higher strength and modulus are achieved by compromising the stretchability in PGS. Secondly, PGS is hydrophobic and lacks the ability of hydration,[20] which makes the polymer impossible to be prepared into a hydrogel on its own. Thirdly, the polymer has no stimuli-responsive properties and bioactive properties which has no ability to induce positive effects on cellular activity on tissue regeneration. Moreover, conventional synthetic procedure of PGS inhibits its architecture of the complex structures as the pre-polymer resin melts at its curing temperature.[26]

This PhD study aimed to create new biomimetic and multifunctional PGS-based elastomeric hydrogels with desirable material properties for soft tissue healthcare such as tissue engineering, wound healing, and drug delivery applications. Design of the PGS-based elastomeric hydrogels included introduction of material synergy by preparing copolymers, and nanocomposites, as well as desired material architectures of solid gels, porous foams and microspheres. The specific objectives are listed as below.

- To create a new PGS-based copolymer system, having mechanical properties mimicking those of soft tissues, the hydration properties, a fabrication method of porous tissue engineering scaffold, as well as the novel pH-responsive behaviours which can be utilised in pH-responsive controlled drug delivery.
- To engineer the desirable properties in a polymer-clay nanocomposite hydrogel system based on PGS, having controllable and biomimetic hydration, mechanical, diffusional, and biodegration behaviours, as well as ability to be fabricated in a porous foam

structure for soft tissue engineering and drug delivery applications.

- To develop and characterise a bioactive PGS-based polymer-clay nanocomposite hydrogel system with novel pro-angiogenic and malodourous diamine-controlling properties as well as tunable hydration and vapour permeability for its potential use in wound healing and soft tissue engineering.

The new synthesis and fabrication approach as well as multifunctionalities of PGS-based elastomer hydrogels are expected to have great potentials in soft tissue healthcare applications as discussed in the following chapters.

Chapter 2 Literature review

2.1 Soft tissue engineering

2.1.1 Definition and characteristics of soft tissues

Soft tissues are wide-ranging biological materials and distributed all over the body. Soft tissues may be distinguished from hard (mineralised) tissues by their soft and elastic mechanical behaviours.[27] In anatomical definition, the term "soft tissue" refers to the tissues that bind, connect, support, surround, or protect other structures or organs.[28] Examples of soft tissues are; (1) connective tissues such as fat, skin, fascia, synovial tissues, tendons and ligaments, and (2) non-connective tissues such as muscles, blood vessels, lymph vessels, nerves, retina in eyes, and gastrointestinal walls in intestines (Figure 2.1). The jobs of soft tissues vary. For example, fat (or adipose) tissues protect, cushion, and insulate the body.[29] It also stores nutrients and biomolecules such as cholesterol.[30] Tendons link bone to muscle, while ligaments are linkages between bones.[31] The skin is the largest single organ (16 wt.% of the adult body) and provides the support and protection to the internal body.[32]

Despite the diversity in their structures and properties is huge, all of the soft tissues can be defined as highly hydrated (65 – 85 wt.% is water),[33] fiber-reinforced composite materials.[32] The major constituents in soft tissues are; (1) cells, (2) fibrous extracellular matrix (ECM) proteins such as collagen and elastin, (3) the ground substances such as glycosaminoglycans, proteoglycans, and glycoproteins, and (4) the vasculature and lymphatics.[32,34] Their mechanical behaviour strongly depends on the concentration and structural arrangement of substances. For example, the ratio between collagen (relatively rigid, Young's modulus (E) = 120 MPa) and elastin (relatively flexible, E = 1.1 MPa) is correlated with the biomechanical behaviours of soft tissues (Table 2.1).[35]

There are several characteristics in the biomechanical properties of soft tissues. First, they undergo large elastic deformations without the mechanical failure, due to the networked structure of ECM.[35] Their maximum physiological stretches range from 5 (tendon) to 200% (mesentery).[36] They show in general nonlinear responses upon strain rate. Soft tissues also tend to behave anisotropically due to the fact that the fibrous extracellular matrix proteins are oriented in the preferred directions.[27,32] Their mechanical behaviours are often inhomogeneous, *i.e.* the mechanical properties depend on the position in the tissues, and viscoelastic. The viscoelastic behaviours are associated with the interaction between protein fibres and proteoglycans, as proteoglycans provide a viscous lubrication between collagen fibrils.[37]

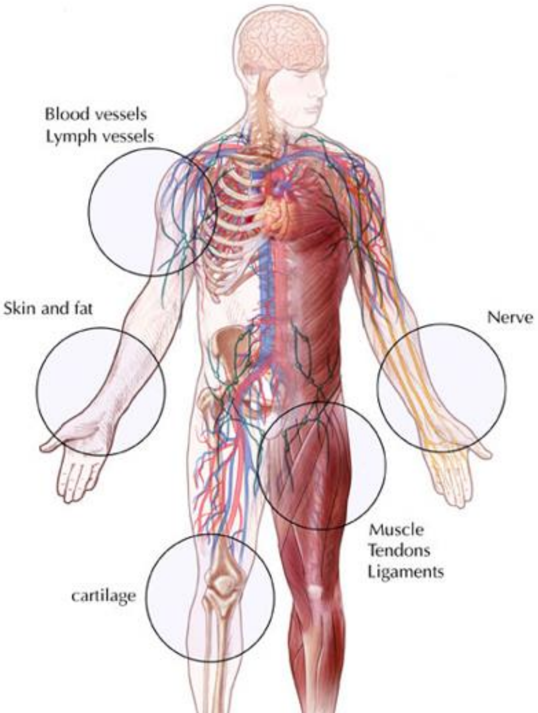

Figure 2.1 Examples of human soft tissues.[29]

Table 2.1 Mechanical properties of soft tissues are correlated with the weight ratio between collagen and elastin.[32]

Material	Ultimate tensile strength (MPa)	Ultimate tensile Strain (%)	Collagen (%, dry weight)	Elastin (%, dry weight)
Tendon	50 – 100	10 – 15	75 – 85	< 3
Ligament	50 – 100	10 – 15	70 – 80	10 – 15
Aorta	0.3 – 0.8	50 – 100	25 – 35	40 – 50
Skin	1 – 20	30 – 70	60 – 80	5 – 10
Articular Cartilage	9 – 40	60 – 120	40 – 70	-

2.1.2 General strategies of tissue engineering

There are three basic tissue engineering strategies founded in the seminal work by Langer and Vacanti: (1) the use of isolated cells or cell substitutes, (2) the delivery of tissue-inducing substances, and (3) growing cells on or within tissue scaffolds.[38] The application of the first two methods have been seriously limited since they can be utilised only when the defect is small and well-confined,[39] or the production cost of tissue-inducing substances such as growth factors is too expensive.[35,40] Therefore, the third method, i.e. growing cells on or within tissue scaffolds, has been the most commonly used tissue engineering strategy. Figure 2.2 shows the general procedure of tissue engineering with implantable scaffolds and injectable scaffolds. This approach relies extensively on the use of scaffold, and the scaffold needs to be engineered to maximise the cell growth and the regenerative potential of tissues. The scaffold material therefore requires a number of design criteria with its interaction with cells (discussed later).

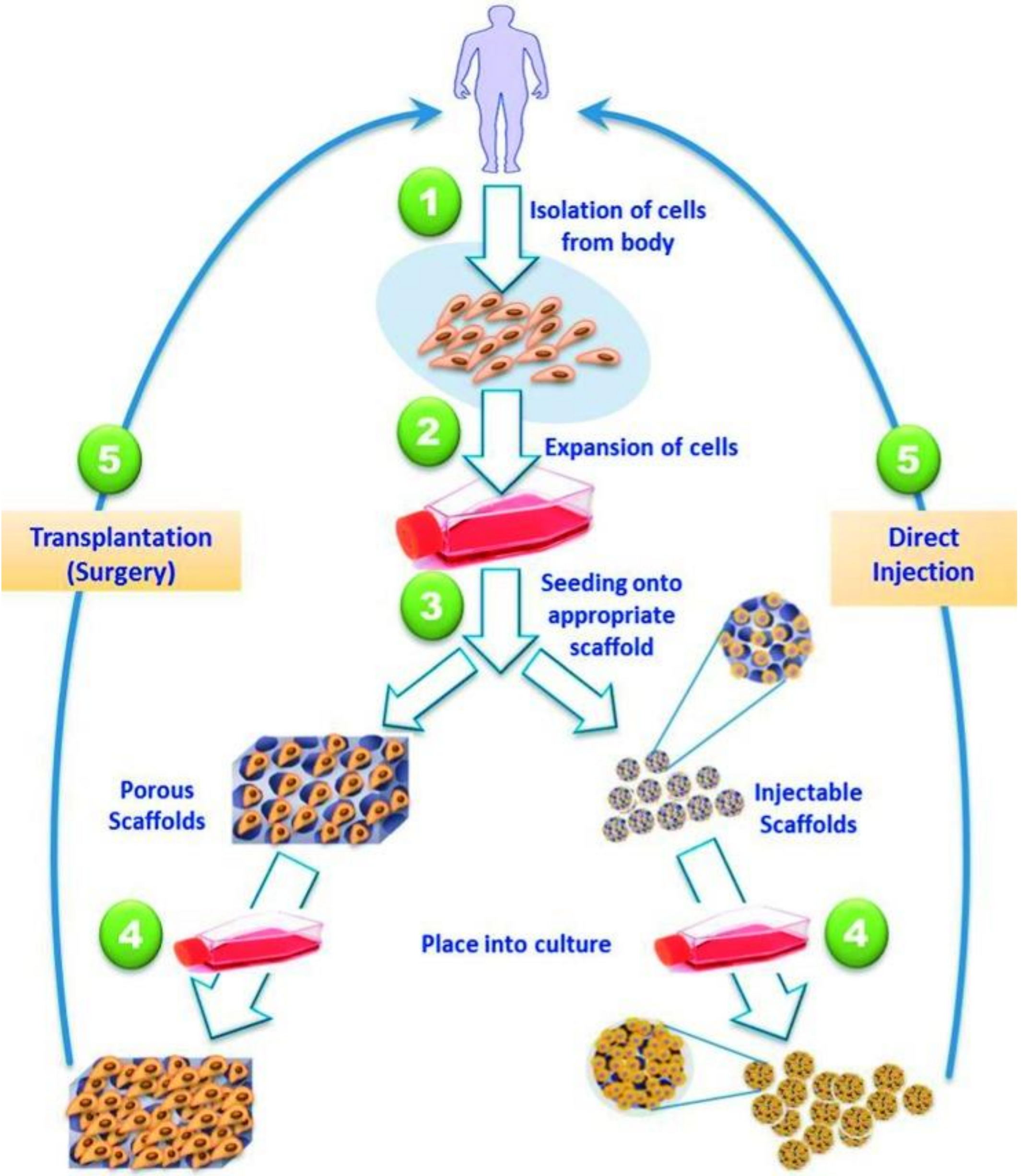

Figure 2.2 Schematic illustration of the most common tissue engineering strategy: (1) Target tissue cells are isolated from body. (2) Cells are cultured and expanded *in vitro*. (3) Cell seeding into the scaffolds; porous scaffolds and injectable scaffolds are being the two most common approach to build the tissue scaffolds. (4) Cells are proliferated on the scaffold. (5) The cell-laden scaffolds are implanted or injected into the defect site.[199]

2.1.3 Scaffolds requirements

Regardless of the tissue type, following fundamental requirements in designing tissue scaffolds has been identified in the literatures. These requirements are potentially interrelated rather than separated,[41] and they will be discussed briefly in the following sections.

Biocompatibility

The very first prerequisite of any tissue scaffold is biocompatibility. Cells must function normally, and proliferate on the scaffold before implantation.[41] After implantation, the scaffold should exhibit a negligible immunogenic reaction in order to prevent the inflammatory response, which can block the flow of nutrients and wastes or even cause rejection by the body.[38,42] The long-term biocompatibility is determined by the bulk material properties, whereas, the short-term biocompatibility immediately after the implantation is subjected to the surface characteristics of scaffold.[35] Achievement of a biocompatible scaffold is generally done by choosing biocompatible materials for its fabrication.[43] If there were one or more harmful chemicals involved in the synthesis of scaffold (organic solvents, crosslinkers or catalysts), a thorough washing process is required.[44–46]

In case of the natural polymers derived from foreign organic bodies, a purification before the synthesis of scaffold might be required to remove potential immunogens.[47] Biocompatibility of a tissue scaffold is normally assessed *in vitro* and/or *in vivo* tests. *In vitro* tests deliver the relatively quick results but it can be tentative, since the immunogenicity is not normally assessed. *In vivo* tests provide more reliable data regarding biocompatibility. However, they can be time and cost-consuming, and the problems in ethics and regulations exist.[41]

Biodegradability

The tissue scaffold is not meant to be implanted permanently in our body. It has to be degraded, and eventually replaced by the natural ECM.[42] In case of the polymeric scaffolds, which are normally used in soft tissue engineering biodegradation depends not only on the origin of polymer, but also the chemical structure, crystallinity, composition, nano-fillers, hydrophilicity, as well as the degrading conditions such as the temperature and pressure.[48–50] The degradation rate of scaffold needs to be engineered to match it with the new tissue formation rate to support the full regeneration of the target tissue.[51] The by-product of degradation process also should not be causing any detrimental effects on surrounding tissues or organs.[42] *In vitro* and/or *in vivo* tests on biodegradability are normally executed, where enzymes are frequently added to mimic biological environment in case of the *in vitro* test.[48,49]

Biomimetic mechanical property

A successful tissue scaffold should have the biomimetic mechanical property consistent with the tissue of interest. While this is important regardless of tissue types, it lays some additional challenges for the load bearing soft tissues such as cardiovascular and cartilage tissues.[42,52] The implanted scaffold must provide the mechanical support during the tissue regrowth until it is degraded and replaced by natural ECM.[42,53] Ideally, the scaffold must maintain its mechanical strength during most part of the tissue regeneration process.[53] Furthermore, it is widely acknowledged that the biomimetic mechanical conditioning appears to encourage the expression of natural ECM and cell growth.[51,54,55] In terms of the clinical practices, the scaffold should be strong enough to be handled by the clinicians.[42]

While the mechanical property of tissue scaffolds primarily depends on the original polymer used in the scaffold fabrication, the crosslinking density of polymer, nano-filler, as well as the storage and synthetic condition also determine the mechanical behaviour of scaffolds.[49,56–60] Since the generation of pore structures in materials usually makes the mechanical strength decreased, for some authors, the balance between the porosity and mechanical property seems to be one of the critical issues in designing tissue scaffolds.[42]

Surface property

The surface properties are important in tissue engineering, since cells primarily interact with tissue scaffolds via the surface. In many literatures, the importance of hydrophilic surface in tissue engineering has been emphasized. In general, hydrophilic surface appears to provide the better cell adhesion and migration.[61–63] Benoit *et al.* demonstrated that the hydrophilic surface also elicits less of an immune response.[64] Furthermore, surface hydrophilicity dictates protein adsorption behaviours, which concomitantly determine cellular activities.[65]

Natural polymers, especially ECM-derived polymers naturally contain biochemically active residues such as a peptide with arginine-glycine-aspartic acid sequence (RGD).[66] However, the surface of synthetic polymers may not be sufficient to induce selective cell adhesion, migration, and proliferation, therefore often require the surface alteration by signalling biomolecules (biofunctiolisation) such as ECM proteins, integrin-binding peptides, and growth factors.[35,42] These biomolecules can be incorporated on the surface either via the chemical conjugation or physical adsorption.[12,15,51,54,67]

The topographical surface morphology is another important factor that modulates the cell behaviours in this realm. Ber *et al.* observed a better cell proliferation with the increased surface roughness.[63] In another study by Bettinger *et al.*, a cell alignment using a patterned substrate was reported.[68]

Scaffold architecture

The architecture of scaffolds for tissue engineering includes: (1) the macroscopic geometry of scaffolds, and (2) the microscopic pore structure. The first one, macroscopic geometry means that the physical size and shape should be designed to mimic those of the biological tissue of interest. For instance, the design of tubular scaffolds is required for intestinal tissue engineering,[69] and the thickness of skin grafts is determined by the anatomical dimension of the tissue defect.[70]

The microscopic architecture of tissue scaffolds, on the other hand, focuses on more cellular (micro-) level. Tissue scaffolds should have an open (interconnected) pore structure and high porosity to let the seeded cells to penetrate and migrate through the scaffold's matrix.[38,42] Without having an adequate pore structure, the diffusion of nutrients for cellular activities also cannot be ensured.[38,42] Furthermore, the proper removal of the waste products such as the cellular wastes and degradation products from tissue scaffold needs the pores.[71] The lack of proper angiogenesis is one of the major challenges in tissue engineering as it will be discussed in the next chapter. The pore structure also plays an important role in the angiogenesis, as it has been demonstrated that the proper pore size encourages the formation of neo vasculature.[72]

Numerous porous scaffolds for soft tissue engineering have been produced from a variety of synthetic skills. For example, electrospinning often used to provide nanofiber matrices.[73] The freeze drying approach with a suitable solvent for polymer can be used especially for a large-scale production of scaffolds.[19] The porogen leaching technique is another.[74,75] Various inorganic, organic, or gaseous porogens can be used to control the porosity and pore size of the scaffolds.

2.2 Wound healing

Wound healing is a complex biological process which requires a proper treatment method including the choice of wound dressing materials and properties. In the following paragraphs, the characteristics of wounds, treatment and factors of wound healing, as well as wound healing materials are discussed.

Definition and Characteristics of Wounds

When the continuity of the epithelial lining of the skin or mucosa from damage, usually by physical and thermal source, we define the medical condition as “a wound”.[76] Depending on the duration of the healing process, there are two different type of wounds; acute and chronic wounds.

An acute wound heals relatively quickly and in a predictable and expectable time of 8 – 12 weeks. The time scale can vary by the size, depth, and extent of the damage in the epidermis and dermis layer of skin or mucosa.

Chronic wounds, on the other hand, do not follow the normal stages of orderly and timely healing stages. Wounds can be caused by many different reasons; surgical injury or accidental injury. Chronic wounds are often originated from underlying medical conditions such as diabetic foot ulcers, burns, pressure ulcers or vascular desease.[77] Wounds can also be categorised into closed wounds, open wounds, wounds without tissue loss, and wounds with tissue loss.[78] For the last type of wounds, the volume of wound dressing material is also important (discussed below).

Another classification method of wounds is based on their appearance; (i) necrotic, (ii) sloughy, (iii) granulating, (iv) epithelialising, and (v) infected and malodourous. For the infected and malodourous wounds, special care is required using the wound dressings with antibacterial agents and deodorants for patients' comfort and optimised healing.[79]

Wound healing is a dynamic and complex biological process but generally includes the following four phases; (i) the coagulation and haematosis immediately after injury, (ii) the inflammatory with swelling on wound site, (iii) the proliferation phase in which new tissues and angiogenesis, and finally (iv) the maturation phase where remodelling of new tissues happens.[76] These phases can be overlapped due to the innate complexity in wound healing process and it largely associated with wound type, but also the wound dressing material and property. Therefore, seeking of proper wound dressing material for a particular wound is important to achieve ideal and fast healing.

In a study in 2016 in UK and Denmark, there are 3 – 4 people with one or more wounds per 1000 population, and many of them are identified as chronic wounds. Based on the figures above, it can be estimated about 3500 people out of a million population will be living with a wound and 525 will live with their wounds over a year.[77] As living with a wound influence greatly the quality of patients' life. The cost in wound treatment can be one of the influential factors, but also other issues such as the pain, discomfort, anxiety, social isolation, morbidity, and even mortality, as well as the burden to patients' families and the society can be preventable by choosing the right treatment of wounds.

General strategies in wound healing

Traditionally, the wet-to-dry gauze has been used. The results have been limited and often made the wound healing worse. The gauze dressings dry the wound site and does not promote the healing of wounds. Besides, it can damage the wounds further when removed.[80] Then the modern wound dressing has arrived in the 20th century. The wound exudate is generated on wound site, which is essentially blood without red blood cells and platelets. It is a bodily reaction to protect the wound site once the haemostasis is achieved.[81] The exudate irrigates continuously and keep the wound moist. Exudates also transport the nutritions and keep the proteinases, chemotactic, and growth factors produced on the wound site to promote the cell migration and mitosis, leading to ephithelialisation, and finally resulting in the proper healing process.[81] The low oxygen tension by the moisture also promote the progress into the inflammatory phase.[76,80]

However, an excessive amount of wound exudate can produce a wet and sloughy mass by a process of autolytic debridement, especially on the chronic wound sites.[81] This leads to medical complications such as prolonged healing time, or even failure to heal the wounds. With the excessive wound exudates, infections by pathogenic bacteria can also happen by *staphylococcus aureus*, *streptococcus pyrogenes*, *pseudo-monas aeruginosa*, as well as some of the genus *proteus*, *clostridium* and *coliform* species, which not only is detrimental for wound healing process, but also cause undesirable malodour.[76,80,81] Therefore, the principle of the modern wound care is based on the choice of proper occlusive dressings with the ideal water swellability and vapour permeability to keep the wound moist based on the wound type and shape. The ideal wound dressing must have the following characteristics according to the literature.[76,77,80,81]

- To be capable of maintaining a high humidity at the wound site while removing excess exudate with adequate water swellability and vapour permeability
- To prevent bacterial invasion by bacterial impermeability and/or antibacterial agents
- To thermally insulating and physically protecting the wound site from the further damages.
- To allow gaseous exchange with optimum oxygen permeability

- To be non-toxic, non-allergenic, and non-antigenic with free of particles and toxic wound contaminants with ease of sterilisation
- To have bioadhesiveness to the wound surface and also to be removed without causing trauma to the wound
- To require only infrequent changes with ease of application, as well as elastic mechanical properties with a high strength to comfortable and conformable uses.
- To promote angiogenesis
- To be able to remove malodour
- Biodegradability
- Compatibility with topical therapeutic agents, cost effective, and long shelf life

Examples of wound dressing

Hydrophilic and mechanically soft polymer materials are most frequently used. There are five main types of wound dressings; (i) film dressing, (ii) foam dressing, (iii) hydrogel dressing, (iv) alginate dressing, and (v) hydrocolloid dressing.

The film dressings are semipermeable. They are impermeable for fluids and bacteria, but permeable to air and water vapour. These dressings usually consisted of polyurethane (PU) or nylon. They are not for highly exudating wounds due to their limited absorption capacity to fluids. However the transparency for inspection and the flexibility as well as stretchability make them ideal for superficial or shallow wounds on the surface requiring mechanical conformation.[76,81]

Secondly, the foam dressings are made of either PUs or silicone polymer. They often have the adhesive layers for proper application. They provide good thermal and physical protection to the wound sites. Their high fluid absorption capacity is ideal for highly exudating wounds.

However they are not suitable for wounds with low exudates, and require frequent replacements.

Thirdly, the hydrogel dressings are made of crosslinked hydrophilic polymers.[81] They are insoluble thus do not leave any particles and debris, which is advantageous by being non-irritant.[76] They have cooling and soothing effects, so frequently applied for burn wounds. They are used for low to moderately exudating wounds. However their low mechanical properties make them difficult to handle and apply.[76,81]

Fourthly, the alginate dressings have a clinical function due to the calcium ions exists within, which promotes the proliferation of fibroblasts and initiates the inflammatory phase. They are applied for moderate to highly exudating wounds. However they are not applicable for the dry wounds as they require moist to function.[81]

Lastly, there are hydrocolloid dressings. The term "hydrocolloid" was derived from colloidal materials made of sodium carboxymethylcellulose, gelatin, or pectin, combined by elastomers or adhesives.[81] They are adhesive to both wet and dry wound sites, and useful for moderately exudating wounds. However, they are naturally malodours and may be mistaken for infection, requiring frequent inspection.[80]

For the advanced and bioactive wound dressings, controlled drug delivery, angiogenesis, malodour-controlling, infection-preventing properties are being actively investigated using the composite stuctrures.[82] An example of a potential bioactive wound dressing which is recently studied in academy is shown in Figure 2.3. Figure 2.3A shows the Ag/ZnO nanoparticles possessing the antibacterial property. Figure 2.3B shows the porous foam wound dressing with Ag/ZnO and chitosan, which is also known for its antibacterial and biocompatible properties. Figure 2.3C shows the antibacterial properties of prepared chitosan-Ag/ZnO nanocomposite porous scaffold dressings with three bacterial species commonly found in soft tissue infection. With the inhibition area of bacterial growth near the nanocomposite wound dressing, the dressing demonstrated its good antibacterial properties. Formation of polymer nanocomposites with functional nanoparticles can introduce various properties which is beneficial to Soft tissue applications.

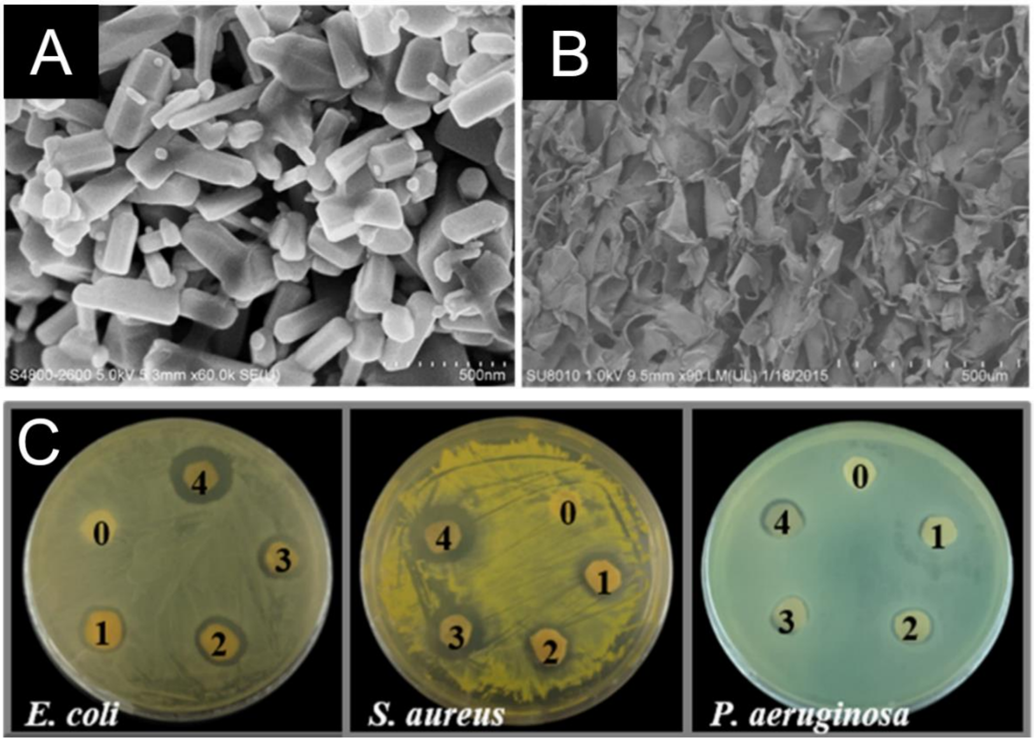

Figure 2.3 Chitosan-Ag/ZnO composite dressing. (A) The Ag/ZnO nanoparticle used to fabricate the composite dressing. (B) Micrograph showing the pore structure of composite dressing. (C) Proven antibacterial property introduced by the Ag/ZnO nanoparticle within the composite dressing

2.3 Angiogenesis

One of the biggest challenges in tissue engineering and wound healing is the lack of vascularisation, *i.e.* the development of new capillaries from existing blood vessels.[83] In our body, the majority of cells are found within 100-200 μm from the nearest capillary network.[84] It has been confirmed that, when the thickness of the implants for tissue engineering is over 2 mm, the diffusion for nutrients, gas, and waste removal is limited, therefore a proper vascularisation is required.[85] A similar observation has also been found in a physiological phenomenon. Solid tumours cannot grow over a size of 2 mm diameter without having their own blood supply,[86] supporting that angiogenesis is essential for metabolism.

One thing needs to be considered, however, the degree of importance of vascularisation varies amongst soft tissues. The reason comes from the natural structure of target tissues in terms of the vasculature. Most of soft tissues are highly vascularised. For instance, skin is well vascularised, therefore achieving rapid vascularisation is essential for skin repair.[70] Oral mucosa (the membranes lining inside of the mouth) is another example of naturally highly vascularised tissue, and a proper angiogenesis would be requested[87]. However, some of the soft tissues such as the hyaline (transparent) cartilage found on joint surfaces contains no blood vessels.[88] Therefore, angiogenesis can be prioritised lower (or even neglected) than other requirements for cartilage tissue engineering.

Several strategies of angiogenesis have been investigated in the literatures. One of the common approaches is to use biological and bioactive molecules that encourage angiogenesis, such as vascular endothelial growth factor (VEGF), heparin, fibroblast growth factor (bFGF), platelet-derived growth factor (PDGF), platelet-rich fibrin, vitamin D, and 17β-estradiol (E2).[84–86,89–93] The mechanism of how these molecules works for angiogenesis is rather complex and different from molecule to molecule. For instance, VEGF is a signal protein that directly stimulates the endothelium cells to induce angiogenesis, whereas heparin more indirectly works by attracting the positively charged residues of VEGF with the electrostatic interaction.[84,94] Scaffolds may be simply loaded or covalently coupled with these angiogenic factors.[84,85,94]

Other methods for angiogenesis include; (1) cell-based, and (2) structure-based approaches. The cell-based approach uses endothelial cells mixed with target tissue cells. The co-culturing of those cells provide a vascularisation throughout the scaffold.[84,95] In the structure-based approach, angiogenesis is induced by the vessel-like microscopic patterns of tissue scaffolds.[96,97] The combination of different approaches has also been studied.[84] Some examples of scaffold design with angiogenesis are shown in Figure 2.4.[85,96] Figure 2.4A1 and A2 shows a scaffold with heparin. With heparin, the number of blood vessels growing towards the sample increased significantly in the fertilised chicken eggs, demonstrating heparin coating can be useful where angiogenesis is required in the soft tissue engineering. Figure 2.4B1 and B2 shows the patterned PGS films to guide the growth of endothelial cells along the patterned capillaries,

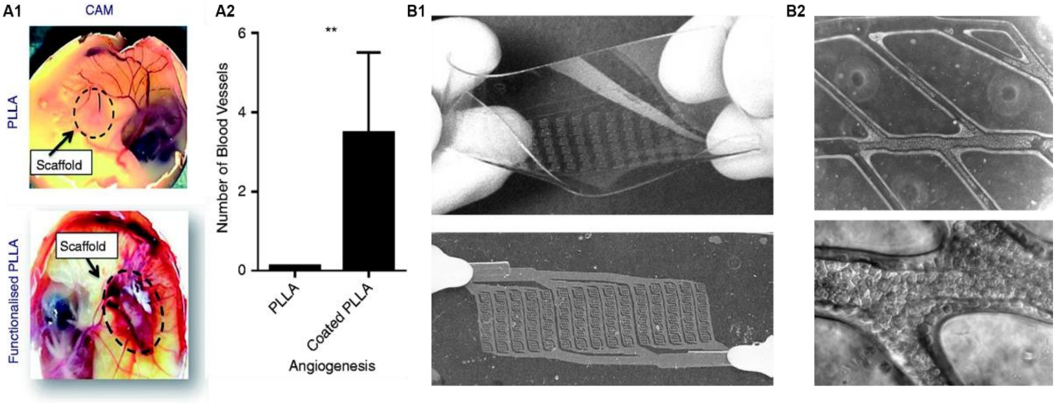

Figure 2.4 The scaffold designs with angiogenesis. (A1) Pristine PLLA scaffold (upper), and heparin-coated PLLA scaffold (lower) implanted in fertilised chicken eggs. (A2) The measured number of blood vessels dramatically increases with the heparin-coated PLLA scaffold. (B1) Patterned PGS films by a moulding process. (B2) Angiogenesis induced by the endothelial cells along the patterned capillaries.[85,96]

forming blood vessels accordingly to the shape of capillaries. As shown in these examples, angiogenesis in tissue scaffolds can be achieved either by the biochemical method or biomechanical method as cells grow in response to the various chemical and mechanical stimuli.[98–100]

2.4 Biomaterials for soft tissue applications

There are three main groups of biomaterials; ceramics, natural polymers, and synthetic polymers. For soft tissue engineering, ceramic scaffolds are not favourable due to their discordant mechanical properties with soft tissues such as too high stiffness, very low elasticity, and a hard brittle surface.[42] In general, polymeric biomaterials (biopolymers) have been used in soft tissue engineering. Biopolymers are often used in copolymer, blend, and composite forms.[51]

2.4.1 Conventional natural polymers

Natural polymers have been widely investigated in the soft tissue healthcare sector for almost all types of soft tissues. There are two types of natural polymers. The first type is ECM-derived polymers such as collagen, gelatin, fibrin and keratin. Among them, collagen and its derivative gelatin are the most commonly utilised polymers. Collagen is usually produced from animal tissues such as skin and tendon, and discarded human tissues such as placenta.[54] While there are total 29 types of collagen discovered,[101] collagen type 1 is most commonly reviewed in the literatures since it is the most abundant type of collagen.[54] Collagen contains the integrin binding sequences such as RGD,[102] which promote cell adhesion, migration, differentiation and proliferation. Gelatin is produced by the denaturisation of collagen, and is an attractive natural polymer for soft tissue engineering because of its biological similarity to collagen. Commercially, two types of gelatin are available; (1) type A gelatin from acid hydrolysis of porcine skin, and (2) type B gelatin from base hydrolysis of bovine skin.[103] Gelatin is less immunogenic compared to its precursor and contains the integrin binding sequences inherited from collagen.[103,104]

Other ECM proteins such as elastin, fibrin, and keratin have also been demonstrated as the good candidates for soft tissue engineering.[56,105] Table 2.2, and Figure 2.5 present the mechanical properties as well as the applications of ECM-derived natural polymers in soft tissue engineering. Figure 2.5A1 and A2 shows a collagen scaffold fabricated by a freeze-drying approach, where collagen is first dissolved in acetic acid aqueous solution and subsequent freeze-drying created the pores by sublimation of ice crystals. The freeze-drying technique is widely used to prepare a porous scaffold, the advantages of this approach includes a large scale production, well-defined and interconnected pores, as well as lack of additional extraction of porogens after the fabrication. Figure 2.5 shows the gelatin hydrogel and its application in adipose tissue engineering. In this case, matured adipocytes were seeded on the gelatin hydrogel and cultured (Figure 2.5B1), showing regenerated adipose tissues studied by

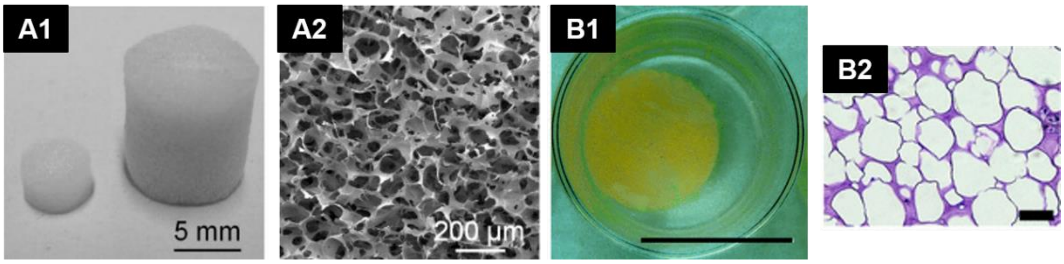

Figure 2.5 (A1 and A2) Collagen scaffolds for cartilage tissue engineering; (A1) scaffolds synthesized by freeze-drying, and (A2) a SEM image showing the pore structure.[334] (B1 and B2) Gelatin hydrogel for adipose tissue engineering; (B1) culturing mature adipocytes (scale bar 1 cm), and (B2) the regenerated adipose tissue (scale bar 50 μm).[335]

tissue histology (Figure 2.5B2).

Table 2.2 A summary of tensile properties and applications of ECM-derived natural polymers used in soft tissue engineering.[35,43,106–108] The mechanical properties of gelatin were measured from a chemically crosslinked gelatin gel with glutaraldehyde, as it is the most commonly used type of gelatin scaffold.[108]

Material	Young's modulus (MPa)	Ultimate tensile strength (MPa)	Elongation at break (%)
Collagen	2 – 1200,[35] 100 – 2900[43]	120,[35] 5 – 500[43]	13 – 50,[35] 5 – 50[43]
Gelatin	5.6 – 15.6[108]	8 – 12[108]	11.9 – 33.1[108]
Fibrin	1.9 – 8.0[106]	-	147 – 226[106]
Keratin	10 – 2500[107]	2 – 530[107]	2 – 50[107]

Another type of natural polymers is derived from foreign biological systems, such as (1) vegetal-sourced proteins such as gluten,[35,49] (2) polysaccharides such as chitosan,[109,110] starch,[111] alginate,[112] and agarose,[109] as well as (3) silk proteins from silk worms and spiders.[35,39,43] They also have been utilised with diverse material designs and structures in order to be applied in soft tissue engineering and wound healing.

Although natural polymers present advantages in biocompatibility, biodegradability, and bioresorbability, as well as the physiologically relevant biochemical and mechanical properties, several limitations are also identified in the literatures. The utilisation of natural polymers often requires tedious purification procedures or chemical treatments to remove pathogen,[39,47] or immunogenic telopeptides.[54] The inherent instability in processing and random properties also limit the use of natural polymers. Furthermore, the issues in regulation and limited supply are exist.[47]

2.4.2 Conventional synthetic polymers

Linear aliphatic polyesters such as polyglycolic acid (PGA), polylactic acid (PLA), and their copolymers, poly(lactic-*co*-glycolic acid) PLGA are frequently used as biomaterials to abricate tissue scaffolds. The chemical molecular structure is shown in Figure 2.6. These polymers gained US Food and Drug Administration (FDA) approval for clinical use,[113] with their well-known and controllable biodegradability as well as acceptable biocompatibility.[56]

PGA is one of the most widely used synthetic polymers.[39] The synthesis of PGA is done by ring opening polymerisation of a cyclic glycolide.[49] PGA is crystalline (45 – 55%) and rigid

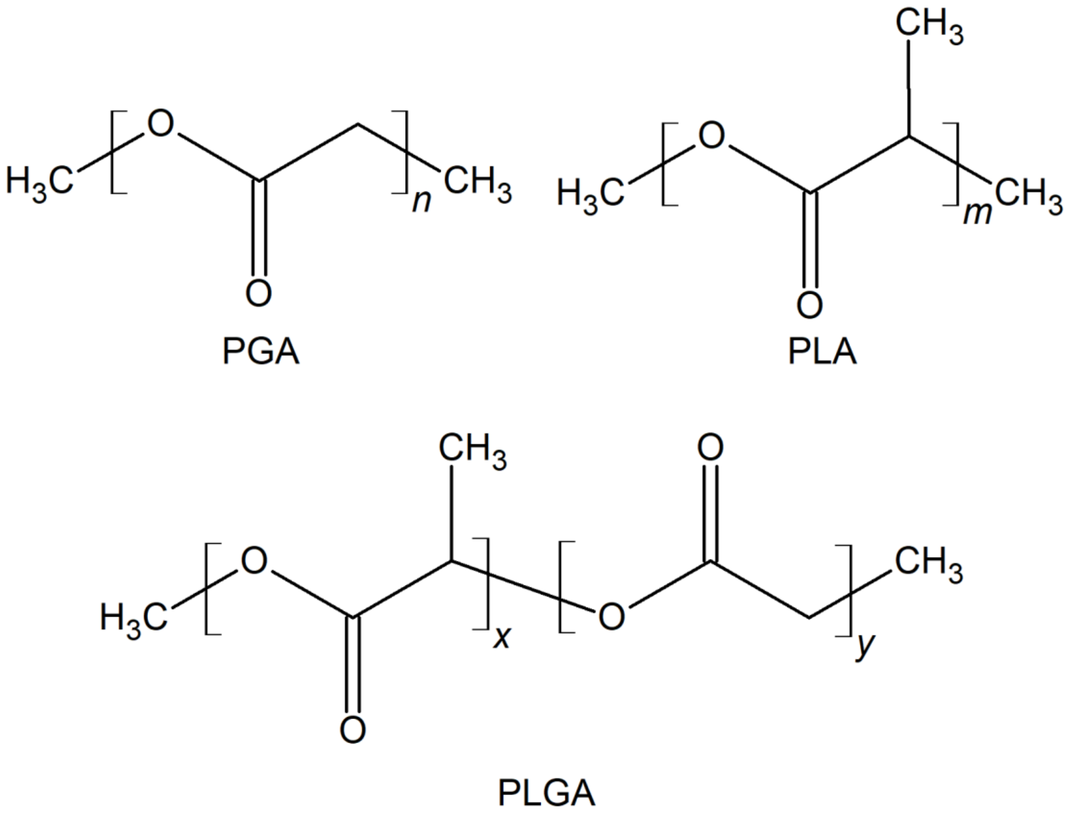

Figure 2.6 Molecular structures of PGA, PLA, and PLGA polymers.

due to the regularity in the chain structure.[114] It is not soluble in most organic solvents and the low solubility often limits its applications.[49]

PLA is usually prepared from polycondensation of D- and/or L-lactic acid and there are three different types of PLA; poly(D-lactic acid) (PDLA), poly(L-lactic acid) (PLLA), or poly(D,L-lactic acid) (PDLLA). The ring opening polymerisation of lactide is also available to obtain this polymer. PLA is generally considered as a hydrophobic polymer because of the –CH3 side groups, and thereby it is more resistive to hydrolysis than PGA.[53] The T_g of PLA is 63.8 °C, so it is rigid at physiological temperature.[49]

PLGA is synthesized by copolymerisation of lactic acid and glycolic acid. The molar ratio of two monomers can change the mechanical properties, degradation rates, and surface hydrophilicity of polymer.[49] However, these polymers do not provide satisfactory mechanical performances for the soft tissue applications.[35] The high stiffness and plastic deformation of these polymers result in the failure under the cyclic mechanical strain, and the consequential and critical decrease in performance and patients' discomfort.[47,115] Furthermore, these polyesters exhibit bulk degradation kinetics, *i.e.* the material properties decay exponentially with the mass loss, which often limits its stable performance *in vivo*.[10]

Poly(ε-caprolactone) (PCL) is another type of biodegradable polyester. PCL is prepared by the ring-opening polymerisation of the cyclic monomer, ε-caprolactone.[53] PCL is a semi-crystalline polymer with a low T_g of -60 °C, therefore it is rubbery at body temperature.[114] PCL degrades significantly slowly than PLA, PGA, and PLGA, which makes it less attractive for general tissue engineering but more attractive for long-term implants.[39] PCL is also relatively cheap and soluble in a wide range of organic solvents.[49]

Poly(ethylene glycol) (PEG) (often called poly(ethylene oxide) (PEO), or polyoxyethylene

Table 2.3 Mechanical properties of synthetic polymers applied in soft tissue engineering.[2,116,117] The mechanical data of PEG was from cylindrical solid specimens (M_w = 600).[116] The mechanical data of PEG hydrogel was from a chemically crosslinked PEG hydrogel.[2]

Material	Young's modulus (MPa)	Tensile strength (MPa)	Elongation at break (%)
PGA	6900[117]	70[117]	< 3[117]
PLA	1200 – 2400[117]	28 – 50[117]	6[117]
PLGA	1.4 – 2.8[117]	41.4 – 55.2[117]	3 – 10[117]
PCL	0.21 – 0.34[117]	20.7[117]	300 – 500[117]
PEG	3.8 – 4.7[116]	0.31 – 0.79[116]	-
PEG hydrogel	0.016 – 0.090[2]	0.013 – 2.200[2]	0.1 – 0.77[2]

(POE), depending on its molecular weight) is widely used for soft tissue engineering since it forms biocompatible hydrogels with similar mechanical properties to soft tissues.[51] In fact, PEG is not biodegradable, and often copolymerised with other PLA, PGA, and PLGA to overcome the deficiency in biodegradability.[51] This copolymerisation induce a hydrophilic surface to the biomaterials as well.[44,118,119]

While synthetic polymers have shown much success as the mechanical properties and degradation kinetics can be easily tailored by the synthetic condition and chemical architecture, the surface of synthetic polymers lacks the biologically active ligands that cells interact with.[42] Therefore, surface modification is often required with biomolecules such ECM proteins, integrin-binding peptides, and growth factors.[35,42] Table 2.3 presents mechanical properties of the synthetic polymers in soft tissue application. Figure 2.7 shows the applications of synthetic

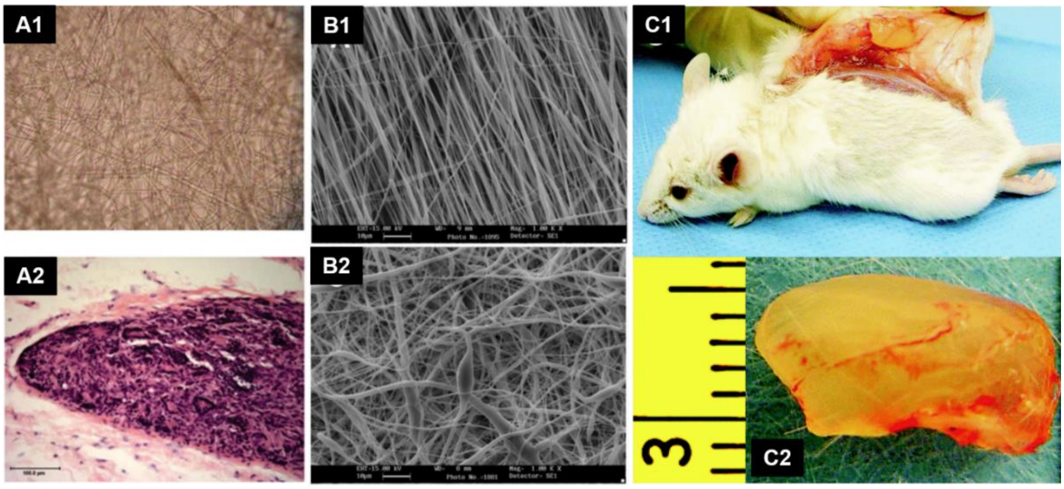

Figure 2.7 Synthetic polymers applied in soft tissue engineering. (A1 and A2) The PLA/PGA electrospun scaffold for skin tissue engineering; (A1) before culture with small vessel endothelial cells, and (A2) three month after the implantation, showing good vascularisation as well as the penetration of granulation tissue.[70] (B1 and B2) The PCL electrospun scaffold for cardiac tissue engineering; (B1) aligned, and (B2) random fibrous structures to control the stem cell differentiation.[336] (C1 and C2) The hydrogel based on PEG synthesized for synovial tissue engineering; (C1) recovery of tissues after 8-week implantation, and (C2) the harvested synovial tissue.[337]

polymers in soft tissue engineering.

2.4.3 Elastomers

As the alternatives to these conventional polymers for biomedical applications, several biodegradable and biocompatible elastomers have been increasingly proposed for soft tissue healthcare in recent years.[35] An elastomer is a polymer with a glass transition temperature (T_g) which is lower than room temperature and exhibit elastic deformation, characterised by high flexibility and stretchability, as well as shape recovery in its size and shape after a mechanical deformation.[47] Elastomers for biomedical applications, often called bioelastomers, can be categorised by their sources; natural elastomers from biological origin, and synthetic elastomers from chemical synthesis. Natural elastomers include elastin, elastin-like peptides (ELP)s, and silk-elastin like protein (SELP) polymers.[47] Their advantages identify the biocompatibility and biomimetic mechanical properties.[19,35,120] The disadvantages are their sourcing, reproducibility in their performance, and often undesirable immune responses *in vivo*.[120–122] Synthetic elastomers can be more finely and predictably engineered in order to meet the requirements in their physicochemical properties by the choice of an appropriate synthetic conditions.[123]

Another way to classify the elastomers can include the thermoplastic elastomers with physical and reversible crosslinking between polymer chains, and the thermosetting elastomers with chemical and usually irreversible crosslinking. Thermoplastic elastomers are easy to process, but the degradation happens in a heterogeneous way, resulting in un-predictable loss of material performance. Thermosetting elastomers have a linear and predictable degradation rate and the following linear performance loss with time, but their poor processability and harsh curing conditions for biochemical molecules have been the problems.[47] An example of the thermoplastic synthetic elastomer is polyhydroxyalkonates (PHAs), including poly(hydroxyalkanoate) (PHA), poly(4-hydroxybutyrate) (P4HB), and Poly(3-hydroxybutyrate-co-3-hydroxyvalerate) (PHBV), which produced by bacterial fermentation of sugar or lipids.

For the thermosetting synthetic elastomer, PUs synthesised by biodegradable polyol segments have been studied for its good mechanical properties and facile engineering of the properties by the synthetic conditions.[44] However, the synthesis of PUs often include toxic chemical crosslinkers and catalysts, requiring an arduous purification of the final products.

Poly(polyol dicarboxylic acid) (PPODA)-based and Poly(diol polybasic acid) (PDOPA)-based thermosetting polyesters also has been widely studied in biomedical applications due to their processability, reproducibility, as well as good biocompatibility and biodegradability in their performance.[43] Table 2.4 summarises the mechanical properties of elastomers for healthcare applications.

Table 2.4 Mechanical properties of natural and synthetic elastomers.[35,43,47,124–127]

Material	Young's modulus (MPa)	Tensile strength (MPa)	Elongation at break (%)
Elastin	0.3 – 1.0[35,126]	0.2 – 0.6[120]	100 – 150[35]
ELPs	1.5 – 400[126]	-	< 420[127]
SELPs	79.6 – 588.9[125]	150 – 700[125]	50 – 250[125]
PHAs	50 – 2000[47,124]	15 – 50[47,124]	1 – 1000[47,124]
PUs	7 – 278[4347]	4 – 38.5[4347]	100 – 1300[4347]
PPODAs	0.08 – 657.4[43]	0.14 – 30.8[43]	10.9 – 737.48[43]
PDOPAs	0.10 – 130[43]	0.21 – 33.35[43]	51 – 1505.5[43]

2.5 Poly(glycerol sebacate)

Amongst synthetic elastomers based on poly(polyol dicarboxylic acid), PGS has attracted significant attention in soft tissue engineering with its biomimetic elastomeric behaviour of soft tissues in our body. *In vivo* and *in vitro* studies exhibited good biocompatibility with adjustable biodegradability and bioresorbability. Additionally, the monomers of PGS are relatively inexpensive, and the synthesis is facile which will be beneficial for large scale applications.[9]

2.5.1 Synthesis of poly(glycerol sebacate)

With its intended application in soft tissue engineering, the following five design criteria were considered in the original investigation of PGS by Wang *et al.*: (1) The polymer degrades through hydrolysis to minimize the number of possible pathways in enzymatic degradation, (2) The polymerisation is governed by the ester bond as it is well established and versatile, (3) The degree of polymerisation is kept low to avoid the formation of rigid and brittle polymers, (4) The chemical bonds that crosslink polymer chains must be hydrolysable and identical to the bonds in the polymer backbone to reduce the possibility of heterogeneous degradation, and (5) The choice of nontoxic monomers is required. At least one of the monomers must be trifunctional and contain hydroxyl groups for hydrogen bonding.[9]

Two monomers were chosen to address the concerns above; glycerol (a polyol, $CH_2(OH)CH_2(OH)CH_2OH$), and sebacic acid (a dicarboxylic acid, $HOOC(CH_2)_8COOH$). The polymerisation mechanism of PGS is step-growth polymerisation.[47] Generally, the synthesis of PGS is carried out in two steps: (1) pre-condensation and pre-polymerisation of monomers, and (2) crosslinking (curing) of the PGS pre-polymer to produce a tough elastomer. In the first step, the hydroxyl groups in glycerol and the carboxylic groups in sebacic acid form the ester bonds by the condensation reaction, resulting a PGS pre-polymer. It has been found that the PGS pre-polymers mainly consist dimer to octamer units of monomers with a study using mass spectroscopy.[22] Another study of PGS pre-polymer using ^{1}H NMR and ^{13}C NMR analysis have shown that the primary alcohol groups of glycerol molecules are responsible for the formation of pre-polymers.[25] In the second step, the remaining secondary hydroxyl groups in glycerol molecule are mostly utilised to further condense the polymer chains to a crosslinked elastomer.

The common synthetic procedure of this polymer is as follows, an equimolar mixture of glycerol and sebacic acid underwent the pre-condensation step at 120 °C to yield a highly viscous pre-polymer resin. A positive pressure of argon gas and a subsequent reduced pressure were applied to minimise the unintended oxidation and hydrolysis. In the second step, the pre-polymer was kept at 120 °C for 48 hours in a vacuum condition to crosslink the polymer chains further through the ester bonds.[9] The chemical reaction scheme of this typical synthetic method is shown in Figure 2.8.

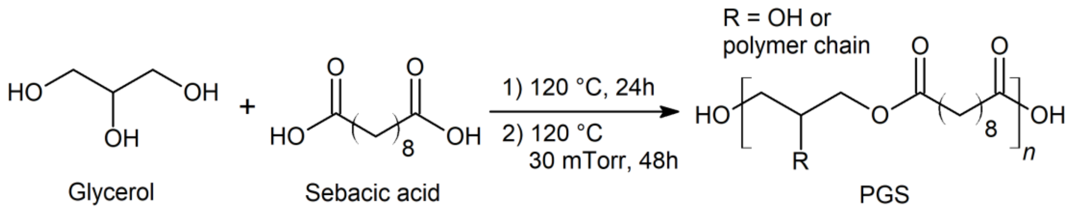

Figure 2.8 Typical synthetic reaction scheme of PGS.

Most of the studies on PGS have followed the thermal synthetic procedure above. However, there have been attempts to change the synthetic parameters to tailor the physicochemical properties as well as the mechanical behaviours of PGS. The modifications have been investigated by; (i) altering molar ratio of monomers,[21,22,128] (ii) modifying the reaction temperature and time,[21,23,25,128] or (iii) employing different chemical mechanisms and monomers such as the ring-opening reaction using diglycidyl sebacate.[20]

Although the thermal synthetic method has been widely used, some notable attempts on photopolymerisation approaches have also been studied to overcome the high temperature synthetic conditions.[129–134] Nijst *et al.* first reported the chemically modified PGS with acrylate moieties, called poly(glycerol sebacate) acrylate (PGSA), and crosslinking of PGSA polymers was achieved via UV light irradiation.[132] Following this study, similar approaches were

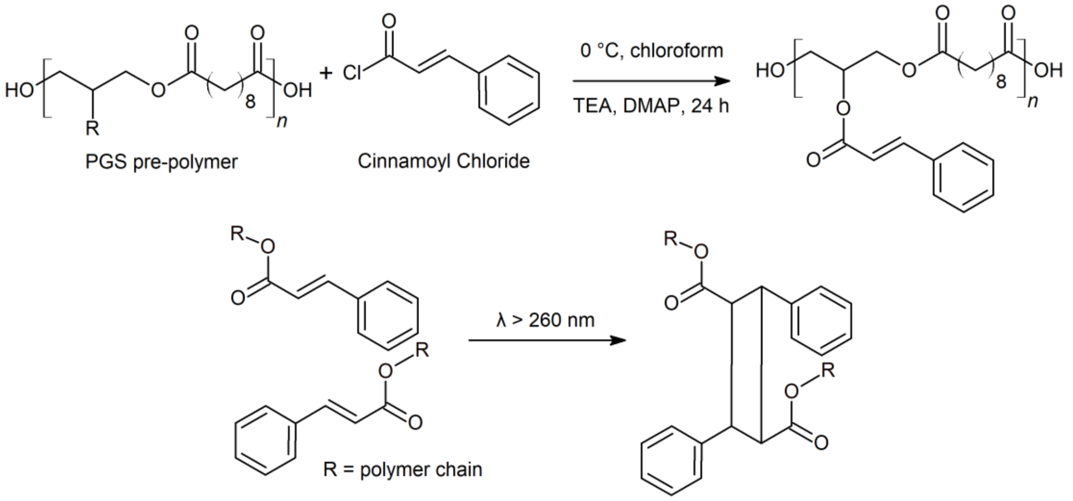

Figure 2.9 Photo-polymerisation method of PGS-cinnamate with UV light. TEA refers to triethlyene amine. DMAP refers to 4-dimethylaminopyridine. Both chemicals were used as catalysts.[135]

investigated by incorporating photo-reactive functional groups such as fumarate, cinnamate and metharcrylate into PGS.[129,133,134] Figure 2.9 shows a photo-polymerisation method of PGS-cinnamate, a PGS modified with cinnamate groups which provides its ability of photo-polymerisation.[135]

To overcome the long preparation time of PGS pre-polymer, the microwave-assisted rapid synthesis was also investigated.[24,136] Only 15 mins of microwave time was found to be as efficient as 6 h of typical thermal pre-polymerisation of PGS. However, the crosslinking of pre-polymer into the cured PGS was done by the typical thermal method in a vacuum oven.

The functional hydroxyl groups of PGS also allow to crosslink the polymer chains chemically via urethane linkages. M. Pereira *et al.* developed Poly(glycerol sebacate urethane) (PGSU) using PGS pre-polymer and hexamethylene diisocyanate (HDI), a hydroxyl-reactive diisocyante crosslinker (discussed in Chapter 4).[45] The hydroxyl groups on PGS pre-polymer were replaced by urethane groups with HDI crosslinker, and the crosslinking density as well as the mechanical properties of PGSU were controlled in a wide range. Young's modulus, tensile strength and elongation at break of PGSU featured 0.09 – 19.7 MPa, 0.14 – 12.1, and 78 – 516%, depending on the amount of HDI added (or the crosslinking density).[45]

2.5.2 Properties of poly(glycerol sebacate)

PGS is a transparent thermosetting polyester.[9] Most of the polyesters in biomedical fields are semi-crystalline and hydrophobic.[20] PGS is also hydrophobic with minimal swelling ratio of 2.11 ± 0.88%, and the water contact angle was determined as 77.5 ± 1.7°.[118] According to the literature, PGS can exhibit amorphous behaviour. However, in a few cases semi-crystalline PGS has been reported. This can be due to the fact that the residual amount of the PGS pre-polymer which is known to be semi-crystalline, depending on its synthetic and purification method.[22] Two T_g at -52.1 °C and -18.5 °C, and two T_m at 5.2 °C and 37.6 °C were revealed by differential scanning calorimetry (DSC), meaning that the polymer is totally amorphous at body temperature.[9,137] PGS is also hydrophobic. PGS swells in water by 2.11 ± 0.88%, and the water contact angle was determined as 77.5 ± 1.7°.[118]

PGS exhibits elastomeric mechanical behaviours. Tensile tests demonstrated that Young's modulus, ultimate tensile strength, and strain at failure of PGS is in the range of 0.025-1.2 MPa, 0.23-0.79 MPa, and 69-448%, depending on the preparation methods.[9,11,12,23,58,138] The chemical crosslinking via ester bonds and hydrogen bonds from free hydroxyl groups between polymer chains are responsible for its elastomeric characteristics.[139–141]

Biocompatibility is one of the essential prerequisites of biomaterials.[51] *In vivo* and *in vitro* examinations demonstrated that PGS has a good biocompatibility with minor fibrotic inflammatory responses,[9,14] which is primarily attributed to the monomers. Both the monomers of PGS are endogenous. Glycerol is a one of the building blocks of lipid molecules.[142] Sebacic acid is a natural metabolic intermediate in the formation of large fatty acids.[143] Use of both chemicals in medical applications has been approved by FDA.[9,18] In addition, the synthesis of PGS includes no organic solvents, which may cause adverse health effects in human body.[144]

PGS is also appeared to be biodegradable *in vitro* and *in vivo* with linear mass loss over time and surface erosion kinetics.[9–11,26,58,145–148] Regarding biodegradability of PGS *in vivo*, tests revealed 70% of weight loss in 35 days, and within 60 days, the polymer was completely absorbed.[10]

2.5.3 Applications of poly(glycerol sebacate)

PGS has been reviewed mostly in the field of biomedical applications, and the majority belongs to soft tissue engineering as the utilisation of its biomimetic mechanical properties of soft tissues. Existing studies include; cardiac,[12,23,154–157,61,138,146,149–153] nerve,[13,14,158] retinal,[15,159,160] vascular,[16,17,55,96,146,161–163] cartilage,[164] and adipose applications in soft tissue engineering (Figure 2.10).[19] Figure 2.10A shows the immunocytochemical analysis for expressions of the mesenchymal stem cells with marker proteins for CD 105 and actinin to evaluate cardiogenic differntiation. Figure 2.10B shows an example of adipose tissue engineering with PGS. The histological analysis of the PGS-based tissue scaffolds shows collagen accumulation by Sirius red staining, indicating the adipose-derived stem cell (ADSC) proliferated well on the scaffolds. The application of PGS in nerve tissue engineering is shown in Figure 2.10C. Several other biomedical applications for PGS include controlled drug delivery system,[165,166] a surgical sealant,[167] a postoperative anti-adhesion barriers.[168] A number of studies on hard tissue engineering applications also exists, such as PGS-hydroxyapaptite nanocomposites,[129] PGS-bioglass® nanocomposites,[169] and PGS-PLLA blends for bone regeneration.[170] PGS has been

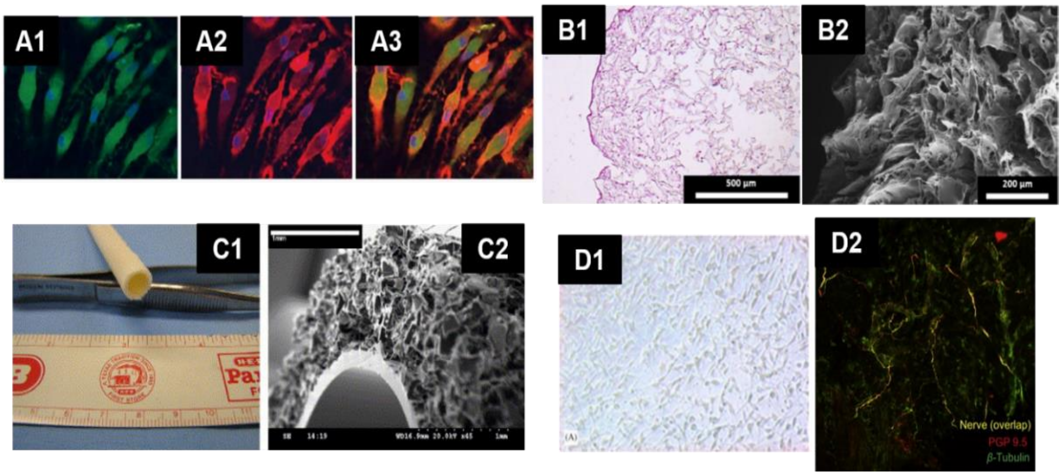

Figure 2.10 Applications of PGS in soft tissue engineering. (A1–3) PGS application on cardiogenic differntiation.[12,153] (B1) ADSC proliferates within the porous PGS-based scaffold.[19] (B2) shows the pore structure of PGS-based scaffold. (C1–2) Artifical blood vessels made out of PGS[16]. (D1) Schwann cells cultured on PGS-coated polystyrene for 7days. (D2) Regeneration of nerves in neoarteries where the nerve is shown in yellow colour.[13,14]

also investigated for its shape memory effects,[46,137] and thermoresponsive properties,[44] depending on the polymer's thermal properties and hydrophilicity/hydrophobicity.

2.5.4 Limitations of poly(glycerol sebacate)

One of the prior limitations of PGS comes from its extreme synthetic condition. The synthesis of PGS generally requires long reaction time of 79 – 149 hours, high temperature of 110 – 160 °C, and a vacuum environment throughout the process.[25] This presents challenges in fabrication of PGS into 3D scaffolds, since the pre-built PGS structures would melt and collapse during the synthetic process.[26]

The hydrophobicity and low water uptake capacity of PGS also pose as hindrance to its use in biomedical applications.[20,119,141] Furthermore, PGS lacks free functional groups for further modification with biomolecules, similar to most of the polyesters.[20] Therefore, the synthesis of PGS with bioactive surfaces is limited.

The materials for tissue engineering should provide sufficient mechanical support during the period of tissue regeneration.[54] However, the degradation kinetics of PGS in vivo can be too fast to sustain in the aggressive environment of human body.[58] Lastly, the acidic degradation products of PGS can cause cytotoxicity.[58,148]

2.6 Polymer-clay nanocomposites

Composites can be defined as the material combination of two or more physically distinct and mechanically separable materials, to provide superior, and possibly unexpected characteristics which are different from the individual components.[171] A nanocomposite is a composite in which at least one of the dimensions of one of its material phases is in the order of nanometre.[172] Polymer-clay nanocomposites (PCNCs) fall in the last category, being consisted by polymer or copolymer as the continuous phase (matrix), and nano-clays as the dispersed phase (filler).[173] Since the seminal work of the nylon-clay nanocomposite by Toyota in 1989,[174] PCNCs have been extensively studied and applied in various applications. The mechanical property,[175] gas permeability,[173,176,177] flame retardancy,[178] thermal stability,[179] electrical property,[180] biodegradability can be modulated or enhanced dramatically by the addition of a small amount of clays (< 10 wt.%).[50,173]

2.6.1 Introduction to clay

Clays are earthy mineral materials with traces of ions and organic matter, produced by natural erosion (particle size < 2 μm).[181] Clays are naturally abundant and non-toxic. There are four main groups of clay minerals; (1) kaolinite, (2) smectite, (3) chlorite, and (4) illite, and a wide range of minerals belong to these groups.[182] Kaolinite group includes the minerals such as kaolite, dickite, halloysite, and nacrite. Smectite group (also known as montmorillonite group) includes montmorillonite, pyrophyllite, talc, vermiculite, sauconite, spaonite, and nontronite. The member of chlorite group is amesite, chamosite, cookeite, and nimite. In illite group, only illite is the common mineral.[183]

Chemically, all clays are hydrous aluminium phyllosilicates, sometimes containing impurities such as magnesium, potassium, sodium, calcium, and iron. Clay minerals contain two-dimensional sheets of silica (tetrahedral) and alumina (octahedral).[181,184,185] The sheet units can be built into two different ratios, known as 1:1 or 2:1 clays (Figure 2.11). In the 1:1 clay, one silica sheets and one alumina sheets form a layer (platelet, 100-200 nm in longitudinal and 1 nm in thickness in case of montmorillonite).[174] The example of this 1:1 clay is kaolinite. Alternatively, in 2:1 clay, one alumina sheet is bonded with and sandwiched by two silica sheets resulting 2:1 ratio. Vermiculite and montmorillonite are the examples of this clay type. Depending on the chemical composition of the sheets, the platelets can be electrostatically neutral or negatively charged. The charge is balanced by coordination between oxygen atoms in the sheets and metal cations such as Li^+, Na^+, K^+, Rb^+, Cs^+, and Ca^{2+}.[174] Water molecules also present in the interlayer spaces.

The general production of clay includes four phases; extraction, blending (if necessary), crushing, and drying.[186] Clay can be manufactured either via a dry or wet (slurry) process. In the dry process, the clay is dried on a fluid bed dryer thereby the moisture content is reduced to 10 - 12%. The product then may be mechanically milled by a roller. The wet process differs from the dry process by using a batch hopper that contains hot water and chemicals. The

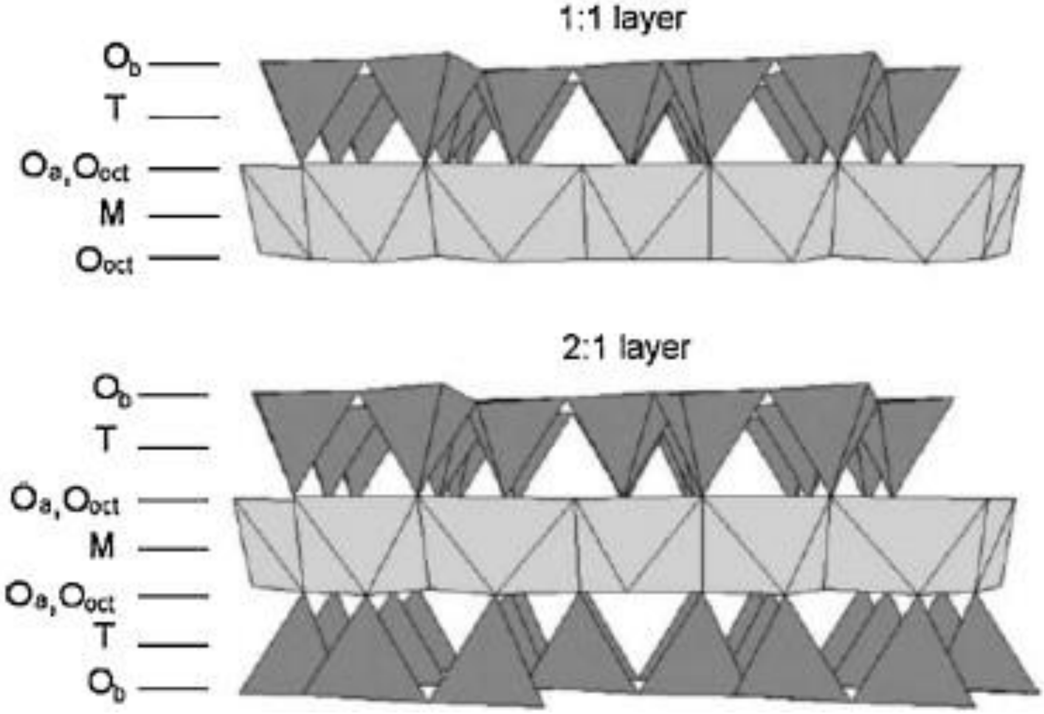

Figure 2.11 The mineral structure of clay: (A) 1:1 clay, and (B) 2:1 clay, where O_a, O_b and O_{oct} refer to tetrahedral apical, tetrahedral basal and octahedral anionic position.[338]

chemicals are to enable the purification of natural organic impurities such as lignin.

Surface modification of clays with organic molecules (surfactants) is often requested to improve the mixing and blending properties with organic solvents and polymers.[187] The resulting modified clays are often called organo-clays. There are two ways to prepare organo-clays; (1) displacement, and (2) grafting. In most cases, water and cations present in the interlayer space (gallery) of clay minerals. The displacement reactions occur non-covalently. Polar organic molecules can replace the water molecules. The exchange of gallery cations is also possible with cationic organic molecules. In case of the neutral organic molecules, the formation of organic-inorganic complexes with gallery cations are responsible for the modification. The grafting reactions, on the other hand, form covalent bonds between clay minerals and organic molecules. Only the 2:1 clays with reactive surface groups can be modified in this manner.[187]

The typical preparation of organo-clays can be achieved either by the solvent-based, or solid-state systems. In solvent-system, the cations in the clay are exchanged by desired organic modifiers in aqueous media.[188] The solid-state reaction is a relatively new method, as it is first reported by Ogawa *et al.* in 1990.[189] Organic modifiers are intercalated via coordination with oxygen atom in silica layers of clay minerals. The gallery cations remain, instead of being replaced. Another mechanism of this method includes ion-dipole interactions between organic molecules and gallery cations.[188] Beall *et al.* reported that the mechanism of self-assembly between polar molecules and cations on the montmorillonite. Not only the polarity of organic molecules, but also the alkyl chain length appeared to be responsible for the interactions. The absence of solvents in the solid-state system makes it more suitable for industrial applications, and eco-friendly as well.[187]

2.6.2 Preparation of polymer-clay nanocomposites

The key for successful preparation of PCNCs is to achieve well-dispersed clay nano-platelets within polymer matrices. A number of synthetic techniques have been identified in the literatures. The three most common methods are; (1) *in situ* polymerisation, (2) solution method, and (3) melt mixing.[172–174] Table 2.5 represents a summary of the fabrication techniques of PCNCs.

The first mentioned method, *in situ* polymerisation, relies on the interaction between polymer monomers and clays. The monomer is directly used as a solubilizing agent for swelling the clays. The monomer is then crosslinked and combined with the clays, allowing the formation of polymer chains between the intercalated clay sheets. The primary drawback of this method is the requirement of suitable monomer/clay pairs.[174]

The solution method is based on a solvent system that can both solubilize the polymer and swell the clay. The clay can be easily dispersed in an adequate solvent owing to its weak forces which stack the layers.[172,190] The polymer then replaces the solvent within the gallery of clays, and the nanocomposite is obtained after the solvent evaporation or precipitation. The solvent used in this regime includes water, acetone, chloroform, or toluene.[172] The choice of solvent is a critical factor here since the intercalation of polymer into clay galleries is dependent on the properties of solvent, such as the polarity.[173] There are several disadvantages in this method. For instance, the removal of solvent can be problematic. The high cost and adverse environmental impacts from the use of solvent also lay a burden on this method.[172]

Table 2.5 Summary of the fabrication techniques of PCNCs.[172–174]

Methods	**Advantages**	**Disadvantages**
In situ polymerisation	Thermosetting nanocomposites are possible	Requirement of monomer/clay pairs
Solution method	Widely available	Requirement of adequate solvent Removal of solvent is necessary
Melt mixing	Simple and economical Use of conventional mixing equipment is possible	Limited clay concentration

The last method, melt mixing, does not require a compatible solvent or suitable monomer. In this method, the polymer is heated and/or sheared above the softening point (T_g) and directly mixed with clays. During the heating and/or shearing, molten polymer chains can migrate into clay galleries to form either intercalated or exfoliated penetrations. This method is more suitable for mass production than the other methods, since it is simple, economical, and environmentally friendly. Furthermore, due to its simplicity in processing, the use of conventional mixing equipment such as twin-roll mills, extruders, and blenders is possible.[173] However, melt mixing method appeared to be successful in only limited cases, since the concentrations of clays over 4 wt.% have not been possible.[174]

There are also several other methods to fabricate PCNCs, such as co-vulcanization, solid-state intercalation, sol-gel, emulsion and supercritical CO_2 fluid methods.[173]

2.6.3 Structure and characterisation of polymer-clay nanocomposites

When clay and polymer are mixed to form a composite, total three different types of structures can be made in terms of the degree of clay dispersion; (1) conventional, (2) intercalated, and (3) exfoliated composite structures (Figure 2.12).[172] In a conventional (also called phase-separated) composite, the clay remains as their original tactoid forms with no intercalation (penetration).[190] In fact, a conventional composite is a microcomposite (the particle size of original clay lies in micro-scale),[181] and only marginal enhancement of properties would be possible.[190] In intercalated composites, the clay is swelled, and one or few polymer chains are intercalated (inserted) into the gallery of clay. The gallery spacing (or basal plane spacing) is increased due to the polymer intercalation, but the clay layers remain stacked forming alternating polymeric and inorganic layers.[173] When the clay layers are completely separated and randomly dispersed in a polymer matrix, an exfoliated (or delaminated) structures are

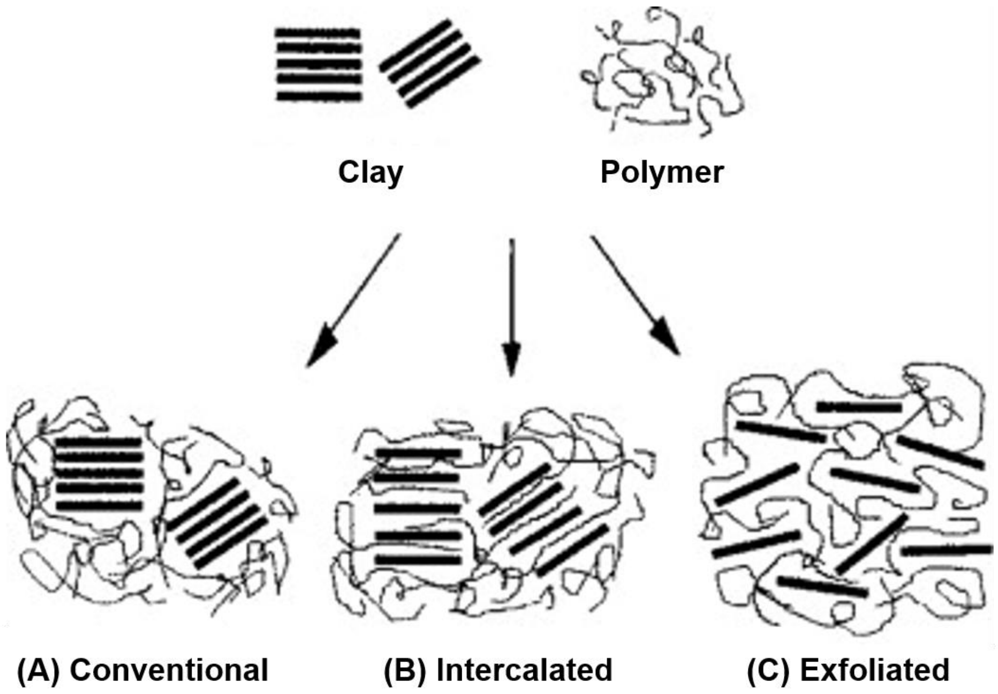

Figure 2.12 Scheme of the types of polymer-clay composites. (A) Conventional microcomposite. (B) Intercalated nanocomposite. (C) Exfoliated nanocomposite.[339]

obtained. Exfoliated nanocomposites are usually preferred because they provide the most dramatic improvements in properties with the maximised surface area.[174] Several other types defined in the literatures include; (1) intercalated-and-flocculated (or just flocculated), and (2) partially (or both) intercalated and exfoliated nanocomposites.[173,190] This is often termed "partial exfoliation". In this partially exfoliated clay structure, dispersed exfoliated clays and stacks of intercalated clays can be seen together. Other sub-types of clay structure in PCNCs include the orientation of clay, when clays exhibit parallel arrangements of layers, it can be called either ordered exfoliated or intercalated. Many PCNCs have complex morphology of dispersed clay by having more than one clay structures within the polymer matrix.[191]

The X-ray diffraction (XRD) assisted techniques, such as XRD, SAXS (small angle x-ray scattering and WAXS (wide angle x-ray scattering), as well as TEM (transmission electron microscopy) are widely used to characterise the dispersion state of clays in PCNCs.[173,174,192] The interlayer spacing (or gallery spacing, or basal layer spacing), d_{001}, correspond to the degree of clay intercalation. In conventional microcomposites, the clay does not swell, so the value of d_{001} remains unchanged (same with the original clay). In the intercalated structure, however, the swelling of clay by one or few polymer chains make d_{001} increase. In exfoliated structure, the *d*-spacing cannot be detected by XRD due to the fact that the clay layers are completely de-laminated and no more stacked layer structures exist.

TEM offers a qualitative knowledge of the composite structure. The individual clay layers can be seen as in the Figure 2.13. TEM, however, is time consuming, and requires an arduous sample preparation process.[173,174]

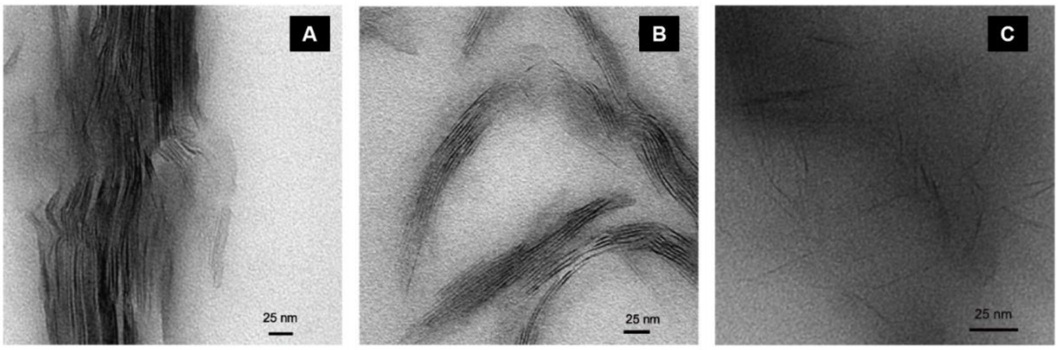

Figure 2.13 TEM micrographs indicating various possible dispersions of clay in the composites; (A) un-intercalated tactoids, (B) intercalated, and (C) exfoliated.[340]

Besides the characterisation methods above, chemical analysis such as FTIR, thermal analysis such as thermogravimetric analysis (TGA) or DSC also can be utilised to characterise the PCNCs. The vibration bands of clay crystal can be detected under FTIR. DSC works with the nucleation effect of clay, which changes the crystallisation of semi-crystalline polymers.[173,193]

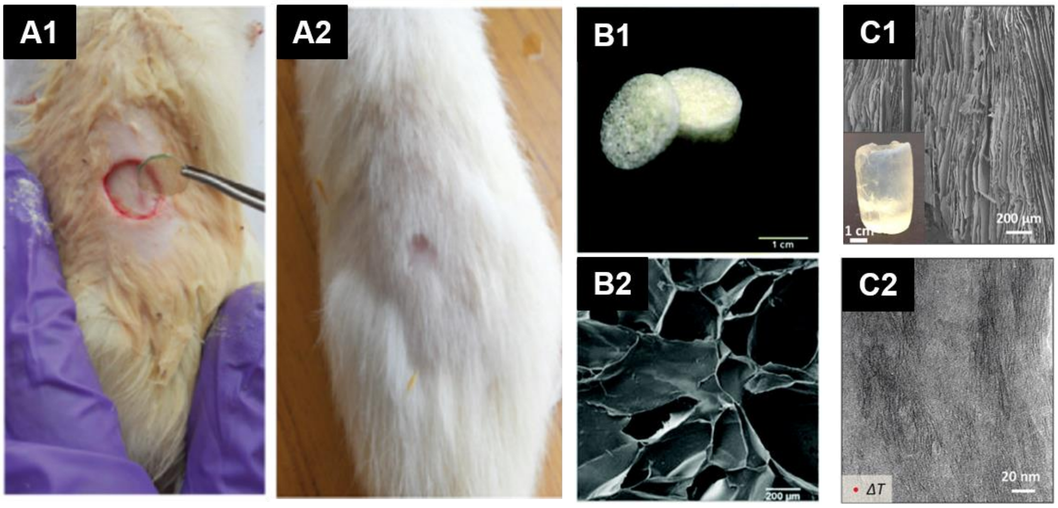

Figure 2.14 (A1 and A2) The epoxy-clay nanocomposite for skin tissue engineering; (A1) application of nanocomposite scaffold, and (A2) a complete wound-healing after 21 days. (B1 and B2) The porous chitosan-agarose-gelatin-halloysite nanocomposite scaffold; (B1) a photograph demonstrating the morphology of porous scaffold, and (B2) a SEM image showing the micro-pore structure. (C1 and C2) PNIPAAm-laponite hydrogel scaffold; (C1) a SEM image showing the aligned structure mimicking the biological tissues (the inlet image shows a macroscopic view of hydrogel), and (C2) a nacre-like clay structure indicated by TEM.[194–196]

2.6.4 Polymer-clay nanocomposites in soft tissue engineering

A number of PCNC scaffolds for soft tissue engineering has been reviewed in the literature (Figure 2.14). Barua *et al.* developed an infection-resistant epoxy-clay nanocomposite for skin tissue regeneration.[194] In their study, the clay acts not only as the mechanical modulator, but also as the substrate of silver nanoparticles, which have a strong infection-resistant property. The synthesis of PCNC was done by a solution method, where 5 wt% of the octadecylamine modified montmorillonite was swelled in THF with the hyper-branched epoxy resin as the polymeric phase. The tensile strength was increased from 54.8 to 60.3 MPa, and the scaffold showed a better wound healing property as well as less infection profile. Complete wound healing in 21 days from a circular wound (20 mm diameter) was confirmed *in vivo*.

Naumenko *et al.* designed a porous chitosan-agarose-gelatin-halloysite nanocomposite fabricated by the solvent method and a subsequent freeze-drying.[195] The enhancement of mechanical strength and higher water uptake was achieved by doping 3 – 6 wt.% of clay. Furthermore, a more homogeneous pore size was obtained with halloysite clay. Human soft tissue cells such as A549 (lung), Hep3B (liver), and HepG2 (liver) cells were cultivated on this scaffold, and no changes in cell viability observed. The biocompatibility as well as biodegradability of the halloysite scaffold was demonstrated *in vivo*.

Natural soft tissues such as tendon and muscle, have well defined hierarchical structures. Inspired by this, Bai et al. synthesized clay nanocomposite hydrogels with aligned macroporous stuctrures.[196] The polymer phase was PNIPAAm (poly(*N*-isopropylacrylamide), and laponite clay was used as the filler. A nacre-like structure of clay was confirmed by TEM analysis. By gradually increasing the clay content, the enhancement in tensile strength (from 48 to 103 kPa) and modulus (from 21 to 108 kPa) was achieved.

2.6.5 PGS-clay nanocomposites

At present, there is a limited set of studies on PGS-clay nanocomposites for soft tissue engineering applications, illustrating the potential of future studies. This is possibly due to the hydrophobic nature of PGS as discussed previously, which hinders a good interaction and dispersion of natural clays which are hydrophilic in general. This can be tackled by using organophilic clays with surface modifiers as we will discuss in Chapter 5. Relatively short history of PGS compared to other polymers can also be another reason why PGS-based PCNCs have not fully explored in the literature.

Chen *et al.* incorporated halloysite nanotubes in PGS polymer matrix to synthesize the PGS-halloysite nanocomposites.[60] Halloysites (3 – 5 wt.%) were mixed in the pre-melted PGS pre-polymer (melt mixing), followed by casting and curing of the polymer. In this study, the nanocomposite showed the increased strain at break values and slowed biodegradability kinetics, which would be beneficial for long-term applications (Figure 2.15).

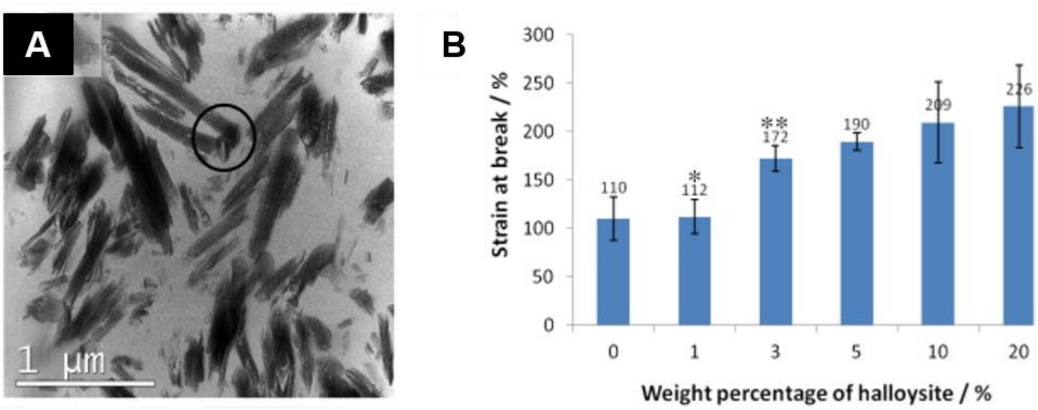

Figure 2.15 (A) The TEM image showing the halloysite nanoclays dispersed in the PGS matrix. (B) The effect of addition of halloysites in PGS on the strain at break values.[60]

2.7 Summary of the literature review

Soft tissue engineering aims to repair or reconstruct soft tissues from the loss or damage after injury, disease, tumour, as well as for aesthetic appearance. Currently, the main strategy in soft tissue engineering is to use a tissue scaffold to host cells and promote tissue regeneration.

Several fundamental requirements in designing a tissue scaffold have been identified such as biocompatibility, biodegradability, biomimetic mechanical properties, and bioactive surfaces. The importance and methods of angiogenesis in tissue engineering was also discussed. A number of different scaffold architectures have been reviewed such as fibrous scaffolds, 3D porous scaffolds, hydrogels, microspheres, and composites.

Among a vast variety of natural and synthetic elastomers which is applicable for soft tissue engineering, PGS has a great potential in soft tissue applications with its biomimetic mechanical behaviours, biocompatibility, and biodegradability, as well as the well-established methods to alter the properties. However, existing literature illustrates the possibilities to modify this polymer further to achieve the optimized tissue scaffold materials for soft tissue applications, through incorporation of bioactive molecules and nanotechnology, which will be discussed in the following chapters.

Chapter 3 Elastomeric and pH-responsive hydrogels based on direct crosslinking of the poly(glycerol sebacate) pre-polymer and gelatin

3.1 Introduction

Hydrogels are of great interest in biotechnology, with their biomimetic macromolecular network structure and soft mechanical properties, as well as the high water content that allows the diffusion of the desired chemical species.[2–6] A critical aspect in designing hydrogels with advanced functionalities is their interaction with biology. The complex physicochemical dynamics *in vivo* drive the need for the development of hydrogels which are capable of responding to biological conditions and stimuli. For instance, hydrogels with elastomeric mechanical properties are great assets for soft tissue engineering applications, with their ability to provide biomimetic and synchronous deformations responding to the mechanical dynamics in native tissues.[1] Another example is the stimuli-responsive properties. Various *in vivo* stimuli such as water, temperature, mechanical stress, pH, ionic strength, and specific chemical species have been extensively investigated in developing hydrogels with their ability to alter the diffusion characteristics for controlled drug delivery.[3,44,197–200] Multifunctional hydrogels which are capable of responding to the various biological dynamics, therefore, are an important class of biomaterials for different biomedical applications such as soft tissue engineering and drug delivery.

The excellent elastomeric mechanical behaviour resulting from the macromolecular network structure, as well as good biocompatibility with minimal inflammatory responses of PGS have attracted much attention in soft tissue engineering such as adipose,[19] cardiac,[12,23,155] cartilage,[18,164] nerve,[14] retinal,[15,159] and vascular applications.[16,55,161] PGS also shows surface-erodible biodegradation with a linear weight loss and good strength retention, which is beneficial for long-term implantations in the body and controlled release of functional molecules incorporated within the polymer matrix.[11,201] While its mechanical properties are tunable by altering the synthesis mechanism,[20] molar ratio of monomers,[21,22] and synthesis conditions such as the reaction time and temperature,[21–25] PGS has poor hydration properties. In spite of the hydroxyl and carboxyl pendant groups present on its polymer backbone, it does not swell in water to form swollen hydrogels owing to the aliphatic carbon chains from the sebacic acid monomer. The hydrophobicity of PGS was shown by a low equilibrium water uptake capacity of 2.1 ± 0.9 wt.%,[118] and high water contact angles ranging between 77.5–85.7°.[59,118,156] As hydration property is an important factor to achieve the optimal biocompatibility, biodegradability, mechanical behaviour, and water-based diffusion characteristics *in vivo*,[65,118] hydrophilic segments such as citric acid and PEG were incorporated to tackle the hydrophobicity in PGS and develop hydrophilic, water-swellable PGS-based copolymers.[44,118,119,133,202] Nevertheless, most of these studies focused on the modification of hydration properties of PGS. Only two reported thermo-responsive PGS-based hydrogels owing to the use of PEG,[44,119] and other types of biological stimuli have not been explored. Moreover, the resulting copolymers did not show full biodegradation, which may limit their wider application in biomedical fields.

Gelatin, a natural hydrophilic polymer derived by collagen hydrolysis, is biocompatible, non-immunogenic, non-antigenic, and biodegradable,[203] and its use in medical applications has been approved by U.S. Food and Drug Administration.[103] Furthermore, gelatin contains arginine-glycine-aspartic acid peptide sequence inherited from its parental collagen that promotes cell adhesion and migration.[204,205] Gelatin hydrogels have been applied in many biomedical applications such as cell signalling,[206] gene and drug delivery,[103] tissue engineering,[207] and bio-sensing.[208] Another virtue of using gelatin to design biomaterials comes from its abundant chemical functional moieties such as amine, carboxyl, and hydroxyl groups, which can incorporate further chemical modifications, induce hydrophilicity, as well as accept or donate protons in response to the surrounding pH changes.[203,209]

Herein, we design a novel elastomeric, pH-responsive, and fully biodegradable as well as biocompatible hydrogel system based on the copolymers of PGS and gelatin. We hypothesised that this new hydrogel system would have synergistic benefits from (1) molecular network structure and elastomeric properties of PGS, (2) hydrophilic and pH-responsive properties of gelatin, and (3) a tunable and full biodegradability as well as good biocompatibility from both biopolymers. To avoid the biocompatibility issues with chemical crosslinking agents, the synthesis was performed in a toxin-free manner without any additional crosslinking agents, but by utilising the chemical functional groups from both biopolymers to form ester and amide linkages which directly crosslinked PGS pre-polymer and gelatin. The chemical structure and mechanical behaviour, as well as surface and bulk hydration properties of these new copolymers were investigated using infrared spectroscopy and tensile tests, as well as water contact angle and swelling ratio measurements. The biodegradation kinetics was studied *in vitro* with lipase and collagenase enzymes. Cytotoxicity was examined by the cell metabolic assay *in vitro* with L929 mouse fibroblast cells. The potential biomedical applications in controlled drug delivery and soft tissue engineering were demonstrated by pH-responsive drug release tests and *proof-of-concept* fabrication of a 3D, elastomeric and interconnected porous scaffold.

3.2 Materials and Methods

3.2.1 Materials

Gelatin (Type A, from porcine skin, 300 bloom), sebacic acid, glycerol, ethanol, glycine, hydrochloric acid, phosphate buffered saline (PBS) tablets, Dulbecco's Modified Eagle's Medium (DMEM) with high glucose, resazurin sodium salt, lipase from porcine pancreas (54 U mg^{-1}) were purchased from Sigma-Aldrich. Collagenase (290 U mg^{-1}) was from Thermo Fisher Scientific. Doxycycline hyclate (DOX) and sodium hydroxide was obtained from Alfa Aesar. Gelatin was dehydrated in a vacuum oven at 25 °C for 24 h before use. Water used in this study was prepared by double distillation.

3.2.2 Preparation of PGS-gelatin (PGSG) copolymers

The copolymerisation of the PGS pre-polymer and gelatin was performed in the following procedure: 1) polycondensation of sebacic acid and glycerol to yield the PGS pre-polymer; 2) preparation of the PGS pre-polymer/gelatin solutions in different weight ratios; 3) synthesis of PGSG pre-polymers; and 4) casting and crosslinking of PGSG pre-polymers into fully cured copolymer films. First, an equimolar mixture of glycerol and sebacic acid was loaded in a three-necked flask, equipped with an oil bath, magnetic stirrer, Dean-stark apparatus, and nitrogen gas line with a bubbler. The monomers were mixed for 30 min, followed by polycondensation at 140 °C for 3 h to produce PGS pre-polymer. In the second step, a specific amount of gelatin (0–20 wt.%) was weighed, and solubilised into the molten PGS pre-polymer by mechanical stirring until transparent and homogeneous solutions were obtained. The yellow to orange coloured low-viscosity PGS pre-polymer/gelatin solutions were then reacted for 24 h at 120 °C to yield viscous resins. The resulting PGSG pre-polymer resins were evenly distributed onto PTFE substrates. After the degassing process in a vacuum oven at 80 °C for 1 h to remove the air bubbles, crosslinking was continued further for 24 h at 120 °C to achieve fully cured copolymer films. The synthetic procedure of PGSG copolymers is shown in Figure 3.1. Finally, all the samples were washed four times using 0%, 30%, 70%, and 100% water-ethanol solutions for 12 h each at 40 °C. The un-crosslinked proportion of cured copolymers was determined by the weight difference on a 4-decimal scale (Sartorius M-power) before and after the washing steps. The solubility of PGSG pre-polymer and cured copolymer samples was evaluated by immersing the samples in various solvents, namely, 1,4-dioxane, acetone, chloroform, dimethylformamide, ethanol, tetrahydrofuran, and water, for 48 h at 37 °C. The nomenclature of the prepared PGSG copolymers is presented as PGSGX, where “X” stands for the weight percentage of gelatin in PGSG copolymers: PGSG0, PGSG5, PGSG10, PGSG15, and PGSG20.

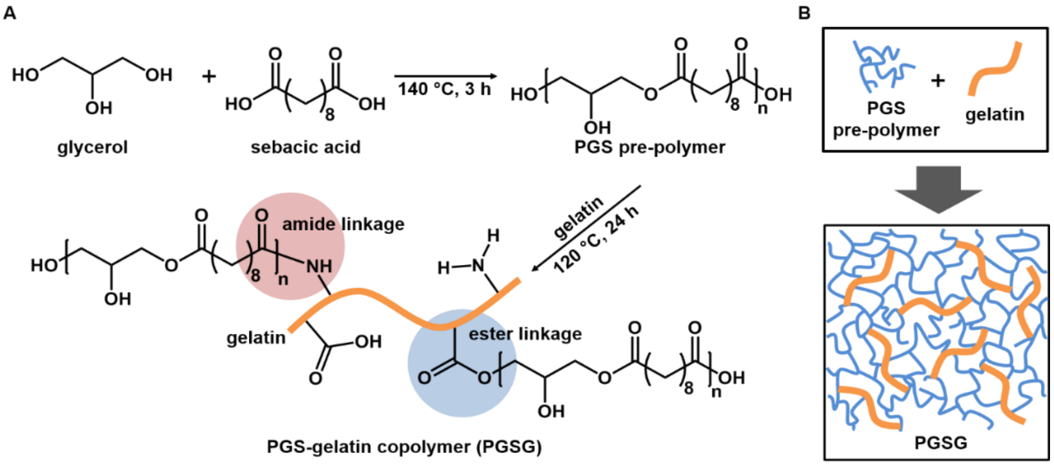

Figure 3.1 (A) Synthetic scheme of PGSG copolymers. (B) Sketch showing the formation of the macromolecular network consisted of directly crosslinked PGS pre-polymer and gelatin.

3.2.3 *Proof-of-concept* fabrication of PGSG20 tissue scaffolds

The fabrication was conducted by a combined technique of salt-leaching and freeze-drying. Salt from a local store was sieved doubly to obtain sizes of 300 μm and mixed with the molten PGSG20 pre-polymer resin at a weight ratio of 3:1 at 65 °C by mechanical stirring (100 rpm) for 15 min. The mixture was then cast into a PTFE petri dish and placed in a vacuum oven at 120 °C for 24 h to cure the pre-polymer. Next, the cured sample was immersed in 0%, 30%, 70%, and 100% water-ethanol solutions at 40 °C for 3 days, during which the salt particles were washed-out by diffusion to create macro-pores in the scaffold whilst the scaffold became fully swollen. Finally, this swollen scaffold was placed in a freeze dryer (FreeZone Triad Freeze Dry System, Labconco) to remove water and create additional micro-pores in order to improve the pore interconnectivity.[210] The freeze-drying cycle consisted of a pre-freezing stage at -40 °C overnight followed by drying at -10 °C for 24 h.

The mechanical property of PGSG20 scaffolds was determined by a compressive mechanical testing with a Hounsfield H100KS (Tinius Olsen). The disk-shaped specimens were prepared using a mould stencil (n = 6; diameter: 10 mm). A 10 N load cell was used at a compressive rate of 50 mm min^{-1}. SEM was also conducted to investigate the microscopic pore structures (Philips XL 30S FEG; spot size = 3, accelerating voltage = 10 kV). The cross-sectional area was examined after a gold-coating.

3.2.4 Characterisation of PGSGs

The number average molecular weight ($\overline{M}_n$), weight average molecular weight ($\overline{M}_w$) and polydispersity index (PDI) of PGS pre-polymer before copolymerization with gelatin were measured by gel permeation chromatography (GPC, Agilent 1260 GPC System), with tetrahydrofuran as the mobile phase and polystyrene standards for calibration.

Attenuated total reflectance Fourier transform infrared (FTIR) spectroscopy was conducted on a Perkin Elmer Spectrum One NTS analyser (500–4000 cm^{-1}, Resolution: 2 cm^{-1}, number of scans: 16). A pressure of 70 N was applied using a built-in screw to increase the extent of sample contact with the diamond ATR crystal.

The microscopic surface analysis was carried out by scanning electron microscopy (SEM) (Philips XL 30S FEG; spot size = 3, accelerating voltage = 10 kV). The samples were cut into small pieces and attached onto an aluminium stub by applying a Pelco® conductive silver paste (Ted Pella, USA). A gold-coating was applied using a high resolution polaron sputter coater (Emscope SC500A) to reduce the charge-up effects.

Mechanical property of dry and hydrated PGSG samples was determined by tensile tests using a Hounsfield H100KS (Tinius Olsen), according to the ISO 527. The specimens were punched-out into dog-bone shapes (n = 6, thickness: 0.32–0.46 mm) using a mould stencil (Ray-ran Test Equipment). A 10 N load cell was used at the strain rate of 50 mm min^{-1}. For the testing of hydrogels, the specimens were swollen in PBS solution at 37 °C for 72 h, and tested under the same tensile condition as above. The test results are reported in a manner of mean ± standard deviation.

The crosslink densities of cured PGSGs were determined by eqn (3.1), based on the theory of rubber elasticity.

$$n = \frac{E}{3RT} \tag{3.1}$$

where n is the density of active network chains, E is the Young's modulus, R is the universal gas constant, and T is the temperature during the tensile test.[26]

The surface and bulk hydration properties of PGSG specimens were determined by water contact angle and swelling studies. The water contact angle on the PGSG samples was measured using a drop shape analyser (DSA-100, Krüss, Germany). A droplet of water (10 µL) was dosed onto the sample surface using a 22-gauge, blunt-end syringe needle. The angle measurement was done by capturing high-resolution images after 10 seconds. The bulk hydration properties were analysed by swelling behaviour of PGSG specimens in PBS. Dry PGSG specimens (n = 5; diameter: 5.3 mm; thickness: 0.41 ± 0.09 mm) with known initial weight (W_{dry}) were prepared by a hydraulic press and disc-shaped mould stencil. The specimens were fully immersed in the medium and incubated at a physiological temperature of 37 °C. At specific time intervals, the swollen specimens were collected, blotted with a filter paper to remove the excessive surface water, and weighed (W_{wet}). The swelling ratio was determined by eqn (3.2).

$$\text{Swelling ratio (\%)} = \frac{W_{wet} - W_{dry}}{W_{dry}} \times 100 \qquad (3.2)$$

3.2.5 pH-responsive swelling and drug release tests

The pH-responsive swelling ratio of PGSGs was measured using the following two buffer solutions: citrate buffer (pH 5.0), and glycine-NaOH buffer (pH 9.1), at 37 °C, and calculated using eqn (3.2). The pH-dependent drug release profiles of the PGSG20 were evaluated. DOX was selected as a model drug, as it is one of the most commonly prescribed antibiotics for soft tissue infections.[211] The drug loaded PGSG20 specimens (n = 5; diameter: 5.3 mm; thickness 0.40 ± 0.11 mm) were prepared by soaking in 10 mL of DOX water solution (pH 6.2, 10 mg mL^{-1}) for 72 h at 4 °C to minimise drug denaturation, followed by washing twice with fresh water to remove the excessive surface-adsorbed drug and drying in a vacuum oven at 37 °C for

48 h. The specimens were then immersed in 10 mL of citrate buffer, PBS, and glycine-NaOH buffer solutions for the release tests. The buffer solutions were used here again not only to modulate the pH values of drug releasing media, but also to minimise the non-specific Coulomb interactions between DOX and PGSG.[212] At scheduled time intervals, 1 mL of the medium was collected and replaced by a fresh medium. The cumulative drug release profiles were obtained by measuring the absorbance of collected media at 345 nm (λ_{max}) and pre-prepared calibration curve of known drug concentrations using an ultraviolet-visible spectrophotometer (UV-vis, Perkin Elmer Lambda 900, US).[213] The drug loading capacity of PGSG20 hydrogels was measured as 0.41 ± 0.05 mg per specimen (*i.e.*, 3.8 ± 0.6 wt.% of the dried specimen) by the same spectroscopic analysis as above using the drug loading solutions before and after the loading procedure.

3.2.6 Biodegradability and cytotoxicity tests *in vitro*

The degradation behaviour of the PGSG hydrogels was investigated *in vitro*. The specimens (n = 5; diameter: 5.3 mm; thickness: 0.43 ± 0.15 mm) were sterilised in 70% ethanol and dried in a vacuum condition until constant weights were observed. The incubation was carried out in the following degradation media: 1) PBS without enzymes, 2) PBS with lipase (110 U L^{-1}), and 3) PBS with collagenase (62 U L^{-1}). The concentration of enzymes in this test was decided based on the serum activity of enzymes in healthy adults found in previous literature.[214,215] The media were kept fresh by replacement daily to ensure the full enzyme activity. The incubation was performed at 37 °C in a shaker incubator at 100 rpm (Stuart SI500). After 3, 7, 14, 21, and 28 days, the weight loss by degradation was determined after washing the specimens with a copious amount of water to remove surface bound enzymes and drying in vacuum. The percentage weight loss was calculated by the following eqn (3.3), where W_{ini} and W_{day} are the initial weight (215 ± 17 mg) before degradation and the weight measured at the specific incubation day, respectively.

$$Weight\ loss\ (\%) = \frac{W_{ini} - W_{day}}{W_{ini}} \times 100 \qquad (3.3)$$

Cytotoxicity of PGSGs was analysed by cell metabolic assay using resazurin *in vitro*. Prior to the cell seeding, all the specimens were sterilised by 70% ethanol, washed thrice with plenty of water and soaked in DMEM overnight in an incubator (37 °C, 5% CO_2). PGSG specimens were then placed in a 12-well plate and fixed by metal rings for cell seeding. After cell trypsinisation with trypsin-ethylenediaminetetraacetic acid, trypsin activity was neutralised with 5 mL of warm medium, and the cells were collected by centrifugation (1000 rpm, 5 min). The optimum cell density (3.0×10^4 cells per specimen) was obtained by dilution with DMEM and seeded onto PGSG specimens. Cell-free and cell-only tests were also performed for negative/positive control, and used to normalise the data. After 3 days of incubation, the DMEM was removed from the well plate and the cell-seeded specimens were washed with PBS and placed in a new well plate. One mL of resazurin solutions (0.1 mM in PBS) was added to each sample and incubated for 2 h. The absorbance at 570 nm was recorded using a colorimetric plate reader (Bio-TEK). This assay was repeated on day 6, 9, 12, and 15. Microscopic images were taken by an optical microscope (Motic, AE2000 Inverted Microscope) to observe cell morphology on the specimen surfaces. The experiments were performed triplicate.

3.2.7 Statistics

All measurements were reported as mean ± standard deviation with a confidence level of 95% unless otherwise stated. Two- way analysis of variance (ANOVA) was used to determine the differences in the in vitro cell metabolic assay results in respect to the test time and material. A p value <0.05 was considered to be statistically significant.

3.3 Results and discussion

3.3.1 Synthesis and characterisation of PGSG hydrogels

PGSG copolymers with varying ratio between PGS pre-polymer and gelatin were synthesised by a thermal crosslinking approach. The first step involved polycondensation of glycerol and sebacic acid to produce PGS pre-polymer. The synthesis of PGS pre-polymer was confirmed by FTIR with the distinct peaks at 1176 cm^{-1} and 1733 cm^{-1}, which is attributed to the formation of ester linkages between hydroxyl groups from glycerol and carboxyl groups from sebacic acid (Figure 3.2).[26,128,137] However, the absorption bands of hydroxyl and carboxyl groups are still shown in the spectrum of PGS pre-polymer. This indicates that the PGS pre-polymer is not fully cured, therefore further chemical crosslinking is possible with the functional groups. GPC analysis affirmed the synthesis of PGS pre-polymer with the $\overline{M}_n$, $\overline{M}_w$, and PDI values of 455, 1875, and 4.12, respectively. It should be noted that the PGS pre-polymer in this study was synthesised by a relatively short reaction time to achieve low molecular weight, which facilitates further copolymerisation with gelatin. In the second step, gelatin was added to and reacted with PGS pre-polymer to yield PGSG pre-polymers. The PGSG pre-polymers were then further crosslinked thermally to produce fully cured PGSG copolymer films. The prepared PGSG copolymers are characterised by soft mechanical properties and the gloss surfaces with the distinct yellow to orange colours depending on the concentration of gelatin as seen in Figure 3.3.

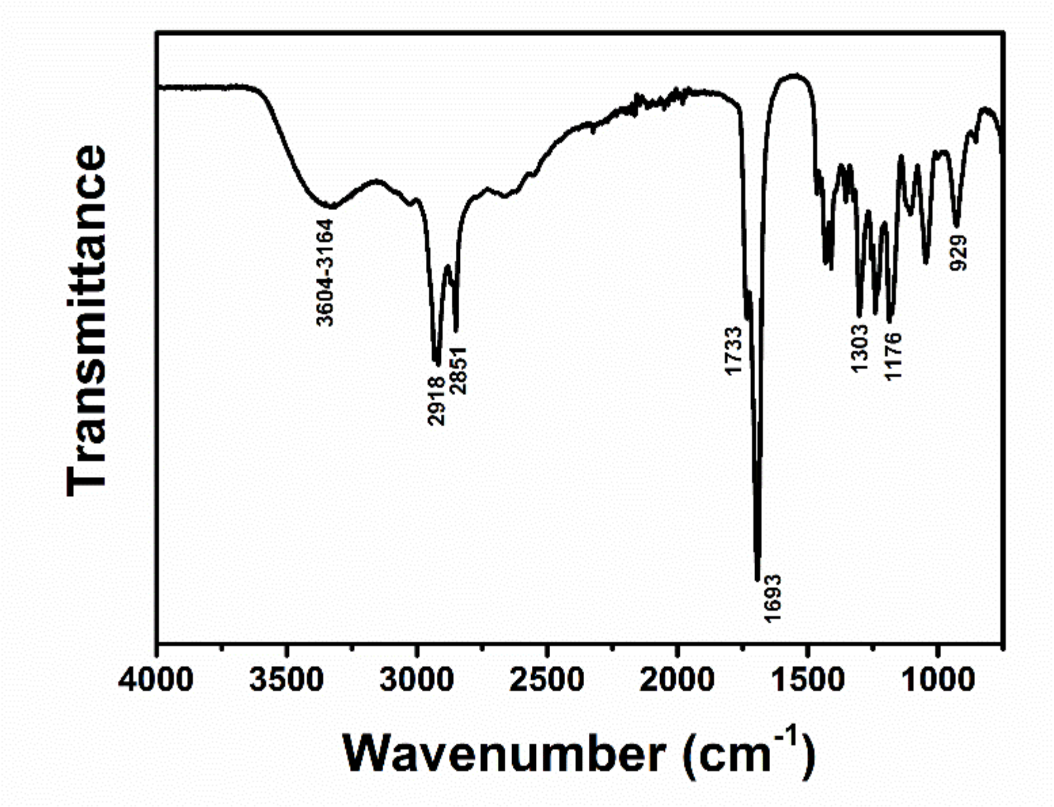

Figure 3.2 FTIR spectrum of poly(glycerol sebacate) (PGS) pre-polymer before copolymerisation with gelatin. The broad band between 3604–3164 cm^{-1} is attributed to the hydroxyl groups (O–H), and the peaks at 2918 and 2851 cm^{-1} are for the stretching vibration of alkane groups (–CH_2).[26,137] Absorption of alkane groups is presented between 1354–1465 cm^{-1}.[136] The intense peak at 1733 cm^{-1} (C=O) and 1176 cm^{-1} (C–O) are the signature band of ester linkages.[137] The absorption peaks at 1693 cm^{-1} (dimer C=O), 1303 cm^{-1} (C–O stretching), and 929 cm^{-1} (O–H bending) are attributed to the carboxylic acid groups.[137]

The PGSG pre-polymers before curing were found to be soluble in 70% ethanol-water solution. Moreover, the pre-polymers were re-meltable and deformable into a desired physical morphology, enabling fabrication of complex architectures such as an interconnected porous scaffold for tissue engineering applications (discussed below). The un-crosslinked proportion

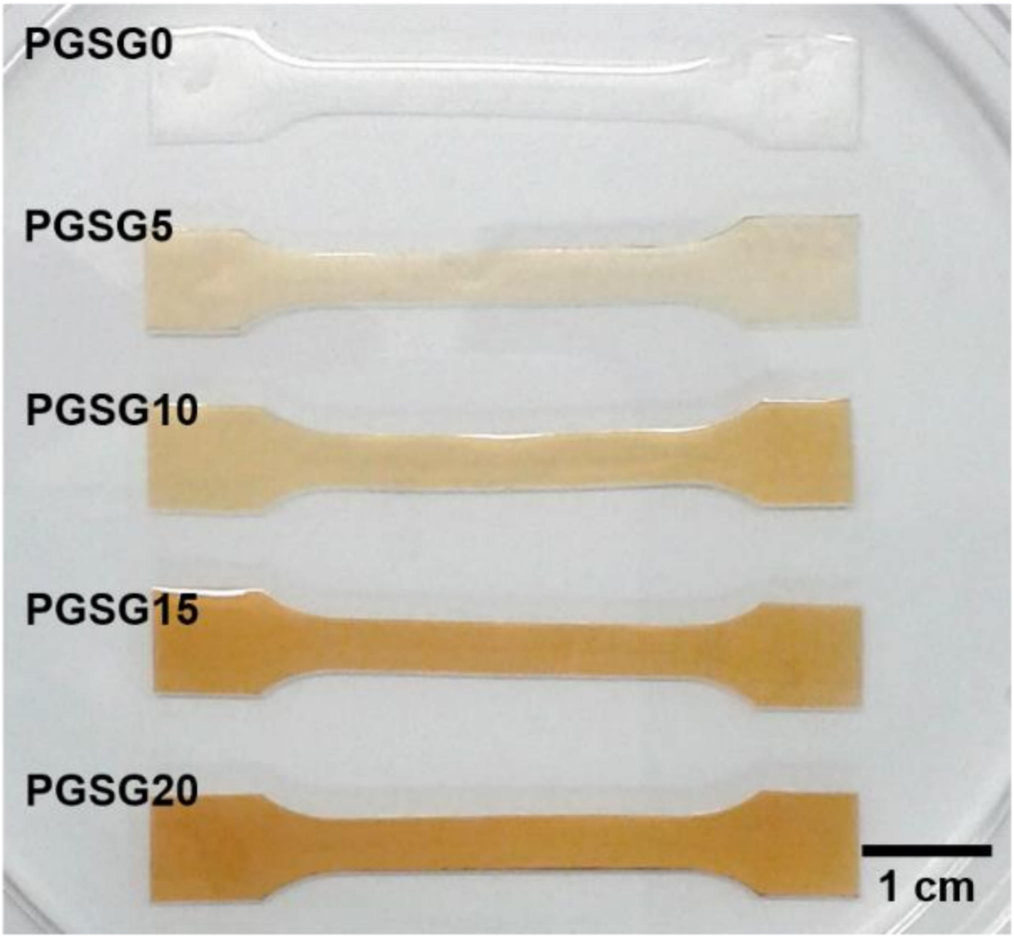

Figure 3.3 A photograph showing fully-cured PGSG copolymer specimens with various gelatin contents. The colour change from pale yellow to orange was observed due to the addition of gelatin in copolymer synthesis.

(sol) of cured PGSG copolymers was determined by the weight loss after extraction with a series of warm water-ethanol solutions and showed a minimal increase from 16.4 to 19.4% with the addition of gelatin (Figure 3.4).

All the cured and purified PGSGs were not dissolved, but rather swelled in 1,4-dioxane, a cetone, chloroform, dimethylformamide, ethanol, tetrahydrofuran, and water. The maximum uptake of ethanol of PGSG specimens after 48 h of immersion at 37 °C was measured as 58.0–69.5% (Figure 3.4), inversely proportional to the amount of gelatin within copolymers. This amphiphilic swelling characteristics in PGSG copolymers, driven by

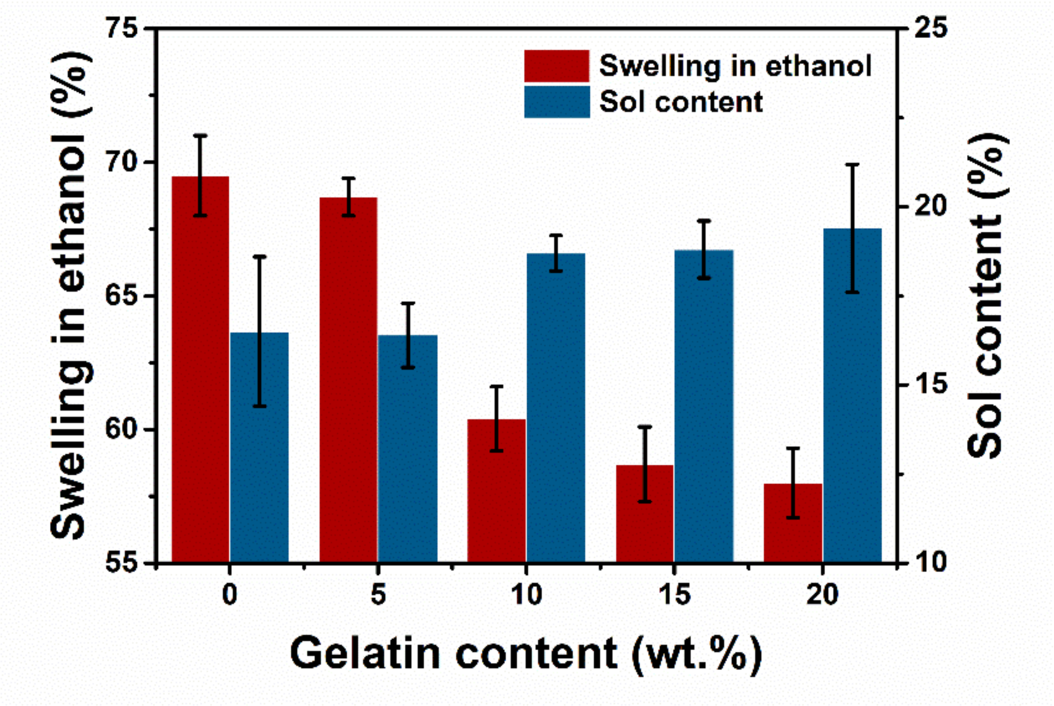

Figure 3.4 The measured maximum ethanol uptake and weight loss after the sol extraction of poly(glycerol sebacate) and gelatin copolymer (PGSG) specimens.

copolymers of hydrophobic PGS and hydrophilic gelatin, suggests that post-functionalisation with desired chemical species is possible, such as the loading of a drug into the hydrogel by diffusion (discussed below).

As we previously discussed, the PGS pre-polymer consisted of a network macromolecular structure with the hydroxyl and carboxyl groups from its monomers, glycerol and sebacic acid (Figure 3.2). Gelatin is a protein, therefore it contains amide backbone structure with amine and carboxyl groups from its amino acid sequence (Figure 3.5). During the thermal curing process of PGS pre-polymer and gelatin by polycondensation reactions, the hydroxyl and carboxyl groups would yield ester bonds, whereas amide bonds would be formed between amine and carboxyl groups (Figure 3.1A).[216] The proposed chemical structure of PGSG copolymers was affirmed under FTIR by comparing PGSG pre-polymers and cured copolymers, as shown in Figure 3.6–8.

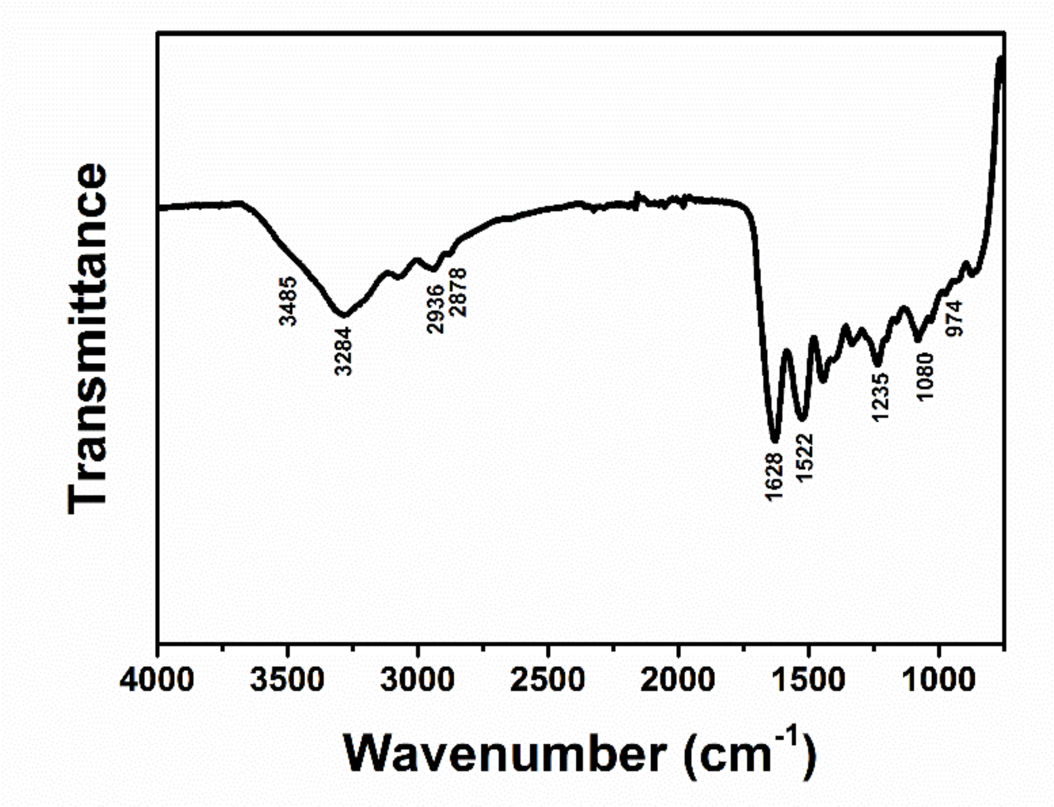

Figure 3.5 FTIR spectrum of gelatin revealing a set of chemical functional groups such as amine, amide, hydroxyl, and carboxyl groups, derived from its abundant amino acid composition.[203,209,341] The broad band at 3485 cm^{-1} and 3284 cm^{-1} are attributed to the hydroxyl groups (O–H) and free amine groups (N–H stretching).[342] The amide peaks in gelatin backbones are identified as follows: amide I peak (C=O stretching) at 1628 cm^{-1}, amide II peak at 1522 cm^{-1} (N-H bending and C-H stretching), and amide III peak (C-N stretching and N-H in phase bending) at 1235 cm^{-1}.[217] The peaks at 2936 cm^{-1} and 2878 cm^{-1} are due to alkane groups (C–H stretching).[228] The peaks at 1080 cm^{-1} (C–O) and 974 cm^{-1} (O–H) are attributed to the carboxylic acid groups in gelatin.[209]

The ester bonds in PGSG pre-polymers were confirmed by intense peaks at 1733 cm^{-1} (C=O) as well as 1159 cm^{-1} and 1095 cm^{-1} (C-O). After the thermal curing of PGSG pre-polymers into

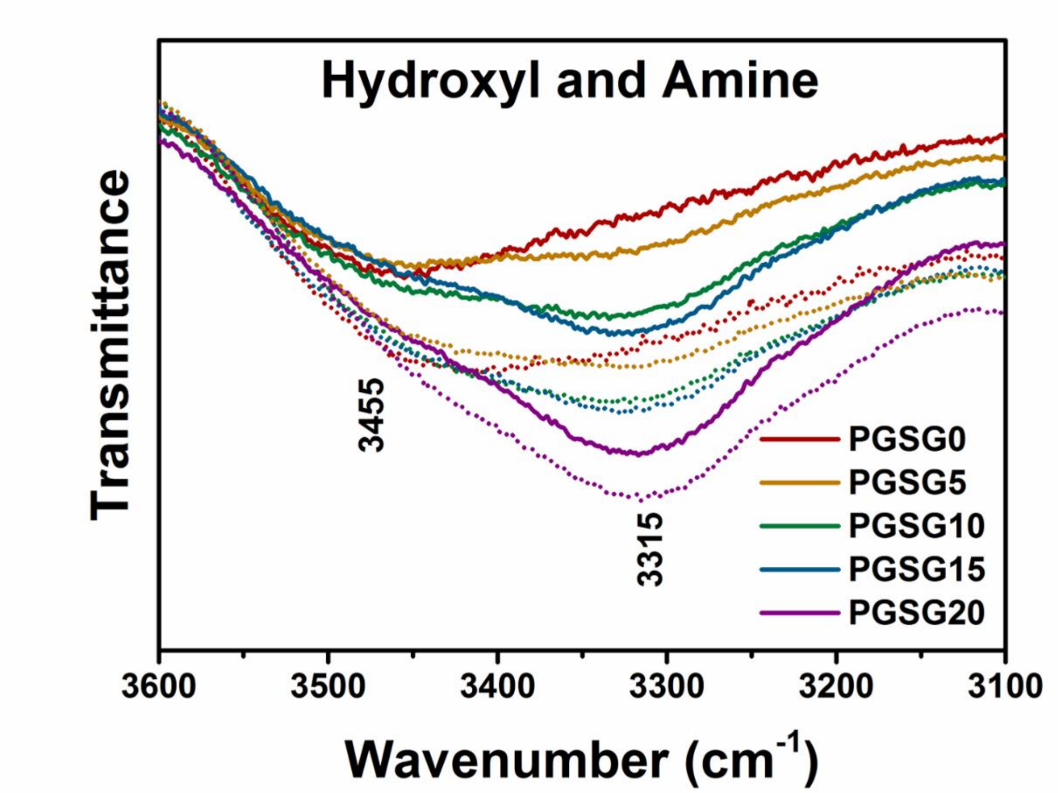

Figure 3.6 ATR-FTIR spectra of PGSG copolymers, highlighting the hydroxyl and amine groups, before and after crosslinking. The dotted lines and solid lines refer to the PGSG pre-polymers and cured copolymers, respectively.

copolymers, the intensity of the ester bond peaks was further enhanced, indicating the newly formed ester bonds between the polymer chains.[26,137] On the other hand, the intensities of hydroxyl peak at 3455 cm^{-1} (O-H) and carboxyl peaks at 1291 cm^{-1}, 1221 cm^{-1} and 1048 cm^{-1} (C-O) were reduced due to the curing process.[26,137] Regarding the amide bond, the peak intensities of amide I at 1644 cm^{-1} (C=O) and amide II at 1537 cm^{-1} (N-H and C-H) in PGSG pre-polymers were also further enhanced in the cured copolymers,[217] whereas the peak intensities of amine at 3315 cm^{-1} (N-H) and carboxyl (also partially due to the ester bonds) were reduced by forming the new amide bonds.

When the cured PGSG copolymers were compared between each other, it was found that

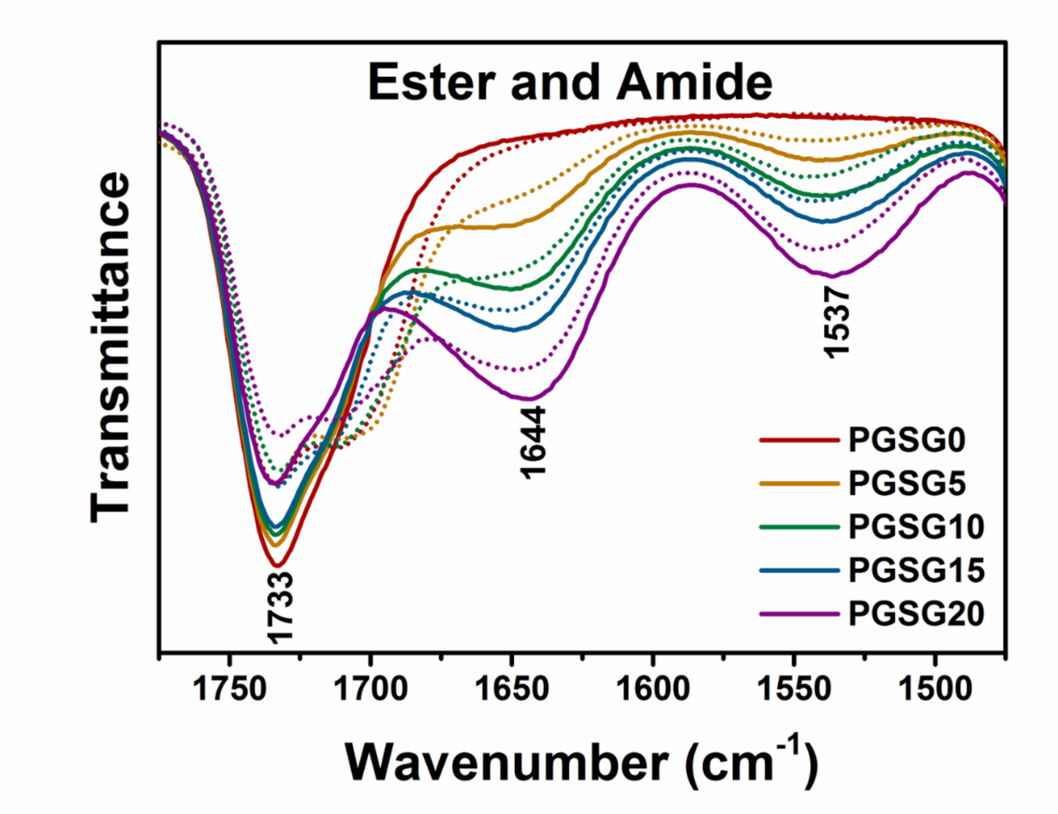

Figure 3.7 ATR-FTIR spectra of PGSG copolymers, highlighting the ester and amide groups, before and after crosslinking. The dotted lines and solid lines refer to the PGSG pre-polymers and cured copolymers, respectively.

with an increasing gelatin content the amide peaks (at 1644 cm^{-1} and 1537 cm^{-1}) became stronger while the ester bond peaks (at 1733 cm^{-1}, 1159 cm^{-1}, and 1095 cm^{-1}) diminished gradually. These results are attributable to two factors: (1) gelatin has amide groups in its backbone, leading to an increase in the amide content in the copolymer with a higher gelatin content; and (2) the amine groups in gelatin react with hydroxyl groups competitively against carboxyl acid groups as previously described, resulting in more amide bonds and fewer ester bonds in the copolymer.

Hydration properties of cured PGSG copolymers were investigated in both surface and bulk characteristics. First, the surface hydration property was analysed by measuring the water

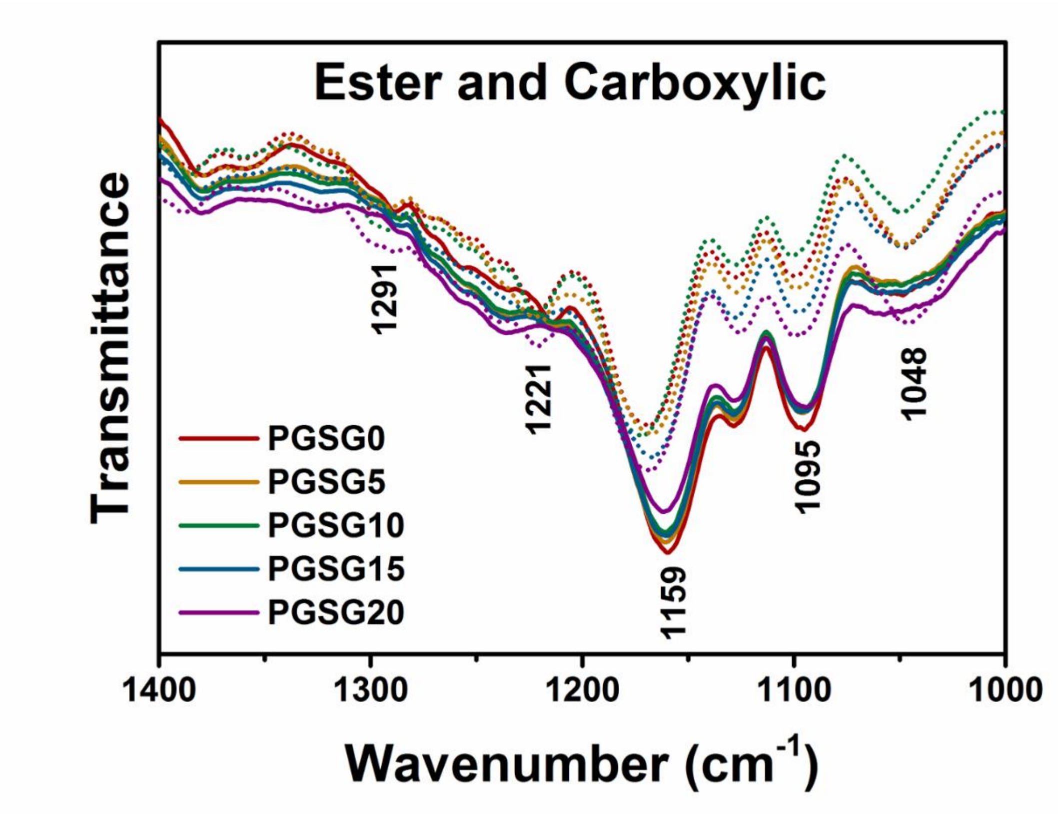

Figure 3.8 ATR-FTIR spectra of PGSG copolymers, highlighting the ester and carboxylic groups, before and after crosslinking. The dotted lines and solid lines refer to the PGSG pre-polymers and cured copolymers, respectively.

contact angles (Figure 3.9). In this test, a droplet of water was dosed on the sample, and the angle between the sample surface and the tangent line to the water drop was measured. A higher contact angle implies lower surface wettability and higher hydrophobic surface characteristics. PGSG0 exhibited a high water contact angle of 85.4 ± 2.9°, similar to the previous report for pristine PGS.[59] Incorporation of hydrophilic gelatin in PGSGs greatly improved the surface wettability with decreases in water contact angle. The lowest water contact angle of 44.2 ± 2.7° was measured from PGSG20, which is generally considered as a hydrophilic surface.[156] This improvement of surface wettability makes the PGSG copolymers more attractive for tissue engineering applications, as cells are known to adhere to and proliferate on hydrophilic surfaces

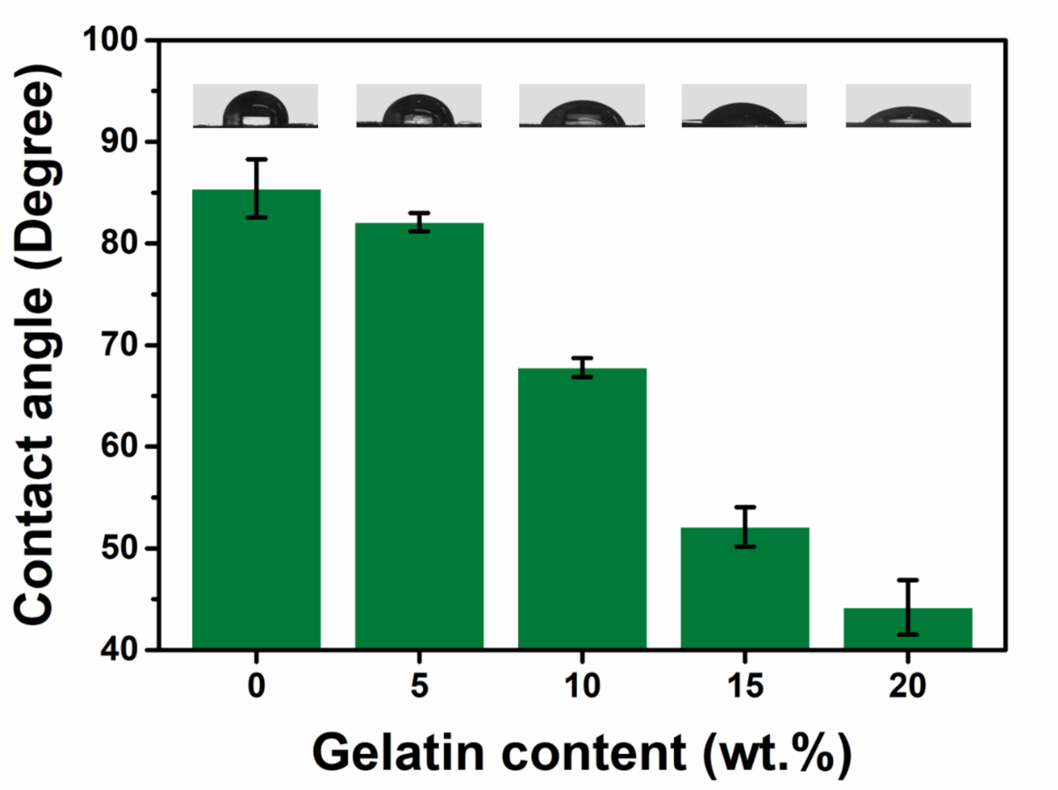

Figure 3.9 The surface water contact angle of PGSG copolymers. The inset photographs show the shape of water droplets on the surface of PGSG specimens.

better than on hydrophobic surfaces.[65] The surface hydrophilicity is also an important parameter in wound dressing applications. The better surface wettability, the higher adsorption of the exudates in the wound sites, promoting healing process.[218,219]

Secondly, the bulk hydration properties of PGSG copolymers were determined by measuring their water swelling ratio. In this test, PGSG copolymers were immersed in PBS at 37 °C, and the amounts of water uptake were recorded in specific time intervals. Figure 3.10 shows the swelling ratio of PGSG up to 120 h. All the PGSG specimens showed the equilibrium water uptake after 72 h of immersion and volume expansion by swollen water (Figure 3.11). While PGSG0 exhibited a minimal water swelling ratio of 5.0 ± 1.9%, incorporation of 20 wt.% gelatin in PGSG20 induced almost a 13-fold increase in water uptake of 67.8 ± 5.9%, resulting

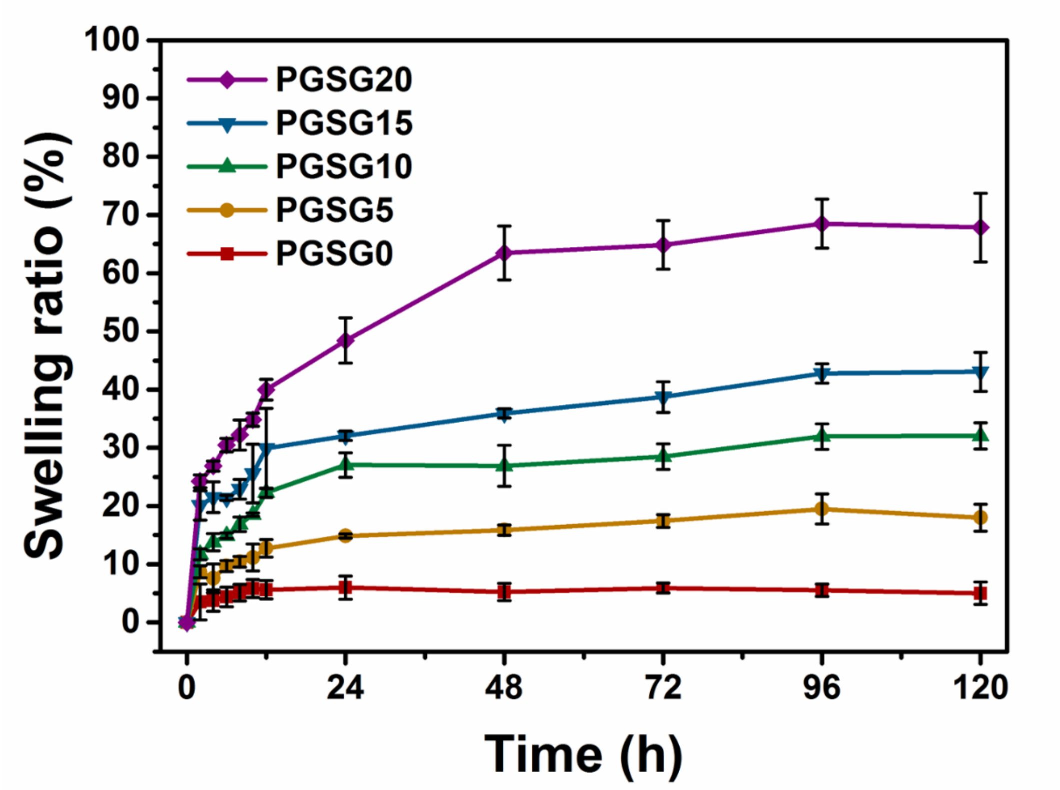

Figure 3.10 Percentage swelling ratio of PGSG copolymers (PBS, 37 °C) from 0 to 120 h. The incorporation of gelatin within PGS greatly improved the water uptake by a maximum 13-fold increase.

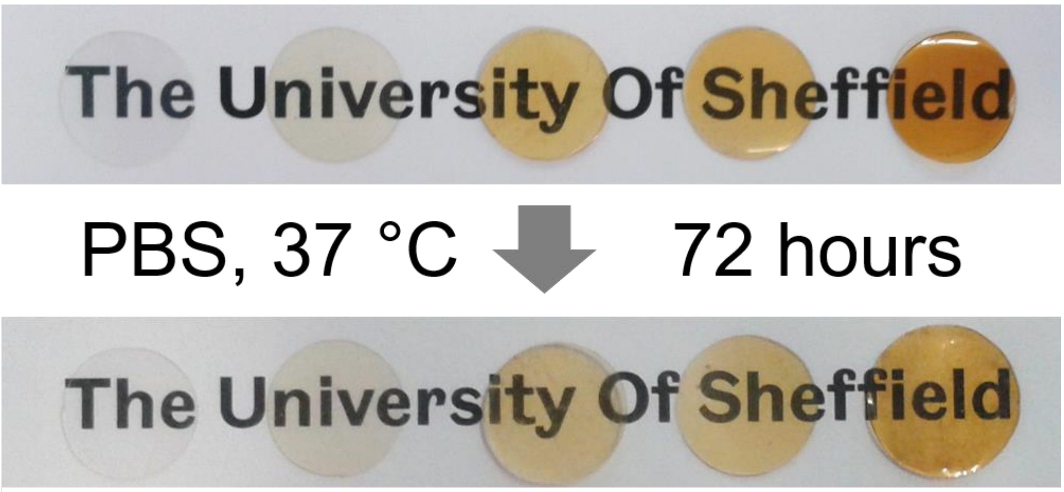

Figure 3.11 Photographs of PGSG copolymers before and after swelling in phosphate buffered saline (PBS) for 72 h at 37 °C (from left to right PGSG0, PGSG5, PGSG10, PGSG15, and PGSG20), showing volume expansions.

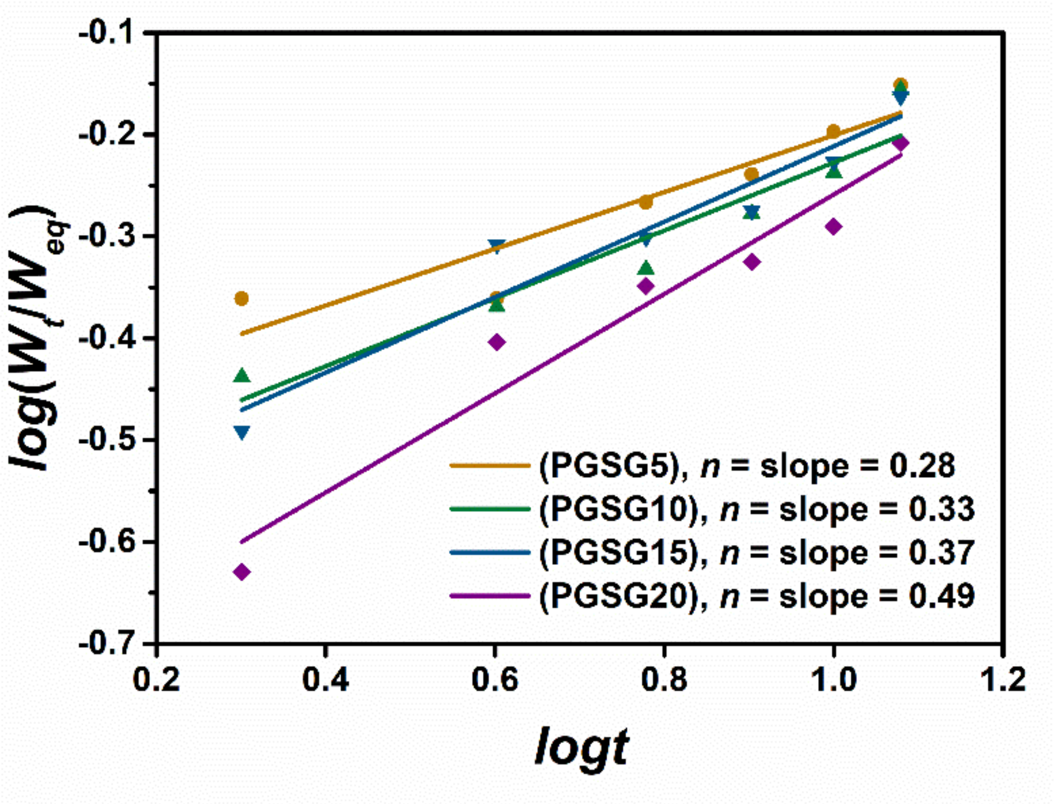

Figure 3.12 The swelling ratio of PGSG copolymers which are fit to Ritger-Peppas equation, with the *n* values shown by the slope of the fitting lines.

in swollen hydrogels.

The kinetics in water diffusion into the PGSG polymer matrix was further investigated mathematically in order to understand the determining mechanisms of swelling process. The data points at the early stage ($W_t/W_{eq} < 0.6$) were fit to the following Korsmeyer-Peppas equation, eqn (3.4),

$$\frac{W_t}{W_{eq}} = kt^n \tag{3.4}$$

where W_t and W_{eq} are the water uptake values at a specific time (t) and at equilibrium, respectively.[6,220] k is the characteristic swelling constant and n is the determining factor of the mode of water transport through the copolymers. The calculated n values for PGSG5, PGSG10, PGSG15, and PGSG20 were 0.28, 0.33, 0.37, and 0.49 respectively (Figure 3.12) (PGSG0 was omitted here due to the minimal water swelling ratio), indicating Fickian diffusion. In this diffusion process, the water penetration rate in the gels is slower than the polymer chain relaxation rate.[221] In other words, the elastic polymer chains in PGSG copolymers instantaneously responded to the stress given by water absorption, thereby the water diffusion through the polymer matrix is not limited by the relaxation of polymer networks. Fickian diffusion is known to be an asset in building diffusion-controlled drug delivery systems from an aqueous stimulus.[118,222,223]

3.3.2 Elastomeric mechanical properties

The mechanical properties of dry and hydrated PGSG copolymers were evaluated by uniaxial tensile tests and the results are shown in Figure 3.13–17. In respect of the tensile properties of

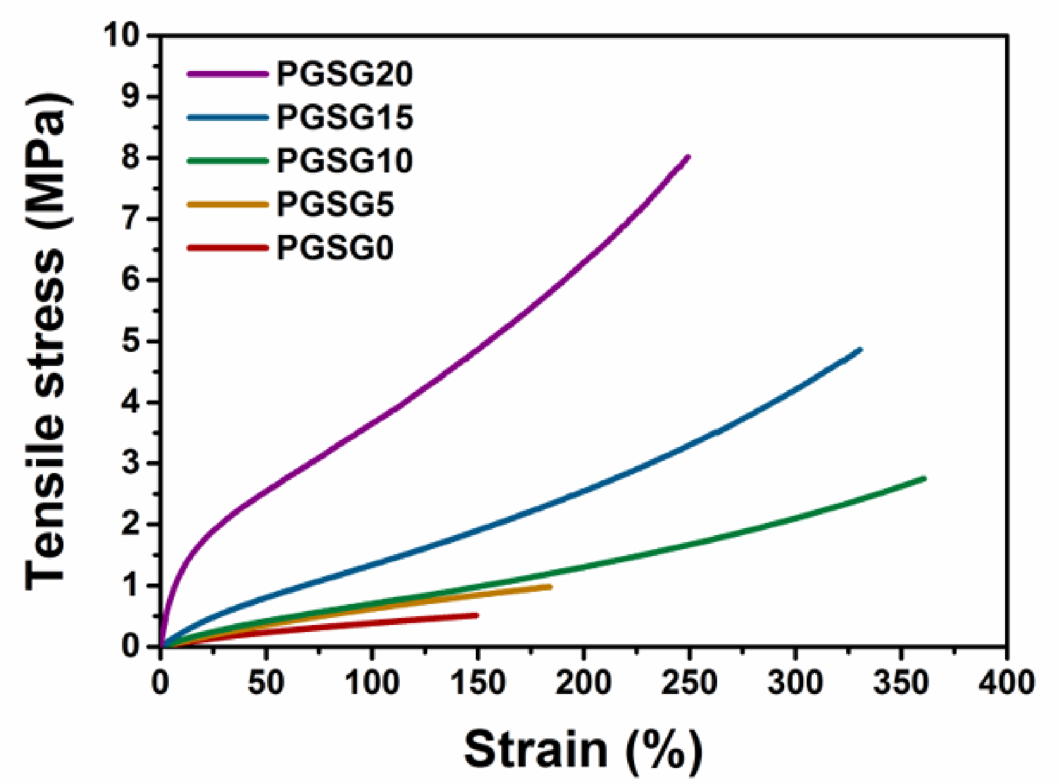

Figure 3.13 Representative tensile stress-strain curves of dry PGSG copolymers.

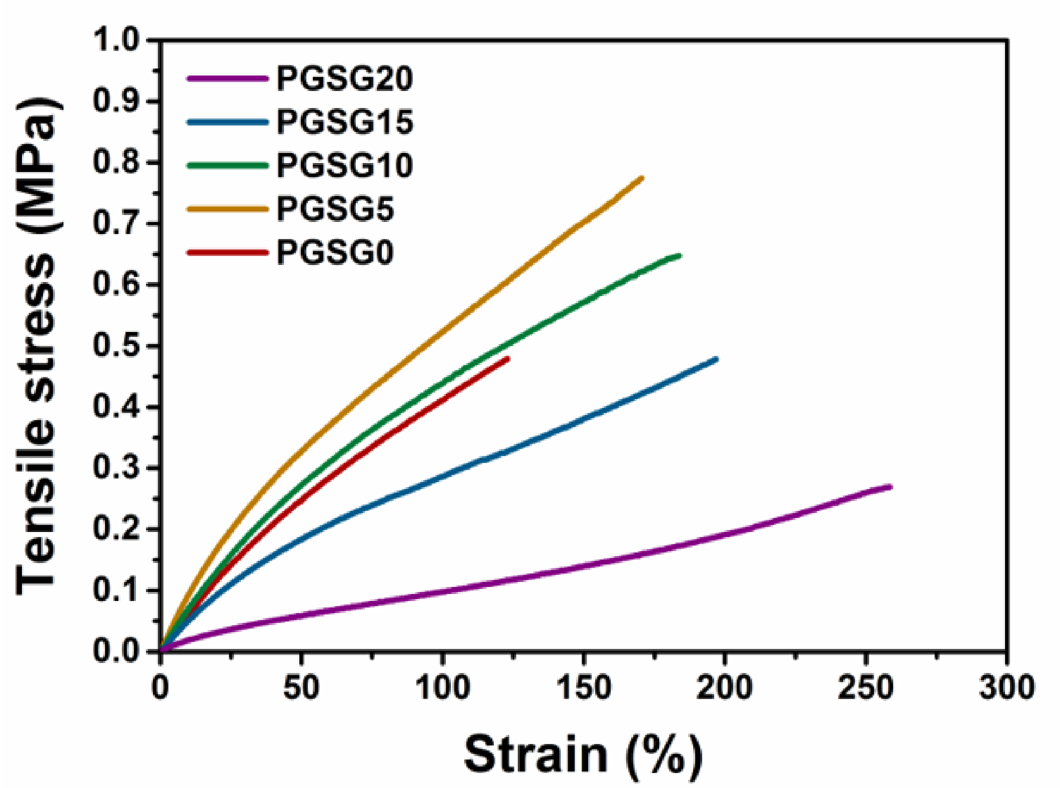

Figure 3.14 Representative tensile stress-strain curves of hydrated PGSG copolymers.

dry specimens, PGSG0 featured Young's modulus, tensile strength, and strain to failure of 0.59 ± 0.05 MPa, 0.55 ± 0.07 MPa, and 142 ± 17%, which are in agreement with PGS homopolymers in previous reports.[9,26] The effect of gelatin on the tensile modulus and strength of PGSGs was measured by an almost 9-fold increase in modulus and 14-fold increase in strength from PGSG0 to PGSG20. The crosslinking densities calculated by eqn (3.1) were 80.2 (PGSG0), 114.1 (PGSG5), 127.7 (PGSG10), 249.9 (PGSG15), and 812.3 mol m^{-3} (PGSG20), respectively, showing an increase in the crosslinking density with increasing gelatin content. When even higher gelatin contents (30 and 40 wt.%) were used, the resultant copolymers were extremely brittle and could not be stretched or bended (hence not tested in this study), confirming that the crosslinking density is increased by the addition of a higher amount of gelatin. The increased

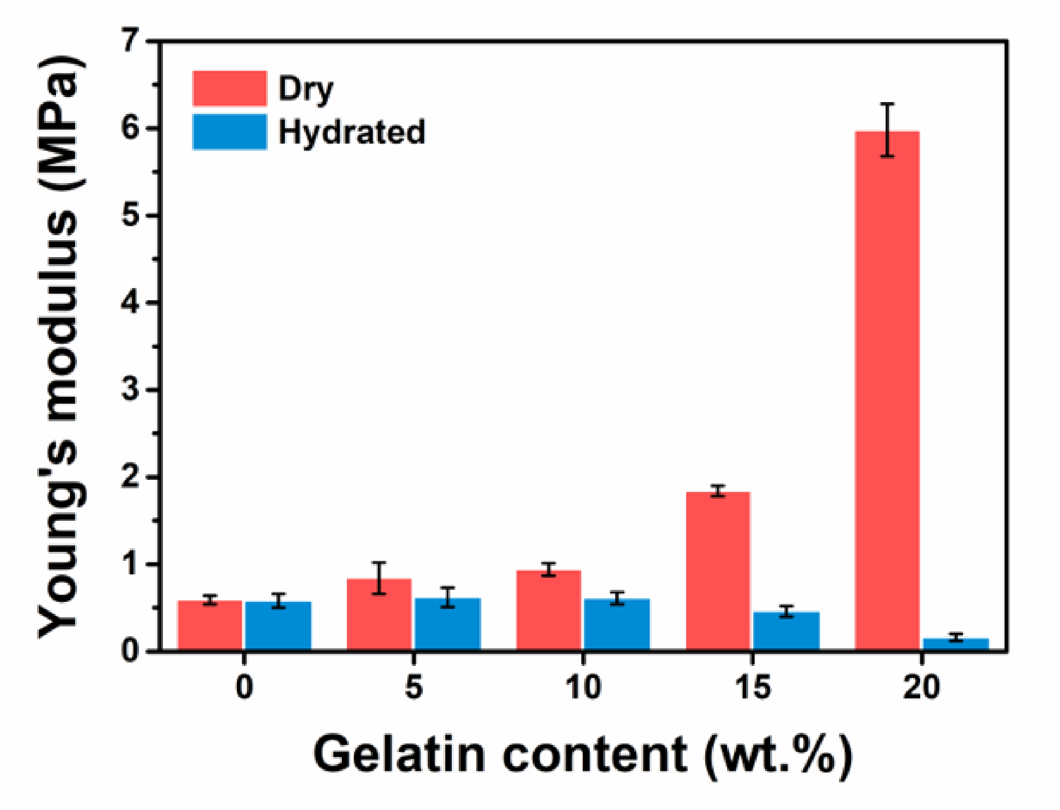

Figure 3.15 The tensile Young’s modulus of PGSGs, both dry and hydrated.

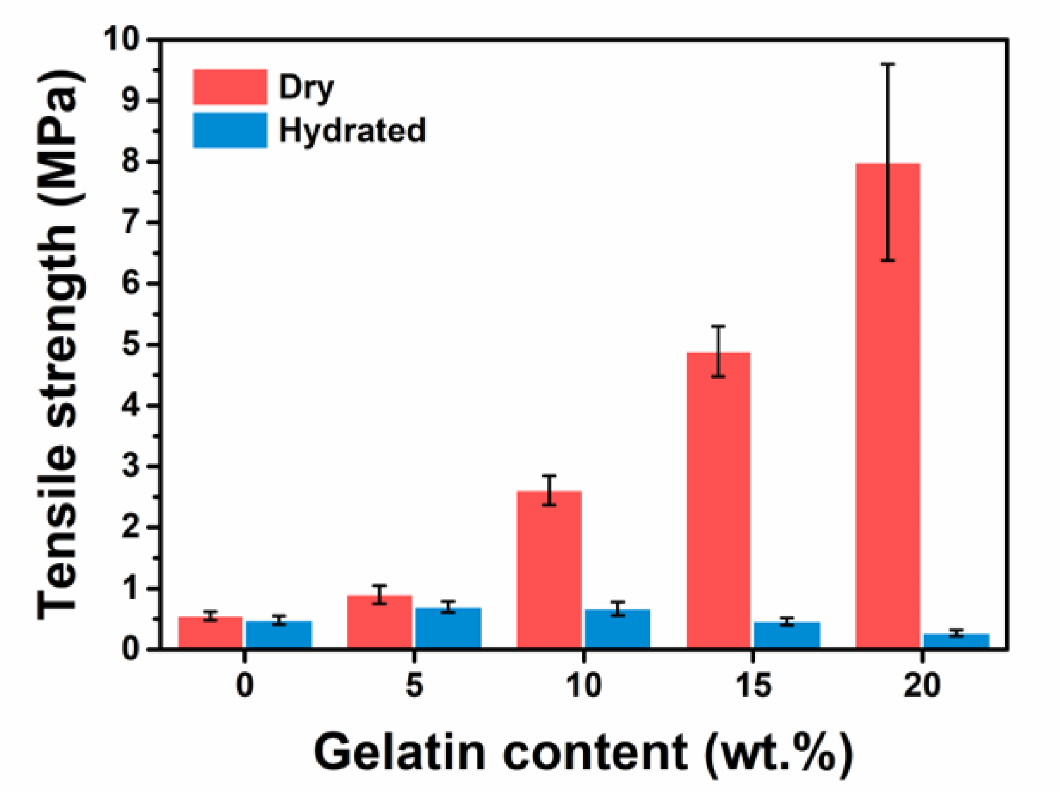

Figure 3.16 The tensile strength of PGSGs, both dry and hydrated.

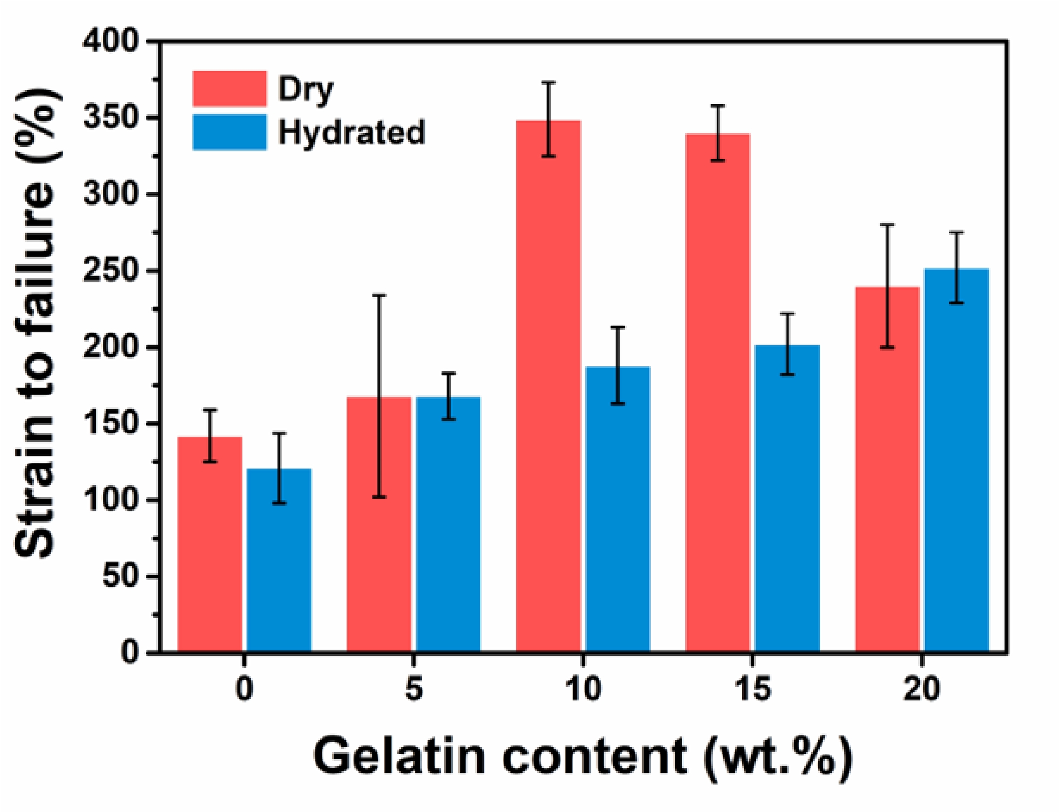

Figure 3.17 The strain to failure values of PGSGs, both dry and hydrated.

crosslinking densities in PGSGs are accounted for by the additional ester and amide linkages provided by the crosslinking between PGS pre-polymer and gelatin, which was confirmed by FTIR previously.

The changes in tensile properties of PGSG copolymers can also be attributed to the mechanical properties of gelatin. As gelatin has relatively high tensile modulus and strength of 3.0 GPa[224] and 63.2 MPa,[225] the addition of gelatin to PGS gives PGSG copolymers with higher stiffness and strength compared to the PGS homopolymer. The amide bond is, in general, known to be more rigid than the ester bond due to the partial double bond character through tautomerism.[226,227] According to the FTIR analysis earlier, the PGSGs with a higher content of gelatin have more amide bonds than those with a lower content of gelatin, thereby showing a higher stiffness.

Interestingly, the strain to failure of dry PGSG specimens also shows an increase between PGSG0 (PGS homopolymer) and PGSG15 copolymers. Although the addition of gelatin increased the crosslinking density in PGSG as calculated above, gelatin has highly coiled molecular structures, therefore one can expect that the relaxation of gelatin coils promoted higher ductility in PGSG.[224,225,228] However, too high crosslinking density in PGSG20 became a dominant factor which drastically decreased free volume in the polymer matrix and restricts the molecular motion, resulting in a decrease in strain to failure.[229]

PGSGs featured highly elastomeric mechanical behaviours even in fully swollen state. Complex deformations such as stretching and knotting were possible with hydrated PGSGs, as demonstrated in Figure 3.18. With the increasing gelatin amount in hydrated PGSGs, the Young's modulus and tensile strength were decreased from 0.62 ± 0.08 MPa to 0.16 ± 0.04 MPa and from 0.70 ± 0.07 MPa to 0.27 ± 0.05 MPa. In contrast, the strain to failure value increased from 121 ± 23% to 252 ± 23%, primarily due to the higher polymer chain flexibility

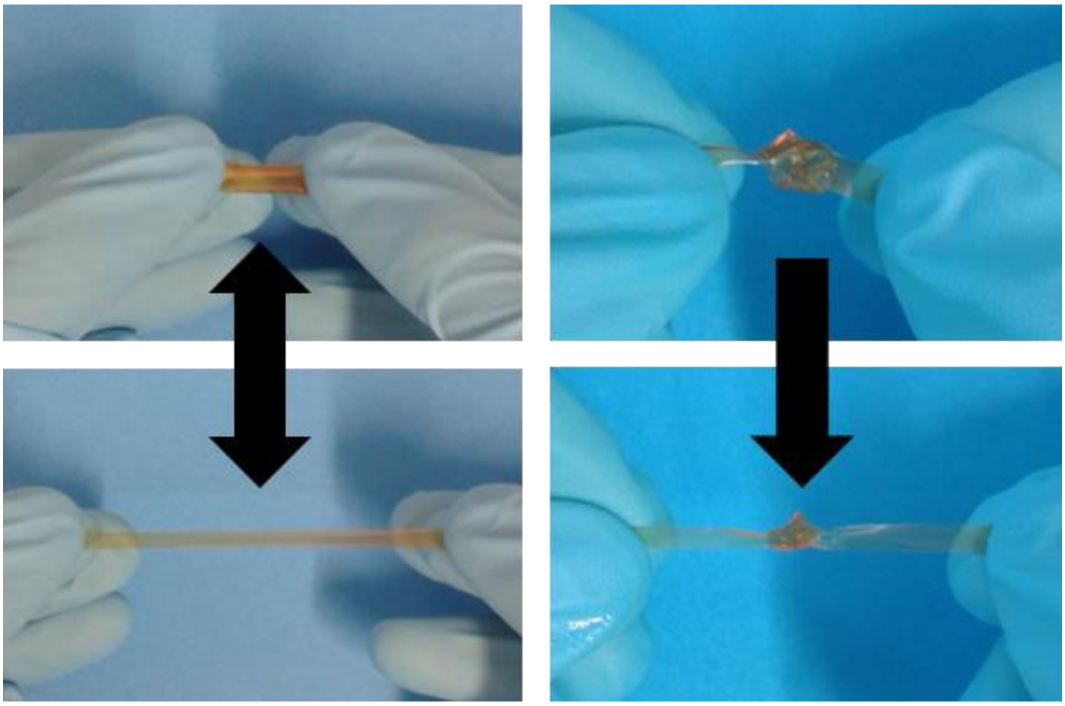

Figure 3.18 Demonstration of mechanical stretching and knotting with hydrated PGSG20 specimens.

led by higher water swelling ratio as discussed previously.

As shown in Figure 3.19, the tensile modulus values of hydrated PGSG copolymers are in the range of soft tissues such as adipose, myocardial, or cartilage tissues,[19,23,230] illustrating a promising future of PGSGs in soft tissue engineering. With their biomimetic mechanical behaviours, porous tissue scaffolds were fabricated with PGSG20 as a *proof-of-concept* (Figure 3.20A). The PGSG pre-polymers were re-meltable and easily deformable into a desired shape, therefore fabrication of a three-dimensional and large scaffold was feasible by a combined technique of salt-leaching and freeze-drying (see SI for the detailed fabrication technique). The macro-pores were generated by salt crystals (300 μm) in the salt-leaching stage, whereas the micro-pores were formed by the ice crystals during freeze-drying. The benefits of well-defined

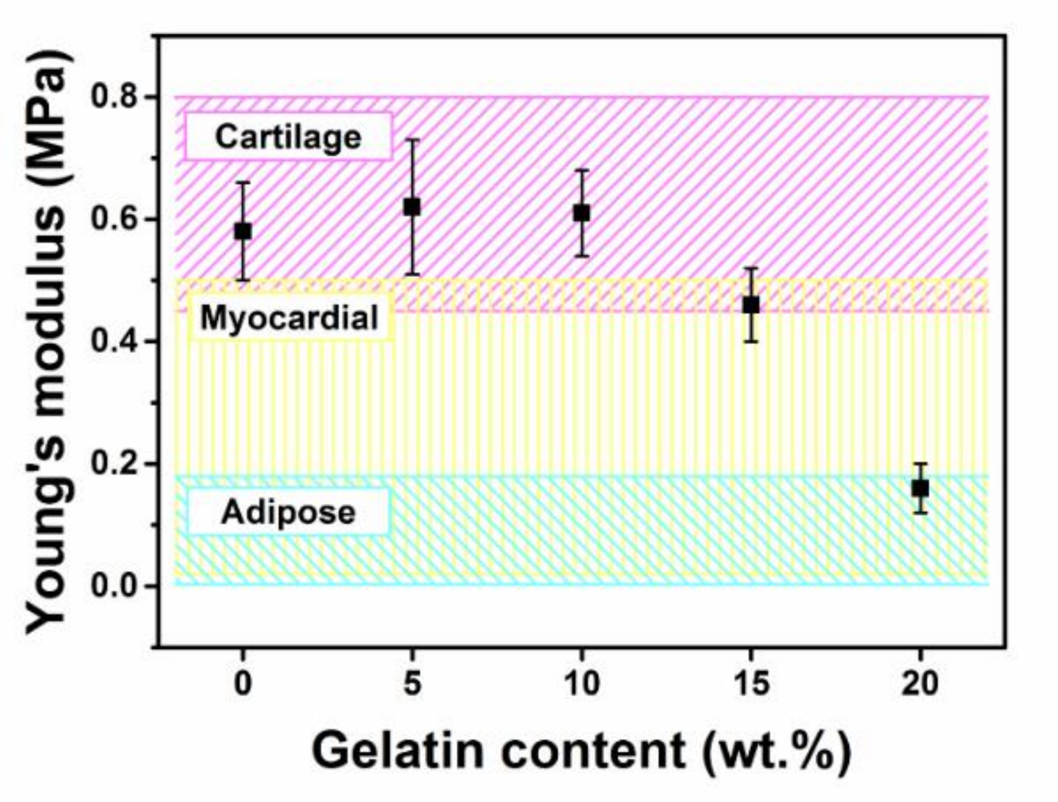

Figure 3.19 Comparison of Young's modulus of PGSG hydrogels to that of native tissues from the literature. Each shaded area represents the range of Young's modulus of cartilage (magenta), myocardial (yellow), and adipose (cyan) tissues.

and interconnected pore structures as well as the micro-pores shown in Figure 3.20B and C are well-demonstrated in tissue engineering fields, with the ability to help cell penetration and proliferation, as well as transportation of chemical species such as water, gas, nutrients, and metabolic waste products throughout the tissue scaffolds.[152,231] The prepared scaffold is also highly elastomeric and exhibits excellent shape recovery after the release of a compressive load, with compressive Young's modulus and compressive stress at 75% strain of 0.19 ± 0.05 MPa and 1.16 ± 0.40 MPa, respectively (Figure 3.21A and B). The interconnected pore structures and elastomeric mechanical properties, as well as good biocompatibility and controllable biodegradation (discussed below) make this PGSG scaffold an attractive candidate for applications in soft tissue engineering. Future work may include dynamic and cyclic mechanical tests with PGSG porous scaffolds under simulated body conditions to fully illustrate the advantages associated with the elastomeric properties of PGSGs and explore them further as potential candidates in soft tissue engineering.

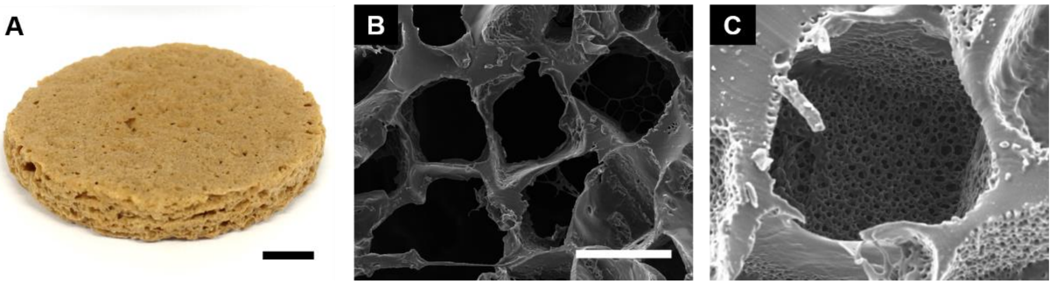

Figure 3.20 (A) Photograph showing a proof-of-concept tissue scaffold fabricated from PGSG20 (scale bar: 1 cm). (B) Well-defined and interconnected porous microstructures seen in an SEM image (scale bar: 300 μm). (C) A closer look at a pore revealing micro-pores on the wall surface (scale bar: 100 μm).

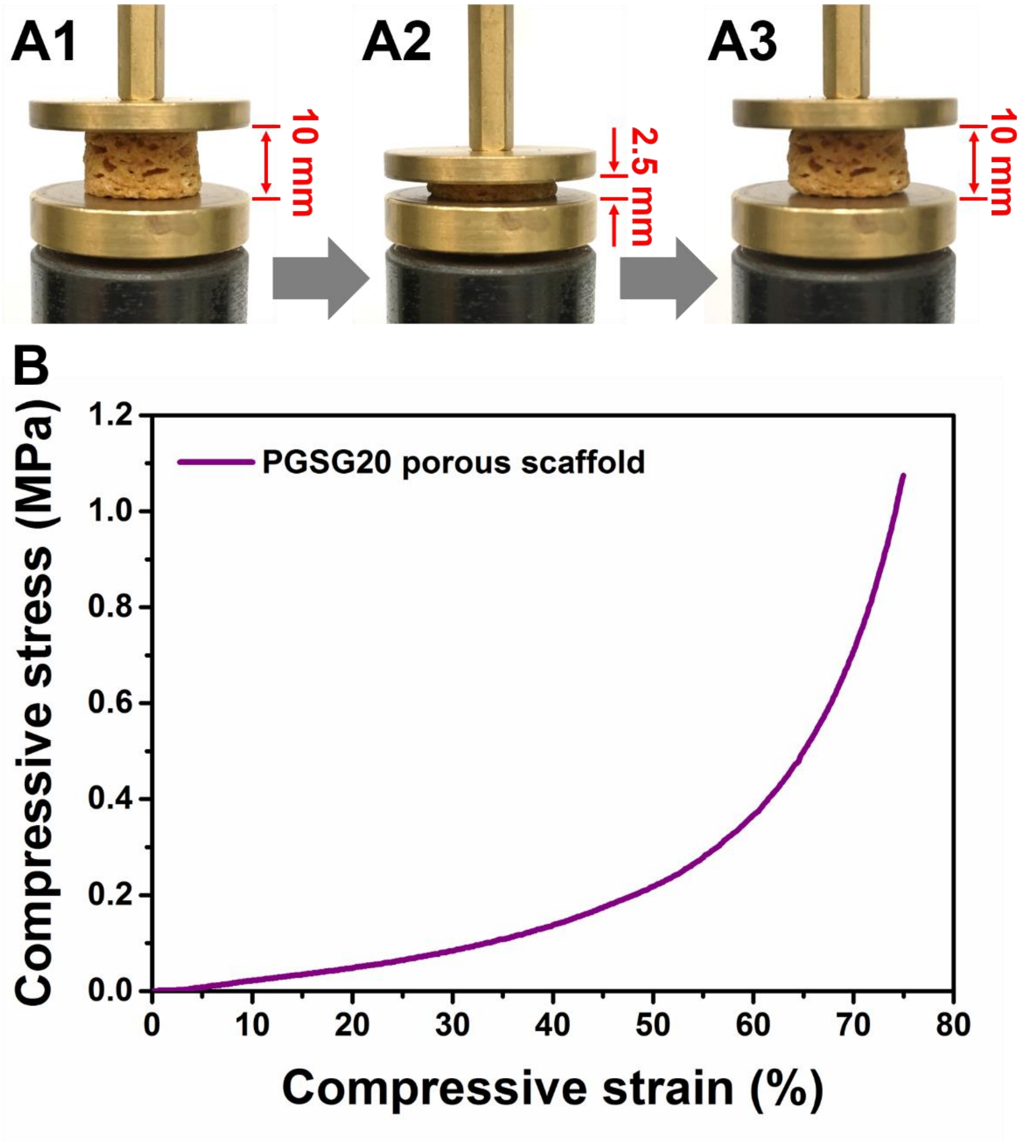

Figure 3.21 (A1 – A3) Elastomeric PGSG20 porous scaffold showing excellent shape recovery after the release of a compressive load. (B) A representative compressive stress-strain curve of PGSG20 scaffold.

3.3.3 pH-responsive behaviours

In our body, there is a large variation in pH in terms of the physiological roles and medical conditions. For instance, the gastric pH is highly acidic ranging between 1.0 and 2.5 (up to 5 when fed), whereas the proximal small intestine exhibits almost neutral pH of 6.6.[232,233] The healthy skin surface has slightly acidic pH of 5.5, however the injured skin tissue in burn patients features basic pH values ranging between 9.5–10.5.[234] Hydrogels with pH-responsive properties, therefore, are of great interest in many biomedical fields, with their ability to alter the material structure and properties depending on the surrounding biological pH values.

Hydrogels containing ionic groups respond to external pH, making them pH-responsive hydrogels.[235] As shown previously in FTIR study, although some amine and carboxyl groups were sacrificed to form covalent linkages in PGSG, there were still ionic functional groups remained in copolymer hydrogels. Therefore, the pH-responsiveness of PGSG hydrogels was examined by swelling tests in three different pHs. Figure 3.22 and 3.23 illustrate the water swelling ratio of PGSG specimens in acidic (citrate buffer, pH 5.0) and basic (NaOH-glycine buffer, pH 9.1) pHs. Figure 3.24 shows the equilibrium water uptake values of PGSGs in three

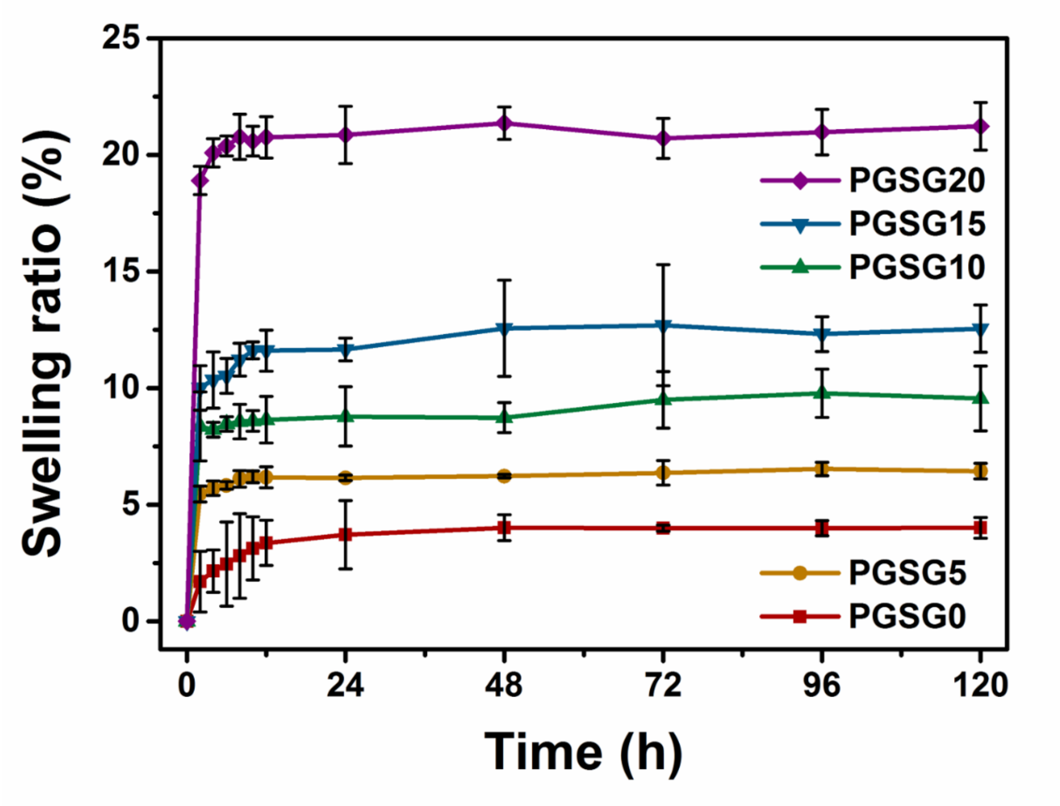

Figure 3.22 pH-responsive water swelling ratio of PGSGs measured at pH 5.0.

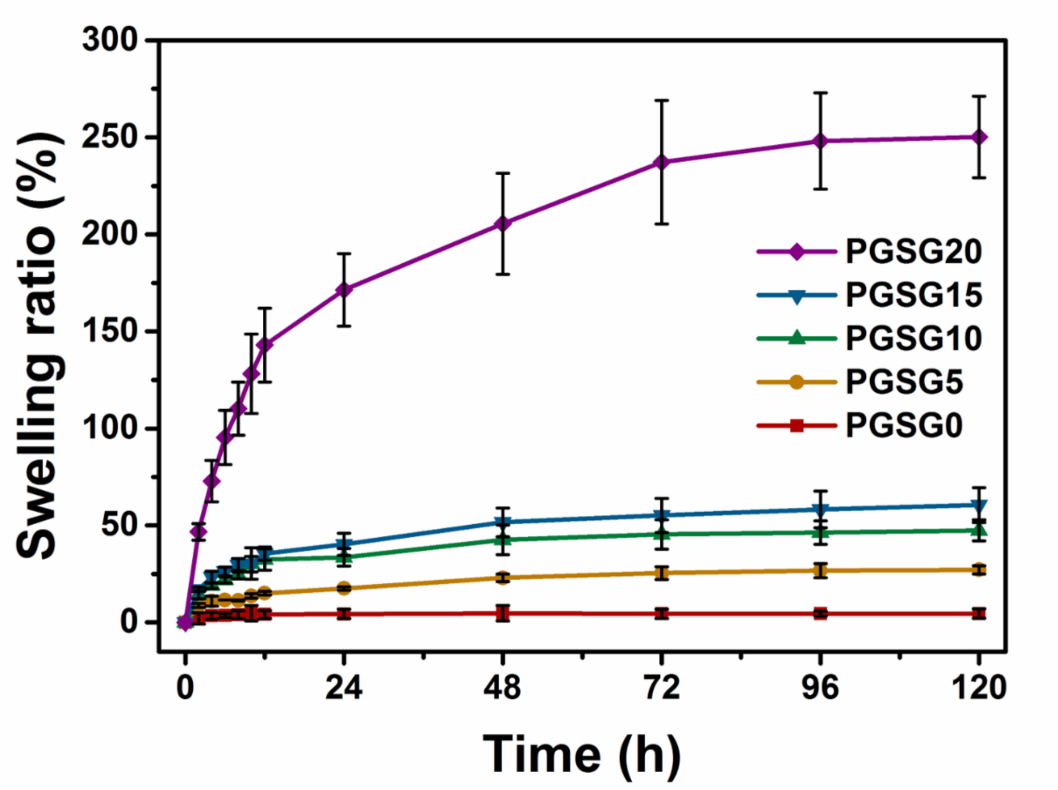

Figure 3.23 pH-responsive water swelling ratio of PGSGs measured at pH 9.1.

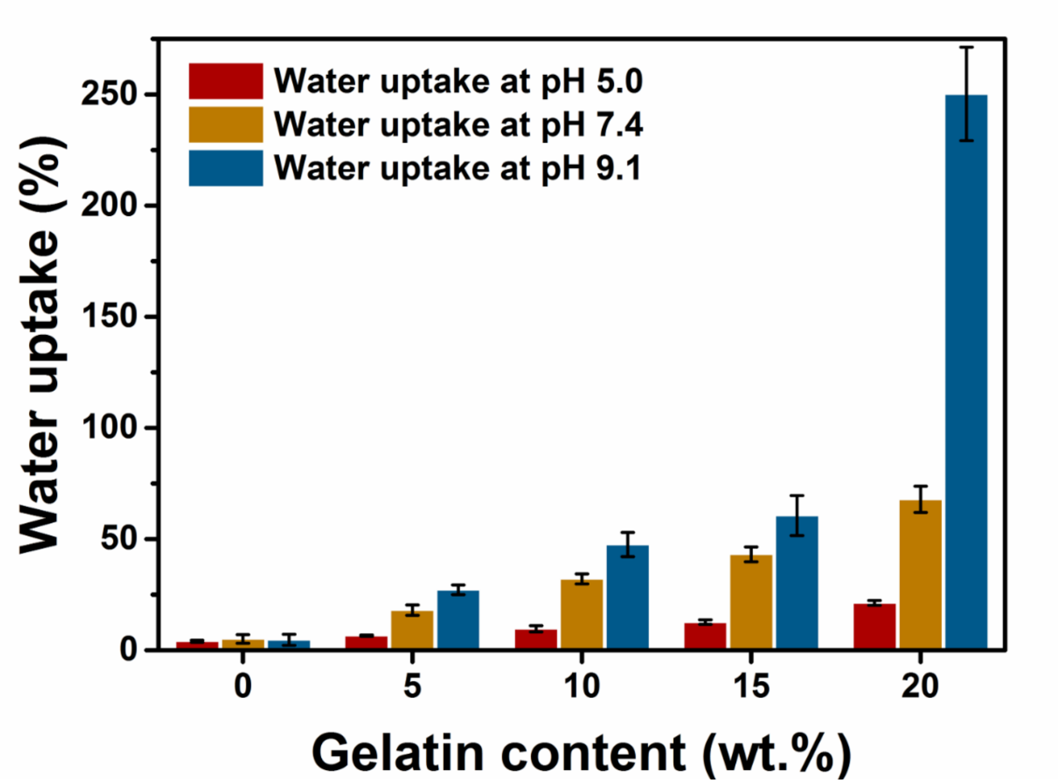

Figure 3.24 Pictures of PGSG20 specimens after 72 h of hydration at pH 5.0, 7.4, and 9.1 (scale bars: 5 mm).

different pHs (pH 5.0, 7.4, and 9.1). The higher the pH value was the higher the water swelling ratio was achieved in PGSG20. The values of the water uptake at equilibrium measured at pH 5.0 were 4.0 ± 0.5% (PGSG0), 6.4 ± 0.3% (PGSG5), 9.6 ± 1.4% (PGSG10), 12.5 ± 1.0% (PGSG15), and 21.2 ± 1.0% (PGSG20), which indicates the PGSG copolymers swell less in an acidic pH than in a neutral pH condition. In contrast, the swelling ratio of PGSG copolymers at pH 9.1 increased greatly, to the values of 27.1 ± 2.1% (PGSG5), 47.5 ± 5.5% (PGSG10), 60.5 ± 9.0% (PGSG15), and 250.2 ± 21.1% (PGSG20), while it was not changed much in PGSG0 homopolymer (4.6 ± 2.5%). The pH also affects the kinetics in the equilibrium of water swelling for the copolymers. It was shown previously that the equilibrium was acquired in 72 h at pH 7.4. In acidic condition (pH 5.0), 12 h was enough to reach equilibrium at pH 5.0, whereas a longer time of 96 h was required at pH 9.1. Figure 3.25 shows the PGSG20 specimens showing the size differences in different pHs.

This pH-responsive swelling behaviour found in PGSG copolymers is different to that of neat gelatin. The latter shows the minimum swelling ratio at the isoelectric point near the neutral pH (pH 7–9, type A, form porcine skin), where anionic and cationic forms are exactly

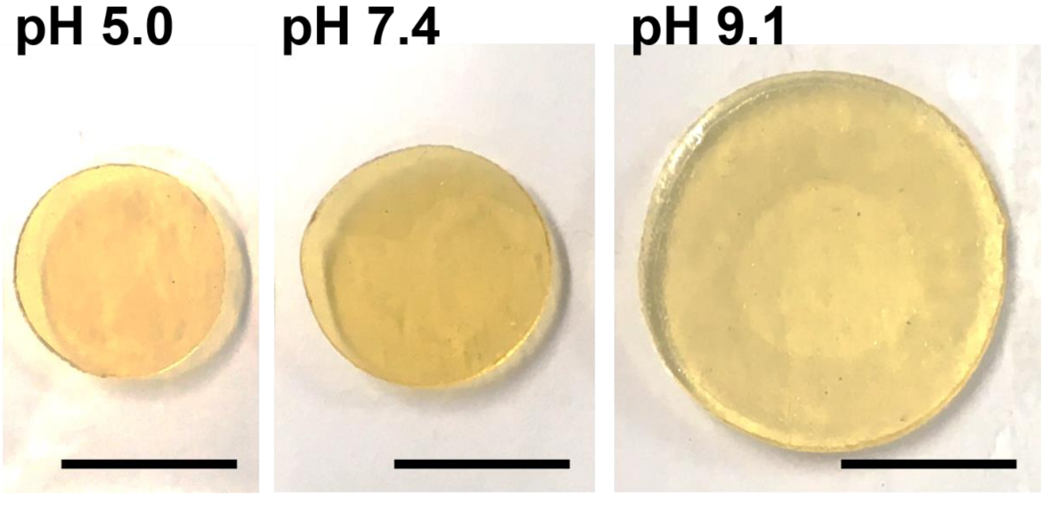

Figure 3.25 Pictures of PGSG20 specimens after 72 h of hydration at pH 5.0, 7.4, and 9.1 (scale bars: 5 mm).

balanced resulting in chain collapse.[103,236] In contrast, PGSG copolymers showed the minimum swelling at the acidic pH and the maximum was achieved at the basic pH. It can be concluded that the number of ionisable carboxyl groups is higher than that of amine groups in PGSG copolymers. The carboxyl group (-COOH) ionises by deprotonation, becoming negatively \charged carboxyl groups (-COO$^-$). The amine group (-NH$_2$), on the other hand, becomes positively charged groups by accepting protons (-NH$_3^+$). To acquire the electrostatic repulsion that leads to the higher swelling ratio of PGSG copolymers in basic pH conditions as described above, the deprotonation of carboxyl group should be dominant and counter the protonation of amine group.[237] This is attributable to the fact that the amine groups are supplied only by the relatively minor amount of gelatin in the synthesis of PGSG copolymers, whereas the carboxyl group was offered by both PGS pre-polymer and gelatin becoming abundant within PGSG copolymers.

It was also noted that the swelling ratio of PGSG20 at pH 9.1 was much greater than that of other PGSGs. In amphiphilic hydrogels such as PGSGs, the ionisation of functional groups is often hindered by the resistive aggregation of hydrophobic polymer chains.[238] The ionisation of carboxyl groups can happen much more easily in PGSG20 compared to the case with other PGSGs, owing to its much better hydrophilicity arising from the higher gelatin content which provides more chain relaxation and much more free space for the ionisation of carboxyl groups, resulting in a significantly higher swelling ratio of PGSG20 at pH 9.1.

The potential application of pH-responsive PGSGs in controlled drug delivery was investigated selectively on PGSG20 with the greatest pH-responsiveness. PGSG20 specimens loaded with a model drug, DOX, were exposed to the same buffer solutions as for the pH-responsive swelling study (pH 5.0, pH 7.4, and pH 9.1) and the cumulative drug release profiles are depicted in Figure 3.26. A quite different drug releasing kinetics was observed from the

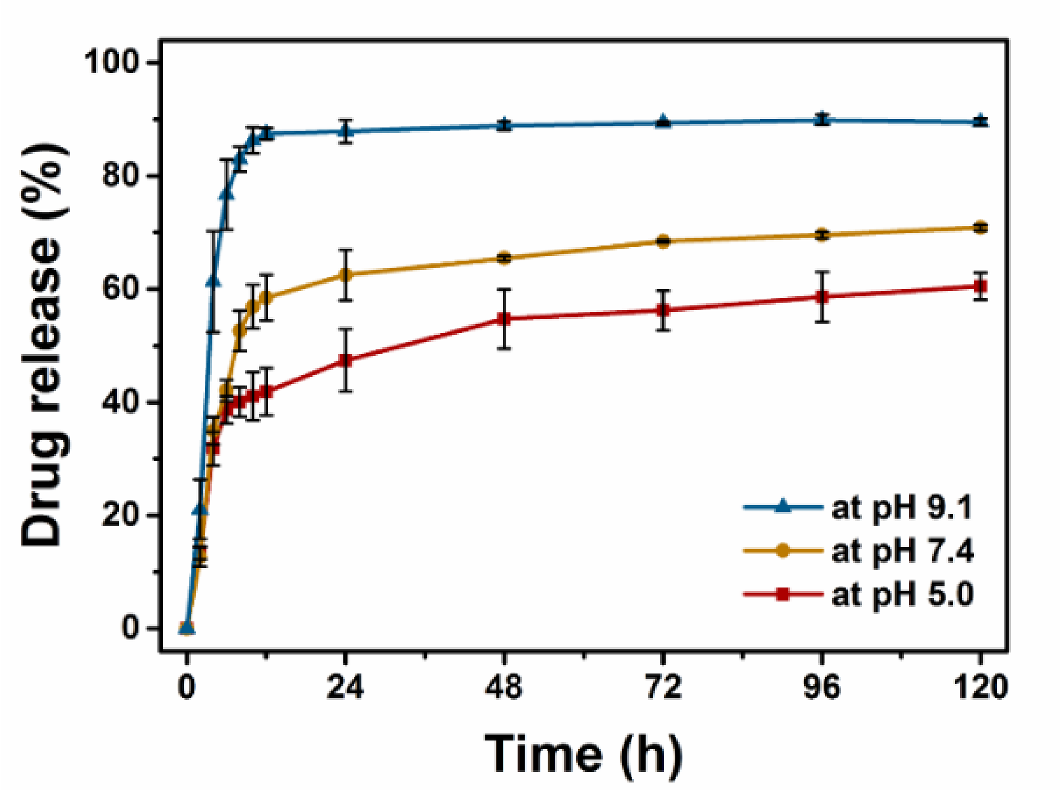

Figure 3.26 Cumulative drug release profile of DOX from PGSG20 at three different pH values.

three different pH values. The drug release kinetics at pH 9.1 quickly reached the equilibrium in 12 h and the cumulative drug release was measured at 89.6 ± 0.6% of the loaded drug amount (or 0.37 mg) initially. However, the cumulative amount of released drug at pH 5.0 was 41.9 ± 4.2% (or 0.17 mg) after 12 h and the equilibrium was not detected even after 120 h. This result suggests a potential use of PGSG copolymers in controlled drug delivery applications. For instance, oral administration of drugs often faces a difficulty in conserving drug stability and drug amount at dynamic gastrointestinal pH conditions.[239] Therefore, pH-responsive PGSG copolymer hydrogels that release drug more slowly and less amount at lower pHs, but more quickly and more amount at higher pHs could be a reliable carrier for controlled drug operations targeting specific organs in the digestive system with pHs ranging from 1 to near 8.[232] The model drug used in this study (DOX) is water-soluble. Since PGSG copolymers exhibit amphiphilic characteristics as discussed previously, future work may also include hydrophobic drugs and steroid hormones to extend their application in controlled drug delivery.

3.3.4 Biodegradability and biocompatibility *in vitro*

Figure 3.27 illustrates the *in vitro* degradation profiles of two selective PGSG samples (PGSG10 and PGSG20) for up to 28 days. Three different degradation media were used in this study; 1) PBS only, 2) PBS + lipase, and 3) PBS + collagenase. Lipase was used to degrade ester linkages, and collagenase was to break down gelatin. Both the PGSG10 and PGSG20 exhibited weight losses of 7.5 ± 3.3% and 8.1 ± 2.1%, respectively after 28 days of incubation in the PBS only medium. In contrast, the presence of enzymes led to accelerated degradation

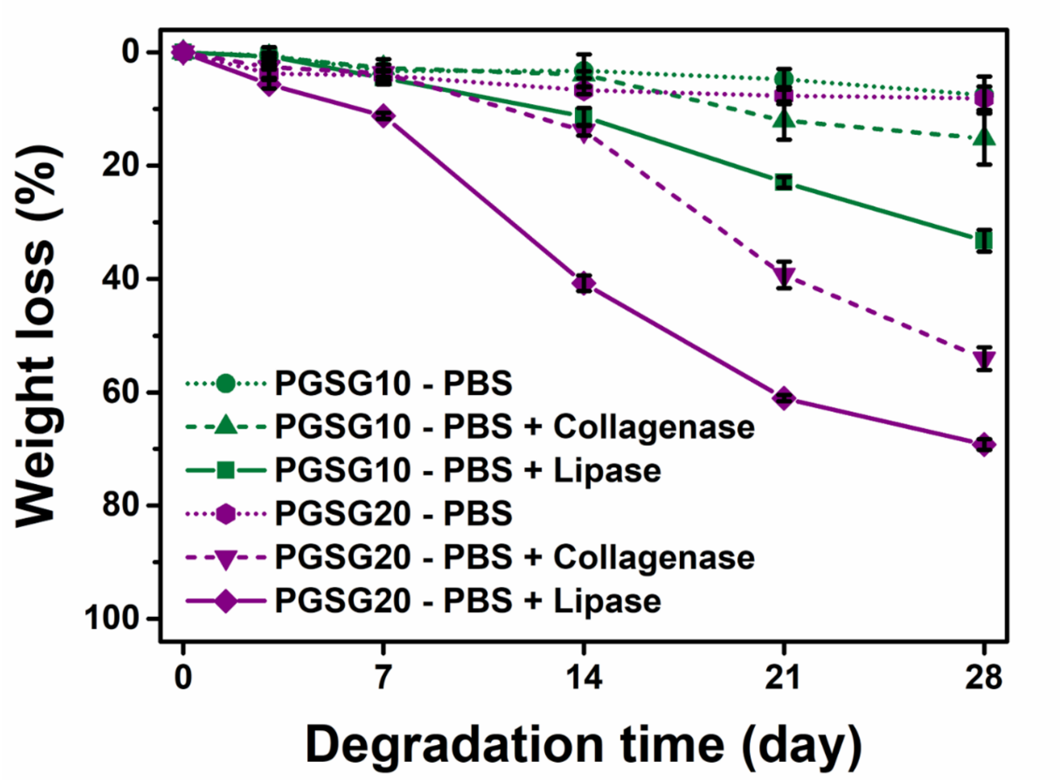

Figure 3.27 Percentage weight loss data of PGSG10 and PGSG 20 incubated in PBS solutions with or without the enzymes (collagenase and lipase) for up to 28 days at 37 °C, showing controllable biodegradation.

kinetics of PGSG specimens, and lipase appeared to be yielding more polymer degradation than collagenase. This was expected as the majority of PGSG copolymers is PGS (polyester) rather than gelatin. PGSG20 presented faster enzymatic degradation kinetics compared to that of PGSG10, which can be assigned to the better hydration properties of PGSG20 as demonstrated previously in water swelling ratio. PGSG10 yielded a weight loss of 33.2 ± 1.9% with lipase and 15.2 ± 4.6% with collagenase, whereas PGSG20 underwent the weight losses of 69.3 ± 1.0% with lipase and 54.1 ± 2.0% with collagenase after 28 days. It should be noted that the degradation rates of PGSGs are faster than that of PGS homopolymer in our previous study with a similar experimental condition (9.6% in enzyme-free media and 29.1% with lipase, after 31 days), which can be attributable again to the presence of gelatin and the higher hydration properties of PGSG copolymers than the PGS homopolymers.[26]

SEM analysis revealed the surface morphology of PGSG specimens after the degradation test with or without enzymes (Figure 3.28). The non-enzymatically degraded PGSG specimens

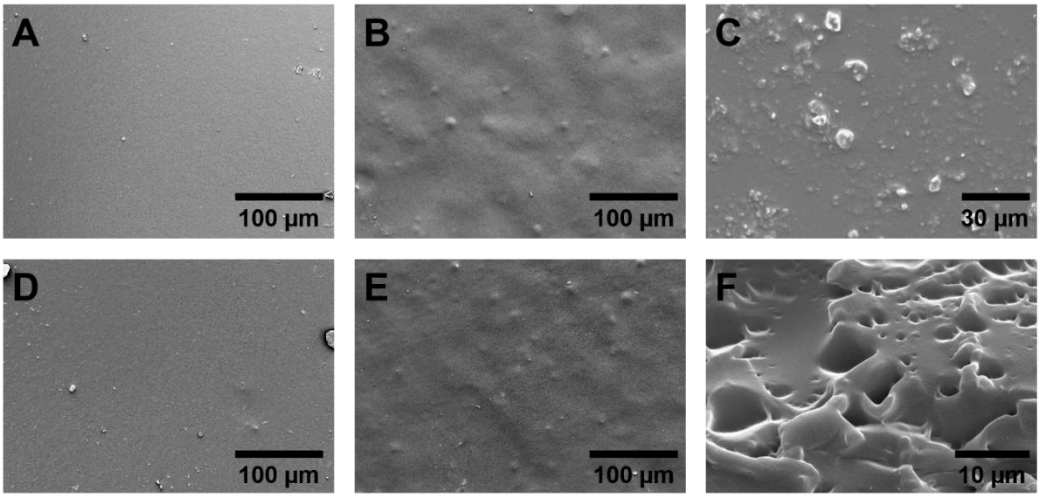

Figure 3.28 SEM images showing the surface of PGSG specimens after degradation. (A-C) PGSG10 incubated for 28 days at 37 °C in (A) PBS only, (B) lipase + PBS, and (C) collagenase + PBS. (D-F) PGSG20 incubated for 28 days at 37 °C in (D) PBS only, (E) lipase + PBS, and (F) collagenase + PBS.

featured smooth surfaces in both PGSG10 and PGSG20 due to relatively minor weight losses (less than 10%) as verified previously. However, enzymatically degraded PGSG specimens showed severe surface damages with irregular swelling and pores, indicating the degradation was catalysed by lipase and collagenase enzymes.[26,145] Especially, PGSG20 with lipase enzymes exhibited extremely rough surface morphology with the greatest weight loss found in this study.

In addition, an ultimate full biodegradability was found in PGSG20 in 77 days with lipase (Figure 3.29). Many biomaterials such as tissue scaffolds and drug carriers are not intended to remain permanently in our body.[42,240] For instance, tissue scaffolds should be designed to have the optimal degradation kinetics to match the rate of new tissue formation regenerated by cells and eventually replaced by native tissues.[39,81] In drug delivery systems based on biodegradable

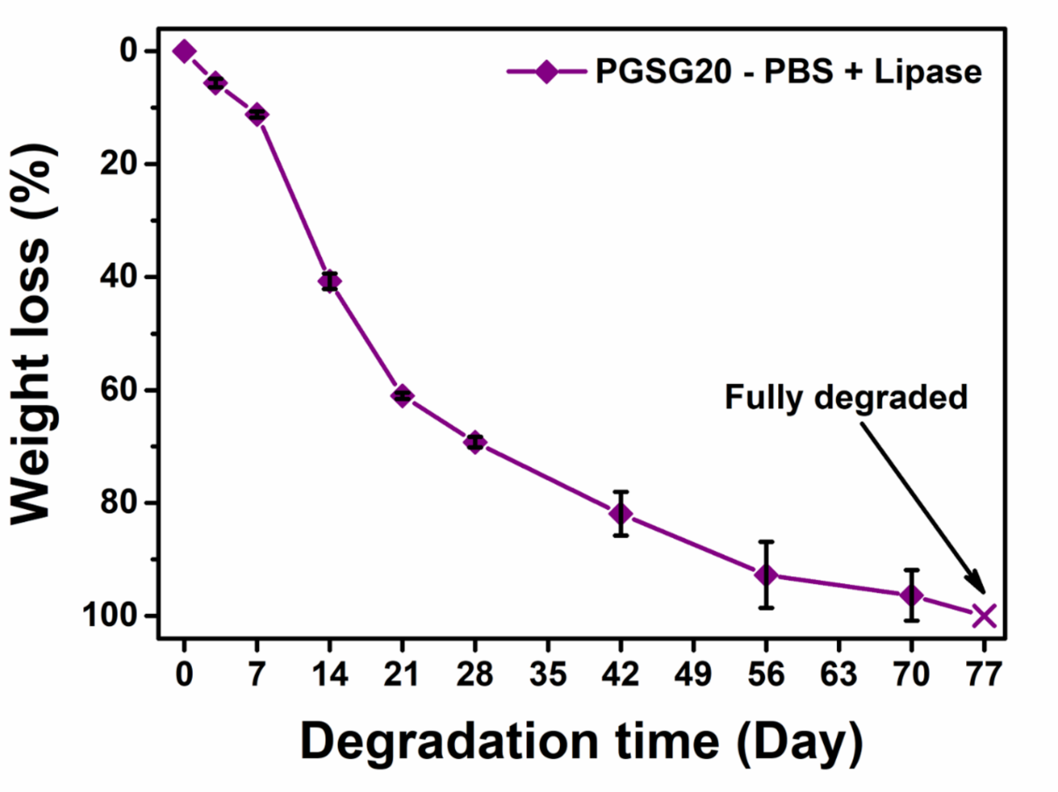

Figure 3.29 PGSG20 incubated in PBS solution with lipase enzyme at 37 °C in 77 days showing full degradation.

polymers, the drug release profile is dependent on the degradation kinetics of polymeric matrix.[240,241] Therefore, the controllable and full biodegradation found in PGSGs is a great asset for their potential uses as biomaterials.

In vitro cell metabolic assay was conducted on PGSG0 and PGSG20 with resazurin dye and L929 mouse fibroblast cells for up to 15 days. Figure 3.30A and B show the morphology of L929 mouse fibroblast cells cultured for 15 days on PGSG0 and PGSG20 specimens. While the cells on both the PGSG0 and PGSG20 appeared to have normal and highly confluent cell populations, PGSG20 showed more adherent, embedded cell morphologies compared to PGSG0. This can be attributed to the better surface wettability of PGSG20, which was demonstrated previously.

No evidence in cytotoxicity was found in the PGSG0 and PGSG20. The cell metabolic activity of both PGSG0 and PGSG20 showed steady growth from day 3 to day 15 (Figure 3.31), with the maximum cell metabolic activity found on day 15 in both cases. The normalised optical density of resazurin dyes increased from 21.5 ± 2.5% to 38.1 ± 6.5% in PGSG0, and from 26.2 ± 5.2% to 42.1 ± 7.6% in PGSG20 from day 3 to day 15. Two-way analysis of

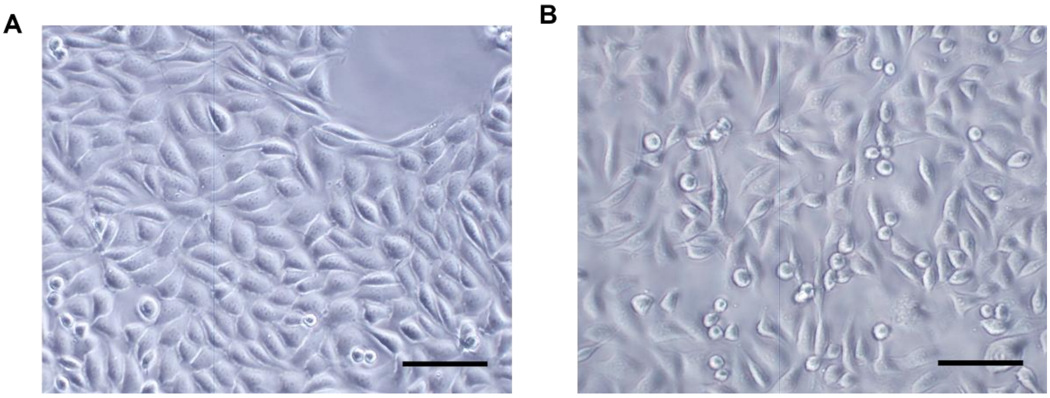

Figure 3.30 *In vitro* cell metabolic assay results. Optical microscopic images show the cell morphology of L929 fibroblasts cultured on PGSG0 and PGSG20 for 15 days; (A) PGSG0 and (B) PGSG20 (scale bars: 50 μm).

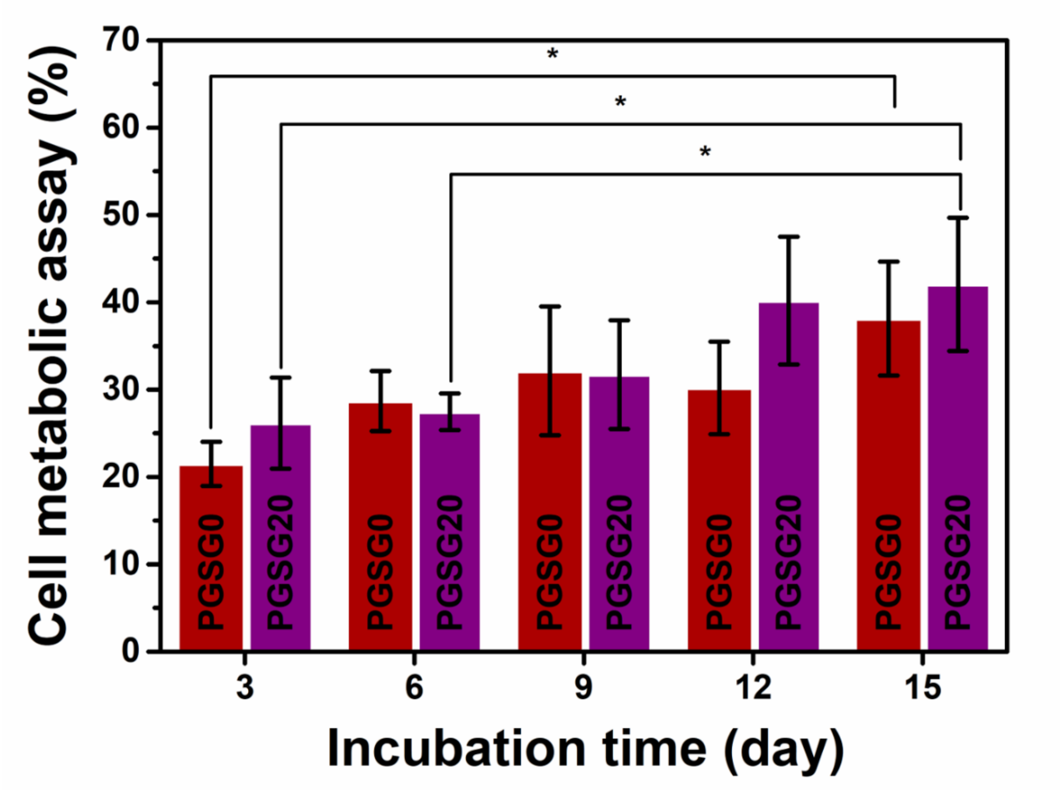

Figure 3.31 The normalised optical density from the resazurin assays of PGS and PGSG20 from 3 to 15 days, demonstrating no cytotoxicity observed for PGSG20 (n =3; * $p < 0.05$ was considered to be statistically significant).

variance (ANOVA) was used to determine the statistical significance in respect to the test time and material. Both the PGSG0 and PGSG20 were found to have a significant increase between day 3 and day 15. PGSG20 also presented another significant increase between day 6 and day 15. There was no statistical significance between PGSG0 and PGSG20 in cell metabolic activity, indicating PGSG20 has similar biocompatibility to PGSG0 (PGS homopolymer) *in vitro*. Since PGS has been investigated for various tissue engineering applications due to its well-known good biocompatibility both *in vivo* and *in vitro*,[9,11,16,165] the result suggests that PGSG20 also has great potential in various biomedical fields with its demonstrated biocompatibility in this test. Full assessment on biodegradability and biocompatibility of PGSG hydrogels, which are critical aspects in developing biomaterials for tissue engineering and drug delivery, should be performed with *in vivo* experiments in the future.

3.4 Conclusion

In this chapter, PGSG copolymer hydrogels with different weight ratios between PGS pre-polymer and gelatin were successfully prepared by condensation copolymerisation followed by swelling in water; the PGS pre-polymer was thermally crosslinked by gelatin during the copolymerisation stage. FTIR studies confirmed that the thermal crosslinking stage induced both ester and amide linkages between the polymers by using the inherent functional groups such as hydroxyl, carboxyl, and amine groups present in both polymers. The improved hydrophilicity of PGSG was determined by the decrease in water contact angle and the increase in water swelling ratio, resulting in the swollen copolymer hydrogels.

Tensile test results showed that the PGSG copolymer hydrogels had excellent elastomeric properties that endure high and complex mechanical deformations such as stretching and knotting. Their biomimetic mechanical properties were tunable in the range of soft tissues by varying the gelatin content in PGSG copolymers. The potential use of PGSG copolymers in soft tissue engineering was further demonstrated by the possibility of manufacturing a 3D, elastomeric, and interconnected porous scaffold.

The pH-responsive behaviour of PGSG copolymers was analysed by the dramatic differences in water uptake at acidic, neutral and basic pHs due to the ionisable functional groups found under FTIR studies. The potential of PGSG copolymers as a pH-controlled drug delivery system was also validated by pH-responsive drug release tests. The controllable and full biodegradation of PGSG was shown by biodegradation tests *in vitro* with lipase and collagenase enzymes. The biocompatibility of PGSG was confirmed, with no evidence in cytotoxicity by cell metabolic assay as well as highly confluent, well adherent morphology of cultured fibroblast cells.

These results suggest that the multifunctional PGSG copolymer hydrogels created in this study have great prospective in various biomedical fields such as soft tissue engineering and controlled drug delivery.

Chapter 4 On the modulation of the physical properties of biocompatible poly(glycerol sebacate)-based polyurethane-clay nanocomposite hydrogels

4.1 Introduction

The widespread use of elastomers in medicine relies on their ability to simulate the viscoelasticity of soft body tissues. Various elastomers have been extensively studied in this realm. Elastomers from natural sources such as elastin, elastin-like peptides, and silk-elastin-like protein polymers exhibit excellent biocompatibility and biomimetic mechanical properties.[19,35,120] However, these natural polymers suffer from their sourcing, reproducibility and undesirable immune responses *in vivo*.[120–122] Synthetic elastomers provide a number of advantages in respect to engineering material properties in a more predictable and reproducible manner. A wide range of physical and chemical properties can be finely tuned for synthetic polymers based on the choice of monomers, reaction condition, and copolymerisation.[123]

Among those, biocompatible PU elastomers have been widely explored in the medical fields with their tunable mechanical properties especially for the soft tissue applications.[45,242] Generally, the synthesis of PUs is performed by various polyols, isocyanates, and chain extenders.[121] A great flexibility in controlling properties of PUs is achieved by the chemical ingredients and stoichiometry. The desired mechanical behaviours, swellability, and surface physiochemistry can be engineered to meet the needs for the specific healthcare applications. Furthermore, biodegradable PUs can be prepared by choosing a biodegradable polyester as a component for their potential *in vivo* applications in tissue engineering, wound healing, and drug delivery.[121,243–245]

As a biodegradable polymer, PGS has been widely explored in soft tissue applications such as tissue engineering,[13,19,138,246] wound healing,[165,247] surgical sealants,[167] and post-operative adhesion barriers,[168] due to its soft tissue-like mechanical properties and good biocompatibility.[248] The mechanical property of PGS can be altered by the crosslinking density which can be controlled by the curing time and temperature, as well as the molar ratio of monomers.[22,23,25] However, higher modulus and strength values from a higher crosslinking density in PGS is made by drastically compromising stretchability of PGS. As soft tissues are supposed to be exposed to large deformation under complex mechanical stress,[249] both good toughness and stretchability are required in elastomers for soft tissue applications. PGS also has a poor water sorption ability with a hydrophobic surface and minimal water swelling ratio.[250] Since water mediates transportation of desired chemical species as well as the cellular activity,[118] this poor hydration property can limit a wider application of PGS in medicine. Furthermore, it is necessary to modulate the biodegradation rate of PGS for designing implantable medical devices such as tissue engineering scaffolds and drug delivery carriers.[42,240]

Therefore, the aim of this study is to develop a new elastomeric hydrogel system of PGS-polyester-based PU-clay nanocomposites (PEUCs) with a range of desired properties for various soft tissue applications. We hypothesized that the addition of a montmorillonite clay would benefit the design of PEUCs with tunable mechanical, sorption, and biodegradable properties, with the high surface area, swellability, mechanical strength, and catalytic behaviour of clay.[251–254] An organically modified montmorillonite clay, Cloisite 30B, was used. The good compatibility of organophilic Cloisite 30B with polymers can provide high homogeneity of clay dispersible within the polymer matrix, which dictates the properties in the resulting nanocomposites.[251,255] The PGS pre-polymer was used as a macromolecular polyol segment with its hydroxyl groups which enable the formation of urethane linkages with an isocyanate, as well as its proven biocompatibility and biodegradability.[9,44,45] An aliphatic isocyanate, hexamethylene diisocyanate (HDI), was chosen not only for its wide application in biocompatible PUs but also for its capability to give good stretchability and flexibility compared to the aromatic isocyanates.[44,45,242] In addition, PEG was introduced as a hydrophilic diol chain extender to modulate the hydration and mechanical property.[244] PEG is one of the most used biomaterials and it has been approved for use in medical applications by the U.S. Food and Drug Administration (FDA), with its non-toxicity and non-immunogenicity.[44] The material structure and properties of PEUCs were analysed by electron microscopy, diffractometry, spectroscopy, and mechanical tests as well as water contact angle and swelling measurements. The drug loading and release properties were tested using three different dye molecules as model drugs. Biodegradability was investigated in a simulated body condition with lipase enzyme. Cytotoxicity was evaluated by cell metabolic assay *in vitro*, with the L929 mouse fibroblast cells. Finally, A *proof-of-concept* fabrication of 3-dimensional and elastomeric foam structure using the PEUC system was also investigated for its potential use in soft tissue applications such as tissue scaffolds and wound healing.

4.2 Materials and methods

4.2.1 Materials

Cloisite 30B (A montmorillonite clay containing 30 wt% of methyl-tallow-bis(hydroxyethyl)-ammonium surface modifier) was provided by Southern Clay Products and dried in a vacuum oven at 80 °C for 1 day prior to use. Tetrahydrofuran (THF) was purchased from Thermo Fisher Scientific. All other chemicals were purchased from Sigma-Aldrich. Water used in this study was prepared by double distillation.

4.2.2 Synthesis of the PGS pre-polymer

The PGS pre-polymer was synthesised by following the previously reported method.[9,26] An equimolar mixture (0.51 mol) of glycerol and sebacic acid was charged in a round-bottom flask and reacted at 120 °C for 72 h with continuous mechanical stirring (300 rpm) and a flow of nitrogen gas. A Dean-stark apparatus was used to help remove water vapour generated from polycondensation reaction. A pale-yellow and highly viscous resin of the PGS pre-polymer was acquired and stored in a glass desiccator with silica gel desiccant (Supelco, 2 – 5 mm in diameter) before use.

4.2.3 Synthesis of PEUCs

PEUCs were prepared by following a combined approach of solvent method and *in situ* polymerisation. A pressure resistant glass container (Duran® Pressure Plus) was used throughout the synthesis after being purged by nitrogen and sealed. First, HDI and PEG (with the number average molecular weight of 950 – 1050 g mol^{-1}) were reacted at 2:1 molar ratio (2.70 mmol and 1.35 mmol) in THF (10 mL) at 50 °C for 1h with tin(II) 2-ethylhexanoate catalyst (tin(II), 0.05% w/v) to prepare the NCO-terminated PEG.[44] It should be noted that this reaction can yield also a polymer through the linkage of PEG by HDI, instead of NCO-terminated PEG. Due to the highly reactive characteristics of NCO-groups, further study to identify the actual chemical structure was not performed here. As the final product will be thermosetting macromolecular network structure, this study focused more on having a full replacement of the hydroxyl groups from both PEG and the PGS pre-polymer into urethane bonds (based on the experimentally determined hydroxyl number of the PGS pre-polymer, discussed below), with the stoichiometric NCO:OH ratio of 1.0. Secondly, a mixture of the PGS pre-polymer (1 g) and the clay (0, 1, 2, 3, and 5 wt% of inorganic clay with respect to the total polymer precursors) was prepared in THF (10 mL) by mechanical stirring and ultrasonication for 30 min each in another container. In the third step, the NCO-terminated PEG in THF was added to the PGS pre-polymer/clay mixture in THF with 0.05% w/v of tin(II). The reaction between the NCO-terminated PEG and the PGS pre-polymer whilst the clay dispersed within was performed for 4 h at 50 °C. The chemical reaction scheme of the organic ingredients is shown in Figure 4.1. The reacted solution was then cast into polytetrafluoroethylene (PTFE) moulds in which the solvent was removed by evaporation first in a fume cupboard at room temperature and then in a vacuum oven at 40 °C for 1 day each. Finally, all the samples were saturated in a copious amount of ethanol thrice for 1 day in total, in which the un-crosslinked sol proportions were extracted and determined by the weight difference before and after the sol extraction (n = 3) on a 4-decimnal scale (Sartorius AG Germany M-power). Ethanol was

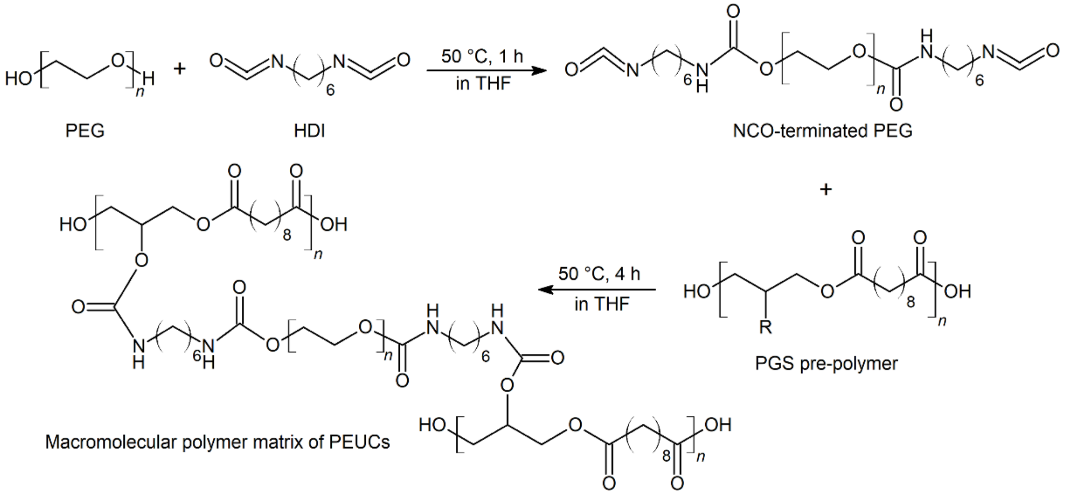

Figure 4.1 Chemical reaction schemes of polymer precursors forming macromolecular polymer matrix of PEUCs by urethane linkages.

removed by drying in a fume cupboard and then in a vacuum oven at 40 ° C for 1 day each before the test. The duration of ethanol extraction and subsequent drying of ethanol was determined based on the constant weight reads on a 4-decimal scale to remove the sol proportions and ethanol as much as possible. The prepared samples were named PEUCX, where “X” represents the weight percentage of the inorganic clay added with respect to the total polymer precursors; PEUC0, PEUC1, PEUC2, PEUC3, and PEUC5.

4.2.4 Characterisation of PEUCs

FTIR spectroscopy was performed on a PerkinElmer Spectrum One NTS analyser (500 – 4000 cm^{-1}, resolution: 2 cm^{-1}, number of scans: 16). A pressure of 70 N was applied on the specimens by a built-in screw to enhance the sample contact on the diamond ATR crystal.

TGA test was performed on the PerkinElmer Pyris 1 TGA, from 50 to 800 °C at 10 °C min^{-1} in a N_2 atmosphere.

XRD patterns were acquired on a STOE STAPI P (Cu Kα, $\lambda = 1.54060$, 40 kV, 35 mA, 2θ: 2.420 – 101.360, scan rate: 0.1°/sec). The cured PEUCs were cryo-milled by the SPEX Certiprep^{TM} 6850 Cryogenic Mill prior to the test.

SEM was conducted on a Philips XL 30S FEG at an accelerating voltage of 10 kV. The specimens were attached onto an aluminium tub by applying a Pelco$^{®}$ conductive silver paste (Ted Pella, USA), followed by gold coating using a high resolution polaron sputter coater (Emscope SC500A).

TEM was carried out on a FEI Tecnai T-12 at an operating voltage of 80 kV. A small specimen of PEUC3 was mounted on a Leica UC6/FC6 cryo-ultramicrotome, frozen *in situ* at -100 °C, and sectioned at ~90 nm using a Diatome cryo-P35 diamond knife. Sections were then collected and placed onto bare TEM copper grids and images were recorded using a Gatan Orius bottom mounted digital camera and using Gatan Digital Micrograph.

The surface water contact angle of PEUC specimens ($n = 3$) was measured by a Krüss DSA-100 drop size analyser. A droplet of water (10 μL) was dosed onto the specimen surface using a 22-gauge, blunt-end syringe needle. High-resolution images were captured after 10 seconds to perform the angle measurements.

Atomic force microscopy (AFM) study was performed on Veeco Dimension 3100 with tapping mode (scan rate: 1.00 Hz, tip velocity: 2.00 $\mu m\ s^{-1}$).

The water swelling ratio was determined gravimetrically. Disk-shaped PEUC specimens ($n = 3$, diameter: 5.3 mm, thickness: 0.50 ± 0.07 mm) were prepared by a punching utensil and dried for 1 day in a closed container with a silica gel desiccant and vacuum pump. The initial dry weight (W_{dry}) was then measured by a 4-decimal scale and the specimens were immersed in phosphate buffered saline (PBS, pH = 7.4) medium at the physiological temperature of 37 °C. At a regular time interval, the swollen specimens were taken out of the medium, blotted by a filter paper to remove the excess surface water, and weighed (W_{wet}). The swelling ratio was defined by eqn (4.1).

$$\text{Swelling ratio (\%)} = \frac{W_{wet} - W_{dry}}{W_{dry}} \times 100 \tag{4.1}$$

Quasi-static uniaxial tensile tests were performed on a Hounsfield H100KS (Tinius Olsen, USA) equipped with a 10 N load cell at a strain rate of 50 mm min^{-1} till failure according to ISO 527. The dog-bone specimens ($n = 6$, thickness: 0.31 – 0.46 mm) were prepared by a mould stencil (Ray-Ran Test Equipment). For the tensile testing of hydrated PEUCs (denoted as PEUC hydrogels herein) ($n = 6$, thickness: 1.20 – 1.50), the specimens were swollen in PBS media at 37 °C for 1 day and tested immediately after being removed from the media.

4.2.5 Drug loading and release tests

To study the drug loading and release behaviours of PEUCs, three dye molecules were used as model drugs; a cationic methylene blue (MB, λ_{max} = 664 nm), an anionic methyl orange (MO, λ_{max} = 463 nm), and a hydrophobic Solvent Green 3 (SG, λ_{max} = 639 nm). The disk-shaped PEUC specimens (n = 3, diameter: 5.8 mm, thickness: 0.44 ± 0.07 mm) were immersed in each dye solution (18.4 μM, 2.5 mL) and incubated at 37 °C, in PBS medium for MB and MO, or ethanol medium for SG. At a scheduled time interval, the solution was examined under an ultraviolet-visible spectrophotometer (UV-vis, Agilent Cary 60). After 96 hours, the maximum dye loading capacity for all dye types was achieved. The dye-loaded PEUC specimens were dried in a vacuum oven for 1 day at 37 °C. The dye-load ed PEUC specimens were then moved into a fresh medium (2.5 mL), in which the dye release profile was recorded. In a specific time interval, 1 mL of medium was collected and replaced by the same volume of fresh medium. The concentration of dye solutions was determined by pre-acquired calibration curves of each of the dyes with known concentrations of 0.1, 0.4, 0.7, 1, 4, 7, and 10 μg mL^{-1} (Figure 4.2–4).

4.2.6 Biodegradation tests

The degradation behaviour of PEUCs was analysed *in vitro* in a simulated body condition. Prior to the test, the disk-shaped PEUC specimens (n = 5, diameter: 10.1 mm, thickness: 0.50 ± 0.09) were sterilised in 70 % ethanol for 1 day and dried in a vacuum condition until constant weights were read. The specimens were moved into a test tube and immersed in PBS medium with or without the lipase enzyme (110 U L^{-1}). The enzyme concentration used in the test was defined based on the serum activity of lipase in healthy adults found in the literature (30 – 190 U L^{-1}).[215] The degradation medium was replaced daily to ensure the full enzyme activity. The test

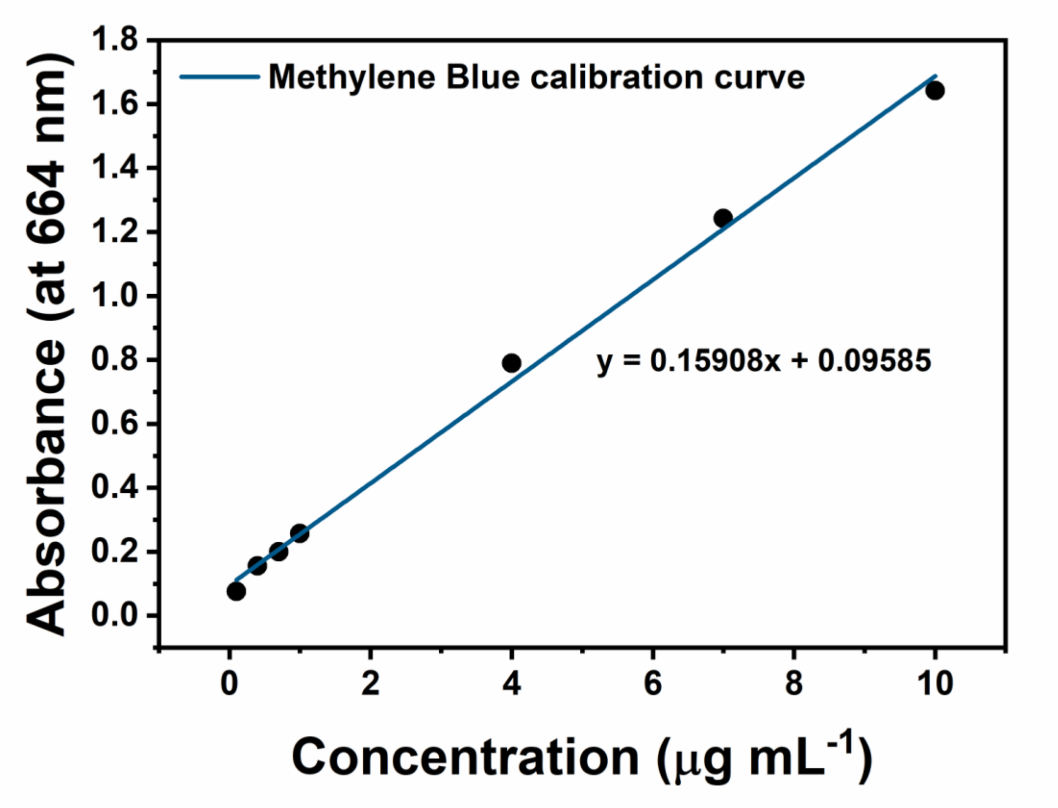

Figure 4.2 Calibration curves of MB acquired under UV-vis.

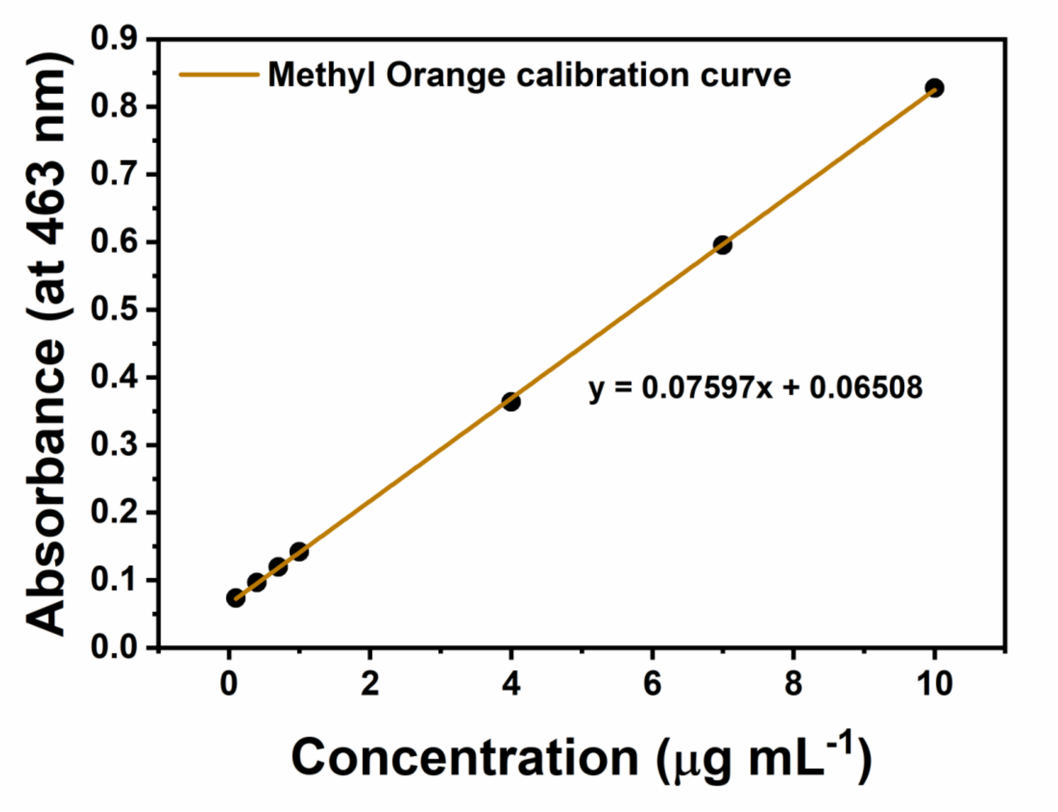

Figure 4.3 Calibration curves of MO acquired under UV-vis.

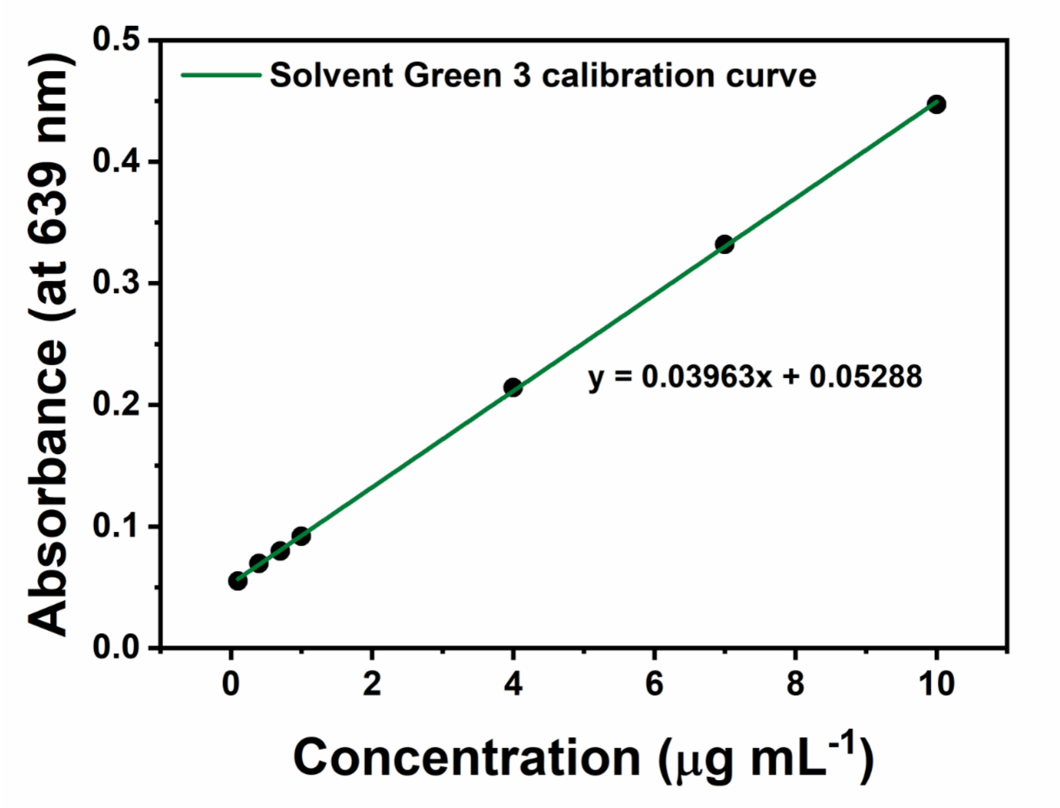

Figure 4.4 Calibration curves of SG acquired under UV-vis.

tubes containing the specimens were then incubated in a shaker incubator (Stuart SI500) at 37 °C and 100 rpm. At a regular time interval, the degraded specimens were removed from the PBS media, washed by a copious amount of water thrice, dried in a vacuum condition overnight, and weighed on a 4-decimal scale. The weight loss by degradation was calculated by the following eqn (4.2), where W_{ini} (53.9 ± 8.3 mg) and W_{day} are the initial weight before the degradation and the weight at a specific day, respectively.

$$\text{Weight loss (\%)} = \frac{W_{ini} - W_{day}}{W_{ini}} \times 100 \tag{4.2}$$

4.2.7 Biocompatibility tests

The biocompatibility of PEUCs was investigated *in vitro* by cell metabolic assay with resazurin *in vitro*. Prior to the test, all the specimens were sterilised in 70% ethanol, washed in water thrice, and soaked in DMEM (Dulbecco's Modified Eagle's Medium) overnight in an incubator (37 °C, 5% CO_2). The specimens were then moved into a 12-well plate and fixed by metal rings. L929 cell line (immortalised dermal mouse fibroblasts) was chosen according to ISO 10993 and also because of the fact that they are one of the most abundant cells found in connective tissues therefore relevant to the clinical applications such as wound healing and tissue engineering.[256] The cells were cultured in a DMEM 10% serum medium. After cell detachment by trypsinisation with trypsin-ethylenediaminetetraacetic acid, 5 mL of warm medium was added to neutralise the trypsin. The cells were then collected by centrifugation (1000 rpm, 5 min). A haemocytometer was used to obtain the optimal cell density (3.0×10^4 cells per specimen) by dilution in DMEM and the cells were seeded onto the PEUC specimens. After defined incubation days (3, 6, ,9, 12, and 15 days), the DMEM medium was removed from the well plate. The cell-seeded specimens were washed with PBS and placed in a new well plate. Subsequently, 1 mL of resazurin solution (0.1 mM) in PBS was added to each well. After 2 h of incubation, a colorimetric plate reader (Bio-TEK) was used to record the absorbance at 570 nm. The negative (cell-free) and positive (cell-only) tests were also carried out and used to normalise the data. The experiments were performed in triplicate. The cell morphology on the specimen surface was observed by an inverted optical microscope (Motic AE2000).

4.2.8 Fabrication and characterisation of the *proof-of-concept* PEUC foams

The PEUC0 and PEUC3 foams were fabricated by using water as a blowing agent. First, HDI and PEG (with a number average molecular weight of 950 – 1050 g mol^{-1}) were reacted at 2:1 molar ratio (2.7 mmol and 1.35 mmol) in 2 mL of THF at 50 °C for 1 h in the presence of Tin(II) (0.05 wt%) to synthesise the NCO-terminated PEG. Second, the mixture of 1 g of the PGS pre-polymer and 124 mg of Cloisite 30B clay (3 wt% of inorganic clay per total polymer) was prepared separately in 2 mL of THF by 30 min of ultrasonication. The NCO-terminated PEG and the PGS-prepolymer/clay mixture was mixed for 5 mins and the crosslinking was continued at 50 °C in an open PTFE mould for evaporation of solvent. To promote the bubble generation, additional 0.10 mL of water, 0.46 mL of HDI, and 0.20 mL of Span 80 surfactant were added. After the solvent was evaporated, the scaffold samples were collected from the mould, washed by ethanol thrice for 1 day, and dried again in a vacuum oven at 40 °C for 1 day.

The pore structure of the PEUC3 foam was examined under a Nikon SMZ800 stereoscopic zoom microscope. For the compression testing of the PEUC foams, cylinder-shaped specimens ($n = 6$, diameter: 10 mm, thickness: 3.42 – 4.66 mm) were prepared and tested at a strain rate of 50 mm min^{-1} till 75% strain compression on the Lloyd LRX mechanical testing machine equipped with a 50 N load cell.

4.2.9 Statistics

All measurements were reported as mean ± standard deviation with a confidence level of 95%, unless otherwise stated. One-way or two-way analysis of variance (ANOVA) was used where appropriate to determine the statistic differences in the results, followed by the Bonferroni post hoc test with the OriginPro 2018 software. A p value < 0.05 was considered to indicate statistical significance.

4.3 Results and discussion

4.3.1 Characterisation of the PGS pre-polymer

The PGS pre-polymer was synthesised by thermal polycondensation of glycerol and sebacic acid. Successful synthesis of the PGS pre-polymer was confirmed by the characteristic ester bond peaks under FTIR (Figure 4.5), and gel permeation chromatography (GPC, Agilent 1260 GPC system, with tetrahydrofuran as the eluent and polystyrene standards for calibration). The measured number average molecular weight ($\overline{M}_n$), weight average molecular weight ($\overline{M}_w$), and the polydispersity index (PDI) were 2035 g mol^{-1}, 6617 g mol^{-1}, and 3.3, respectively. Determination of the hydroxyl number of the PGS pre-polymer was also performed by colorimetric titration method following ISO 14900, for use in preparation of the polyester-based PU clay nanocomposites (PEUCs). Briefly, the PGS pre-polymer (n = 3) was acetylated by phthalic anhydride and the excess reagent was hydrolysed with water and the resulting phthalic acid was titrated by the NaOH solution (0.5 N) in the presence of phenolphthalein indicator. The hydroxyl number of the PGS pre-polymer was calculated by eqn (4.3),

$$\text{Hydroxyl number} = \frac{(V_b - V_s)\times 0.5\times 56.1}{w} \tag{4.3}$$

where V_b is the volume of NaOH solution required for titration of test samples, V_s is the volume of NaOH solution required for titration of the blank, 0.5 is the concentration of the titrant, NaOH solution, 56.1 is the molecular weight of NaOH, and w is the sample weight. The resulting hydroxyl number was 148.8 ± 2.9 mg of KOH g^{-1}, or 2.7 mmol of hydroxyl end group per 1 g of the PGS pre-polymer on average. Therefore, the NCO-terminated PEG with 2.7 mmol of free NCO groups were used to prepare PEUCs (discussed above), aiming a full

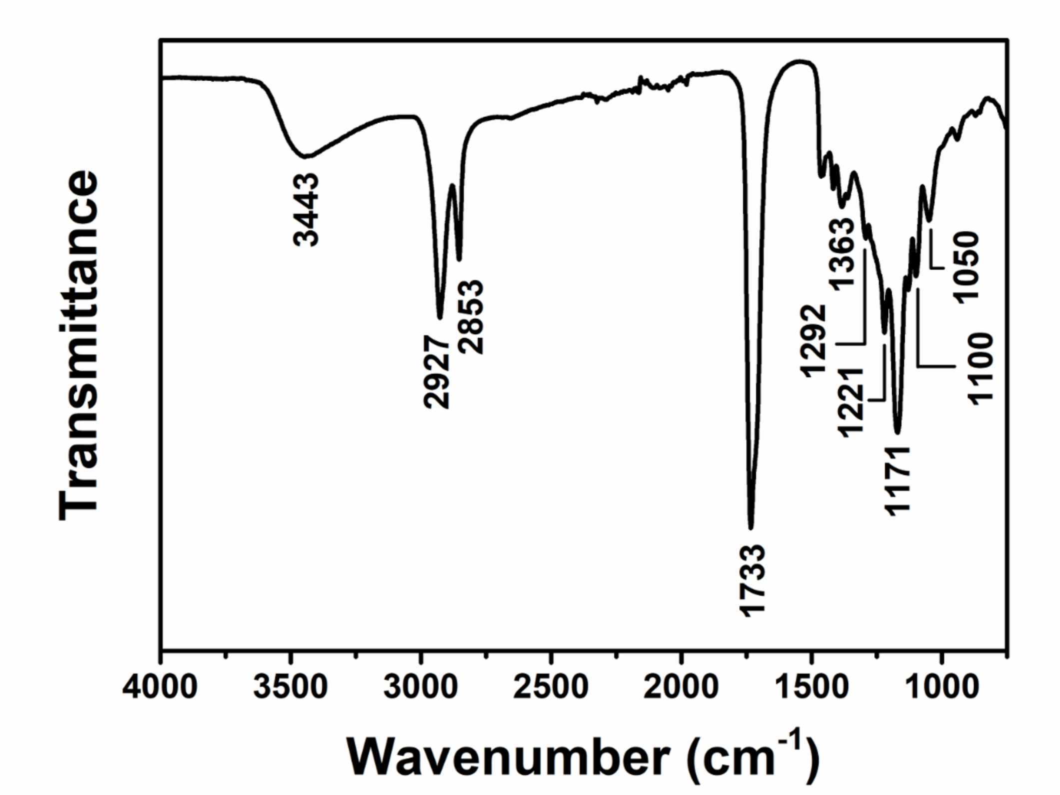

Figure 4.5 FTIR spectrum of the PGS pre-polymer. The broad peak at 3443 cm^{-1} is associated with the hydroxyl group from glycerol (O–H).[26,137] The peaks at 2927, 2853, and 1363 cm^{-1} are related to the alkane groups (–CH_2).[26,136,137] The intense peak at 1733 cm^{-1} and 1171 cm^{-1} are signature bands for the ester bond; C=O and C–O, respectively.[137] The distinct peaks at 1292, 1221, 1100, and 1050 cm^{-1} are also belong to the stretching vibration of C–O.[139]

conversion of the hydroxyl groups in the PGS-prepolymer into the urethane bonds.

4.3.2 Material characteristics of PEUCs

PEUCs with varying clay content (0 to 5 wt%) were synthesised in a three-step process as shown in Figure 4.6A; synthesis of the NCO-terminated PEG step, preparation of the PGS pre-polymer/clay mixture in THF step, and crosslinking step of the PGS pre-polymer and the NCO-terminated PEG by urethane linkages while the clay was dispersed within the polymer matrix.

The isocyanate functional groups (NCO) in the NCO-terminated PEG reacted with the hydroxyl groups in the PGS pre-polymer, forming a macromolecular by the urethane bonds. It should be noted that the organic surface modifier of Cloisite 30B contains hydroxyl groups which can react with the NCO-terminated PEG to form the urethane bonds. However, the amount is very small; 0.0 – 0.9 wt% in respect to the total polymer precursors. Thus, the reaction of the organic surface modifier in Cloisite 30B is neglected here. Under TGA, thermal degradation of organic modifier was not visible due to its very small amount (discussed later). There were also no absorption peaks of organic modifier under FTIR (discussed later). Moreover, the synthesis of PEUCs is based on THF solvent system, including total 5 hours of mechanical stirring and sonication, in which any un-bound organic surface modifier of Cloisite

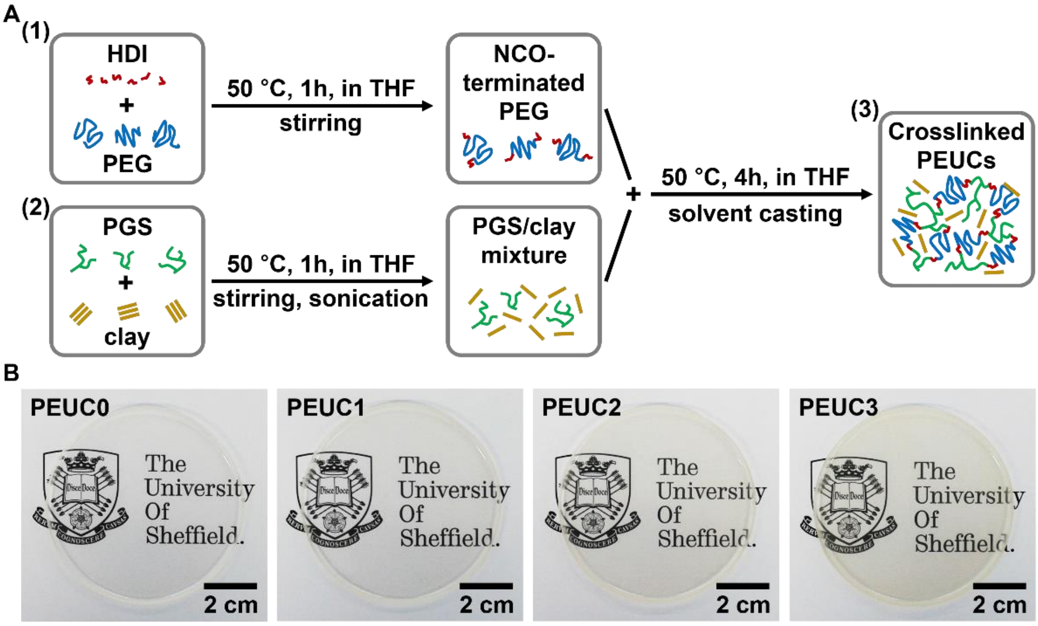

Figure 4.6 (A) Synthesis scheme of PEUCs; (1) synthesis of NCO-terminated PEG, (2) preparation of mixture of the PGS pre-polymer and clay in THF, and (3) crosslinking of the polymers by urethane linkage to produce PEUCs. (B) Photographs of the PEUC films with various clay contents, showing the optical transparency and macroscopic homogeneity.

30B would be solubilised due to its high organophilicity and lowering the concentration in the synthesis chamber, which further reduces the chance for it to be involved in the reaction. All the PEUC films showed their excellent transparency with a slight yellow tint by the addition of clay, which indicates the homogeneous dispersion of clay platelets throughout the polymer matrix (Figure 4.6B),[257] except PEUC5 with its visible clay agglomerates, hence not studied further here (Figure 4.7).

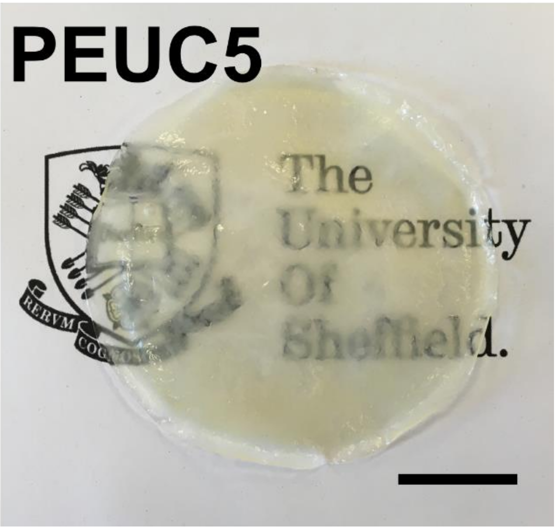

Figure 4.7 Photograph showing a PEUC5 films with visible clay agglomerates (scale bar: 2cm).

The compositions of PEUCs are shown in Table 4.1, columns 2, 3, and 4. It should be noted that the inorganic clay proportion of Cloisite 30B used in this study was evaluated to be 70.0 wt% by TGA (Figure 4.8), which is in agreement with previous reports.[258] After the synthesis of PEUCs, the un-crosslinked sol proportions ($W_{\text{un-crosslinked}}$) were extracted by ethanol and measured as shown in Table 4.1, column 5. The addition of clay resulted in a minor increase in $W_{\text{un-crosslinked}}$, which indicates that the formation of urethane linkages between polymer segments may have competed with either the physical bonding effect of clay between hydroxyl groups in clay and polymer, or the direct chemical crosslinking between clay and the PGS pre-

Table 4.1 Compositions of PEUCs

Sample	**NCO-terminated PEG (g)**	**PGS pre-polymer (g)**	**Cloisite 30B (g)**	$W_{\text{un-crosslinked}}$ **(wt%)**	$W_{\text{inorganic-clay}}$ **(wt%)**
PEUC0	1.80	1.00	0	23.5 ± 0.2	0
PEUC1	1.80	1.00	0.04	24.1 ± 0.5	1.32
PEUC2	1.80	1.00	0.08	24.6 ± 0.6	2.68
PEUC3	1.80	1.00	0.12	25.0 ± 0.3	4.12

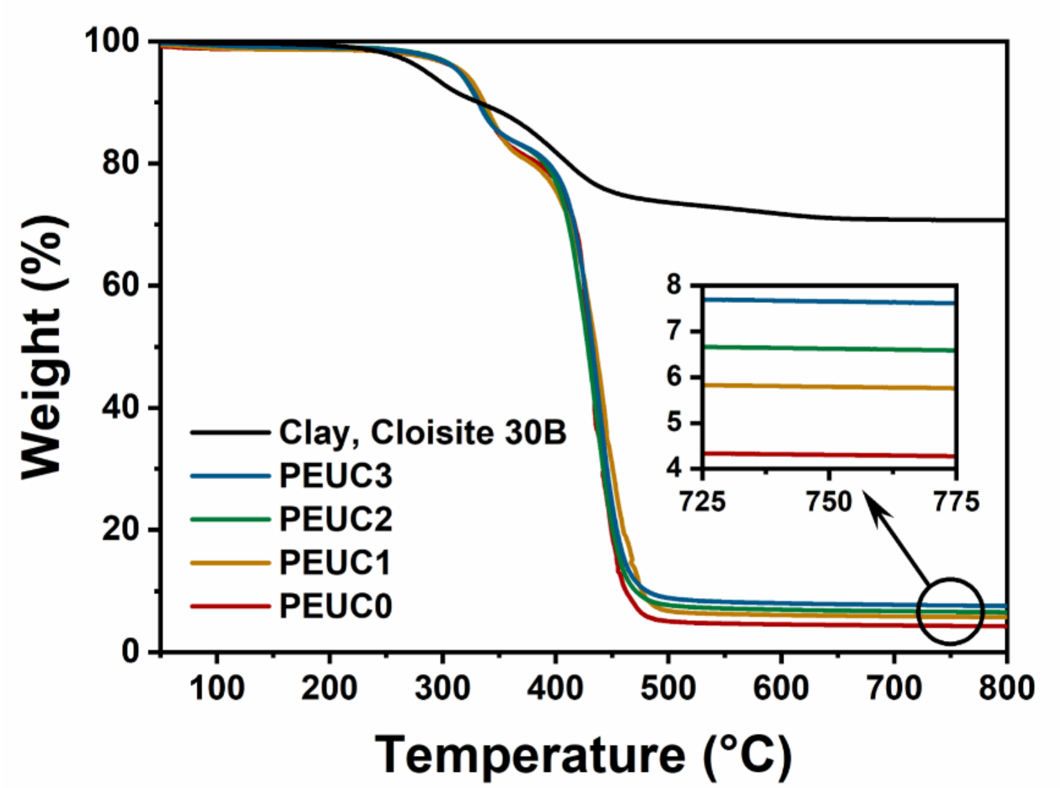

Figure 4.8 TGA of an organically modified montmorillonite clay used in this study, Cloisite 30B, and PEUCs with 4 different clay contents.

polymer.[46,259] The actual weight percentages of inorganic clay in PEUCs after the sol extraction are listed in Table 4.1, column 6. TGA confirmed the presence of clay within PEUCs. Increases in the residual weights after thermal decomposition up to 800 °C found as follows; 4.2% (PEUC0), 5.7% (PEUC1), 6.5% (PEUC2), and 7.5% (PEUC3) (Figure 4.8), confirming the loading of clay in PEUCs. The residual weights found in TGA are higher than $W_{\text{inorganic-clay}}$ in Table 4.1, column 6. This is possibly due to carbonaceous char formation under the TGA testing condition. All the nanocomposites did not exhibit the degradation of surface organic modifier of Cloisite 30B, due to its small amount as discussed above.

PEUCs were not dissolved but rather swollen in various solvents (acetone, dimethyl carbonate, dimethylformamide, dimethyl sulfoxide, ethanol, isopropyl alcohol, methanol, tetrahydrofuran, and water), confirming the formation of covalently crosslinked macromolecular structure. It should be noted that the amphiphilic swelling ability of PEUCs, as expected by their molecular components of hydrophobic PGS and hydrophilic PEG, makes them a novel drug carrier candidate for various drug types (discussed below).

The dispersion of clay layers in PEUCs was analysed under XRD. As shown in Figure 4.9, the (001) peak of pristine Closite 30B clay, disappears in PEUCs within the testing 2θ degree range, indicating increase in the clay interlayer spacing or full exfoliation of clay. We can see that there can be a peak indicating the increased clay interlayer spacing at a low angle region as the peak intensity rises with the addition of clay, yet the peak location cannot be seen in the current XRD pattern of the nanocomposites. Further XRD study in the low angle region is required to achieve the interlayer spacing changes of clay in the nanocomposites in the future. It should be also noted that the semicrystalline characteristic peaks of the PGS-prepolymer found under XRD disappeared after synthesis of PEUC nanocomposites (Figure 4.10),[139] suggesting inhibition of polymer crystallisation by formation of the covalently crosslinked

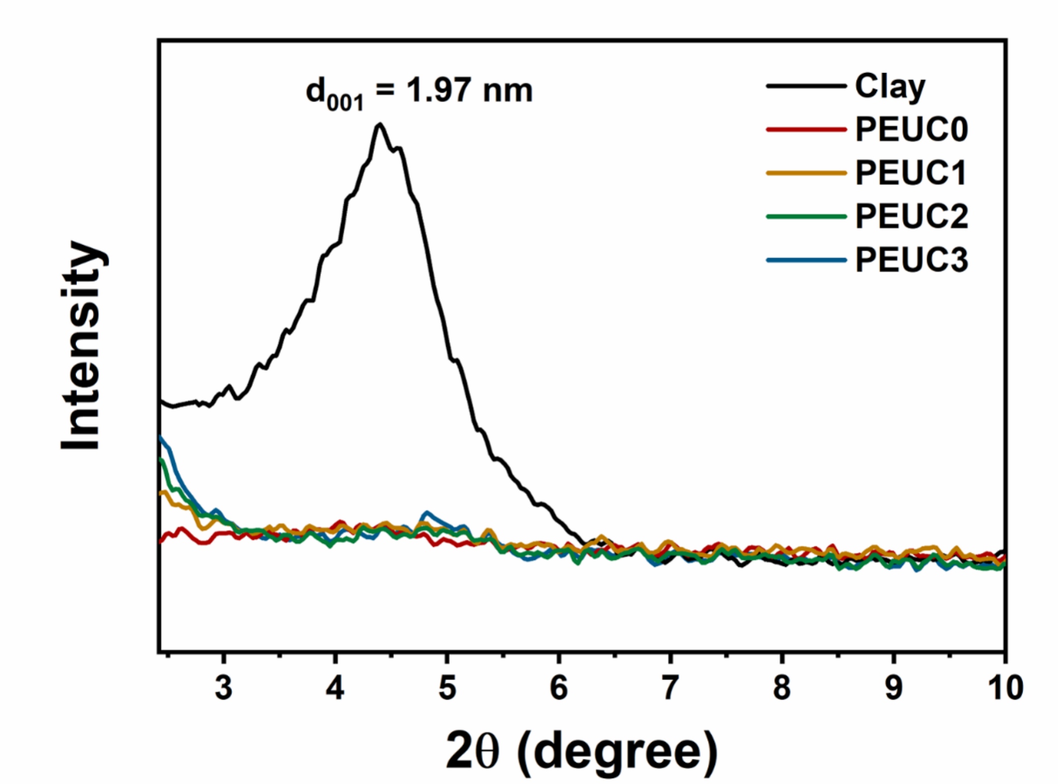

Figure 4.9 XRD patterns of the pristine clay (Cloisite 30B) and PEUCs. The absence of the original (001) peak of clay in the PEUCs within the test range demonstrates the clay dispersion by exfoliation/intercalation.

macromolecular structure in PEUCs. This is different from other PGS-based semicrystalline elastomers in the literature.[22,129,260] Stretchability and flexibility, which are important mechanical properties for soft tissue applications, can be further enhanced with this amorphous characteristic of PEUCs (discussed below).[261]

Post-functionalisation of amorphous polymers in general have higher absorption capacity with their greater degree of free space within polymer matrix than crystalline polymers.[262] Moreover, the fact that biodegradation of polymer preferentially occurs on amorphous region, leaving crystalline lamellar intact, suggests that the amorphous PEUCs can be utilised to design a fully biodegradable medical devices.[263]

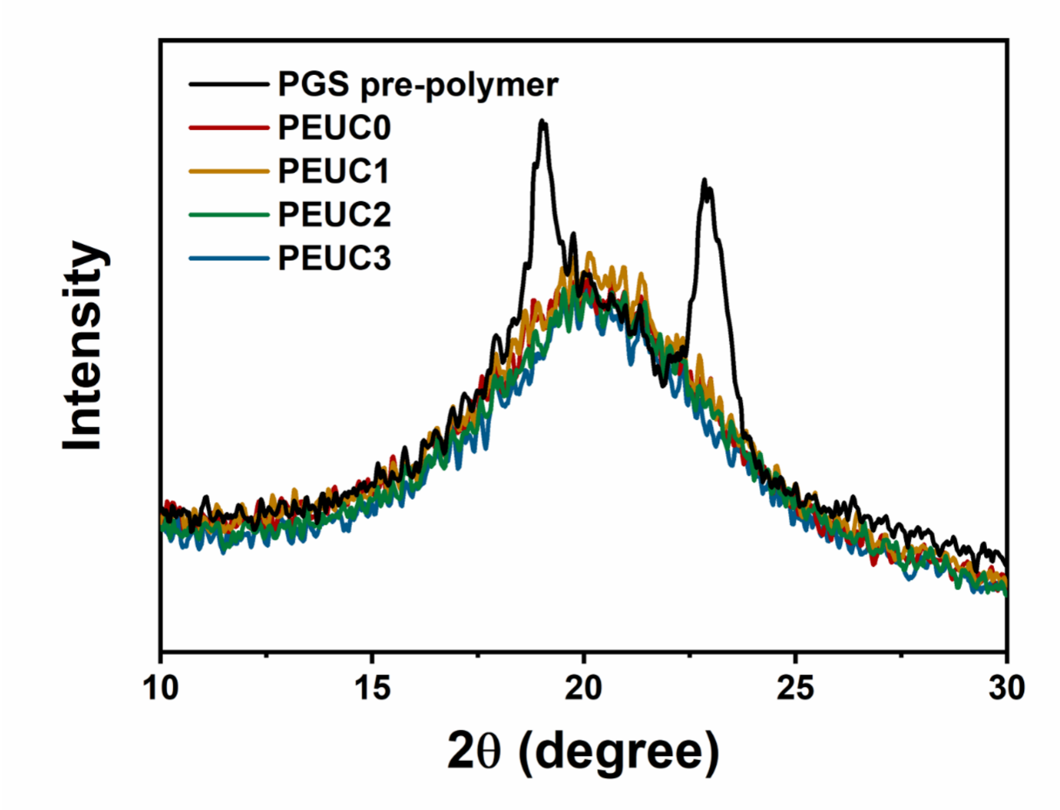

Figure 4.10 The XRD patterns of the PGS pre-polymer and PEUCs. The semicrystalline characteristic peaks of the PGS pre-polymer disappears after the fabrication of PEUCs.

Successful dispersion of clay within the polymer matrix of PEUCs was also shown under electron microscopy. Under SEM, some clay platelets are exposed at the cryo-fractured surface of PEUC3 (Figure 4.11). In Figure 4.12, the uniform distribution of clay platelets within the polymer matrix, either by intercalation and exfoliation, is affirmed under TEM. Figure 4.2D displays a closer look of intercalated clay platelets. The interlayer spacing of 3.47 ± 0.20 nm was measured by using ImageJ software (n = 20), compared to the 1.97 nm of pristine Closite 30B clay.

The chemical structure of PEUCs was examined under FTIR (Figure 4.13). The formation of urethane linkages was confirmed by the stretching vibration of N–H at 3333 cm^{-1}, the

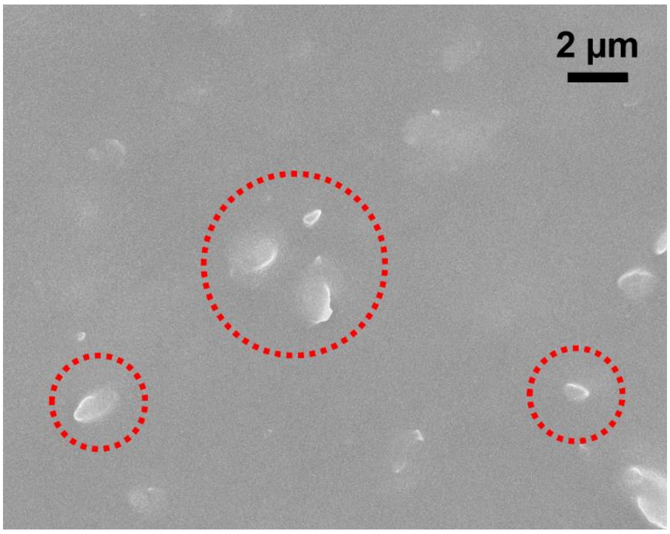

Figure 4.11 SEM micrograph shows the clay platelets exposed on the cryo-fractured specimen surface of PEUC3 (marked in circles).

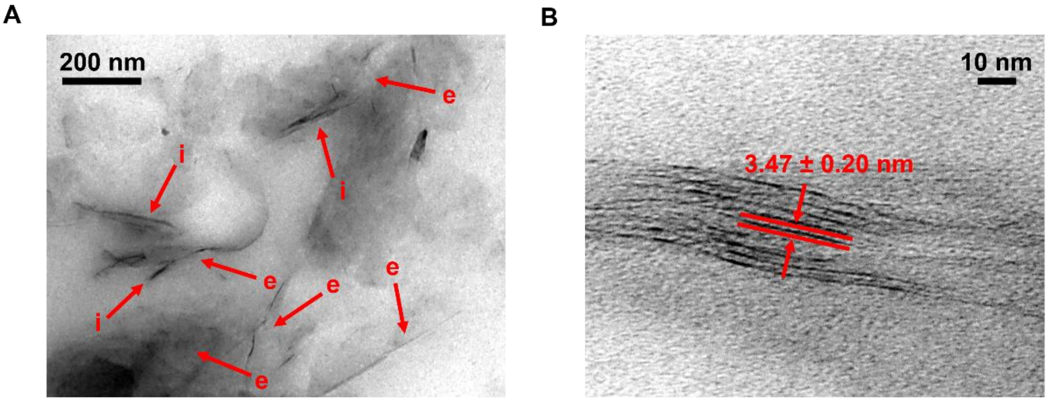

Figure 4.12 (A) TEM micrograph reveals the exfoliated (denoted by “e”) and intercalated (denoted by “i”) clay within PEUC3. (B) A higher magnification TEM image showing the increased interlayer spacing of clay. The average clay interlayer space was measured as 3.47 ± 0.20 nm (n = 20), confirming again the increased clay interlayer spacing by polymer intercalation.

stretching vibration of C=O at 1733 cm^{-1} (also partially originated from ester backbone of the PGS prepolymer), amide I (C=O stretching vibration) at 1624 cm^{-1}, amide II (N–H bending,

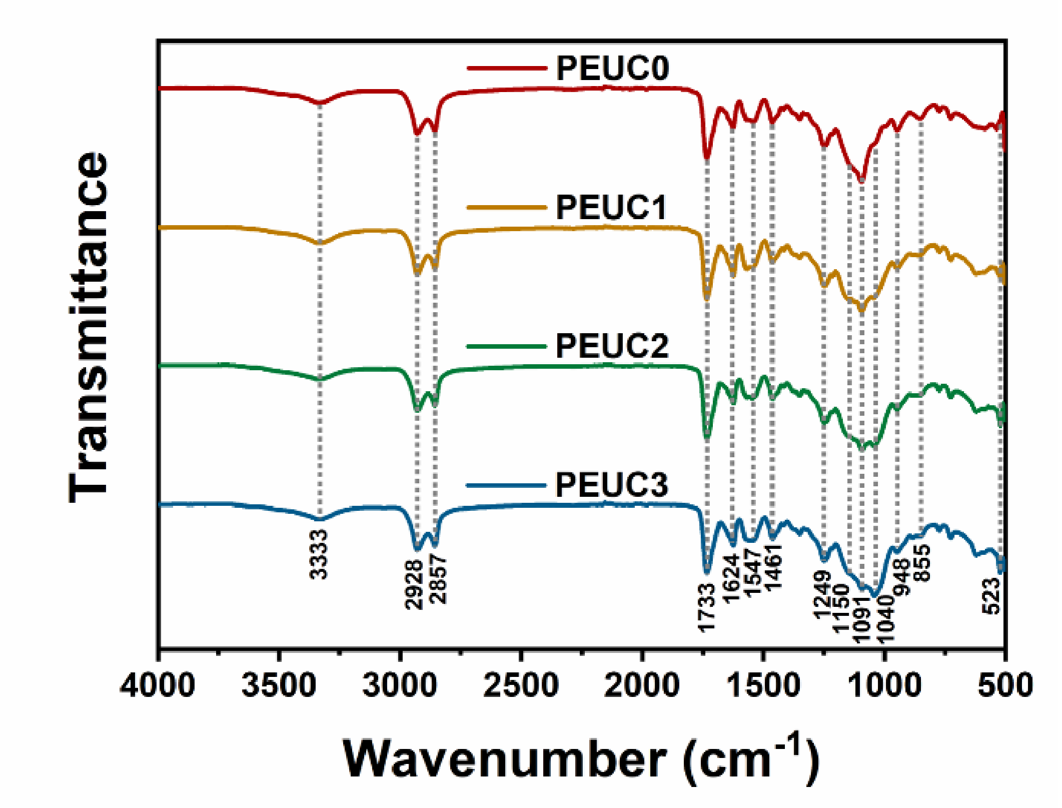

Figure 4.13 FTIR spectra of PEUCs. The spectra were shifted vertically for clarity.

C–N stretching, and C–C stretching vibration) at 1547 cm^{-1}, amide III at 1249 cm^{-1}, and amide IV at 845 cm^{-1}.[26,44–46,245] The ester bond peaks from the PGS pre-polymer are also at 1150 and 1091 cm^{-1} (C–O stretching vibration).[26] Stretching vibration of PEG-related C–O–C is at 948 cm^{-1}. The peaks at 2928 and 2857 cm^{-1} belongs to the stretching vibration of methyl and alkane groups.[26] The peak at 1461 cm^{-1} is due to the C–H bending vibration.[46] The peaks from Cloisite 30B are at 1040 (Si–O–Si asymmetric stretching vibration) and 523 cm^{-1} (Si–O–Al bending vibration).[255,264] The peak intensity of these peaks increases with the loading of clay from PEUC0 to PEUC3. The absence of O–H stretching vibration band at 3443 cm^{-1} (Figure 4.5) and characteristic peak of isocyanate group at 2250 cm^{-1} (Figure 4.14) in PEUCs confirms the complete reaction between hydroxyl groups in the PGS pre-polymer and isocyanate groups in HDI-PEG crosslinker. Under the FTIR study, the absorption peaks of the organic modifier of Cloisite 30B was not visible. Overall, FTIR study confirms that PEUCs are consisted of

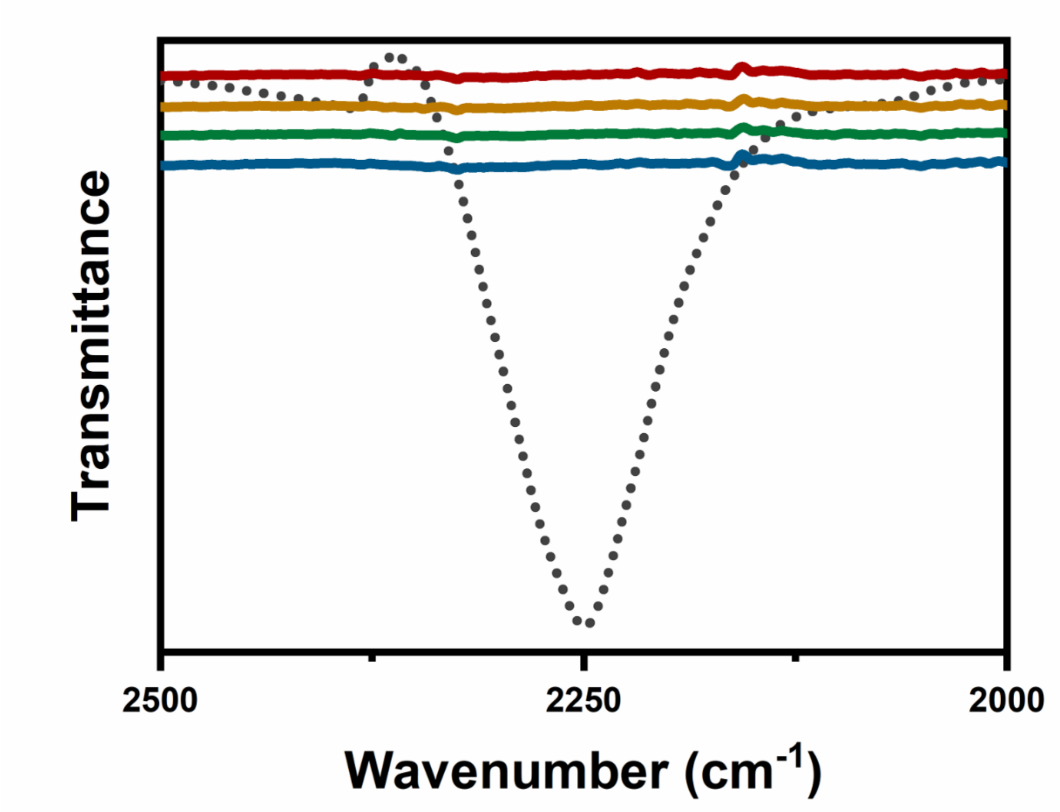

Figure 4.14 The FTIR spectra showing absence of the characteristic peak of HDI (grey dotted line) at 2250 cm^{-1} in PEUC specimens.[44] The coloured solid lines are from PEUC specimens and they were shifted vertically for clarity

urethane linkages and the existence of clay within the polymer matrix.

The surface hydrophilicity of PEUCs was determined by measuring the surface water contact angle as shown in Figure 4.15. It is generally considered that a surface is hydrophobic when its water contact angle is > 90° and is hydrophilic when the angle is < 90°.[265] PEUC0 exhibited a hydrophobic surface with a high water contact angle of 103.7 ± 3.4°. Despite the presence of hydrophilic PEG segments within the polymer network, the abundant hydrophobic aliphatic carbon chain segments from HDI (6 carbons) and sebacic acid (8 carbons) within the polymer matrix may have rendered a hydrophobic surface in PEUC0. The incorporation of clay improved the surface wettability, yielding a hydrophilic surface in PEUC3 with the lowest

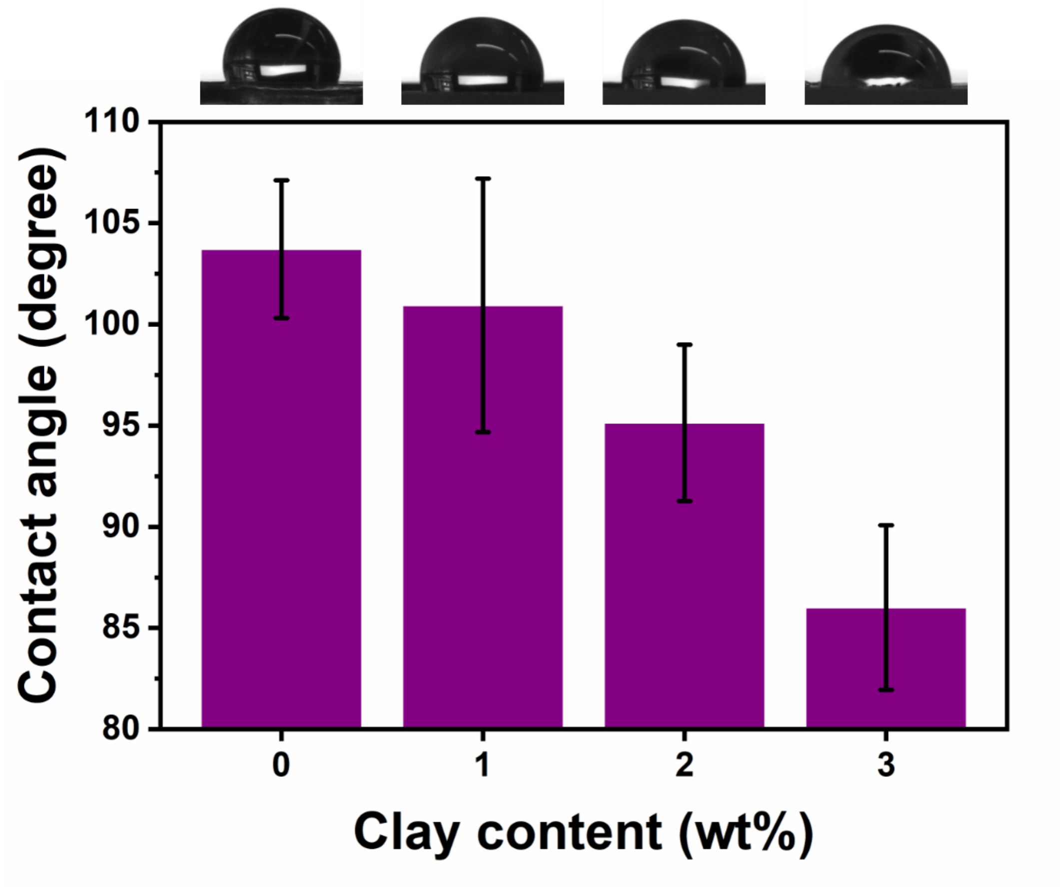

Figure 4.15 The surface water contact angle of PEUCs decreases with the addition of clay. The photographs above the graph show the shape of water droplets on the surface of PEUC specimens.

water contact angle amongst the PEUCs of 86.0 ± 4.1°.

One-way ANOVA test revealed the statistically significant differences in the water contact angles between PEUC0 and PEUC2, as well as between PEUC3 and all the other PEUCs. The better wettability found in PEUCs with the addition of clay is in part attributable to the increased surface roughness. The root mean square roughness of PEUCs, measured by AFM, increases from 203.7 nm (PEUC0) to 290.8 nm (PEUC3) (Figure 4.16). This change in surface roughness due to the presence of surface clay may reduce the water contact angle by forming favourably more interfacial area between water and clay surfaces, when the contact angle is

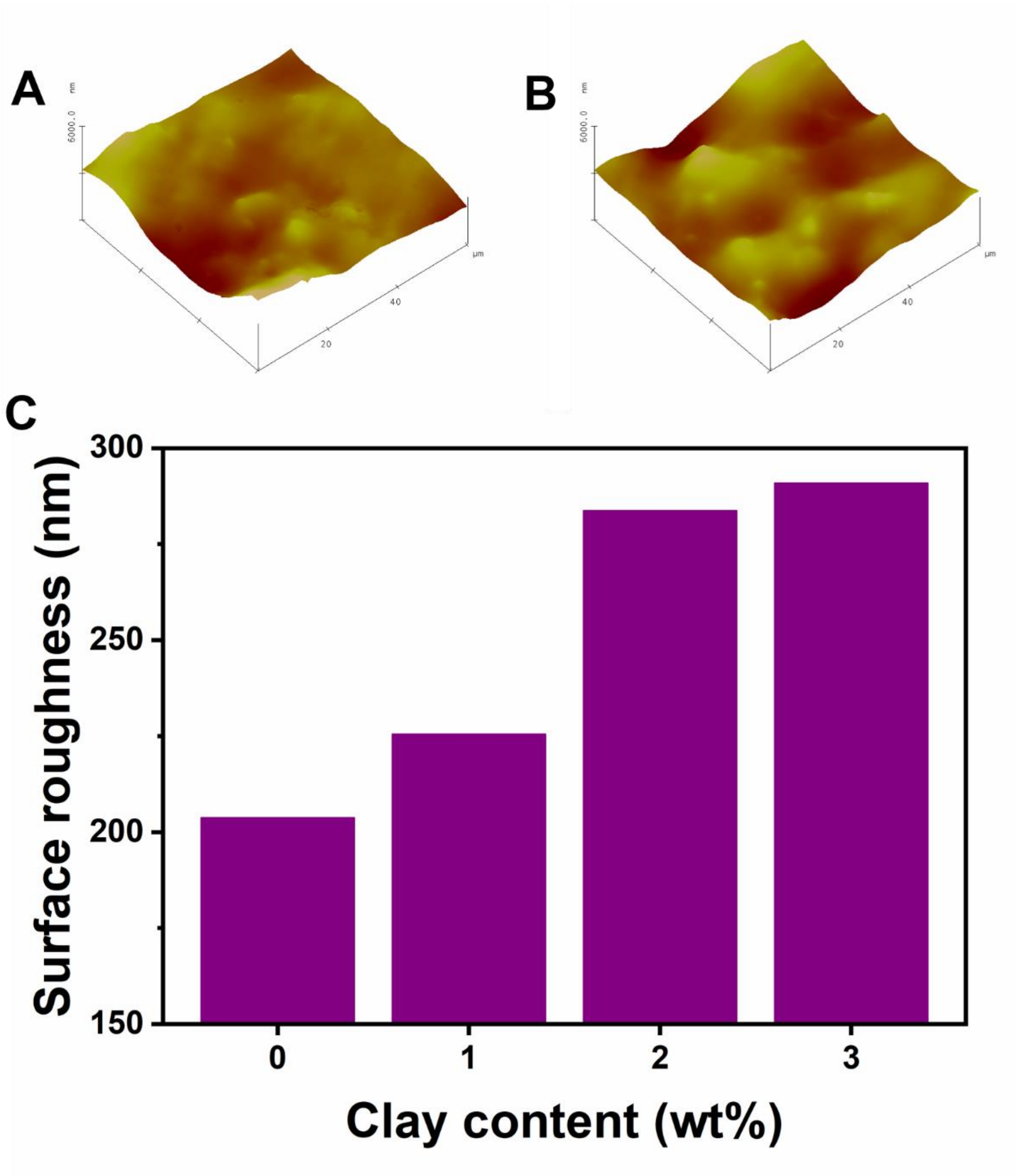

Figure 4.16 AFM study results on PEUCs. The surface topography of PEUC0 (A) and PEUC3 (B). (C) The root mean square (RMS) surface roughness were measured as 203.7 nm (PEUC0), 225.5 nm (PEUC1), 283.7 nm (PEUC2), and 290.8 nm (PEUC3).

not greatly higher than 90°.[266–268] Moreover, the uncrosslinked organophilic surface modifier of Cloisite 30B may have been removed during the solvent-based synthetic procedure of PEUCs and the washing procedure after synthesis, exposing hydrophilic surface of clays on PEUCs specimens.

This improved surface wettability of PEUCs is a beneficial property designing medical devices. For tissue engineering, cells are known to adhere and proliferate better on the hydrophilic surfaces than hydrophobic surfaces.[65,99] For wound healing applications, the better surface wettability means higher adsorption of the wound exudates, promoting the healing process.[218,219]

Bulk hydration property of PEUCs was determined by measuring water swelling ratio. With the hydrophilic PEG and swellable clay, PEUCs were designed to swell in water, resulting in PEUC hydrogels. As shown in Figure 4.17, all the PEUCs showed a rapid water uptake initially. In case of PEUC0, the equilibrium water uptake was achieved only after 4 h. Both PEUC1 and PEUC2 reached at equilibrium after 8h. However, PEUC3 required the longest time of 12 h to reach at equilibrium. The result suggests that the loading of clay in PEUCs resulted in a slowed

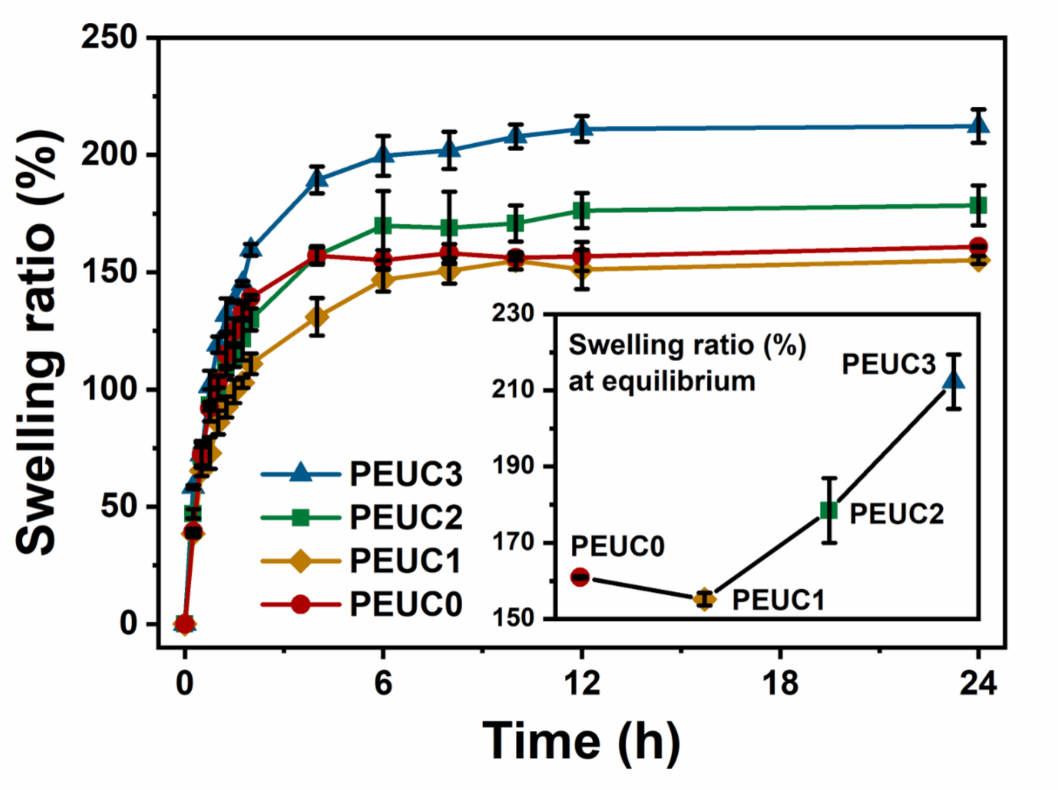

Figure 4.17 The percentage water swelling ratio of PEUCs (PBS, 37 °C) up to 24 h.

swelling kinetics. The clay swelling does not occur instantly at the contact with water and involves several different swelling phases and mechanisms.[269] Moreover, the clay in PEUCs was not free-swelling, but spatially surrounded by polymeric phases, requiring enough osmotic pressure to induce polymer chain relaxation.[270] The measured equilibrium water swelling ratios were 160.1 ± 0.3% (PEUC0), 155.2 ± 1.7% (PEUC1), 178.5 ± 8.5% (PEUC2), and 212.3 ± 7.2% (PEUC3), respectively.

It can be seen that the equilibrium water swelling ratio decreases from PEUC0 to PEUC1, then increases in PEUCs with higher clay contents. This is a consequence of the competition between the physical crosslinking effect and swellable characteristic of clay. PEUCs are consisted of chemically crosslinked polymer matrix by urethane linkages. Although it is limited due to the chemical crosslinking, the addition of clay may exert a small degree of physical crosslinking of polymers and restricts the free volume in polymer matrix for water molecules to permeate. At a higher clay content, however, the swellable characteristic of clay from its ionic surface dominates the physical crosslinking effects of clay, introducing more water into the composite matrices.[270,271] This controllable bulk hydration property of PEUCs can be utilised to design the swelling-controlled drug release devices.[272]

The swelling kinetics of PEUCs were analysed further by the Korsmeyer-Peppas power-law equation shown in the following eqn (4.4),

$$\frac{W_t}{W_{eq}}=kt^n \tag{4.4}$$

where W_t and W_{eq} are the water uptake at a specific time (t) and at equilibrium, respectively.[118,243] The k is a structural/geometric constant which identifies the swelling of polymer matrix. The n determines the type of water transport mechanism through the polymer matrix; (i) n = 0.5 for Fickian diffusion, (ii) $0.5 < n < 1.0$ for non-Fickian diffusion, (iii) $n \geq$

1.0 for the polymer chain relaxation controlled diffusion, and (iv) $n < 0.5$ for less-Fickian diffusion.[243,273] This equation is used for thin film polymer samples and valid for the initial swelling data ($W_t/W_{eq} \leq 0.6$).

The calculated n values of PEUCs were 0.66 (PEUC0), 0.54 (PEUC1), 0.53 (PEUC2), and 0.53 (PEUC3) (Figure 4.18), indicating non-Fickian diffusion. In this diffusion mode, both the water diffusion rate and polymer relaxation rate control the overall water swelling of materials. Non-Fickian diffusion mechanism is often explained by "lumped models" in which swelling is essentially localised separating un-swollen glassy phases. This was expected as PEUCs are amphiphilic and consisted of both hydrophilic PEG and hydrophobic PGS segments.[274]

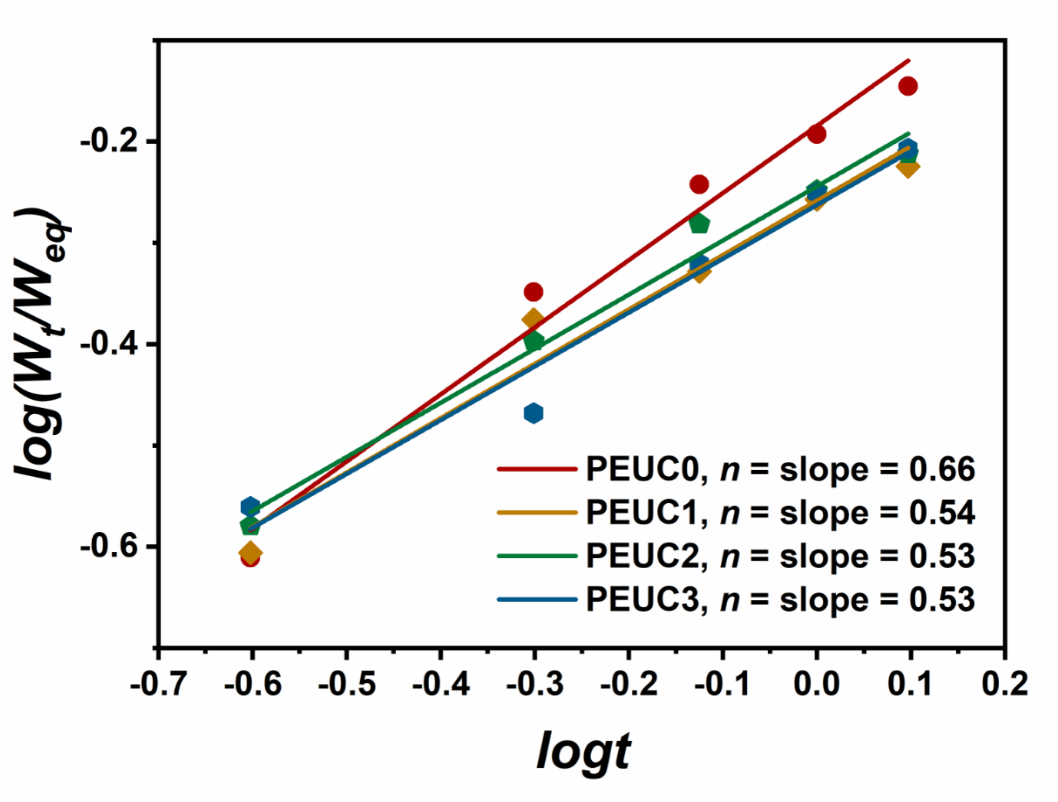

Figure 4.18 The swelling ratio of PEUCs fit to the Korsmeyer-Peppas power-law expression, with the n values shown by the slope of the fitting curves.

4.3.3 Mechanical strengthening and toughening by clay

The mechanical properties of PEUCs were evaluated by tensile tests and the parameters are listed in Table 4.2.

Table 4.2 Tensile properties of PEUCs

	Sample	**Young's modulus** E **(MPa)**	**Ultimate tensile strength** $\sigma_{\max}$ **(MPa)**	**Elongation at break** ε_{tb} **(%)**	**Energy at break** T **(MJ m^{-3})**
Dry	PEUC0	0.48 ± 0.01	0.77 ± 0.04	353 ± 22	1.57 ± 0.17
	PEUC1	0.67 ± 0.02	1.51 ± 0.10	394 ± 22	3.26 ± 0.34
	PEUC2	0.83 ± 0.05	2.21 ± 0.35	459 ± 47	5.20 ± 0.93
	PEUC3	0.82 ± 0.02	2.64 ± 0.33	529 ± 44	6.99 ± 1.29
Hydrogel	PEUC0	0.16 ± 0.01	0.29 ± 0.03	385 ± 38	0.29 ± 0.05
	PEUC1	0.19 ± 0.01	0.38 ± 0.03	446 ± 23	0.94 ± 0.09
	PEUC2	0.25 ± 0.02	0.44 ± 0.02	533 ± 25	1.38 ± 0.10
	PEUC3	0.38 ± 0.02	0.51 ± 0.02	574 ± 44	1.92 ± 0.25

As shown in Figure 4.19 and 20, all the PEUCs exhibited elastomeric mechanical behaviours. The energy at break values, which is energy that specimen has absorbed up to point of failure, were calculated by the area under the tensile stress-strain curves from the test start to the failure. Clay in PEUCs significantly improved all the tensile parameters and mechanical

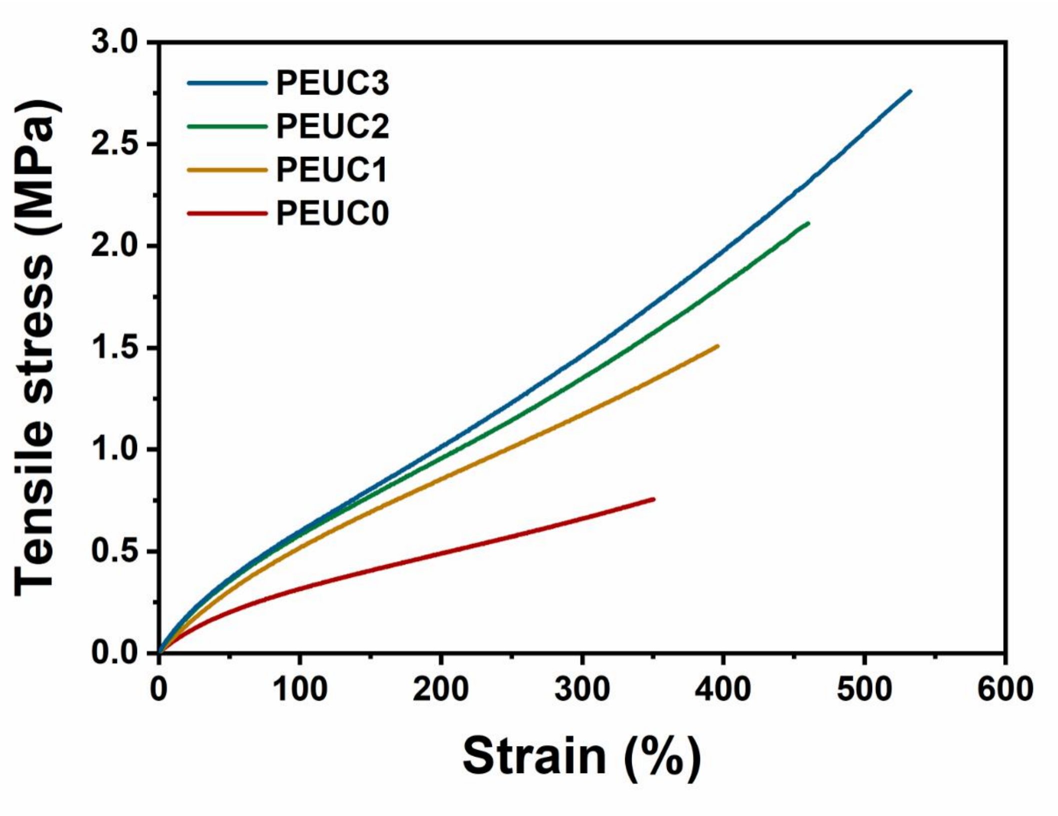

Figure 4.19 The representative tensile stress-strain curve of dry PEUCs.

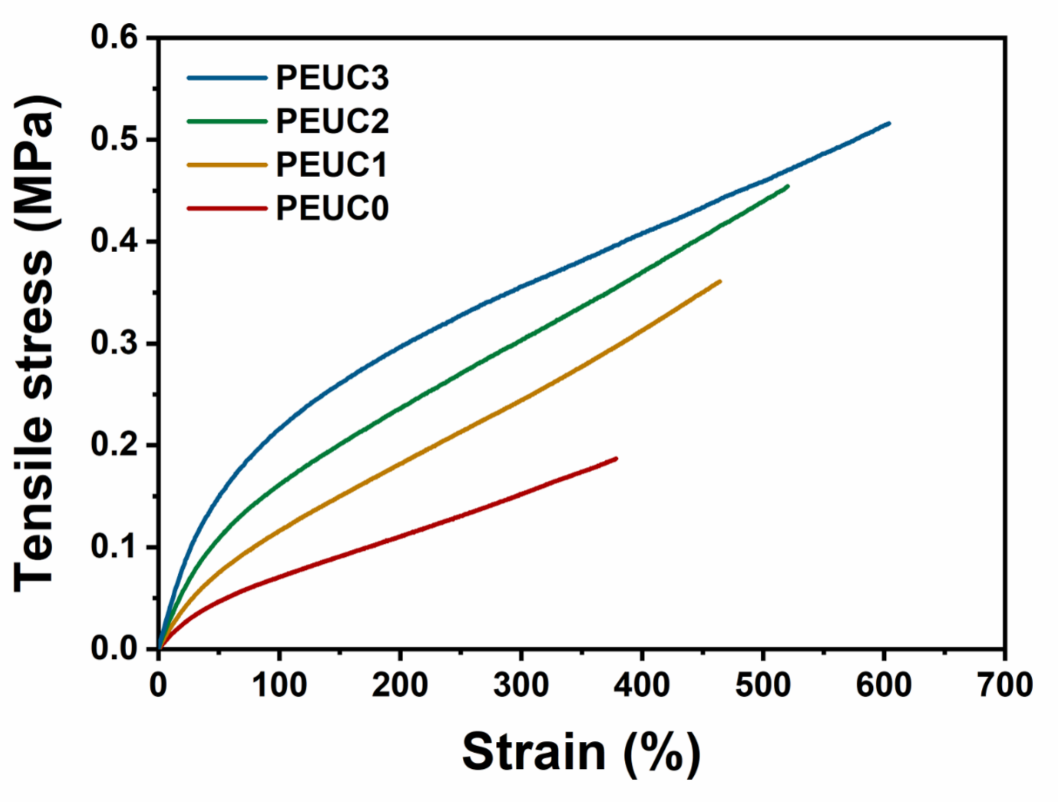

Figure 4.20 The representative tensile stress-strain curve of PEUC hydrogels.

performance, with increasing stiffness, strength, elongation at break, and energy at break from PEUC0 to PEUC3. In case of dry PEUCs, the increase between PEUC0 and PEUC3 was by 140% for Young's modulus, 164% for tensile strength, 59% for the elongation at break, and 373% for the energy at break (Figure 4.21).

In respect to the hydrated PEUC hydrogels, the increase between PEUC0 hydrogel and PEUC3 hydrogel was by 70% for Young's modulus, 242% for tensile strength, 50% for the elongation at break, and 346% for the energy at break (Figure 4.22). The lower tensile modulus and strength and the higher elongation at break found in PEUC hydrogels compared to the dry samples are primarily due to the polymer chain relaxation by swollen water, where the water permeates through the polymer matrix by breaking the polymer-polymer interactions such as dispersion forces and hydrogel bonds. This provides higher polymer chain flexibility. With the

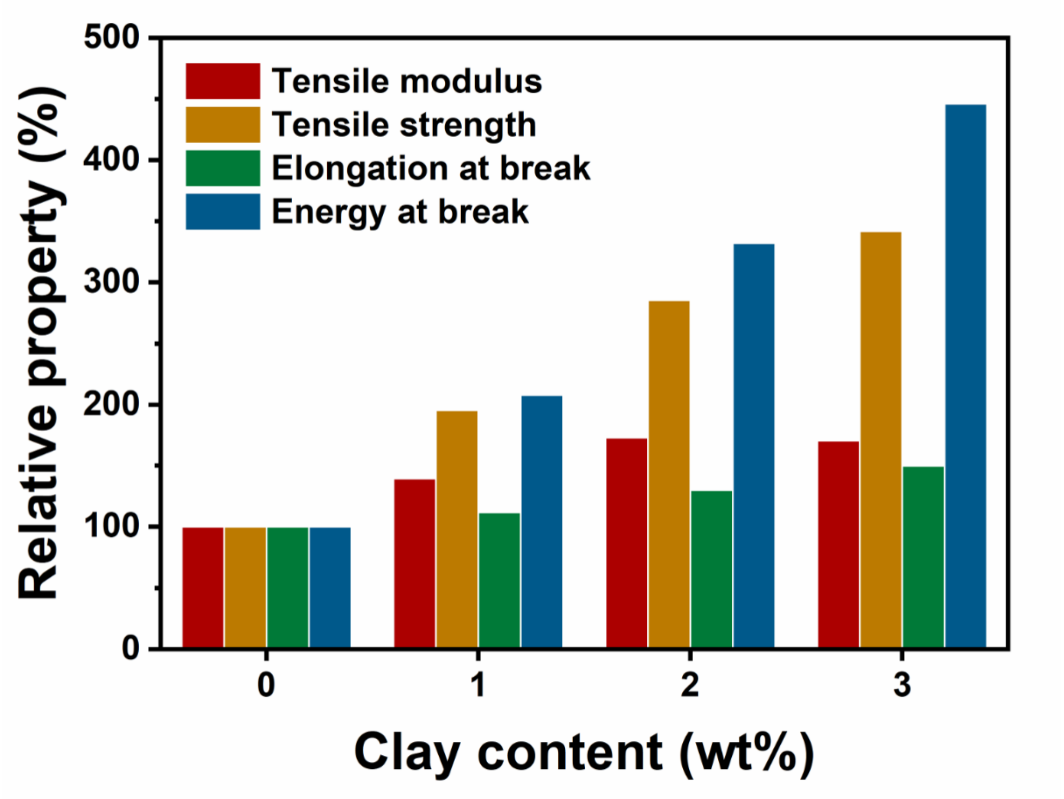

Figure 4.21 The relative tensile parameters of dry PEUCs, where the parameters of PEUC0 are 100%

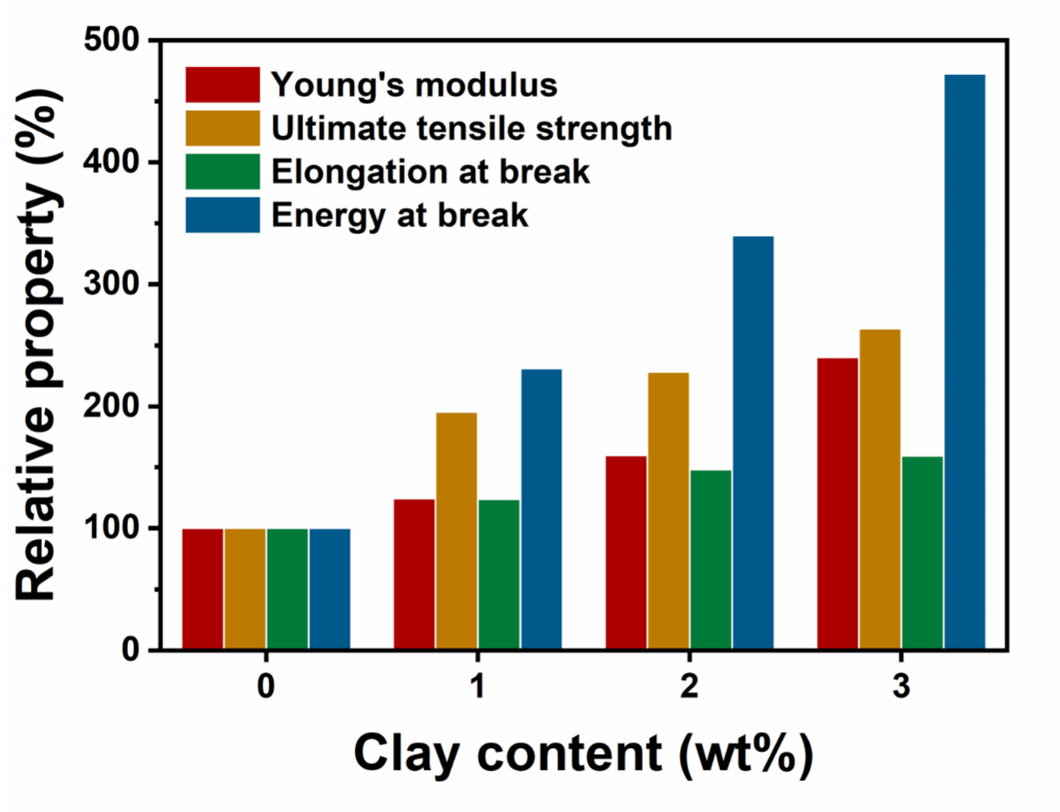

Figure 4.22 The relative tensile parameters of PEUC hydrogels, where the parameters of PEUC0 are 100%

excellent elastomeric properties improved by clay, complex mechanical deformations such as stretching and knotting were possible with PEUC3 hydrogel specimens even in the fully hydrated state as shown in Figure 4.23.

In general, higher crosslinking densities in polymer yield higher stiffness and strength by compromising the stretchability with the reduced chain flexibility.[275,276] The unusual improvement in all the tensile parameters in PEUCs indicates the strong interaction between the clay nano-layers and polymer matrix, transferring the load from the polymer matrices in PEUCs to the rigid clay platelets.[275] In addition, this concordance increase in the modulus, strength, and elongation at break can be explained by elastomeric macromolecules adsorbed on the surface of clay uncoil and stretch at higher stress levels, providing an additional deformation source.[60,149,277] A nano-filler with a great specific surface area, such as

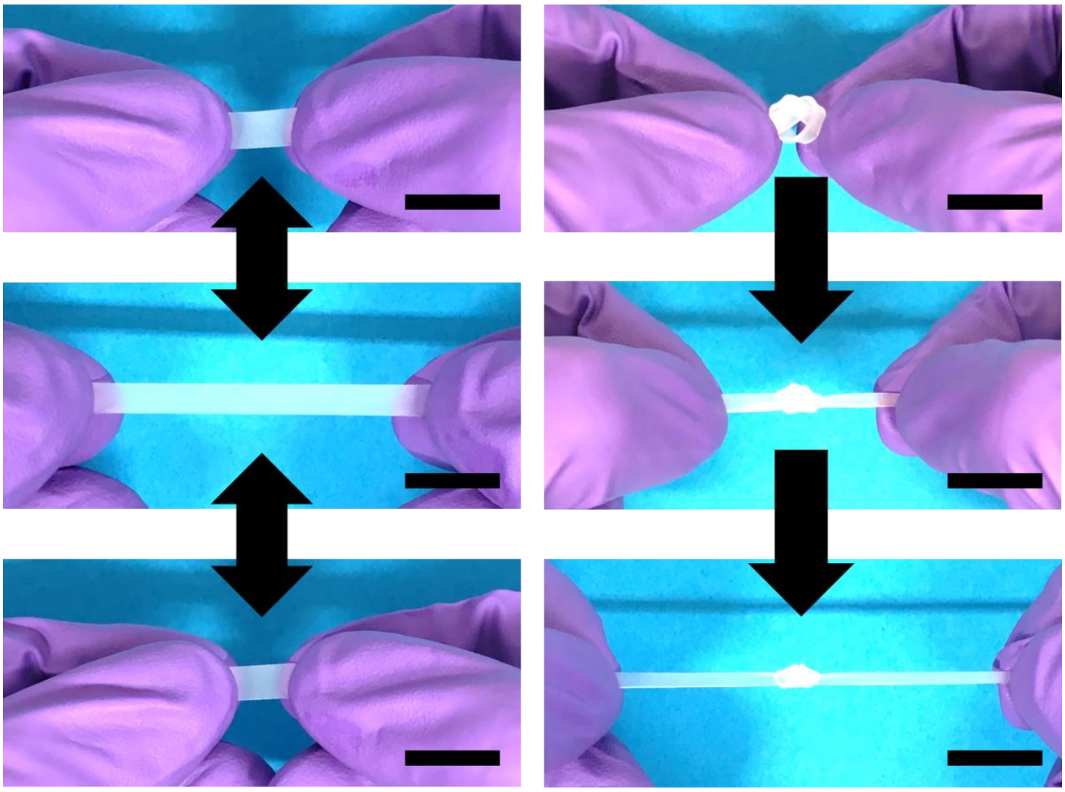

Figure 4.23 Demonstration of mechanical deformation (stretching and knotting) with the PEUC3 hydrogel specimens (scale bar: 1 cm).

montmorillonite clay in this study, would provide higher elongation at break as demonstrated in our study. Finally, this increased elongation at break is combined with the improved modulus and strength to provide further increases in the energy at break value in PEUCs.

As shown in Figure 4.24, the tensile Young's modulus of PEUC hydrogels are in the range of soft tissues such as adipose (0.0003–0.180 MPa), vascular (lower modulus region; 0.2–0.6 MPa), and myocardium (0.01–0.5 MPa).[19,23,278] PEUC hydrogels with lower clay content can be applied for adipose and myocardium tissues, whereas PEUC hydrogels with higher clay content can be more suitable for myocardium and vascular tissues. Biomimetic mechanical behaviour is an important design criterion for soft tissue applications, as it determines the cellular behaviours and patients' comfort during the treatment.[19,98]

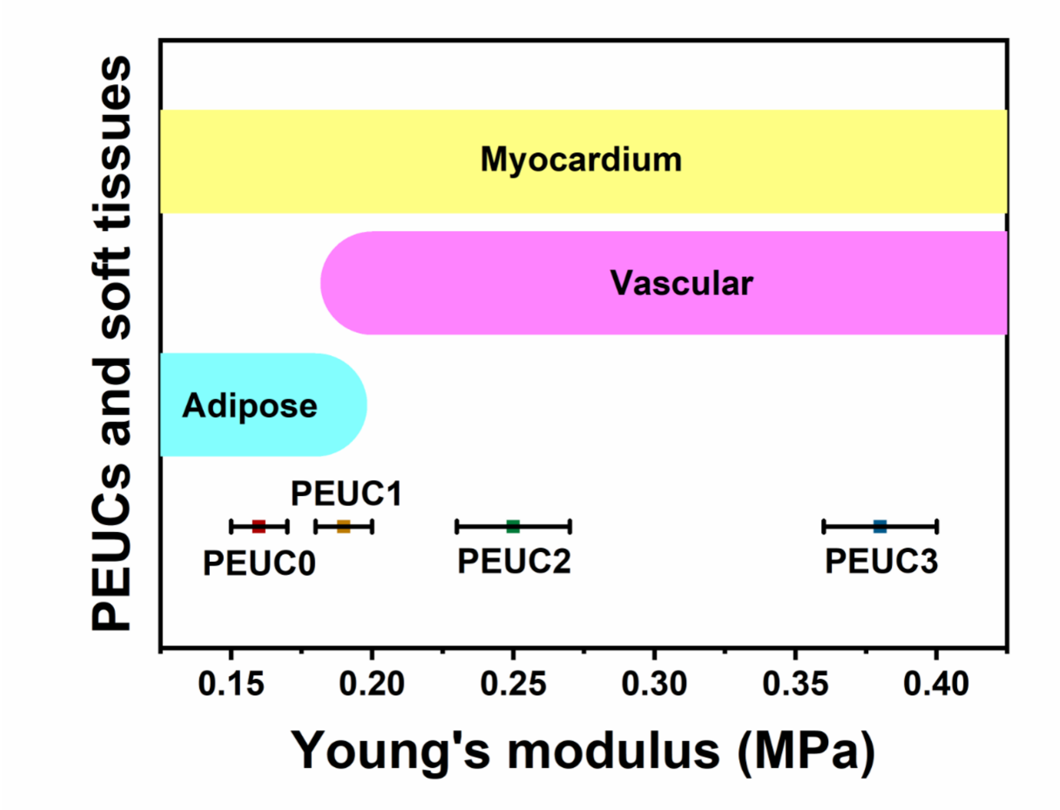

Figure 4.24 Comparison of the Young's moduli of PEUCs with them of natural soft tissues from the literature. Each shaded area represents the range of Young's moduli of adipose (cyan), vascular (low modulus region) (magenta) tissues, and myocardium (yellow).

4.3.4 Tunable drug loading and release behaviours by clay

The drug loading and release behaviours of PEUCs were studied with three dye molecules as model drugs; MB, MO, and SG. The MB and MO are hydrophilic and water-soluble dyes with similar molecular weights (319.9 and 327.3 g mol^{-1}, respectively), but with opposite ionic charge in water; MB is a cationic dye with +1 ionic charge per molecule and MO is an anionic dye with -1 ionic charge per molecule. SG is an organophilic and water-insoluble dye. Therefore, the dye loading and release tests were performed in PBS medium (pH 7.4) for MB and MO, and in ethanol medium for SG. In this test, the PEUC0 and PEUC3 disk specimens were immersed in each dye solutions and the loading of dye molecules by PEUC specimens were recorded in a percentile manner in respect to the initial concentration of dye solutions of 18.4 µM. After the dye loading test, the dye-loaded samples were moved into the fresh solvents (PBS or ethanol), in which the dye release test was performed.

Figure 4.25 shows the dye loading and release profiles. The colour of dye solutions before (pristine dye solutions) and after the loading test, as well as the dye-loaded PEUC0 and PEUC3 specimens are shown in Figure 4.6B. The highest dye loading capacity was observed between MB and PEUC3, with 100% loading capacity in respect to the initial dye concentration after 72 h. The blue colour of the pristine MB dye solution becomes completely clear after the dye loading by PEUC3 as shown in Figure 4.26, indicating the excellent and selective MB loading capacity of PEUC3 with the highest clay content.

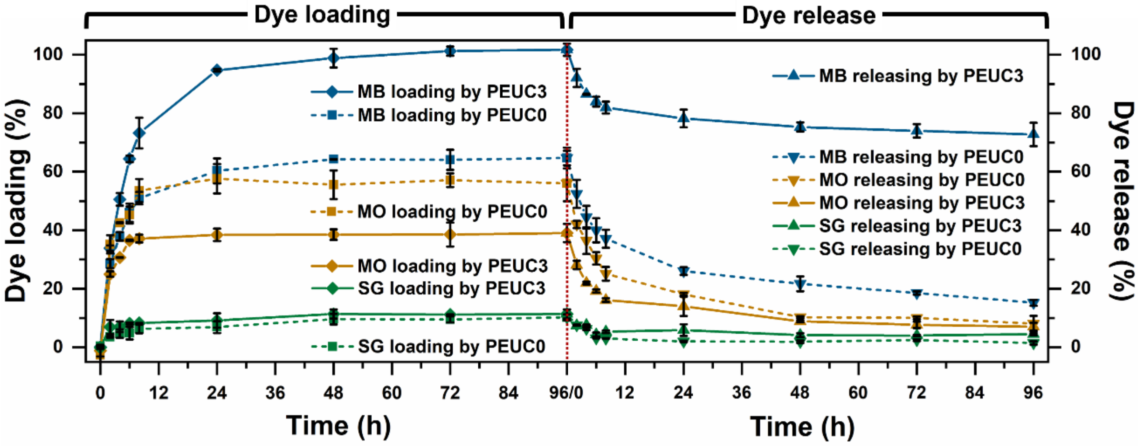

Figure 4.25 Dye loading and release profile by PEUC0 and PEUC3 specimens.

On the other hand, PEUC0 showed a lower MB loading of 64% with no clay added. The clay in PEUC3 promoted the higher loading capacity of MB compared to the PEUC0. This can be attributable to the attractive Coulomb interaction between positively charged MB and the negative surface charge of montmorillonite clay.[279] In case of MO, PEUC0 showed higher

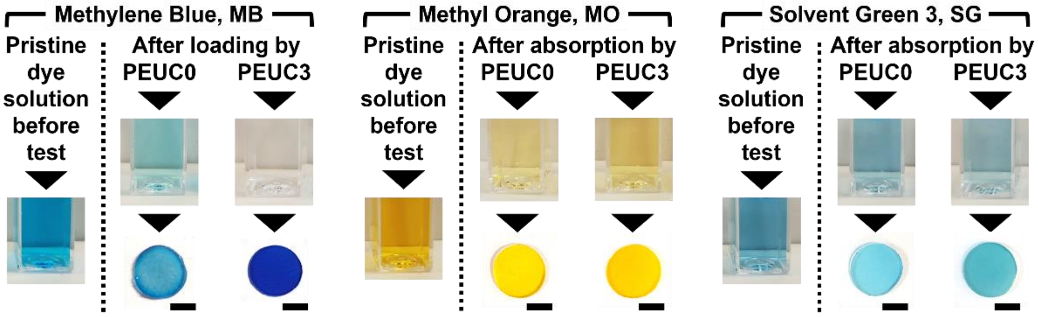

Figure 4.26 Photographs show the colour of pristine dye solutions of MB, MO, and SG before the tests (left columns of each dye section). After the loading test, the dye solution and the dye loaded specimens are also shown (scale bars: 3 mm).

loading capacity of 56% than PEUC3 (39%). As MO is a negatively charged molecule, the repulsive interaction with the clay surface may have lowered the loading capacity of MO in PEUC3.

It should be also noted that the loading capacity of MB in PEUC3 was much higher than that of MO in PEUC3, even though the Cloisite 30B clay contains a positively charged organic surface modifier. This suggests that the organic surface modifier in Cloisite 30B was presumably washed out during the solvent-based sample preparation and washing procedure. In respect to SG, the loading capacity resulted in relatively lower values compared to MB and MO; 10% and 11% for PEUC0 and PEUC3, respectively. This can be due to the higher molecular weight of SG (418.5 g mol^{-1}) than MB and MO, impeding the diffusion into the polymer matrix. Furthermore, the undesirable interaction between hydrophobic SG and hydrophilic components in PEUCs, such as PEG and clay, may have resulted in a weaker physical bonding of SG within PEUCs.

The release profile of all dyes showed rapid release in the initial 8 h, which is associated with the higher drug concentration on the outer layer of samples.[44] The release kinetics was then reduced in proceeding times. Especially, the MB-loaded PEUC3 showed sustained release of MB, compared to the PEUC0, suggesting the prospective use of PEUCs with clay in sustainable drug delivery devices. This is mainly attributable to the Coulomb affinity between the cationic MB and negatively charged clay surfaces. As clays can have different surface charge and area values,[280,281] one can expect that it is possible to design a PEUC with desirable drug loading and release behaviours in terms of the target drug, loading capacity, and release behaviour.

The drug release mechanism was further investigated by the Korsmeyer-Peppas model (eqn (4.4)) and Kopcha model equation (eqn (4.5)),

$$Q_t = A\mathrm{t}^{1/2} + B\mathrm{t} \tag{4.5}$$

where Q_t is the quantity of model drugs (dyes) at a specific time (t). The A and B are constants which are related to the contribution of diffusion and polymer relaxation.[243] The higher A values suggest that the release is diffusion controlled (Fickian diffusion), whereas the higher B values mean that polymer relaxation is dominant in the release mechanism. The initial 60% of dye release data were fit to these models and shown in Figure 4.27 and 28. The SG release data was omitted here due to the relative low loading capacity. From the Korsmeyer-Peppas model, the calculated n values were all between 0.5 and 1.0, indicating non-Fickian diffusion mechanism as proven previously in swelling studies. From the Kopcha model, all the A/B ratios were lower than 1, confirming again the polymer relaxation is the main mechanism for dye release in all cases.

4.3.5 Controllable biodegradation and non-cytotoxicity

The PEUCs are designed as biodegradable materials by containing the PGS segments, which degrades predominantly by hydrolysis of ester bonds in its backbone chain.[11] Figure 4.29 shows

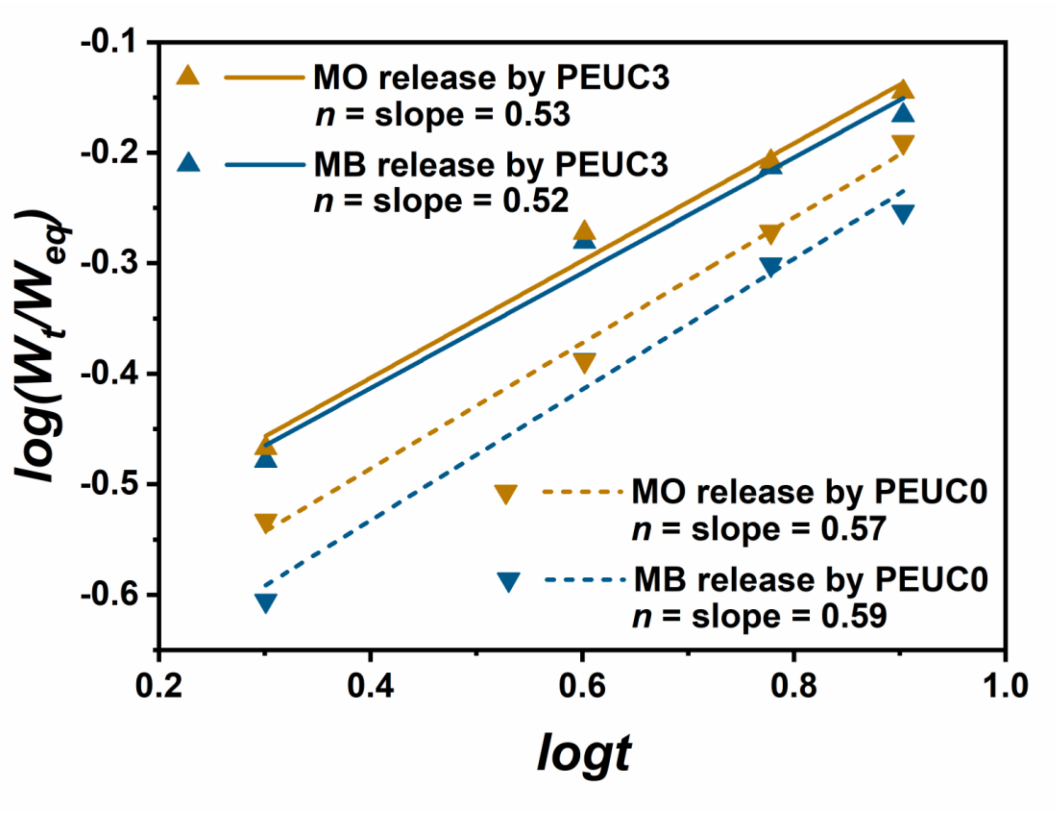

Figure 4.27 Fitting of dye release data to mathematical Korsmeyer-Peppas model.

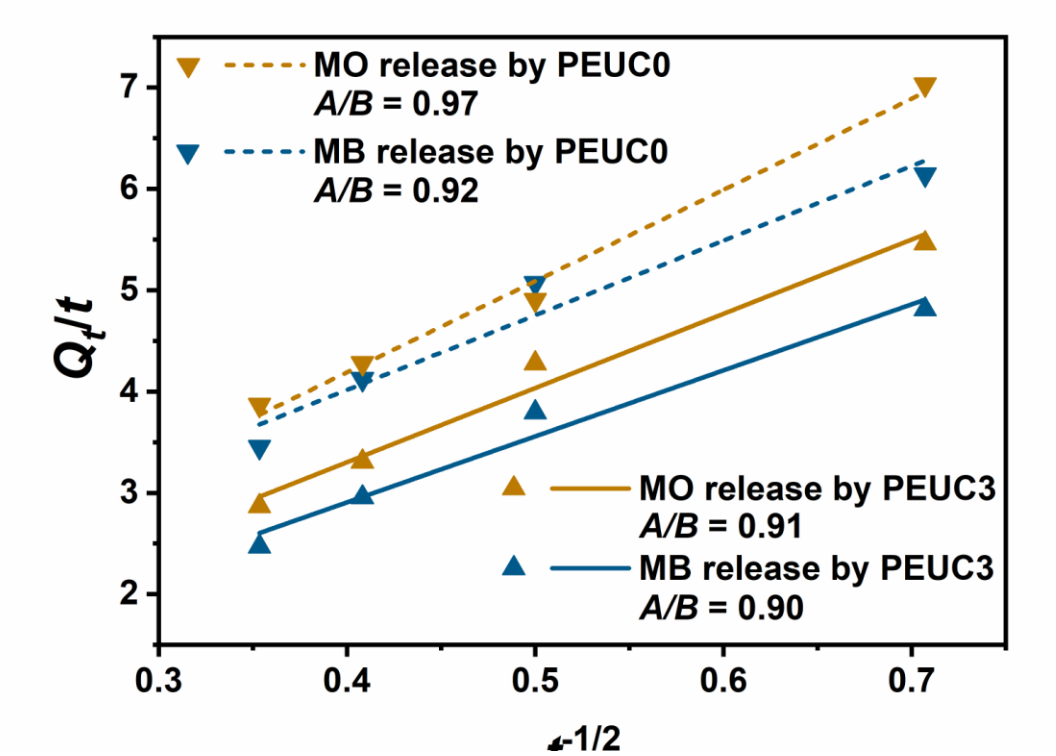

Figure 4.28 Fitting of dye release data to mathematical Kopcha model.

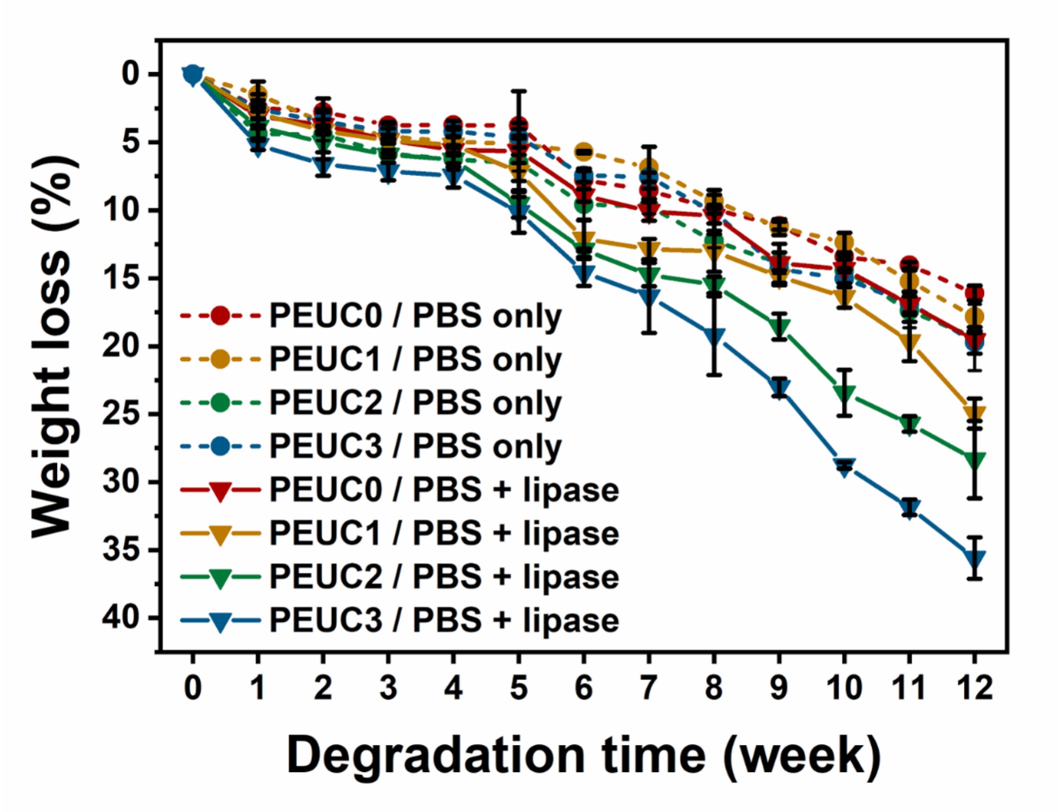

Figure 4.29 Percentage weight loss of PEUC0 and PEUC3 from the biodegradation test in a simulated body condition with or without the lipase enzyme for up to 12 weeks, showing that the controllable degradation rates can be achieved by incorporation of clay in PEUCs.

the percentage weight loss records of PEUCs with or without the enzyme lipase to catalyse hydrolysis of ester bonds in a simulated body condition. Without lipase, the weight losses after the 12 weeks of degradation were 16.1 ± 0.5% (PEUC0), 17.8 ± 1.2% (PEUC1), 19.3 ± 2.4% (PEUC2), and 19.7 ± 0.8% (PEUC3). With lipase, the results were recorded as 19.6 ± 1.0% (PEUC0), 25.0 ± 1.1% (PEUC1), 28.3 ± 2.8% (PEUC2), and 35.6 ± 1.5% (PEUC3). All the samples exhibited a linear degradation profile without compromising their overall structural integrity.

The weight loss data indicate that the rate of degradation increases with an increasing clay content in PEUCs for both with or without lipase. This can be assigned to the improved hydration properties of PEUCs with clay as previously demonstrated in the water swelling ratio results, promoting hydrolysis and removal of the degradation products through diffusion. Moreover, clays are known to catalyse the hydrolytic degradation of polymers.[252–254] This catalytic effect of clay explains the further acceleration in enzymatic degradation rate in PEUCs with higher clay contents. SEM was utilised to examine the surface of PEUC0 and PEUC3 after degradation for 12 weeks (Figure 4.30). The enzymatically degraded surfaces of PEUCs featured severe surface damages with irregular wrinkles, voids, and pores, due to the catalysed and accelerated degradation by lipase. Especially, PEUC3 with lipase exhibited extreme

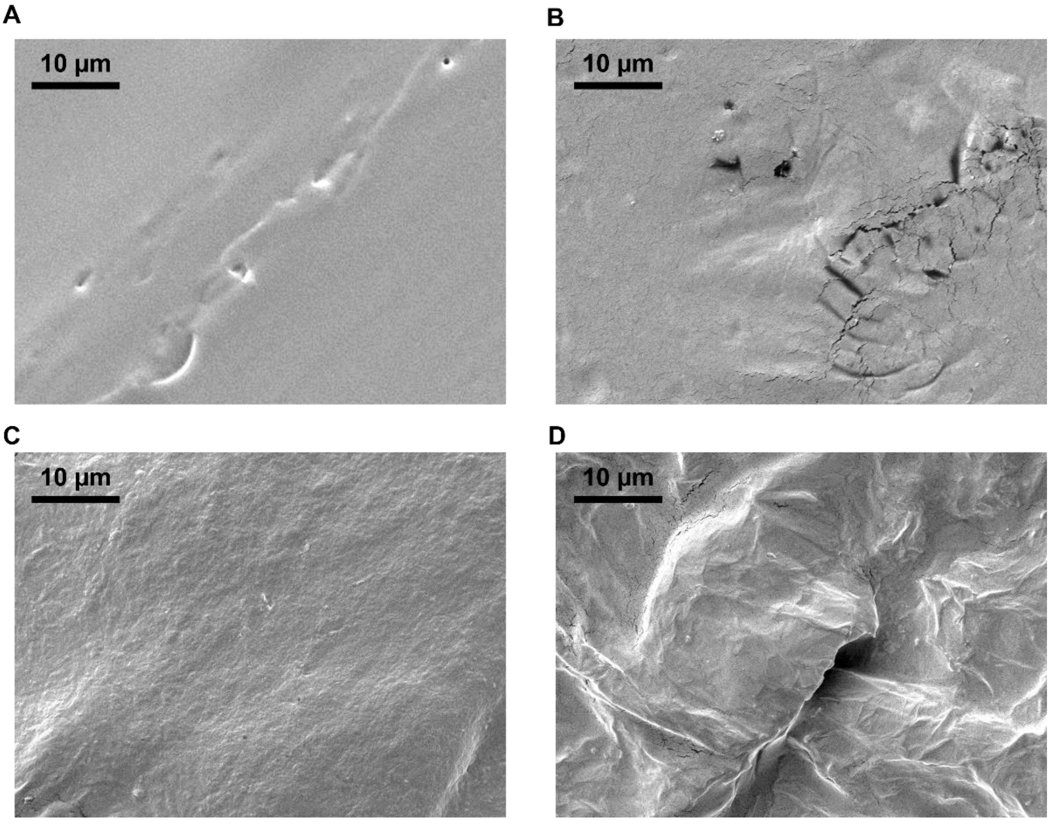

Figure 4.30 SEM images showing the surface of PEUC specimens after degradation for 12 weeks in a shaker incubator (37 °C, 100 rpm). (A) PEUC0 in PBS only media. (B) PEUC0 in PBS + lipase media. (C) PEUC3 in PBS only media. (D) PEUC3 in PBS + lipase media. The scale bars represent 10 µm.

surface damage with the greatest weight loss after degradation test. On the other hand, the non-enzymatically degraded PEUC specimens showed relatively smooth surfaces, owing to the lower weight loss compared to the case of enzymatic degradation.

Optimisation of biodegradability is one of the key design criteria in biomaterials involving implantation. For tissue engineering applications, the degradation kinetics of the implanted tissue scaffolds must be synchronised to the body tissue regeneration, so that the scaffold can be adequately replaced by the newly formed extracellular matrix.[9] For drug delivery systems based on degradable polymers, the degradation rate of drug carriers directly dictates the drug administration.[165] For the postoperative barrier application, the implanted anti-adhesives are designed to be degraded and resorbed by body at the time when wound healing is complete.[168] Therefore, PEUCs are attractive candidates in applications of the implantable biomedical devices with their controllable biodegradation rate with clay.

Cell metabolic assay with the resazurin dye and L929 mouse fibroblast was performed to evaluate the *in vitro* cell viability and proliferation on PEUC0 and PEUC3 for up to 15 days (Figure 4.31 and 32). In this test, the optical density was recorded by colorimetric measurements for the colour change of the blue resazurin dye to the pink resorufin, in response to cellular metabolic reduction.[100] For both PEUC0 and PEUC3, the measured cell metabolic activity showed steady growth during the test period. The normalised optical density increased from 12.4 ± 3.0% to 34.8 ± 13.4% in PEUC0, and 10.7 ± 7.6% to 33.4 ± 8.1 % in PEUC3, between day 3 and day 15 of incubation.

Two-way ANOVA test found no statistically significant difference in the cell metabolic activity in terms of the sample type between PEUC0 and PEUC3. In respect to the incubation time, a significant difference was found between day 3 and day 15. One-way ANOVA test was conducted to evaluate the significant differences in cell metabolic activity in terms of the

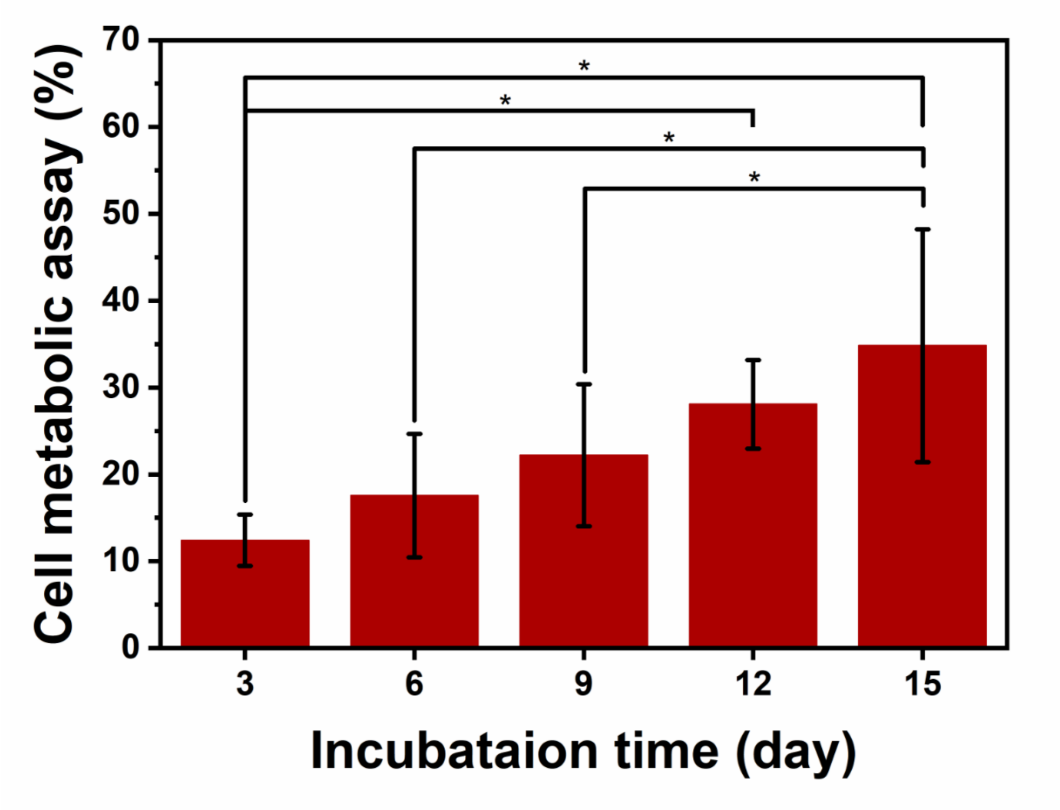

Figure 4.31 The normalised optical density from the resazurin assay from 3 to 15 days of incubation L929 cells on PEUC0. The data are presented as mean ± SD (n =3; * $p < 0.05$ was considered statistically significant, One-way ANOVA).

incubation time and found that both PEUC0 and PEUC3 presented significant increases from day 3 to day 12 and day 15, as well as day 6 and day 15. PEUC0 showed another significant increase from day 9 to day 15, whereas PEUC3 exhibited two more significant increase from day 3 to day 6 and 9. The statistical analysis confirms the steady growth in cell metabolic activity due to the cell proliferation in both PEUC0 and PEUC3 from day 3 to day 15 of incubation.

Figure 4.33A and B show the cell morphologies of L929 after 15 days of incubation on PEUC0 and PEUC3, respectively. In both cases, high confluency as well as normal cell size and shape were observed, with a small number of spherical and detached cells. However, it was found that the cells on PEUC3 have more stretched and adherent cell morphologies with more

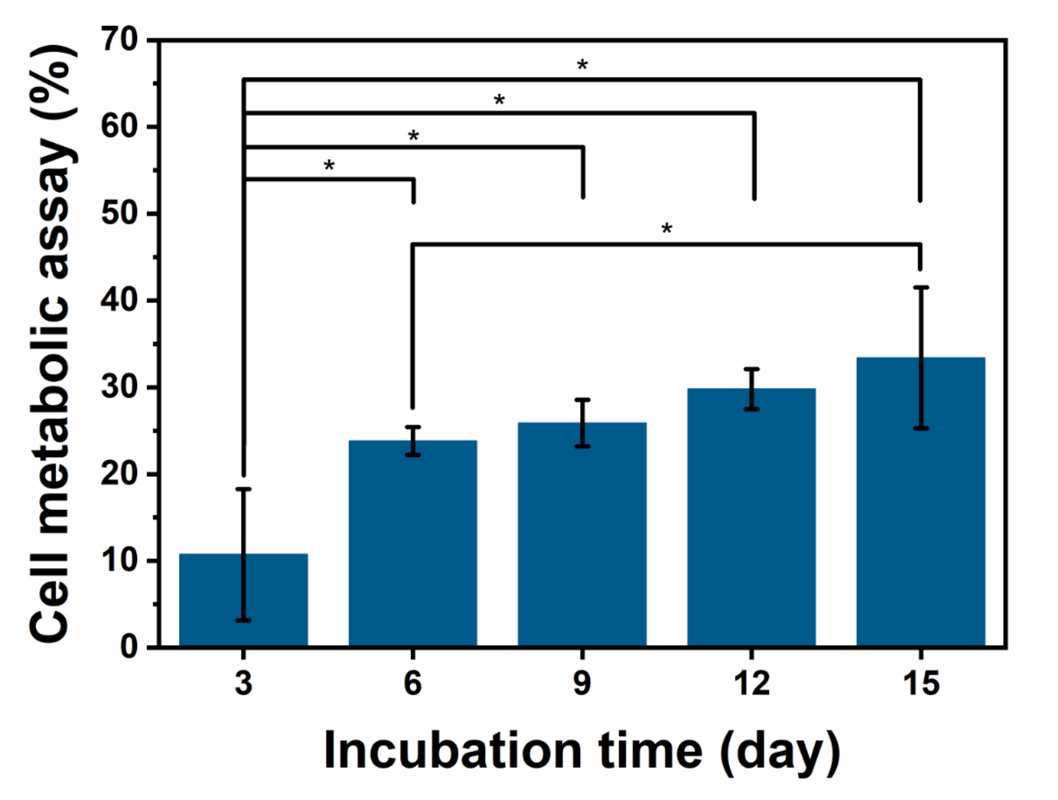

Figure 4.32 The normalised optical density from the resazurin assay from 3 to 15 days of incubation L929 cells on PEUC3. The data are presented as mean ± SD (n =3; * $p < 0.05$ was considered statistically significant, One-way ANOVA).

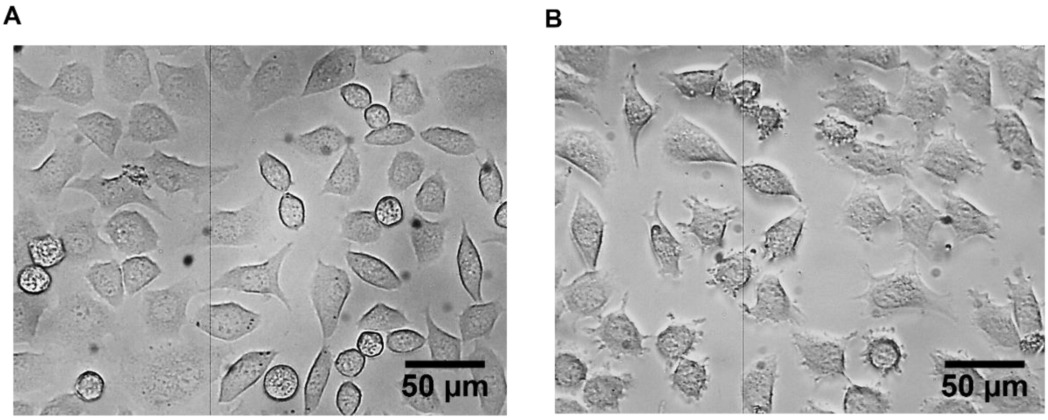

Figure 4.33 Optical micrographs show the cell morphology of L929 fibroblasts cultured on the PEUC specimens for 15 days; (A) PEUC0 and (B) PEUC3.

prominent actin stress fibres. This can be attributed to the higher stiffness in PEUC3 as previously demonstrated.[256] The improved surface hydrophilicity and increased surface roughness in PEUCs with a higher clay content are also known to induce better cell-surface adhesion.[99] This manipulation of cell adhesion property found in PEUCs is beneficial in biomedical applications which involve cell transfer such as tissue engineering.[282]

Overall, the results above showed that the L929 cells were proliferated and adhered well on the surface of PEUCs for up to 15 days, indicating good biocompatibility of PEUCs. Although there have been a few reports about the mild cytotoxicity of organically modified clays due to their organic surface modifiers,[283] the low clay content in PEUCs may have resulted in non-cytotoxicity in PEUCs.[284,285] Furthermore, PEUCs were subjected to the extraction of sol by copious solvent after the nanocomposite synthesis. Where the un-crosslinked organic surface modifiers would be washed off during the extraction procedure, as also suggested by the discussion on the lower drug loading results of the nanocomposites with the MO dye above.[286,287]

The good biocompatibility and controllable biodegradability, as well as the previously proven biomimetic mechanical property make PEUCs as a great candidate in a variety of medical applications. As a *proof-of-concept* study, foam structures were fabricated from PEUC0 and PEUC3 for potential uses in wound healing or soft tissue engineering (see the supplementary information for the detailed fabrication and characterisation methods). As the PEUCs are fabricated based on a solvent system, one can expect that a foam with the desired shape and size can be easily achieved by using a pre-designed casting mould. For the sake of simplicity, the disk-shaped foams were prepared in this study by using the same casting mould as the film samples. The highly elastic mechanical property of PEUCs yielded the foam structures with a full shape recovery after deformation (Figure 4.34A). The well-defined and interconnected pore structure are shown in Figure 4.34B, which is beneficial in tissue engineering fields, with the ability to help cell penetration and transportation of chemical species such as water, gas, nutrient, and cellular wastes.[152,231]

The pore sizes measured by micrographs with the ImageJ software (n =100) were 104.6 ± 16.3 μm for PEUC0 foam, and 94.3 ± 13.0 μm for PEUC3 foam. The porosities of PEUC0 and PEUC3 foams were 85% and 83%, respectively (measured by the density ratio between the dry film samples and foams). A small decrease in the pore size and porosity from PEUC0 to PEUC3 is possibly due to the dispersed clay acting as a shield preventing the coalescence of bubbles.[288,289] Nevertheless, the pore structure of PEUC foams is suitable for tissue engineering and wound healing applications.[290]

The mechanical properties of PEUC0 and PEUC3 foams were determined by the compression tests (Figure 4.35). The measured compressive Young's moduli were 0.04 ± 0.01 MPa (PEUC0 foam), and 0.10 ± 0.02 MPa (PEUC3 foam). The compressive strength at 75% strain values were 0.12 ± 0.02 MPa (PEUC0 foam), and 0.29 ± 0.04 MPa (PEUC3 foam) (The foams did not collapse during the compression tests). The lower compressive moduli and strengths compared to the film samples are largely due to the porous structural factor.

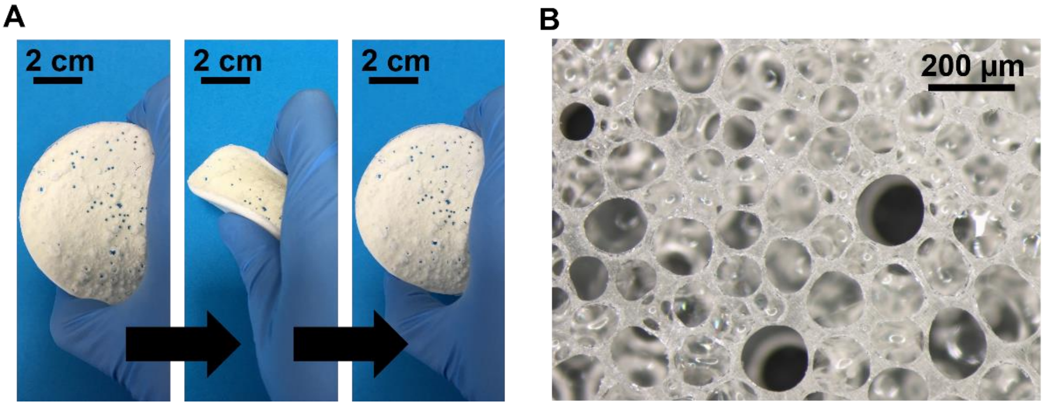

Figure 4.34 (A) The porous foam structure fabricated from PEUC3 demonstrating instant shape recovery by folding and unfolding. (B) A micrograph showing the internal pore structure of the PEUC3 foam.

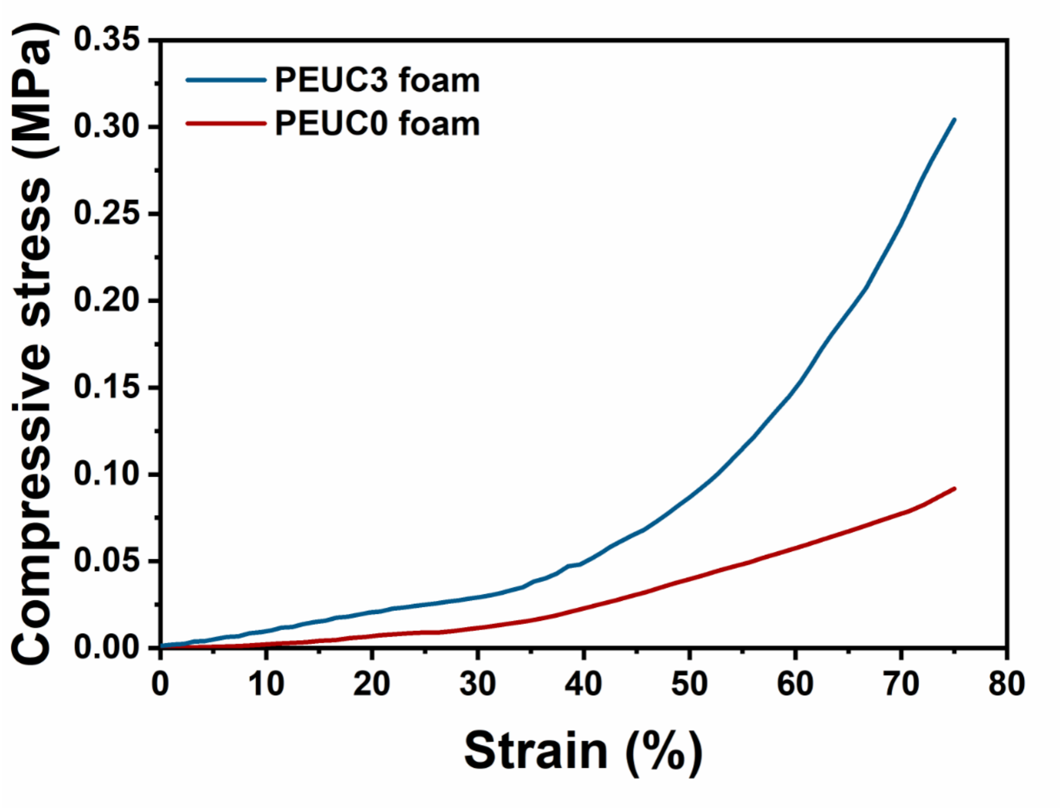

Figure 4.35 The representative compressive stress-strain curves of the PEUC0 and PEUC3 foams.

The biodegradability and biocompatibility are critical design criteria for developing biomaterials. Therefore, further investigations *in vivo* are necessary to fully illustrate the potential of PEUCs as tissue scaffolds, wound dressings, and drug carriers. To address the needs of different applications, future work can also include the design of PEUCs into a variety of macroscopic architectures resembling the shape of actual soft tissues, by utilising a pre-shaped casting mould with a negative impression of the target soft tissue trauma.

4.4 Conclusions

PEUC nanocomposites with varying clay contents were successfully synthesised by a combined approach of the *in situ* polymerisation and solvent method; the PGS pre-polymer and NCO-terminated PEG were crosslinked into a macromolecular network through the urethane linkage whilst an organically modified montmorillionite clay was dispersed within the polymer matrix by THF solvent. The XRD and electronic microscopy study found good clay dispersion within the polymer matrix by both intercalated and exfoliated morphologies.

The addition of clay improved the hydration properties of PEUCs, resulting swollen PEUC hydrogels in water. The mechanical properties of PEUC hydrogels were also improved by clay, enabling the complex mechanical deformations at fully hydrated state with the higher stiffness, energy at break, and stretchability. The biomimetic moduli of PEUC hydrogels were in the range of various biological soft tissues.

Three different dye molecules were used as model drugs to investigate the potential application of PEUCs in drug delivery, and selective dye loading and release behaviours were found, by the Coulomb interaction between clay and dye molecules. Biodegradation rate was also tunable with the clay. The higher clay content in PEUCs, the faster biodegradation rate was resulted for both non-enzymatic and enzymatic conditions. Cell metabolic assay found no evidence of cytotoxicity in PEUCs, with the increasing cell metabolic activity and good cell morphology on the PEUCs surface. Finally, a highly porous and elastomeric foam structure was studied.

Overall, the results suggest that PEUCs with tunable mechanical, drug delivery, biodegradable, and structural properties, as well as good biocompatibility have a great potential in various healthcare applications for soft tissues such as tissue engineering, wound healing, and controlled drug delivery.

Chapter 5 Pro-angiogenic, malodourous diamine-controlling poly(glycerol sebacate-co-ethylene glycol)-based polyester-clay nanocomposite hydrogels

5.1 Introduction

In the previous chapter, the importance of achievement of angiogenesis in wound healing is discussed. As a highly vascularised tissue, regeneration skin essentially depends on the angiogenesis.[70] Another functionality could be beneficial in wound healing is the control of malodour especially in chronic wounds.

In this chapter, a new polyester-clay nanocomposite hydrogel system is developed based on a copolymer of poly(glycerol sebacate-*co*-ethylene glycol) (PGS-*co*-PEG) with an interesting pro-angiogenic and malodourous diamine-controlling properties. The synthesis was performed in a combined approach of melt intercalation and *in situ* polymerisation methods to achieve well dispersed clays within the polymer matrix. Montmorillonite clay was used for its well-known biocompatibility as well as high specific surface area with the ability to adsorb growth factors.[173,291,292] The PGS pre-polymer was used as a crosslinker as a branched polymer with an excessive amount of carboxylic functional groups which can be utilised to form the ester bonds, leading to a macromolecular network structure. PEG was used as an intercalated polymer in MMT, as well as the source of hydration as a hydrophilic polymer.[293] Furthermore, the hydroxyl groups in PEG enabled the reaction with the PGS pre-polymer. The material structure as well as the dispersion structure of MMT is characterised with FTIR, XRD, and TEM. The hydration properties as well as the surface hydrophilicity and vapour permeability were investigated. A porous foam architecture was fabricated as a *proof-of-concept* study. Mechanical properties are examined by tensile tests. Biodegradability and biocompatibility are also studied *in vitro*. Pro-angiogenic property is studied by a chick chorioallantoic membrane (CAM) assay with an additional pro-angiogenic substance of E2. The hypothesis was that the MMT will provide a controlled release of E2 to obtain the optimum activity as demonstrated by the E2 release tests with or without MMT. The high specific surface area and negative surface charge of MMT were expected to adsorb malodourous-diamines, and the removal of diamines are tested with the loading of the MMT in the nanocomposite hydrogels. The benefits and potential applications of this new nanocomposite hydrogel system are also discussed based on the materials property and structure, mainly in wound healing and also in soft tissue engineering.

5.2 Materials and methods

5.2.1 Materials

Glycerol, sebacic acid, PEG (with a number average molecular weight of 2000 g mol^{-1}), 17β-estradiol (E2), putrescene (PUT), cadaverine (CAD), mercaptoacetic acid (MAA), o-phthalaldehyde (OPA), methanol, ethanol, phosphate buffered saline (PBS) tablets, lipase from the porcine pancreas (54 U mg^{-1}), Dulbecco's Modified Eagle's Medium (DMEM) with high glucose, and resazurin sodium salt were purchased from Sigma-Aldrich (Bioreagent or BioXtra grade was used, where appropriate). Natural sodium MMT clay was provided by Southern Clay Products and purified and dried before use.[294] A desired amount of MMT was dispersed in water (1 w/v %) by mechanical agitation for 24 h and allowed to sediment large aggregates. The rest of supernatant suspension was transferred into a dialysis bag in water to remove excessive cations. The water was changed thrice daily for 4 days, until the conductivity was measured as 10 μS (initial conductivity measured as 321 ± 1 μS). Finally, the purified clays were dried at 60 °C for 48 h in a vacuum oven for further uses. Water used in this study was prepared in ultrapure water by Barnstead™ Smart2Pure™ system (resistivity: 17.1 ± 1.0 MΩ cm at 25 °C).

5.2.2 Preparation of the PGS pre-polymer

The PGS pre-polymer was prepared following the previously reported manner with modifications.[9,250] Glycerol (16.2 mmol) and sebacic acid (26.0 mmol) were charged in a three-necked flask. The monomers were first mixed and reacted at 130 °C for 1 h under a flow of nitrogen. A Dean-Stark apparatus was used here to help removal of the water vapour generated by the polycondensation. The reaction was further continued for another 2 h with a vacuum pump attached on the reactor to remove the water vapour more actively. The prepared PGS pre-polymer was collected from the reactor and used for the synthesis of the nanocomposite hydrogels below. The gel permeation chromatography (GPC) was used to affirm the successful preparation of the PGS pre-polymer. The measured number average molecular weight ($\overline{M}_n$), weight average molecular weight ($\overline{M}_w$) and polydispersity index (PDI) were 1645 g mol^{-1}, 4993 g mol^{-1}, and 3.04. Attenuated total reflectance Fourier transform infrared spectroscopy (FTIR) were also confirmed the synthesis of the PGS pre-polymer with the peaks attributable to the ester bond (Figure 5.1).

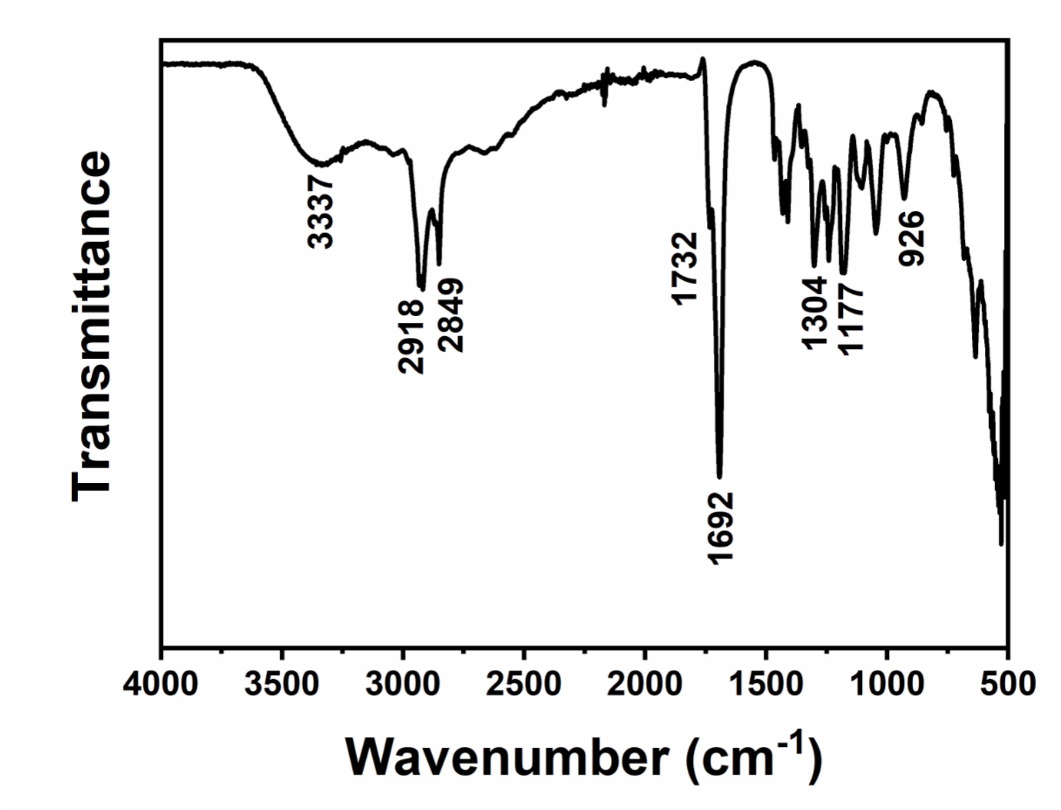

Figure 5.1 The attenuated total reflectance Fourier transform infrared spectroscopy (FTIR, PerkinElmer Spectrum One NTS analyser) spectrum of the PGS pre-polymer. The broad band between at 3337 cm^{-1} is from hydroxyl groups (O–H).[26,137] Two peaks at 2918 and 2849 cm^{-1} are stretching vibration of methyl groups (C–H).[26,137] The peaks at 1732 cm^{-1} (C=O) and 1177 cm^{-1} (C–O) are the characteristics of ester bonds.[137] Carboxyl group peaks are shown at 1692 cm^{-1} (dimer C=O), 1304 cm^{-1} (C–O stretching), and 926 cm^{-1} (O–H bending).[137]

5.2.3 Synthesis of the nanocomposite hydrogels

The synthesis was conducted in a combined approach of melt intercalation and *in situ* polymerisation. Without concerning about the inorganic MMT component, the chemical reaction scheme of organic components in shown in Figure 5.2. First, MMT (0, 5, and 10 wt%

in respect to the total weight of ingredients) was mixed into the molten PEG (1.6 mmol) by a mechanical agitation at 80 °C for 15 h under a nitrogen atmosphere. Subsequently, the PGS pre-polymer prepared above was added and the polycondensation reaction was performed at 130 °C for 72 h. A vacuum pump was used to remove the water vapour generated throughout the synthesis. The resulting molten resin of nanocomposite was collected from reactor and poured on to a PTFE mould. The nanocomposite resins were then degassed in a vacuum oven at 80 °C for 30 min to remove the voids. As the molten resin was extremely cohesive, a non-stick baking paper (purchased form a local store) was topped on the resin and 10 N of force was applied gently. The capillary action between the base of PTFE dish and baking paper on the top maintained the resin spread. After the curing at 130 °C for 32 h, the synthesised nanocomposite samples were cooled down to room temperature and peeled off from both the PTFE dish and baking paper. After the samples were collected, the surface exhibited visibly no residues from the baking paper. The baking paper is a food grade and has the layers of silicone which can be used up to 220 °C. Extraction test was performed using 30%, 50%, 70%, and 100% ethanol at 37 °C for 2 days (12 h each) to estimate the un-crosslinked proportion. After washing, the nanocomposite samples were first dried in a fume cupboard for 1 day, followed by drying in a vacuum oven at 37 °C for another day. Finally, dry nanocomposite samples were swollen in the PBS medium to prepare swollen nanocomposite hydrogel samples.

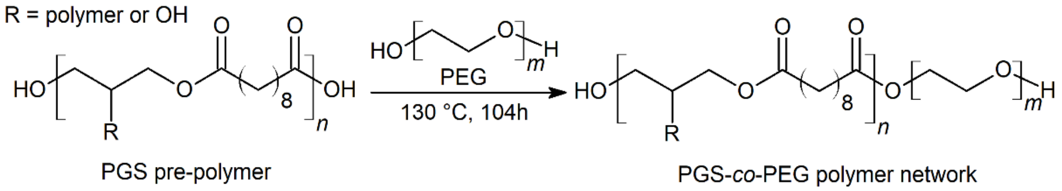

Figure 5.2 Chemical synthesis scheme showing the reaction between organic components forming PGS-*co*-PEG polymer network by ester bonds.

5.2.4 Characterisation of the nanocomposite hydrogels

FTIR study was performed on a PerkinElmer Spectrum One NTS analyser (500 – 4000 cm^{-1}, resolution: 2 cm^{-1}, number of scans: 16). A pressure of 70 N was applied on the specimens by a built-in screw to extend the degree of sample contact on the diamond ATR crystal.

GPC was conducted on an Agilent Technologies 1260 Infinity. The eluent was tetrahydrofuran containing 2.0% v/v triethylamine and 0.05% w/v BHT inhibitor. The GPC was calibrated using PMMA standards. For the nanocomposite resin samples, additional filtration was performed thrice to removed MMT which hinders the machine operation.

XRD patterns were acquired on a STOE STAPI P (Cu Ka_1, $\lambda = 0.15406$ nm, 40 kV, 35 mA, scan rate: 0.1° sec^{-1}). Dry nanocomposite samples were cryo-milled by the SPEX Certiprep™ 6850 Cryogenic Mill to obtain fine powers and tested.

TEM was performed on a FEI Tecnai T-12 at an operation voltage of 80 kV. The dry nanocomposite samples were cut into a small size and sectioned by a Leica UC6/FC6 cryo-ultramicrotome at -100 °C using a Diatome cryo-P 35 diamond blade. Sections were moved onto bare copper grids and images were recorded using a Gatan Orius bottom mounted camera and Gatan Digital Micrograph.

SEM was conducted on a Hitachi FlexSEM 1000 (spot size = 3, accelerating voltage = 10 kV). The dry nanocomposites were cut into small pieces, mounted onto an aluminium stub by applying a Pelco conductive silver paste (Ted Pella, USA), and gold-coated by a high resolution polaron sputter coater (Emscope SC500A).

Water swelling ratio was recorded gravimetrically. Disk-shaped dry nanocomposite specimens (n = 3, diameter: 5.3 mm, thickness: 0.71 – 0.88 mm) were prepared by a punching utensil and kept in a vacuum oven at 37 °C for 1 day until constant weights were read. The initial dry weight (W_{dry}) was obtained at this point by a 4-decimal scale (Sartorious M-power). The dry nanocomposite specimens were then immersed in PBS medium. At a specific time interval, the specimens were collected, blotted to remove the surface medium and weighed to record the swollen weight (W_{wet}). The water swelling ratio was calculated by eqn (5.1)

$$\text{Swelling ratio (\%)}=\frac{W_{wet}\text{-}W_{dry}}{W_{dry}}\times 100 \tag{5.1}$$

Surface water contact angle was measured by a Krüss DSA-100 drop size analyser. A droplet of PBS medium (10 μL) was dosed onto the sample surface using a 22-guage, blunt-end syringe needle. High-resolution images were captured after 10 seconds by a built-in digital camera to perform the angle measurements (n = 3).

Water vapour transmission rate (WVTR) was measured according to ASTM E96. The dry nanocomposite samples (n = 3, thickness: 0.53 – 0.58 mm) were fixed tightly onto the mouth of plastic dish containing water by applying a wax (60% of microcrystalline wax and 40% of paraffin wax). The dish assembly was then incubated at 37 °C and 50% relative humidity.[295] The weight loss was recorded on a 4-decimal scale and WVTR was defined by eqn (5.2) as below.

$$\text{WVTR}=\frac{\Delta W}{tA} \tag{5.2}$$

ΔW (g) is the weight change of dish assembly, t (h) is the time during which G occurred, and A (m^2) is the tested area. WVTR is reported in a unit of g h^{-1} m^{-2}. The calculation was performed where the weight change was steady.

Quasi-static uniaxial tensile test was performed on a Lloyd LRX, equipped with a 50 N load cell at a strain rate of 50 mm min^{-1} till failure according to ISO 527. The dog-bone specimens (n = 6) were prepared by a mould utensil (Ray-Ran Test Equipment) for both dry (thinkness: 0.64 – 0.84 mm) and hydrogel samples (thickness: 1.19 – 2.05 mm).

5.2.5 Fabrication and characterisation of the *proof-of-concept* porous foam structure

The tissue scaffold was fabricated by a combined salt-leaching and freeze-drying approach. First, molten nanocomposite resin with 10 wt% of MMT was mixed with of doubly sieved NaCl particles (300 µm) by an overhead stirrer at 80 rpm for 20 min (1:3 weight ratio). The mixture was then casted into a PTFE dishes and cured in a vacuum oven at 130 °C for 32 h. The salt was extracted out by a copious amount of water for 2 days. Compressive mechanical tests were performed on (n = 3) on a Lloyd LRX, equipped with a 50 N load cell at a strain rate of 50 mm min^{-1} till 75% strain.

5.2.6 Biodegradability and biocompatibility tests *in vitro*

Biodegradability was investigated *in vitro* with or without lipase enzyme to catalyse the hydrolysis of ester bonds. Disk-shaped specimens (diameter: 5.3 mm, thickness: 0.93 – 1.82 mm) were sterilised in 70% ethanol solution and dried in a vacuum condition for 1 day until constant weights were read (W_{ini}). The specimens were moved into test tubes and 10 mL of PBS medium with or without 110 U L^{-1} of lipase (from the average serum activity of lipase in healthy adults in the literature; 30 – 190 U L^{-1}).[19] The test tubes were then placed in a shaker incubator (Stuart SI500) at 37 °C and 100 rpm. The test medium was replaced daily to ensure the full enzyme activity. At a specific time interval, the specimens were collected, washed thrice by a copious amount of water, dried in a vacuum desiccator overnight, and weighed on a 4-decimal scale (W_{day}). The weight loss by degradation was determined by the following eqn (5.3).

$$\text{Weight loss (\%)} = \frac{W_{ini} - W_{day}}{W_{ini}} \times 100 \tag{5.3}$$

Biocompatibility was tested *in vitro* by the cell metabolic assay. Prior to the test, all the disk specimens (diameter: 5.3 mm, thickness: 1.03 – 1.91 mm) were sterilised in 70% ethanol for 1 day, washed thrice with plenty of water, soaked in DMEM overnight, and placed in an incubator (37 °C, 5% CO_2). The specimens were then placed in the well-plates and fixed by sterilised metal rings to seed the cells. L929 immortalised dermal mouse fibroblast cell line was chosen according to ISO 10993. The fibroblast is one of the most common cells found in soft tissues, therefore relevant to the soft tissue healthcare applications.[256] Cell trypsinisation was performed by trypsin-ethylenediaminetetraacetic acid, followed by neutralisation by addition of warm medium 5 mL, The cells were collected (centrifugation at 1000 rpm for 5 min) and the optimum cell density of 3.0×10^4 cells per specimen was seeded in DMEM. Cell-free test was also done as the negative control, to be subtracted by the data from the actual sample tests. After 1 day of incubation, the old DMEM was removed and cell-seeded specimens were washed by PBS and moved into new well-plates. The resazurin dye solution (0.1 mM in PBS) was added to each well and incubated for 2 h for colour change. The colourimetric analysis was performed on a Bio-Tek plate reader at the absorbance wavelength of 570 nm. The test was continued after 4 and 7 days of incubations. After the cell metabolic assay, microscopic cell images were recorded on a Motic AE2000 microscope to examine the cellular morphology. The experiments were triplicated.

5.2.7 E2 release test and CAM assay

E2 was loaded by mixing directly into the nanocomposite resins at 70 °C for 20 min before curing (5 wt%). The complete mixing was confirmed by transparent (in case of resins with 0 wt% MMT) and homogeneous colour of E2/resin mixtures. The curing was performed in the same manner as above and disk specimens (n = 3, diameter: 5.3 mm, thickness: 0.90 – 1.01 mm) were immersed in 4 mL of PBS. At a specific time intervals, the solution was collected and replaced by fresh PBS. The absorption intensity at λ = 220 nm of the collected PBS containing E2 was examined under an ultraviolet-visible spectrophotometer (UV-vis. Agilent Cary 60). A pre-prepared calibration curve was used to determine the concentration of E2 in PBS (Figure 5.3).

An *ex-ovo* CAM assay was used to evaluate the angiogenic activity of the gels as described previously.[296–298] Fertilised chicken eggs (Gallus Domesticus) were purchased from Henry Stewart & Co. MedEggs and wiped with 20% Industrial Methylated Spirit solution in order to remove dirt and feathers from the shell. Eggs were then incubated at 37.5 °C for 3 days lying horizontally in a humidified rotating egg incubator (RCOM King SURO, P&T Poultry). At the end of embryonic day 3, the embryos were transferred gently into sterile petri dishes by cracking the eggs, and the embryos were incubated at 38 °C in a humidified cell culture incubator (Binder). On day 7, the gels were implanted to CAM, and the chicks were incubated for further 7 days. On day 14, angiogenesis was quantified by counting all discernible blood vessels growing towards the sample specimens in a spoke wheel pattern, as described previously.[299,300] Three independent CAM experiments were conducted and in each independent experiment, and nine embryos were allocated for each group for statistical analysis. The test was done by following the institutional policies on ethical use of animals in research, registered with and inspected by the ethical review committee. The embryo cultures were only allowed for up to 14 days.

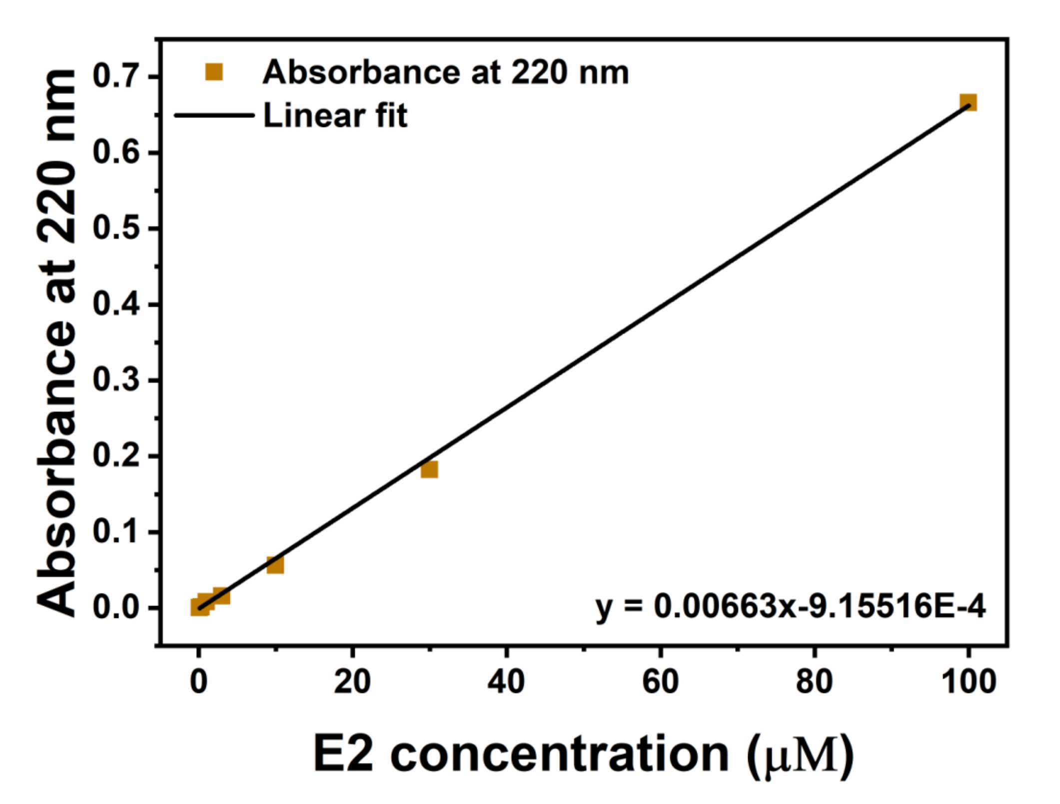

Figure 5.3 Calibration curve of 17β-estradiol (E2). The standard solution of E2 prepared at 7 different concentrations (100, 30, 10, 3, 1, 0.3, and 0.1 μM). The stock solution of E2 was prepared first in ethanol at 10 mM and diluted in PBS to achieve the above concentrations.

5.2.8 Malodourous diamine-controlling test

The removal capacity of PUT and CAD by nanocomposite hydrogels was determined utilising the OPA derivatisation reaction coupled with MAA.[301] OPA and MAA were dissolved separately in methanol at 0.2 M, and kept at 4 °C for 24 h prior to use. The nanocomposite hydrogels specimens (n = 3, diameter: 5.3 mm, thickness: 1.12 – 2.07 mm) were immersed in

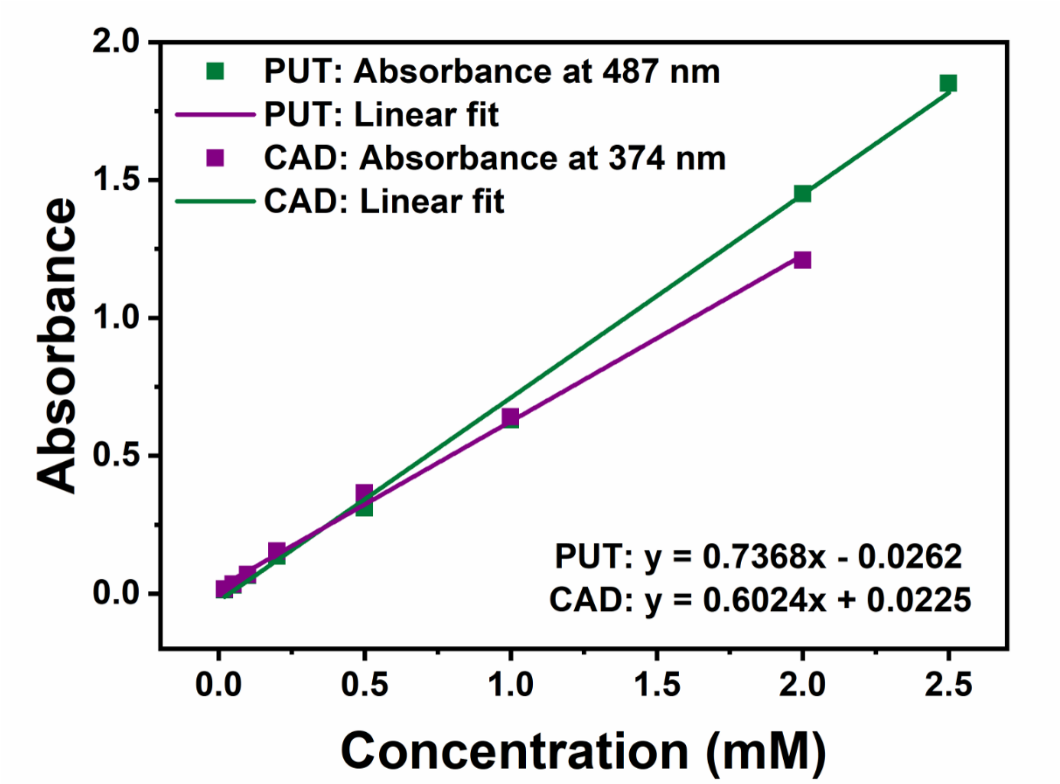

Figure 5.4 Calibration curves of putrescene (PUT) and cadaverine (CAD) acquired under an ultraviolet-visible spectrophotometer (UV-vis. Agilent Cary 60). The standard solutions of PUT and CAD were prepared at the eight or seven different concentrations (2.5 mM, 2.0 mM, 1.0 mM, 0.5 mM, 0.2 mM, 0.1 mM, 50 µM, and 20 µM) and used to generate the calibration curves.

PBS (3 mL) containing PUT (2.11 mmol) or CAD (0.77 mmol), sealed tightly in a tube, and incubated at 37 °C for 39 h. The initial concentration of PUT and CAD was determined by their average contents in the necrotic tissue of patients with diabetic foot in the literature.[302] The incubation time of 39 h was from the average time of one wound dressing being used before being changed by another during the treatment of patients in the literature.[77] PUT or CAD only samples without the nanocomposite hydrogels also tested and used to adjust the final result. After the incubation, 10 µL of PBS media containing PUT or CAD were collected. OPA and

MAA in methanol (20 µL each) were added. The final volume was adjusted to 2.0 mL by PBS. The compound was then sealed and heated at 60 °C for 12 min using a heating bath. Colourimetric analysis was performed under the ultraviolet-visible spectroscopy (UV-vis, Agilent Cary 60) to determine the concentration of PUT (λ_{max} = 487 nm) and CAD (λ_{max} = 374 nm) with calibration curves prepared beforehand (Figure 5.4).

5.2.9 Statistics

All measurements were reported as mean ± standard deviation with a confidence level of 95%. One-way and/or Two-way analysis of variance (ANOVA) was performed where appropriate, with the Bonferroni post hoc test by the OriginPro 2018 software, where appropriate. The degree of significance was indicated with number of stars; *** $p \leq 0.001$, ** $p \leq 0.01$, and * $p \leq 0.05$. Error bars in the graphs indicate standard deviations.

5.3 Results and discussion

5.3.1 Synthesis and characterisation of nanocomposite hydrogels

The synthesis of nanocomposite hydrogels is performed in a combined approach of melt intercalation of PEG into MMT, followed by *in situ* polymerisation between PEG and the PGS pre-polymer while MMT (0, 5, or 10 wt %) was intercalated by PEG. Finally, the nanocomposites were swollen in water, resulting in swollen nanocomposite hydrogels (Figure 5.5). The PGS pre-polymer was prepared by polycondensation between glycerol and sebacic acid. It should be noted that the PGS pre-polymer in this study was prepared by a relatively short reaction time to achieve a low molecular weight, as well as excessive sebacic acid which provides additional carboxyl groups to accommodate further reaction with PEG. The branched molecular structure of the PGS pre-polymer enabled the formation of crosslinked polyester with PEG (PGS-*co*-PEG), without any additional crosslinking agent. The molar ratio between the organic compounds was 8:13:1 = glycerol:sebacic acid:PEG, giving a stoichiometric ratio between hydroxyl group and carboxyl group of 1:1.

All the nanocomposites were not dissolved but swollen strongly in various solvents such as acetone, dimethylformamide, dimethyl sulfoxide, ethanol, isopropyl alcohol, and water, indicating a covalently crosslinked network structure. Amphiphilic swelling behaviour was expected as the nanocomposites are consisted of organophilic PGS and hydrophilic PEG. Furthermore, the addition of MMT on the nanocomposites greatly modified the ability to swell in water, making the nanocomposites into nanocomposite hydrogels in contact with water (discussed later). The residual sol proportion in the nanocomposites was determined after the extraction by ethanol/water solutions; 22.6 ± 3.4%, 23.7 ± 2.7%, and 22.9 ± 1.7%, with 0, 5, and 10 wt% of loading of MMT, respectively. The molecular weight of nanocomposite resins before curing were analysed under GPC to see whether the addition of MMT modulates the covalent polymerisation between the PGS and PEG segments.

The $\overline{M}_n$, $\overline{M}_w$, and PDI listed in Table 5.1. The molecular weight of nanocomposite resins exhibited a minor increase with the addition of MMT, indicating MMT does not hindered the formation of ester bonds between the PGS pre-polymer and PEG during the resin synthesis. As

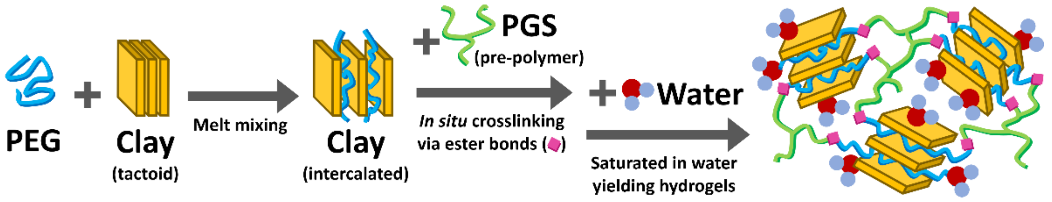

Figure 5.5 A cartoon showing the synthesis of nanocomposite hydrogels.

PGS segments are organophilic mainly due to its 8 carbon aliphatic chain in polymer backbone which originated from sebacic acid, organic compound of PEG must have been selectively reacted with PGS segments, leaving MMT with the hydrophilic and ionic mineral surfaces out of the reaction.[250,303]

Table 5.1 The molecular weights of nanocomposite resins before curing.

	$\overline{M}_n$	$\overline{M}_w$	PDI
with 0 wt% of MMT	4148	24712	5.96
with 5 wt% of MMT	4571	24929	5.45
with 10 wt% of MMT	4507	25332	5.62

Overall, the nanocomposites are consisted of copolymerised polymer network of PGS and PEG segments, while the MMT forms intercalated structure by PEG. From the similar molecular weight distribution of nanocomposite resins before the curing as well as the sol contents determined by the extraction test after the curing of nanocomposites suggest that no big difference has been caused in the chemical bonding structure and crosslinking density between the PGS and PEG segments by the loading of MMT. This covalent network structure has also an advantage in wound healing applications, as many physically crosslinked hydrogels can break and dissolve and it causes unideal damages on the wound site before the wound is healed completely.[304]

Chemical structure of the nanocomposites was evaluated by FTIR as shown in Figure 5.6. The polymer backbone consisted of ester bonds can be seen by the characteristic ester bond peaks at 1732 cm^{-1} (C=O stretching) and 1096 cm^{-1} (C–O stretching).[26] The intensity of ester bond peaks does not change with the loading of MMT, confirming again MMT does not largely participates in or hinders the ester bonds. The broad band at 3455 cm^{-1} is from hydrogen bonded O–H stretching vibration either by MMT or free hydroxyl functional groups from polymer segments.[46] The peaks at 2934 cm^{-1} and 2854 cm^{-1} are attributable to the stretching vibration of methyl groups from the polymer chain. Stretching vibration peak of PEG-related C–O–C can be also seen at 948 cm^{-1}.[44] With the addition of MMT, most notable changes are the appearances of Si–O–H and Si–O–Si stretching vibration peaks,[255,264] and the peak intensifies from 5 wt% to 10 wt% due to the increasing loading of MMT. It should be noted that the Si–O–Si peak blue-shifted from original 980 cm^{-1} in pristine MMT to 1033 cm^{-1} in the nanocomposites. This is attributable to the distorted bond angle caused either by molecular confinements from the adsorbed PEG and surrounding elastomeric PGS segments.[305]

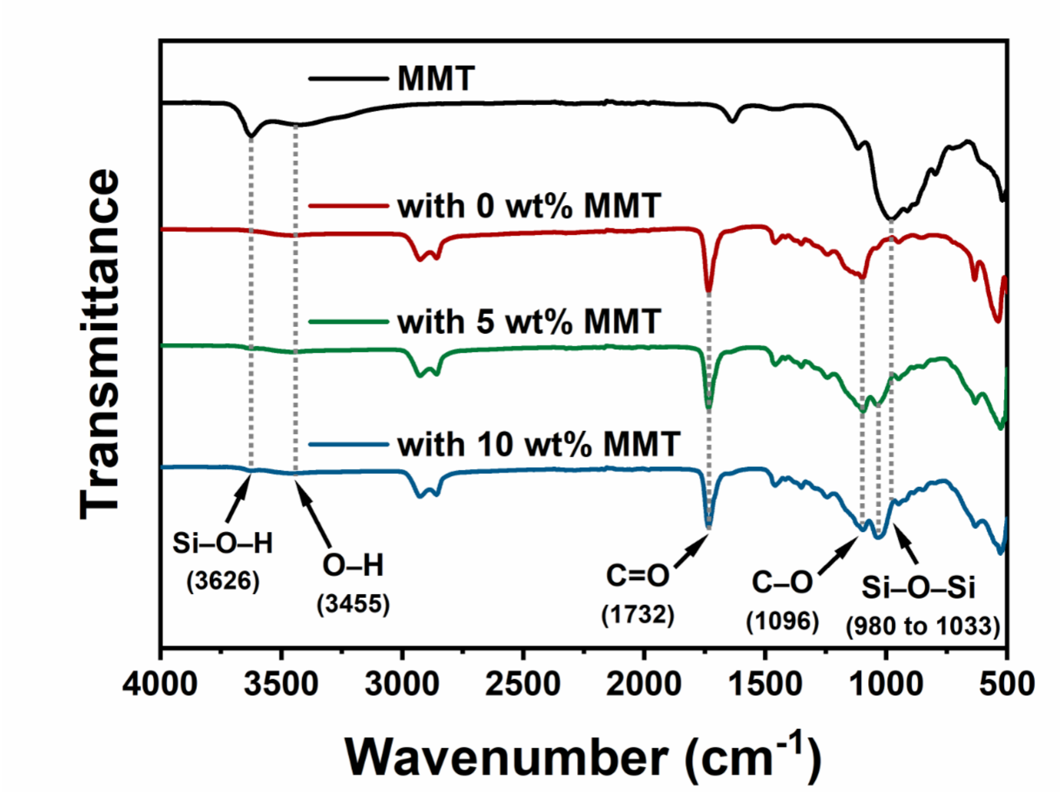

Figure 5.6 FTIR spectra of MMT and the nanocomposites.

The presence of MMT in the nanocomposites was also affirmed by TGA study (Figure 5.7). The residual weights after the thermal decomposition of organic compounds at 800 °C were 1.2%, 6.1%, and 11.1%, showing a sequential increase of 5% by each 5 wt% loading of MMT. This suggests that MMT was not extracted out during the ethanol/water extraction before the test. This is beneficial for wound healing applications, as it is important to have no particles released form the dressings not to irritate the wound sites.[80,306]

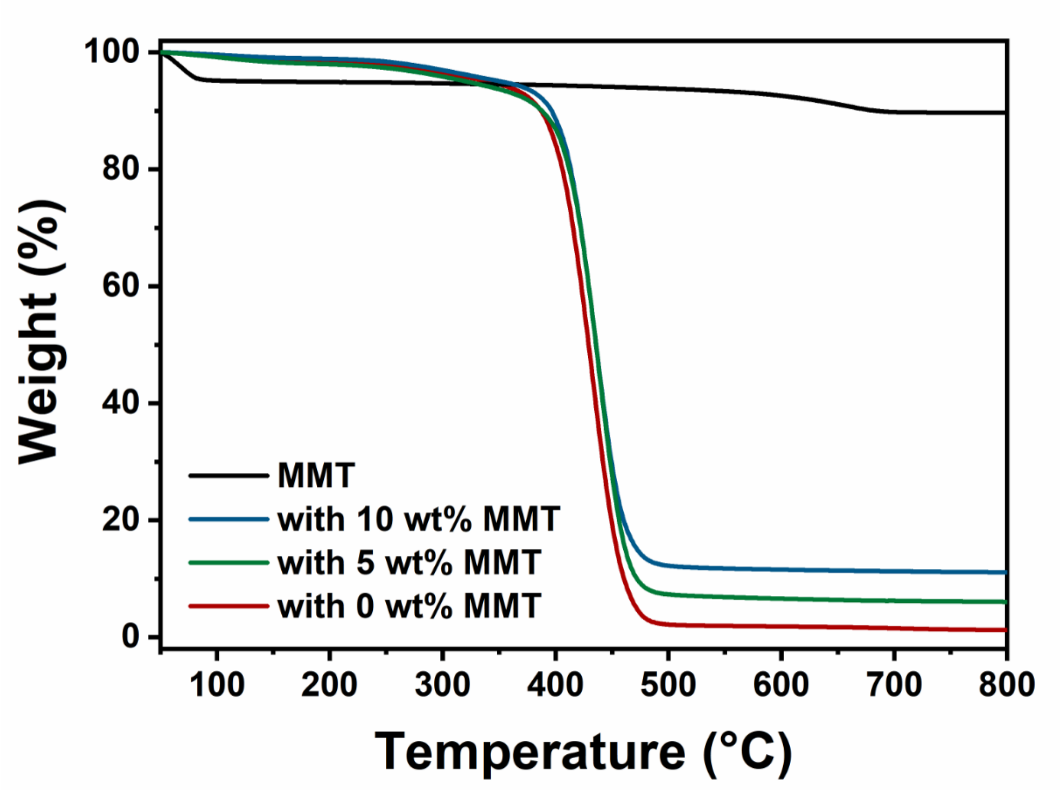

Figure 5.7 TGA analysis result of MMT and the nanocomposites

MMT dispersion structure was analysed by XRD as shown in Figure 5.8A. The clay interlayer spacing (d_{001}) of MMT was determined as 1.32 nm ($2\theta = 6.68°$). After the melt intercalation of MMT by PEG, the interlayer spacing of 2.08 nm ($2\theta = 4.24°$) was recorded (Figure 5.8B). As we can see, the interlayer spacing remains the same 2.08 nm for the

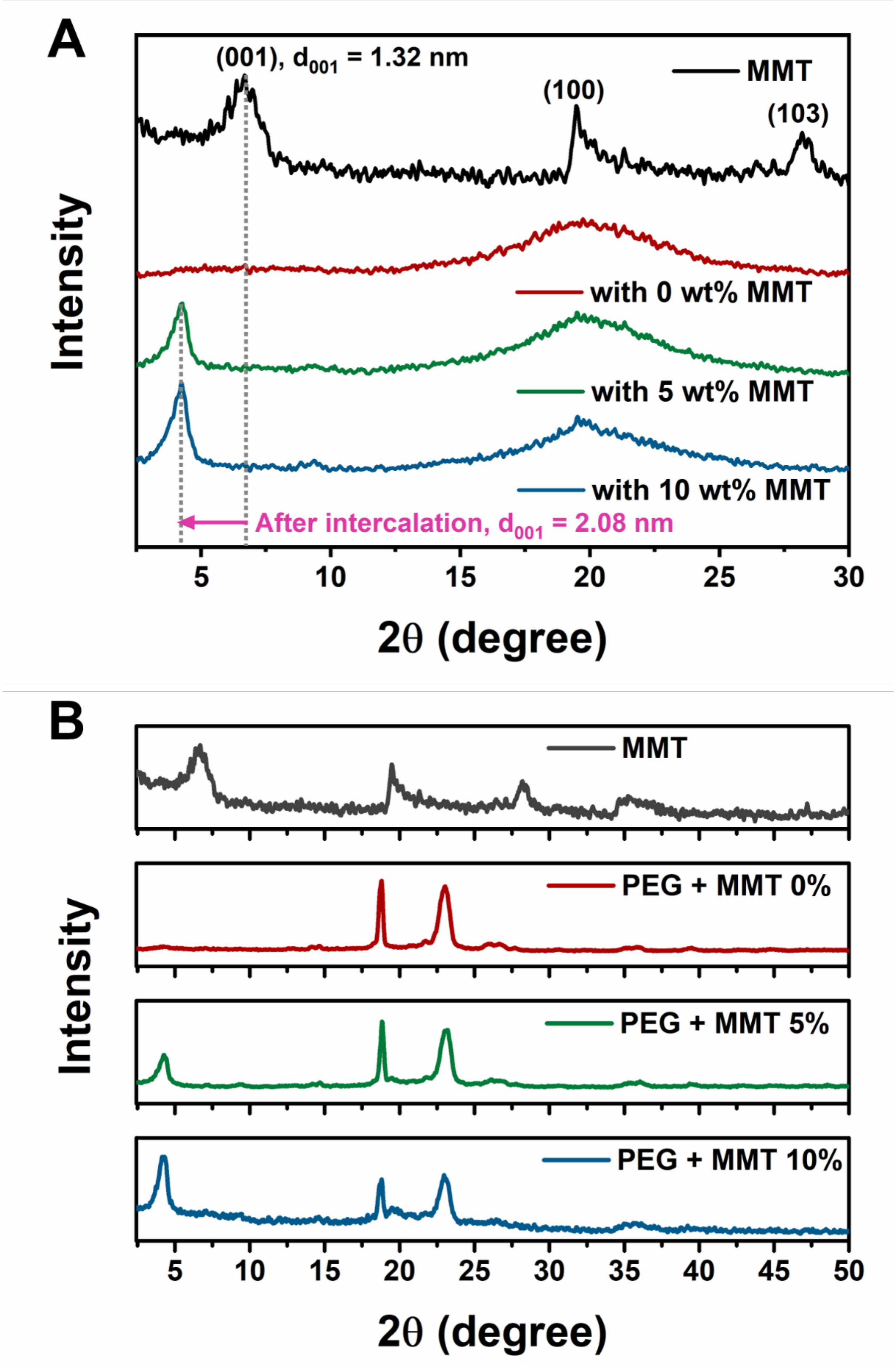

Figure 5.8 (A) XRD patterns of MMT and the nanocomposites. (B) Comparison of XRD patterns between MMT and MMT intercalated by PEG.

nanocomposites. The addition of PGS segments and subsequent copolymerisation with PEG does not change the interlayer spacing. This affirms again that the organophilic PGS segments does not interact with or intercalate into hydrophilic and ionic MMT, due to the mutual repulsion.[307] It can be also seen that the crystalline characteristics of PEG found under XRD (Figure 5.8B), disappeared in the nanocomposites with the amorphous halo at around $2\theta = 20°$.[308]

Chemical crosslinking of PEG by PGS segments forming a thermosetting network structure interfere the recrystallization of PEG. The intercalated MMT dispersion structure was also confirmed by TEM study. Figure 5.9A shows a lower magnification image, showing intercalated MMT. Some exfoliated MMT can be also seen, but minimal. The interlayer spacing of MMT was measured as 1.97 ± 0.11 (n = 20) in a higher magnification image (Figure 5.9B) which in a good agreement with the previously determined interlayer spacing of 2.08 nm from XRD.

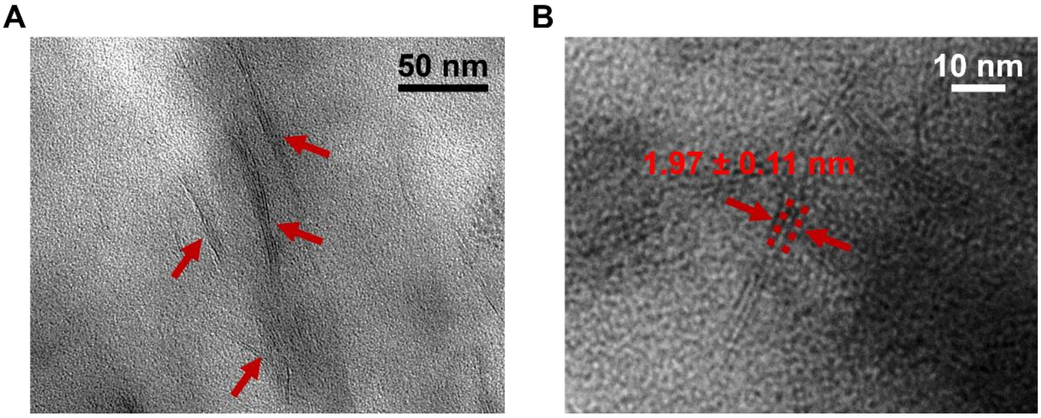

Figure 5.9 (A) TEM micrograph of the nanocomposite with 5 wt% of MMT showing intercalated clay structure (indicated by arrows). (B) A high magnification TEM micrograph showing the clay interlayer spacing of intercalated MMT in the nanocomposite (5 wt%).

As we discussed earlier, the nanocomposites are consisted of covalently copolymerised PGS and PEG segments, while MMT is intercalated by PEG. The additional hydrophilic components of PGS and MMT gives the nanocomposites water swelling properties, resulting in the swollen nanocomposite hydrogels. The swelling ratio of the nanocomposite hydrogels was evaluated as shown in Figure 5.10. Whilst pristine PGS has a minimal water swelling ratio of 5%, copolymerisation with hydrophilic PEG first rendered a higher water swelling ratio of 119 ± 1% before the addition of MMT. The additional hydrophilic and swellable MMT further improved the maximum hydration capacity together with osmotic pressure generated by intercalated PEG segments.[271] With the loading of 5 and 10 wt% of MMT, the water swelling

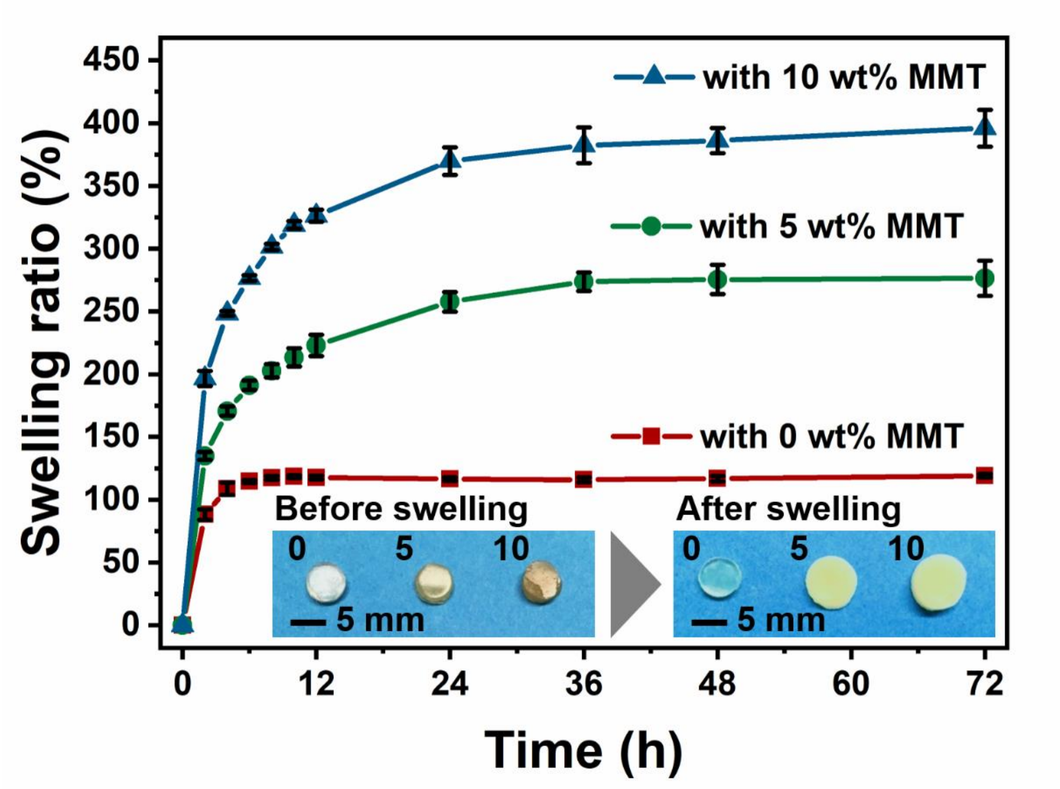

Figure 5.10 The water swelling ratio of the nanocomposites with 3 different MMT contents (0, 5, and 10 wt%). The inserted photographs show the size of nanocomposite specimens before (dry nanocomposites) and after swelling (nanocomposite hydrogels).

ratio values at equilibrium were 258 ± 8% and 396 ± 15%, respectively. The nanocomposite hydrogels with 5 and 10 wt% of MMT took a longer time of 36 h to reach at equilibrium, whilst it was shorter 10 h with 0 wt%. Clays do not swell instantly, but take a number of swelling phases and mechanisms.[269] Furthermore, MMT in the nanocomposite hydrogels was not free-swelling. The osmotic pressure of clay must be stronger to induce the polymer chain relaxation to be fully swollen.[270] Nevertheless, the control of swelling properties in the nanocomposite hydrogels with MMT plays an important role in wound healing applications by maintaining a moist wound site while absorbing the excessive wound exudates.[306,309] An adequately moist wound environment allows the migration of growth factors and cells for an optimised healing process.[81,306] The controllable swelling properties can also be utilised to design a swelling-controlled drug release devices as it dictates the diffusion of active molecules or drugs from the hydrogel.[272]

The surface water contact angle was measured as 84.0 ± 2.8° (0 wt% MMT), 78.9 ± 1.2° (5 wt% MMT), and 68.0 ± 1.7° (10 wt% MMT) (Figure 5.11), rendering a better surface wettability with the loading of MMT.[265] The presence of surface hydrophilic MMT may have induced this decrease in water contact angle. This controllable surface hydrophilicity is beneficial in wound healing applications as it dictates adsorption of wound exudates to optimise the healing process.[218,219] Additionally, cells are known to adhere better onto the hydrophilic surfaces which makes the nanocomposite hydrogels in this study as an attractive candidate in medicine where the cell transfer and culture are involved such as tissue engineering.[65,99]

After an injury, the water loss from the wound site through the evaporation is approximately 20 times greater than that of the normal skin surfaces. When a wound is exposed to air, the wound site dehydrates and a scab is formed. This is the body response to protect the site from bacterial infection. By doing so, however, the cells in dry microenvironment will die and tissue

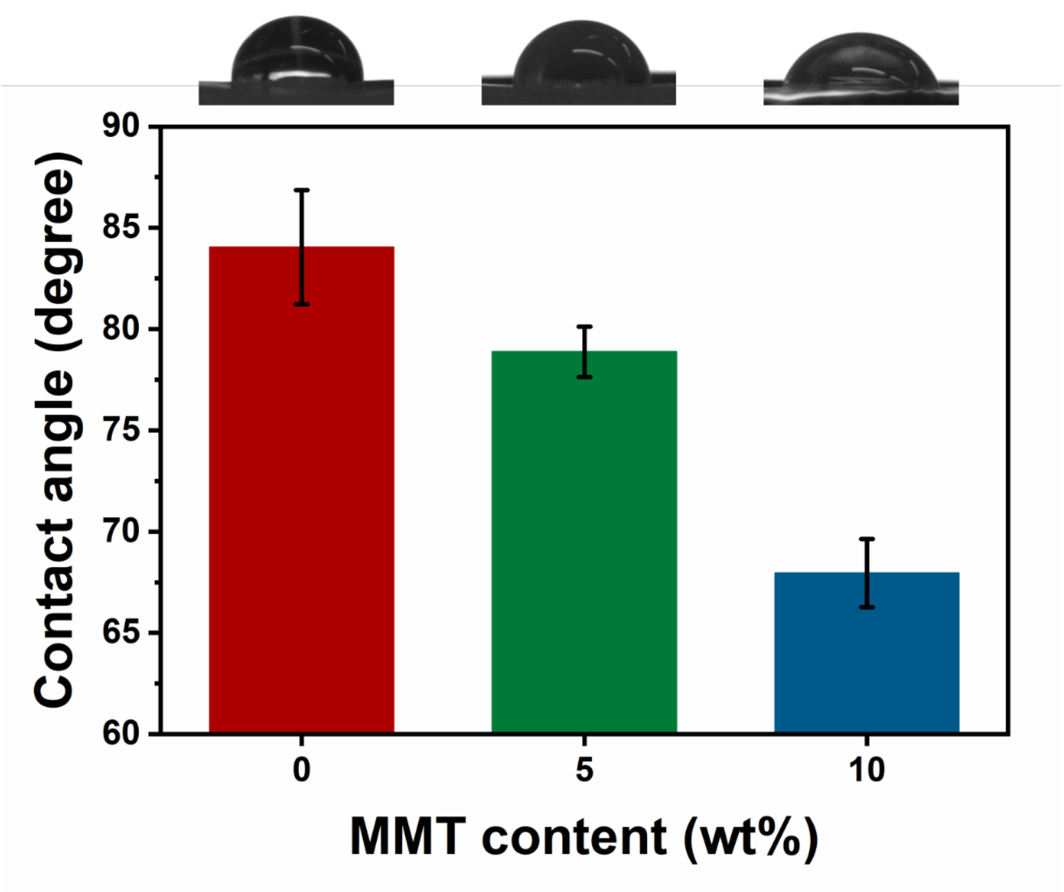

Figure 5.11 The surface water contact angles. The photographs on the top show the shape of water droplets on the surface of the nanocomposites.

lose its ability to heal substantially.[295] Therefore, a suitable wound dressing with its ability to retain an adequate amount of moist in the wound site to optimize the healing process. This ability depends on WVTR; a measurement of water vapour passes through an unit area during a fixed time period. Too high WVTR may result to dehydration of a wound site which not only delays the healing process, but also gives a scar tissue.[76,295] Too low WVTR may lead to the undesirable accumulation of wound exudates which often leads to the bacterial infection, and malodour, as well as patients' discomfort. WVTR of the nanocomposites were measured as shown in Figure 5.12; 154 ± 20, 87 ± 19, and 65 ± 15 g h^{-1} m^{-2} for the nanocomposites with 0, 5, and 10 wt% of MMT, respectively. This decreasing WVTR with the increasing loading of

MMT is mainly due to the barrier effect of clays, where water vapour diffusion takes the tortuous path due to the intercalated silicate layers of MMT.[310] A wound dressing with a specific WVTR must be chosen based on the wound specification. For instance, WVTR of 80–100 g h^{-1} m^{-2} is known to be adequate for burn wounds. In another study, 84.5 ± 10 g h^{-1} m^{-2} was found optimal for proliferation of epidermal cells and fibroblasts. In general, WVTR of the nanocomposites in this study is adequate for wound dressing applications.

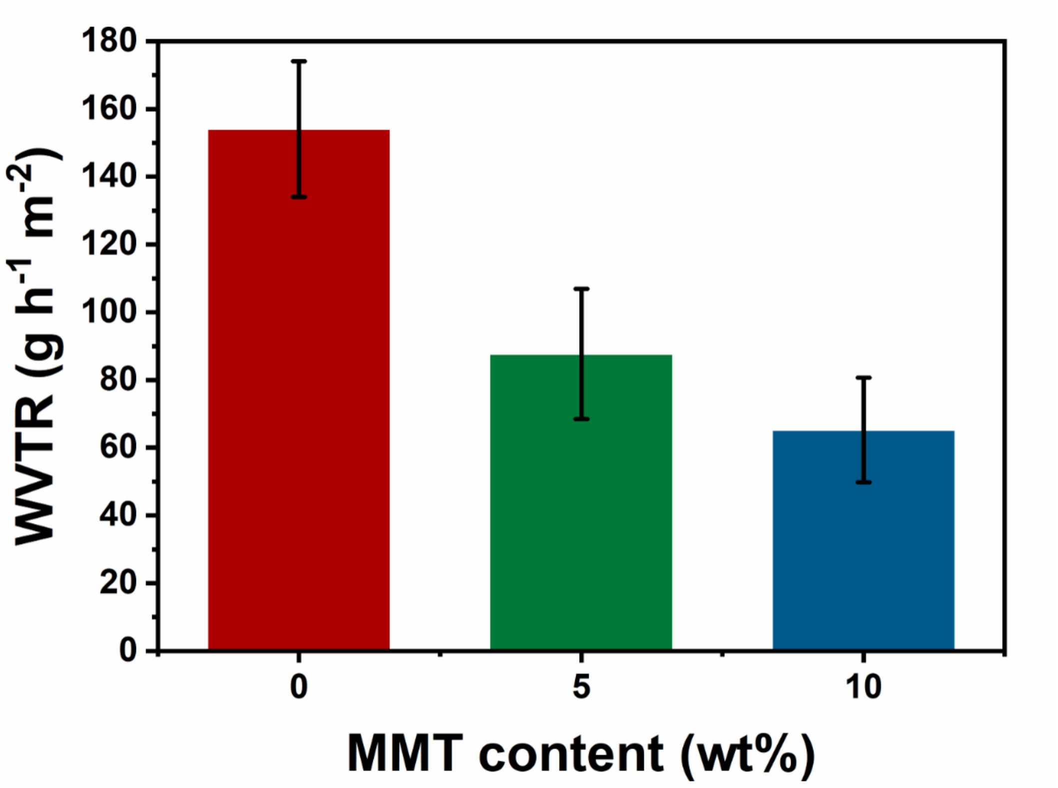

Figure 5.12 WVTR of the nanocomposites showing a decreasing trend with increasing MMT content.

5.3.2 Elastomeric tensile behaviours of hydrogels and porous foam structures

The mechanical properties of the nanocomposite hydrogel system were investigated. The summary of tensile parameters of the nanocomposite hydrogels are shown in Table 5.2. As we can see from Figure 5.13, the nanocomposite hydrogels exhibit elastomeric tensile stress-strain curves with high stretchability. The elongation at break value is inversely proportional to the loading of MMT, higher the MMT, lower the elongation at break. Whereas, the Young's modulus and ultimate tensile strength values increase with the loading the clay. This suggests that there is a strong physical crosslinking effect between MMT and PEG segments.[310–313] The increasing crosslinking density by additional MMT with PEG exerted the higher modulus and ultimate tensile strength, whilst compromising stretchability. However, even with the highest loading of 10 wt% of MMT, the nanocomposite hydrogel exhibited nearly 300% of elongation at break which is well beyond the range of the dynamic mechanical loading of soft tissues, which is typically around 15%.[60] The nanocomposite hydrogels also exhibited full-shape recovery after the tensile tests as shown in Figure 5.14. Figure 5.15 demonstrates the stretchability and conformability to the bodily movement of the nanocomposite hydrogels with 10 wt% MMT. Additionally, it is important for a wound dressing not to lose its mechanical integrity while replacement, otherwise it can lead their undesirable breakage or eventual

Table 5.2 A summary of tensile properties of the nanocomposite hydrogels

MMT (wt%)	**Young's modulus E (kPa)**	**Ultimate tensile strength σ_{max} (kPa)**	**Elongation at break ε_{tb} (%)**	**Energy at break T (mJ m^{-3})**
0	12.7 ± 2.6	37.1 ± 8.0	560 ± 38	10.0 ± 3.4
5	44.6 ± 2.9	120.4 ± 19.6	412 ± 75	28.1 ± 8.9
10	105.2 ± 6.0	228.5 ± 15.1	299 ± 45	41.1 ± 7.3

dissolution before complete tissue healing or regeneration. As shown in Figure 5.16, the hydrogel nanocomposite with 10% MMT show no evidence of mechanical failure and debris on the applied surface during the detachment.

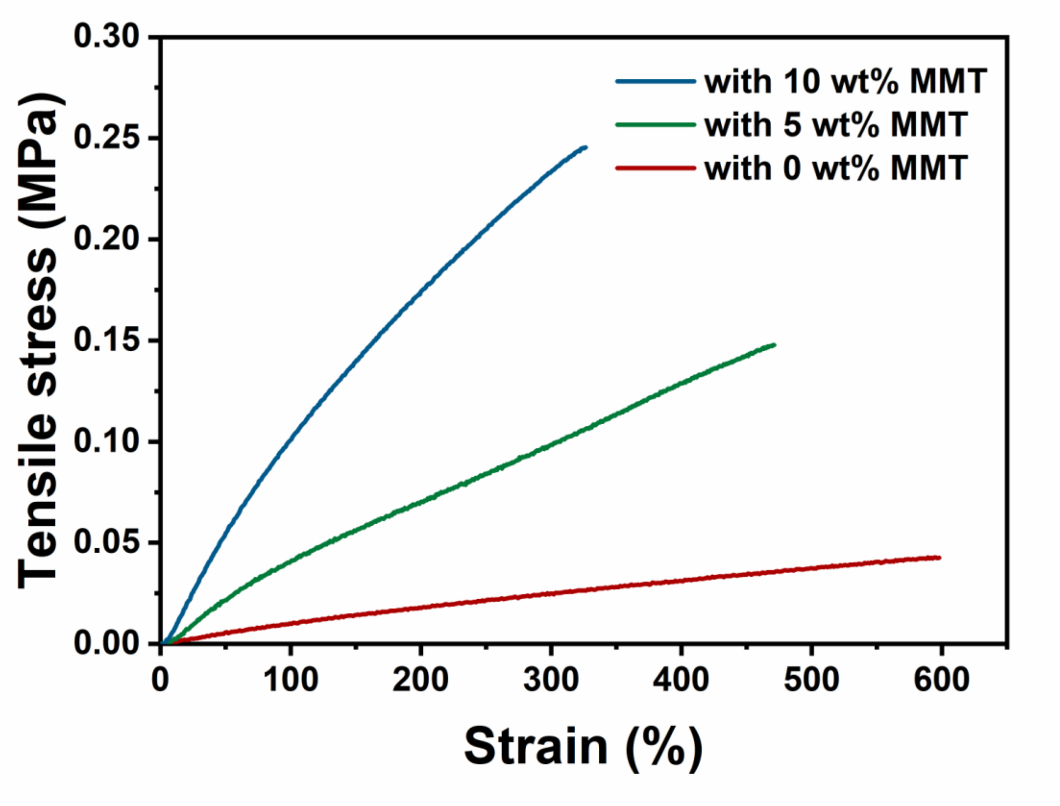

Figure 5.13 Representative tensile stress-strain curves of the nanocomposite hydrogels.

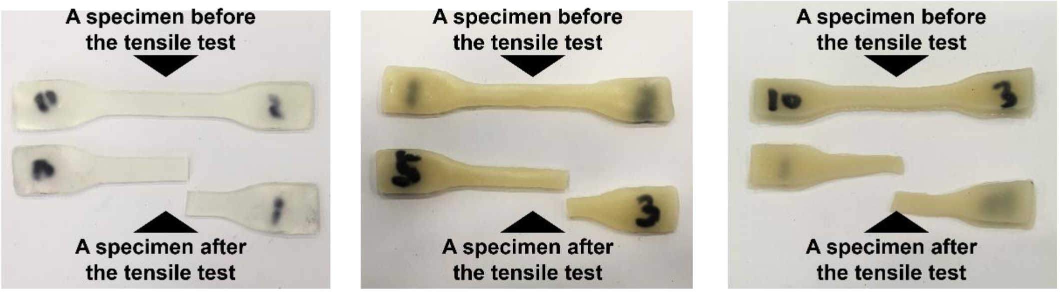

Figure 5.14 Representative images of the nanocomposite hydrogel before and after the tensile test revealing minimal creep and full shape recovery (from left to right; nanocomposite hydrogels with 0, 5, 10 wt% of MMT).

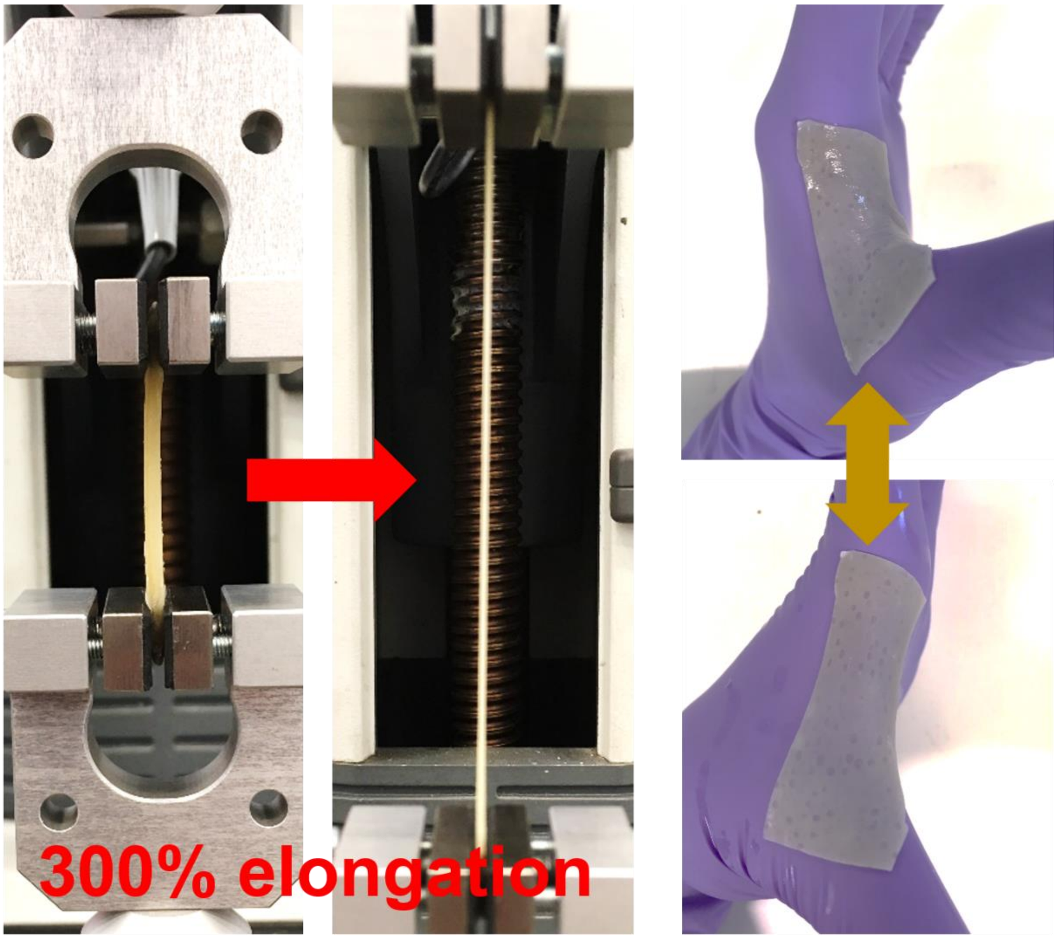

Figure 5.15 Demonstration of stretchability of the nanocomposite hydrogel (with 10 wt% MMT) during the tensile testing (left), as well as the same nanocomposite hydrogel placed on a hand joint withstanding a full stretch of the joint without failure (right).

The resins of the nanocomposite system before the curing are meltable and deformable into a desired shape, opening a possibility of building a complex structure. As a *proof-of-concept*, a porous foam structure was fabricated for the potential applications in tissue engineering and wound healing applications. As shown in Figure 5.17A, a large-scale fabrication is feasible, the shape and size will be determined by the mould that is used to contain the molten resins. Under a microscope, interconnected pores are visible, yet the connectivity of pores can be improved

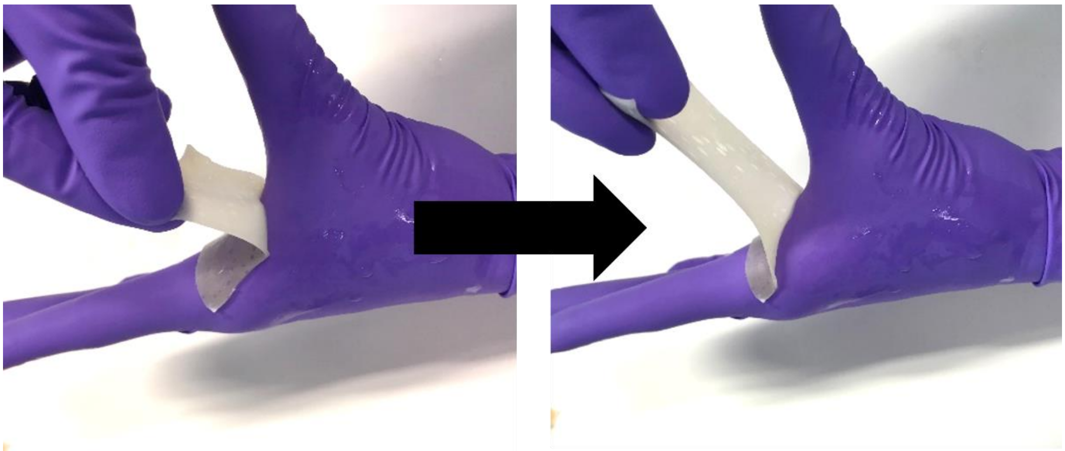

Figure 5.17 Detachment of the nanocomposite hydrogels (with 10 wt% of MMT) leaving no visible residues on the surface.

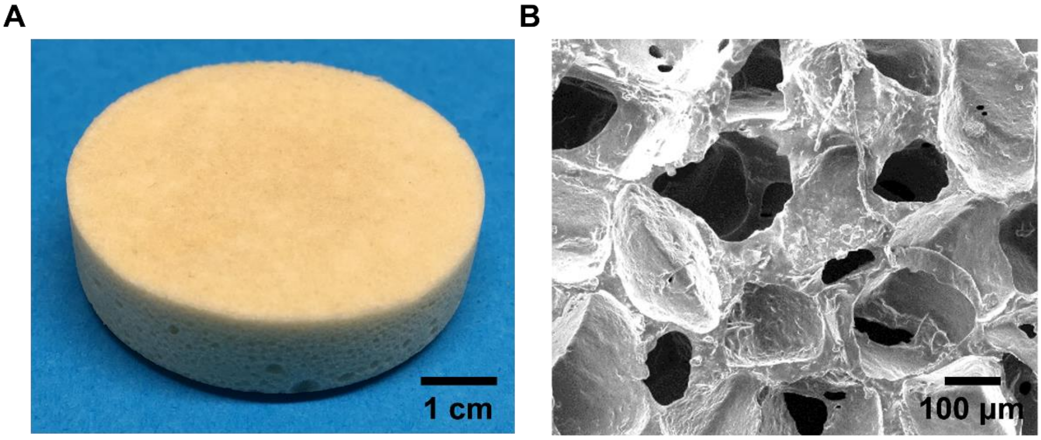

Figure 5.16 The mechanical behaviours of the proof-of-concept nanocomposite porous foam structure with 10 wt% of MMT. (A) Photograph showing a macroscopic view of the fabricated foam structure. (B) Porous microstructure seen in a SEM image.

by using a different type or amount of the porogens for higher cellular penetration and proliferation as well as the transportation of chemical species (Figure 5.17B).[314] The porosity calculated as 79 ± 4%, based on the ratio in the density between non-porous samples and the porous foam structures. A representative compressive stress-strain curves are shown in Figure

5.18, with the compressive Young's modulus and compressive stress at 75% strain of 0.26 ± 0.04 MPa and 1.11 ± 0.02 MPa, respectively. The fabricated porous foam structures are highly elastomeric, exhibiting the full shape-recovery as shown in Figure 5.19. This porous foam structure, together with good biodegradability and compatibility (discussed later), make an attractive candidate biomaterial for foam type wound dressing and soft tissue engineering.

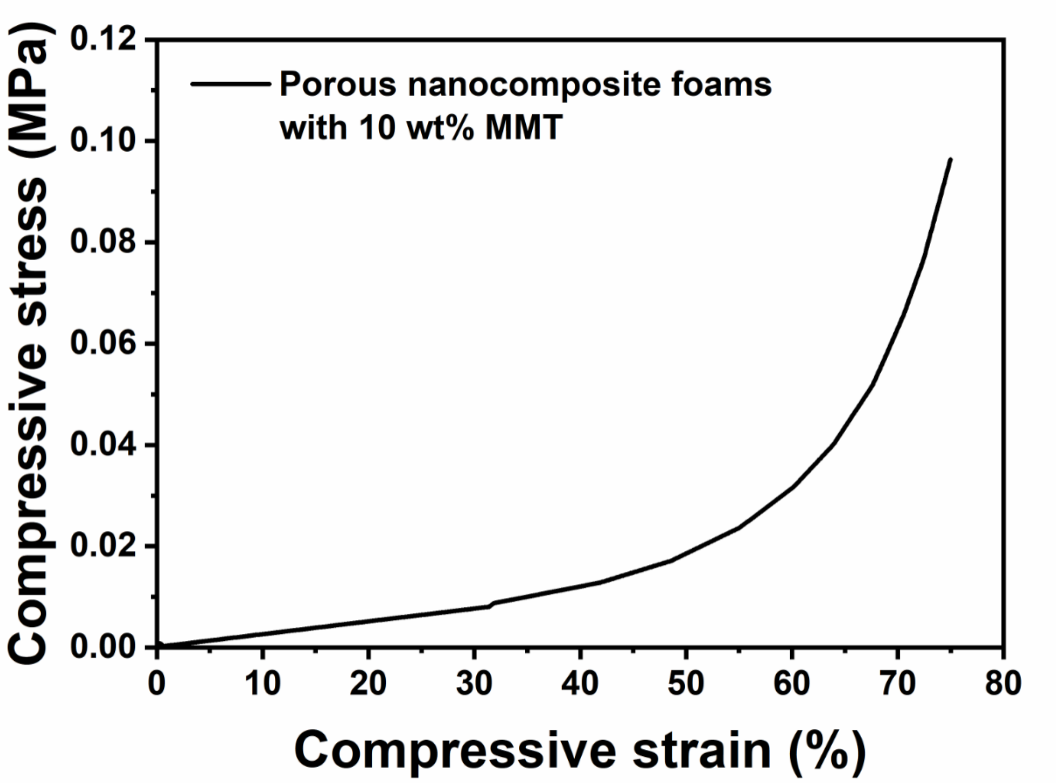

Figure 5.18 A representative compressive stress-strain curve of the *proof-of-concept* foam structure till a 75% of compressive strain.

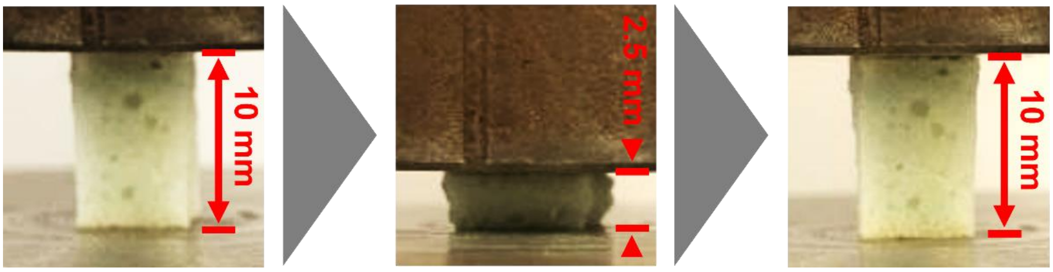

Figure 5.19 The elastomeric foam structure showing a full and immediate shape-recovery after a 75% of compressive strain.

5.3.3 Biodegradable and biocompatible properties

The effect of the loading of MMT on the nanocomposite hydrogels were investigated by the *in vitro* biodegradation test. Two different PBS media were used with or without lipase enzyme to catalyse the degradation ester bonds by hydrolysis. Figure 5.20 shows the percentage weight loss by the degradation for 28 days. Without lipase enzyme, the percentile weight losses after 28 days of degradation were 70.8 ± 3.7%, 36.3 ± 3.0%, and 21.0 ± 1.9%, with 0, 5, and 10 wt%, respectively. The degradation of nanocomposite hydrogels was faster with lipase enzyme, resulting in the weight losses after 28 days of 91.4 ± 2.0%, 60.6 ± 1.2%, and 50.1 ± 0.8%. With the loading of MMT, the weight losses from degradation decreases. The results suggest that the degradation of ester bonds from the PGS segments as well as between the PGS and PEG segments were hindered by the presence of MMT. This is due to the formation of hydrogen

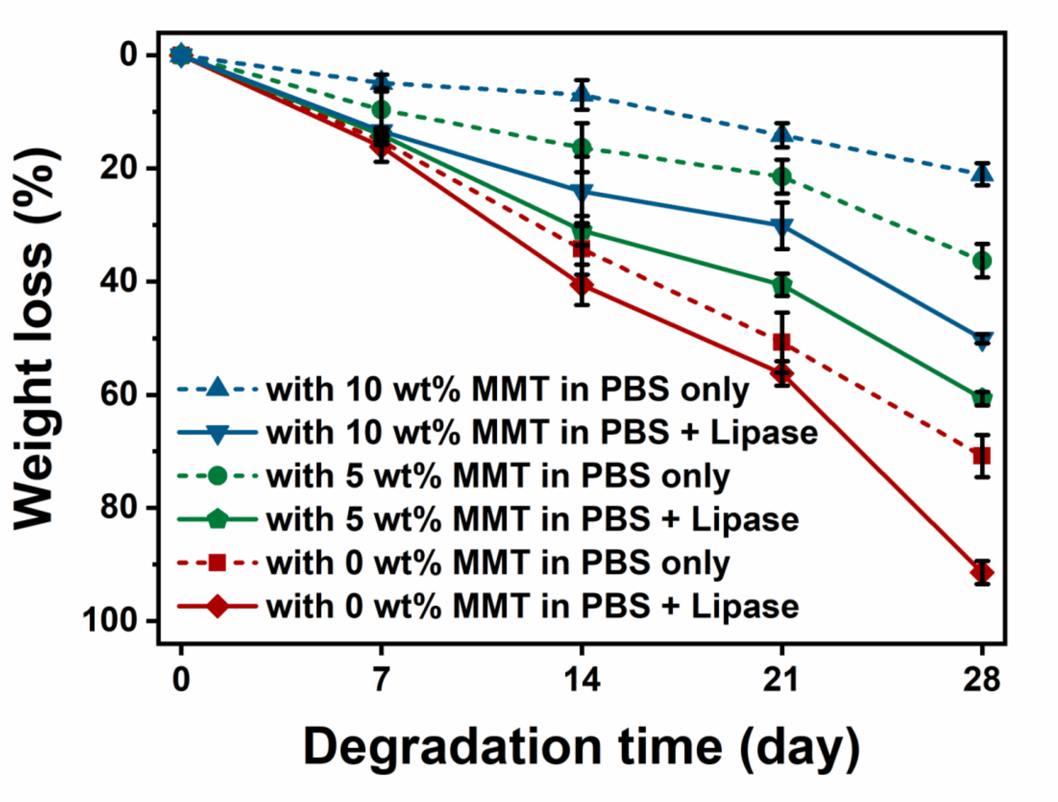

Figure 5.20 Percentage weight loss from the biodegradation test *in vitro*, showing different degradation rates by the MMT contents in the nanocomposite hydrogels.

bonds between the components and the barrier effect from MMT. Nevertheless, the controllable degradation behaviour with the loading of MMT is a beneficial for designing medical devices such as tissue scaffold, and degradation-controlled drug delivery devices, where the performance is directly dictated by the degradation rate of materials.[240,315]

The biocompatibility was investigated by the cell metabolic assay *in vitro* as shown in Figure 5.21. For all the nanocomposite hydrogels, the cell metabolic activity showed steady growths, with the maximum cell metabolic activity at day 7. Two-way ANOVA test revealed that there was no statistically significant difference in cell metabolic activity between the nanocomposite hydrogels in terms of the MMT content as well as the incubation time. One-way ANOVA found statistically significant increases in the nanocomposite hydrogels with 10 wt% of MMT between day 1 and day 4, as well as between day 1 and day 7. This suggests, fibroblasts were

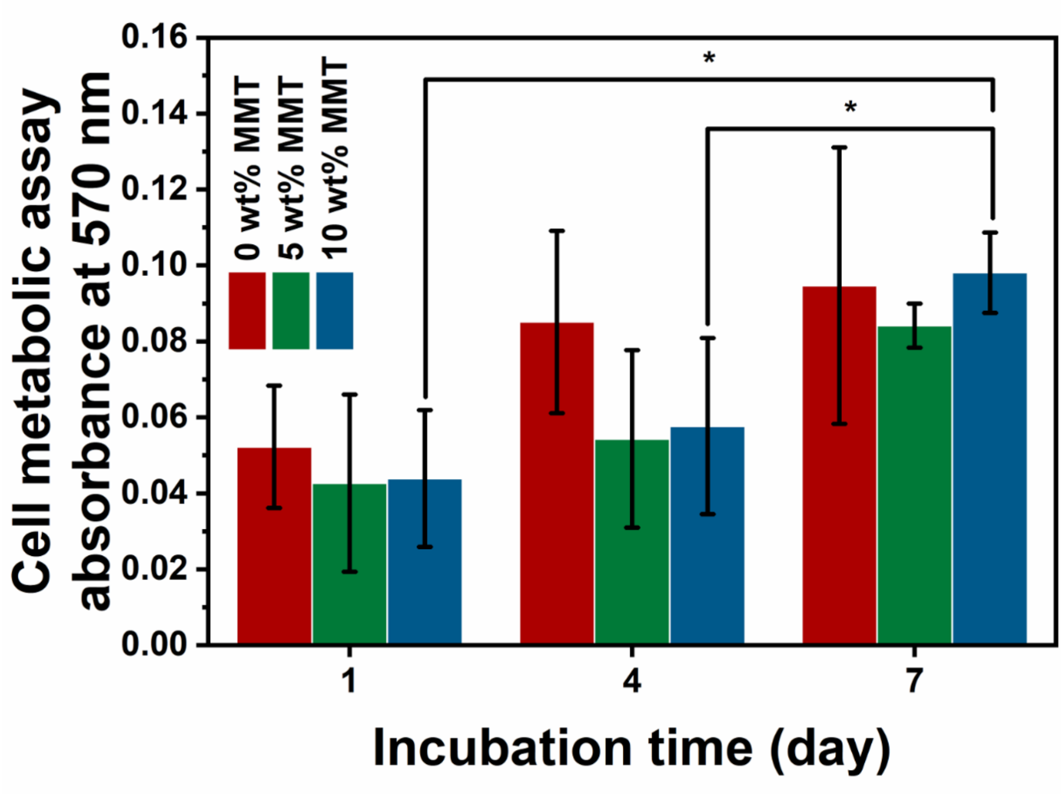

Figure 5.21 The *in vitro* cell metabolic assay results of L929 cultured on the surface of nanocomposite hydrogels, after subtracting the data for cell-free tests.

grown on the nanocomposite hydrogels with 10 wt% more rapidly.

The cell morphologies are examined under microscopy on the nanocomposite hydrogels with 0 and 10 wt% of MMT (Figure 5.22A and B). The cells on both cases appeared normal with adherent cell morphologies. Actin stress fibres can be seen indicating the fibroblasts are attached well on the specimen surfaces.[256] In both cases, the cells were highly confluent. Overall, no evidences in cytotoxicity from the nanocomposite hydrogels were found with the increasing cell metabolic activity and the good cell morphologies.

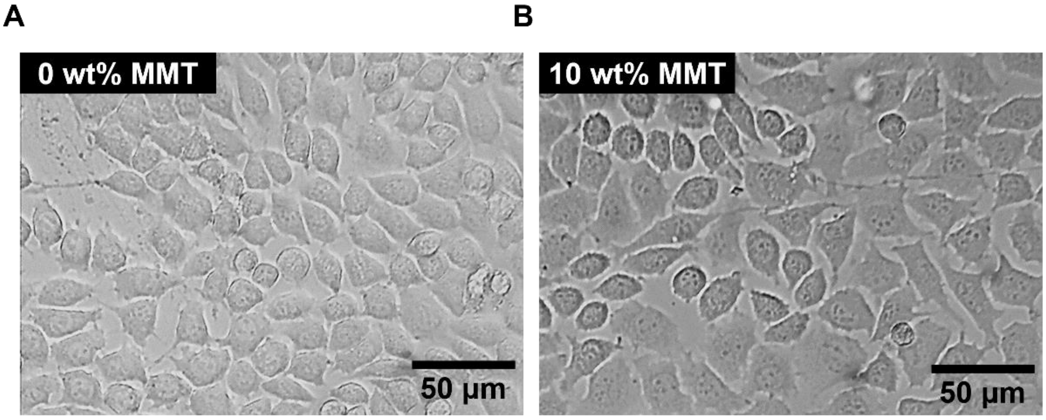

Figure 5.22 Micrographs show the L929 cell morphologies cultured for 7 days on the surface of (C) the nanocomposite hydrogel with 0 wt% MMT and (D) the nanocomposite hydrogel with 5 wt% of MMT.

5.3.4 Pro-angiogenic and malodourous diamine-controlling properties

The pro-angiogenic ability of the nanocomposite hydrogels was tested by CAM assay. E2 was also introduced, with its well-known ability to induce angiogenesis. The hypothesis was that the presence of MMT in the nanocomposite hydrogels would physically interfere the diffusion of E2 out of the nanocomposite hydrogels, showing a more sustained and controlled release of

E2 for optimal E2 release and activity. Total 4 different conditions were tested for CAM assay; (i) control; no MMT and no E2 were added into the hydrogel, (ii) MMT only; nanocomposite hydrogel with 10 wt% MMT, (iii) E2 only; 5 wt% of E2 was added into the hydrogel without MMT, and (iv) MMT and E2; nanocomposite hydrogel with 10 wt% of MMT together with 5 wt% of E2. The representative CAM images are shown in Figure 5.23. None of the gels have incorporated with CAMs, showing no vessel growth into the gels and no tissue infiltration. Gels were easily separable from CAMs at the end of the experiments. There was no obvious

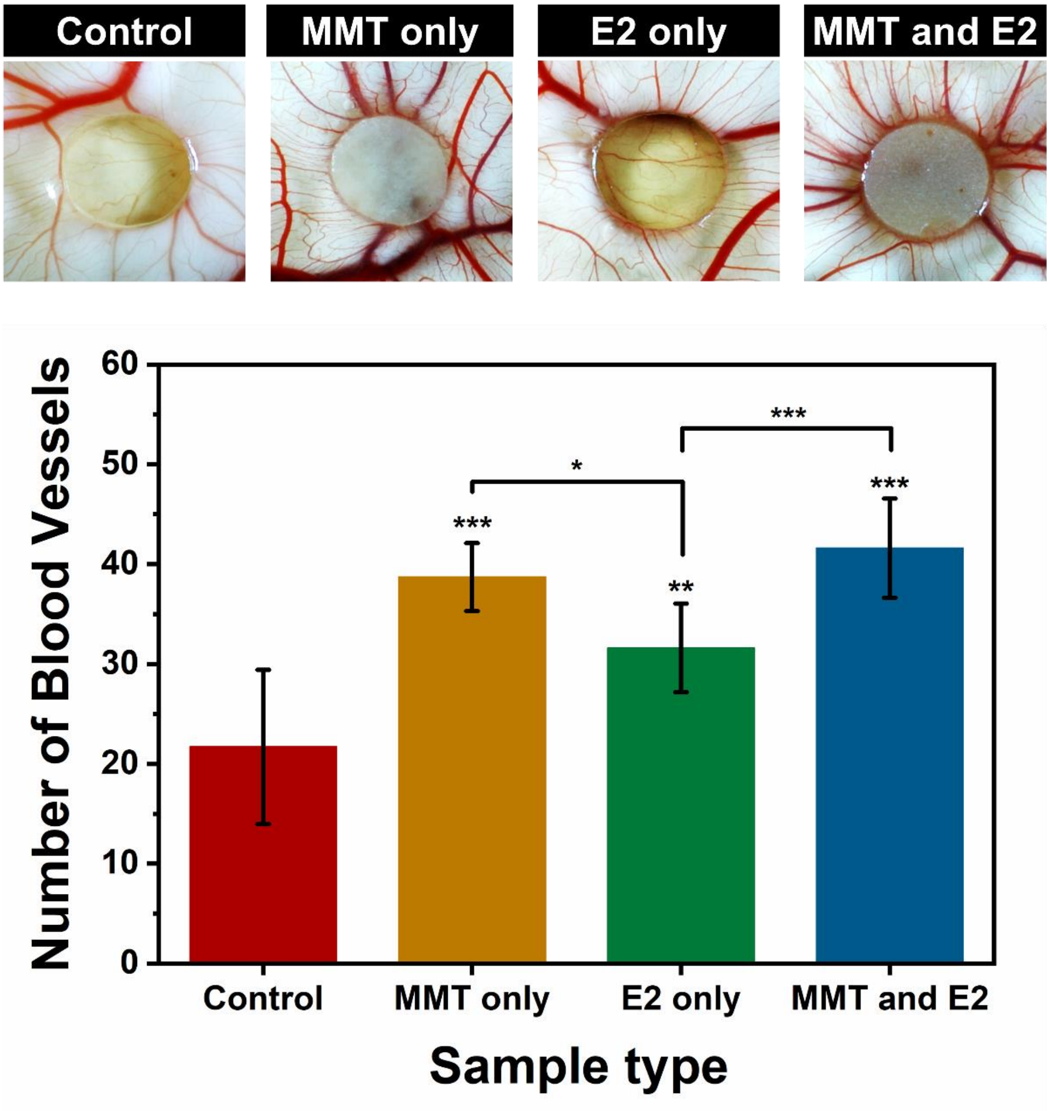

Figure 5.23 (Top) Representative CAM images from each test conditions. (Bottom) The counted number of blood vessels.

inflammation. As the samples are hydrogels with no macroscopic pores, this was expected. The embryo survival rate was the same in all types (77 %), confirming again good biocompatibility of the nanocomposite hydrogels together with the cell metabolic assay.[297]

The counted number of blood vessels are also shown in Figure 5.23. Between the control condition sample and the E2 only condition, there was an increase in the counted vessel number from 21.7 ± 7.7 to 31.6 ± 4.4, which is attributable to the addition of pro-angiogenic E2 into the system. Another increase is from the E2 only condition to the MMT and E2 condition; the vessel count number was further increased to 41.6 ± 5.0, showing the highest amongst the all other groups. This is first attributable to the controlled and sustained release of E2 with the addition of MMT. Figure 5.24 shows the cumulative E2 release profile from the nanocomposite hydrogels with 0 and 10 wt% of MMT. In both cases, the initial burst release can be seen up to

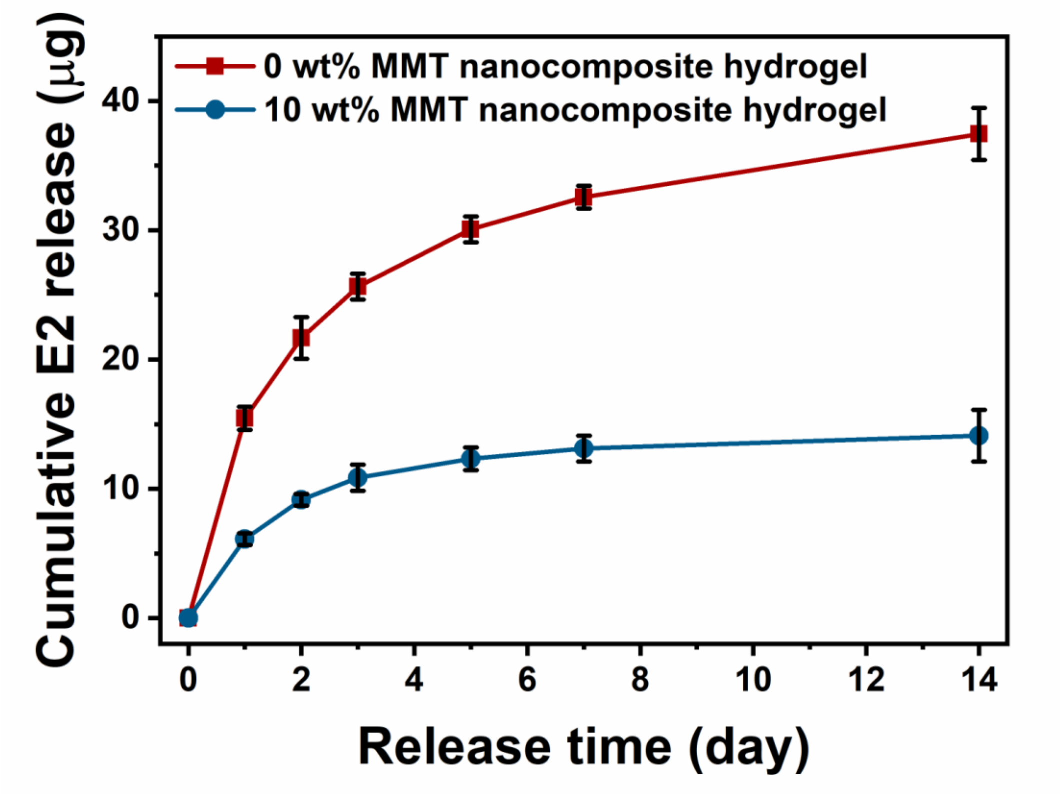

Figure 5.24 Release profile of E2 from the nanocomposite hydrogels with or without 10 wt% of MMT.

2 days. With the addition of MMT, the release kinetics decreased with a lower slope in the release curve, as MMT with in the nanocomposite hydrogels act as physical barrier for the E2 diffusing out. With 0 wt% of MMT, the released amount of E2 may have been too high to promote angiogenesis, resulting a lower vessel count.[316–318] Interestingly, the MMT only condition showed a higher vessel count of 38.7 ± 3.4, compared to the control condition. It was even higher than the E2 only condition. This is attributable to the high specific surface area of MMT, which are known to adsorb various growth factors such as VEGF.[292,319] The local microenvironment with adsorbed VEGF might have induced further angiogenesis with the conditions include MMT. Overall, the results suggest that MMT and E2 can have a synergetic pro-angiogenic properties in the nanocomposite hydrogels, which is useful in wound healing and tissue engineering applications.

The high specific surface area, together with the negatively charge surface ionic charge in MMT created another novel property of malodourous diamine-controlling in the nanocomposite hydrogels.[173,279] The malodourous diamines such as PUT and CAD, generated by the breakdown of amino acids in the necrotic tissues are positively charged. Therefore, the hypothesis was that the attractive Coulomb interactions between the MMT with a negative surface charge and cationic diamines would effectively lower the concentration of diamines in the surrounding environment of nanocomposite hydrogels.

Figure 5.25 shows the control of malodourous diamine compounds; PUT and CAD. One-way ANOVA revealed that there are statistically significant differences between the nanocomposites with different MMT contents. After 39 h of incubation with nanocomposite hydrogels, the concentrations of PUT in the solution were decreased by 21.3 ± 7.4% (with 0 wt% of MMT), 51.7 ± 4.1% (with 5 wt% of MMT), and 81.0 ± 8.0% (with 10 wt% of MMT). The percentile decreases of CAD after the incubation with the nanocomposite hydrogels were

16.4 ± 6.5% (with 0 wt% of MMT), 32.0 ± 4.6% (with 5 wt% of MMT), and 61.1 ± 5.9% (with 10 wt% of MMT). The lower decreases of CAD are possibly due to the higher molecular weight of CAD compared to PUT. The excessive generation of PUT and CAD on the wound sites not only disturbs the patients' comforts with the malignant odours, but also affects the tissue regenerations.[76,79,80] For instance, a decreased putrescene level is one of the conditions for the

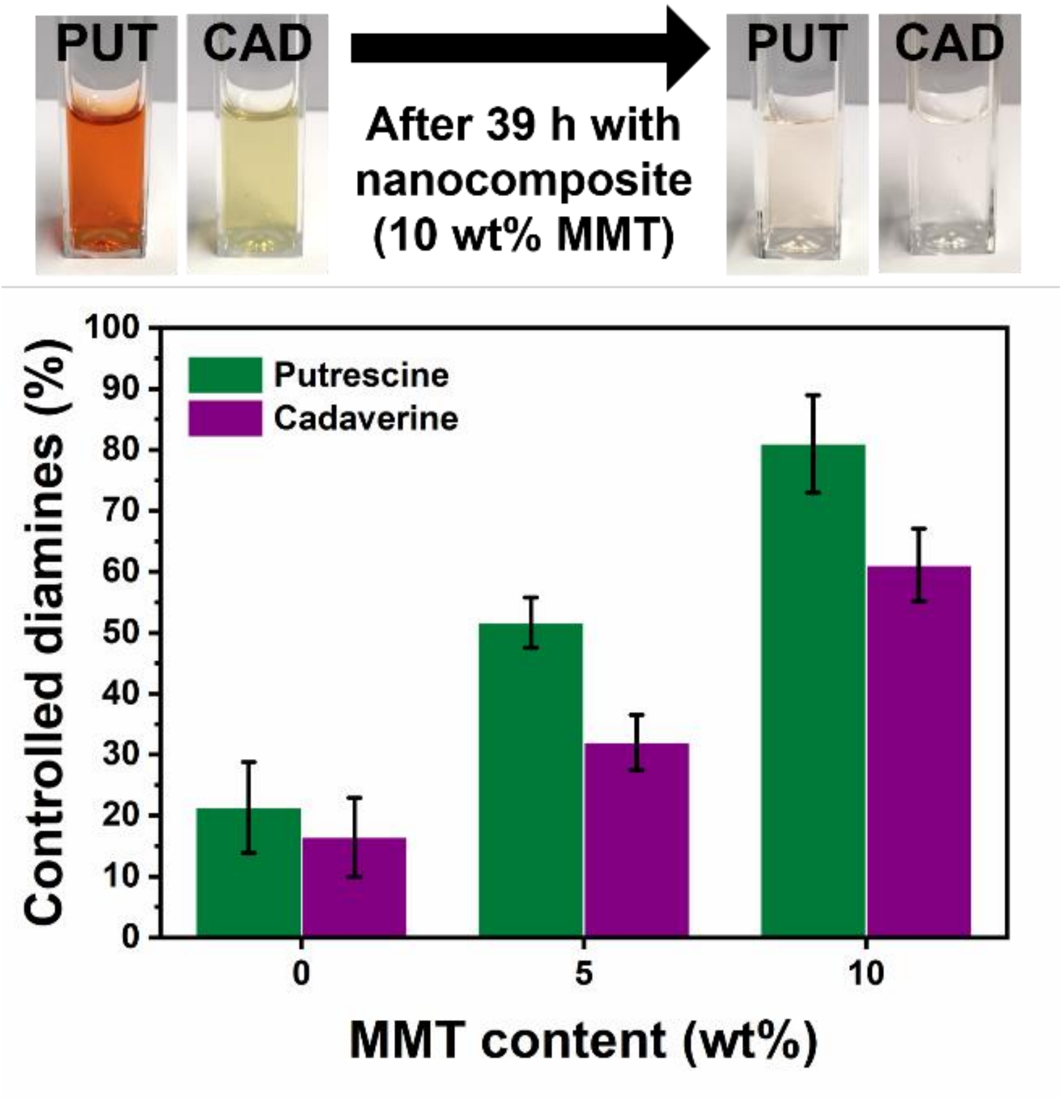

Figure 5.25 PUT and CAD controlled by nanocomposite hydrogels after 39 h. The photograph shows the colour of PUT and CAD solution after the reaction with OPA and MAA for the colourimetric determination. The stronger the colour is the higher the concentration.

cells to migrate across the wounds.[320] The ability to control the diamine products with MMT in the nanocomposite hydrogels can be studied further to regulate the optimised regeneration of target tissues.

5.4 Conclusions

A bioelastomer-clay nanocomposite system was developed with the PGS pre-polymer, PEG, and MMT. The synthesis was performed in a combined approach of melt intercalation and *in situ* polymerisation. PEG was first intercalated into MMT. The PGS pre-polymer with an excessive number of carboxyl groups and a relatively small molecular weight induced the crosslinking of polymers together with the hydroxyl groups in PEG to form a polymer network through ester bonds, as confirmed in FTIR. The intercalated MMT dispersion structure was confirmed under XRD and TEM studies. The loading of MMT greatly improved the hydration properties of the nanocomposites, resulting in swollen nanocomposite hydrogels in contact with water. The addition of MMT also increase the surface hydrophilicity and decrease the WVTR. All the nanocomposite hydrogel exhibited good flexibility, stretchability, and full shape recovery, even at a fully swollen state. The tensile properties were altered with the increasing loading of MMT, showing higher modulus due to the additional physical crosslinking between MMT and PEG segments.

A porous foam structure was also studied as a *proof-of-concept*, broadening the future applications of this new nanocomposite system in foam type wound dressing and tissue engineering.

The addition of MMT on the biodegradability was also investigated in vitro, showing a highly tunable degradation kinetics inversely related with the increasing loading of clay. No evidence in cytotoxicity was found in the cell metabolic assay with L929, with the increasing cell metabolic activity as well as the normal and confluent cell morphologies discovered under a microscopy study.

The addition of MMT on the pro-angiogenic ability of the nanocomposite hydrogels was also examined. A pro-angiogenic agent of E2 was added in the test. The addition of MMT controls the release behaviour of E2. The results also suggested that there is a synergistic activity when MMT and E2 were added together into the nanocomposite hydrogel system. The addition of MMT also gives the ability to control the malodourous diamine compounds.

Overall, the loading of MMT into the nanocomposite system can alter its hydration, vapor transmission, mechanical, and degradation properties. Furthermore, new bioactive properties such as pro-angiogenic and diamine-controlling behaviours were achieved with MMT. Together with its proven biocompatibility and porous foam architecture, this new nanocomposite hydrogel system has a great potential in soft tissue healthcare such as wound healing, tissue engineering, and controlled drug delivery. Future studies can include the exploration of pro-angiogenic activity of MMT, and in vivo application studies to fully address the functionalities of the nanocomposite system as well as its biocompatibility and biodegradability.

Chapter 6 Other exploratory studies

This chapter addresses other preliminary studies that has led to the work in the previous chapters and exploratory studies which could not be concluded due to the problems in the material designs or process methods, as well as lack of time. However, from these studies, I could learn the valuable knowledges on characteristics and properties of PGS polymer, general biomaterials and biopolymers, as well as polymer chemistry, synthesis, processing, and characterisation techniques. I would like to mention here that the process of doing the literature review, thinking about new possibilities, and designing a new material were one of the most entertaining and educational moments in my PhD study.

6.1 Polyester-clay nanocomposites based on poly(glycerol sebacate) and Closite 30B

The mechanical properties of PGS can be tailored by the synthetic condition and molar ratio of monomers.[9,21–23,25] For instance, the longer synthesis time yields a PGS with a higher crosslinking density, having greater modulus and strength than one with a lower crosslinking density. However, there is a limitation in terms of the range of mechanical properties which can be acquired in pristine PGS. To engineer a wider range of properties, polymers are often mixed with nano-sized fillers with a greater modulus and various morphologies to achieve polymer nanocomposites. In this study, Closite 30B clay was used as the nano-filler and mixed directly with PGS by a simple solvent method with THF. We hypothesised that the mechanical properties would be greatly improved with the addition of Cloisite 30B with its greater modulus than PGS and high surface area, as well as the good compatibility with organic PGS.[251,303]

Furthermore, interesting additional properties such as the surface wettability and drug loading capacity can be achieved through the superior adsorption property of clay, which normally cannot be seen in the pristine PGS.[321]

The PGS pre-polymer (8 g), prepared at 120 °C for 72 h with the same reaction set-up as Chapter 4, was dissolved together with 0, 0.5, 1, 2, and 4 wt% of Cloisite 30B (in respect to the PGS pre-polymer) in THF (20 mL) for 1 h on a magnetic stirrer (300 rpm) at room temperature, followed by 1 h of ultrasonication in a sonication bath. The mixtures were then cast on a nonstick PTFE dish and the solvent was removed by evaporation for 1 day in a fume cupboard at ambient temperature and another 1 day in a vacuum oven at 40 °C. After the complete removal of solvent (defined by the weight), the samples were cured in a vacuum oven at 120 °C for 48 h, followed by a washing procedure with ethanol for 48 h with agitation to remove the uncrosslinked sol proportion within the polymer matrix. The measured sol proportion was 18.4 ± 2.3%, 18.6 ± 1.9%, 19.9 ± 1.4%, 21.1 ± 2.6%, 23.7 ± 2.5%, with the addition of 0, 0.5, 1, 2, and 4 wt% of Cloisite 30B, respectively. The increasing sol proportion is attributable to the clay interfering the chemical crosslinking of PGS through the ester bonds.

The tensile testing was performed on a Hounsfield H100KS (Tinius Olsen), according to the ISO 527, equipped with a 10 N load cell at a strain rate of 50 mm min^{-1}. The dog-bone specimens (n = 6, thickness: 0.57–0.66 mm) were used The test results are reported in a manner of mean ± standard deviation. The XRD test was performed on a STOE STAPI P (Cu $K\alpha_1$, λ = 0.15406 nm, 40 kV, 35 mA, scan rate: 0.1° sec^{-1}).

Figure 6.1A shows the fabricated nanocomposite films. The colour of samples becomes more yellowish as the clay content increases, due to the presence of Cloisite 30B clay (pale-yellow colour). To understand the clay dispersion structure within the PGS matrix, the samples

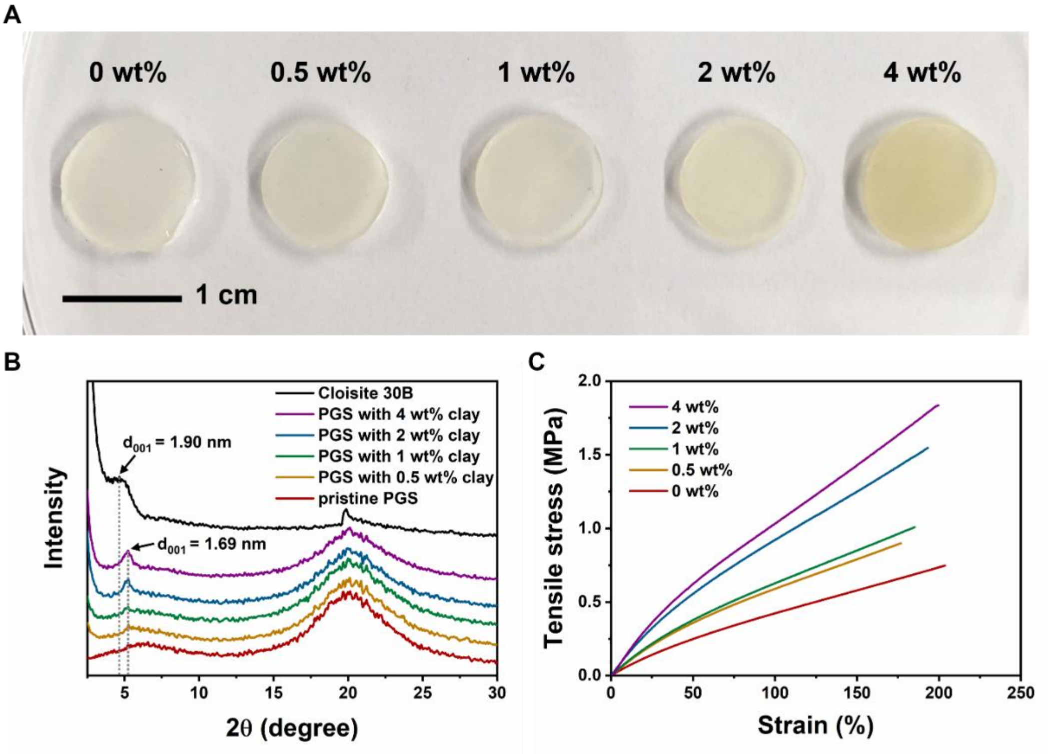

Figure 6.1 (A) the fabricated PGS-Cloisite 30B composite films. (B) XRD patterns showing the decrease in the clay interlayer spacings in the composites. (C) The representative tensile stress-strain curves of PGS-Closite 30B composite films.

were tested under the XRD. Unfortunately, an increase in the clay interlayer spacing (d_{001}) was found from 1.90 nm ($\theta = 2.33°$) to 1.69 nm ($\theta = 2.61°$), indicating the aggregation of clay layers (Figure 6.1B). One can expect that the crosslinking of PGS reduces the free space in the polymer matrix, resulting in segregation and aggregation of clay.[322] Furthermore, competitive co-intercalation of clay may occur by both the solvent and the PGS pre-polymer in this solvent method. The clay intercalation by PGS might have not been possible when the clay intercalation by solvent is much more favourable, having the clay interlayer spaces occupied primarily by the solvent molecules, not by the PGS polymer segments.[323] Lastly, as the solvent method relies on the entropy gained by desorption of solvent which would be compensated by the decrease in conformational entropy of intercalated polymers, temperature decrease can be detrimental to achieve intercalated clay structure. The evaporation of highly volatile solvent THF, might have reduced the temperature of material system and weakened the entropy effect in the solvent method.[323] As a result, the mechanical property achievable from this composite system was not greater than the range of pristine PGS only (Figure 6.1C). The measured tensile Young's modulus, ultimate strength, and elongation at break are shown in Table 6.1 together with those values of pristine PGS in the literature.

Table 6.1 The tensile properties of PGS-Cloisite 30B composites and the pristine PGS in the literature.[20,23,24,128,136]

Clay content (wt%)	Young's modulus (MPa)	Ultimate strength (MPa)	Elongation at break (%)
0	0.55 ± 0.11	0.70 ± 0.07	198 ± 17
0.5	0.79 ± 0.03	0.82 ± 0.11	183 ± 10
1	0.84 ± 0.09	0.91 ± 0.09	177 ± 31
2	1.31 ± 0.22	1.53 ± 0.20	202 ± 25
4	1.52 ± 0.14	1.68 ± 0.23	189 ± 23
Pristine PGS[20,23,24,128,136]	0.06–1.67	0.23–1.83	41–448

The research work was not performed further here. However, this experience helped me to design a better nanocomposite system in Chapter 4 and 5. Introduction of PEG as a chain extender and the *in situ* polymerization approach in both chapters was successful to develop new PGS-based polymer-clay nanocomposite systems.

6.2 Poly(glycerol sebacate)/chitosan semi-interpenetrating polymer network

Chitosan is a natural polysaccharide produced from N-acetylation of chitin under an alkaline condition.[324] The chemical structure of chitosan is shown in Figure 6.2. It has been widely studied in the biomedical applications, with its interesting biochemical properties as well as good biodegradability and biocompatibility. Chitosan is also haemostatic, antibacterial, and hydrophilic. This project aimed to develop a new elastomeric hydrogel system by mixing PGS and chitosan. The hypothesis was that the elastomeric, hydrophobic, and biochemically inert PGS would be modified to have hydrophilicity, haemostatic, and antibacterial properties by the addition of chitosan, which can be an attractive collection of properties for wound healing applications.[76] It must be also noted that there was a personal interest in investigating the possibility of making a new polymer structure with PGS, instead of copolymers and polymer nanocomposites we discussed in the previous chapters.

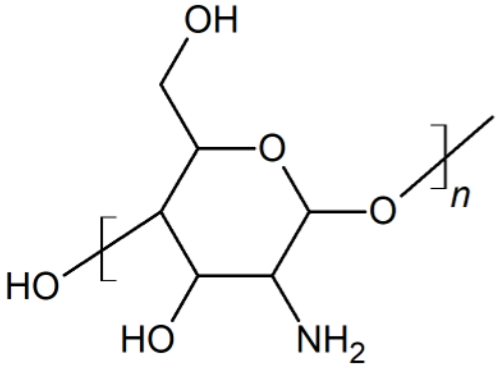

Figure 6.2 Chemical structure of chitosan, showing 1-4 linked 2-amino-2-deoxy-β-D-glucopyranose.

As PGS forms a macromolecular network and chitosan is a linear polymer, we aimed for a semi-interpenetrating polymer network (SIPN) hydrogel structure with PGS and chitosan (Figure 6.3A). In the SIPNs, one polymer forms a network structure and the other physically interpenetrates the first one without forming another network.[325] The advantages of SIPNs include the enhanced mechanical properties and swelling/deswelling response, which are beneficial for wound healing applications. Furthermore, the bioactive functional groups of chitosan can be preserved in this case, by not participating in crosslinking of polymers.

Three different preparation attempts were made. The first approach involved a passive diffusion method. A fully cured PGS film swollen in a solvent and chitosan were dissolved in the same solvent. This test was to see if the passive diffusion is enough to create a SIPN structure. One of the difficulties here was that the solvent for both swelling hydrophobic PGS and dissolving hydrophilic chitosan. After a number of tests, a suitable solvent mixture system for this was found; the acetic acid aqueous solution (80%). The same PGS pre-polymer from Chapter 4 was used and cured in the vacuum oven at 120 °C for 36 h. The cured PGS (2 g) was swollen in the acetic acid aqueous solution (20 ml). Chitosan was dissolved in the same solution (1 w/v%) and incubated in a closed vessel at 70 °C for 3 days with mechanical agitation. The PGS was then collected from the solution, washed by water thrice, and tested under the FTIR. However, no evidence of chitosan was found in the sample (data are not presented). This is possibly due to the repulsive interaction between the hydrophobic PGS and hydrophilic chitosan. The cured PGS also must have not enough free space for chitosan to penetrate in the PGS networks.

The second approach was a melt mixing method. Chitosan was directly mixed into the molten PGS pre-polymer. The PGS pre-polymer synthesised in the same method as Chapter 4 was molten at 60 °C and chitosan was mixed. The resulting mixture of the PGS pre-polymer

(2 g) and chitosan (0.1, 0.2, and 0.4 g) was then cured at 120 °C for 36 h in a vacuum oven. However, this method yielded a polymer film with visible chitosan aggregates.

In the third approach, a solvent method was used. Chitosan (2 g) and the PGS pre-polymer (0, 0.1, 0.2, 0.4, and 0.8 g) were mixed together in the acetic acid aqueous solution, followed by solvent removal by evaporation and curing of PGS. The evaporation was done in a fume cupboard at ambient temperature for 2 days and in a vacuum oven at 60 °C for 3 days. The curing was performed at 120 °C for 36 h. This method yielded relatively homogeneous films as shown in Figure 6.3B. The samples were flexible in some extent, but not stretchable, making them not suitable for use in soft tissue applications. Thereby, further study on this work was

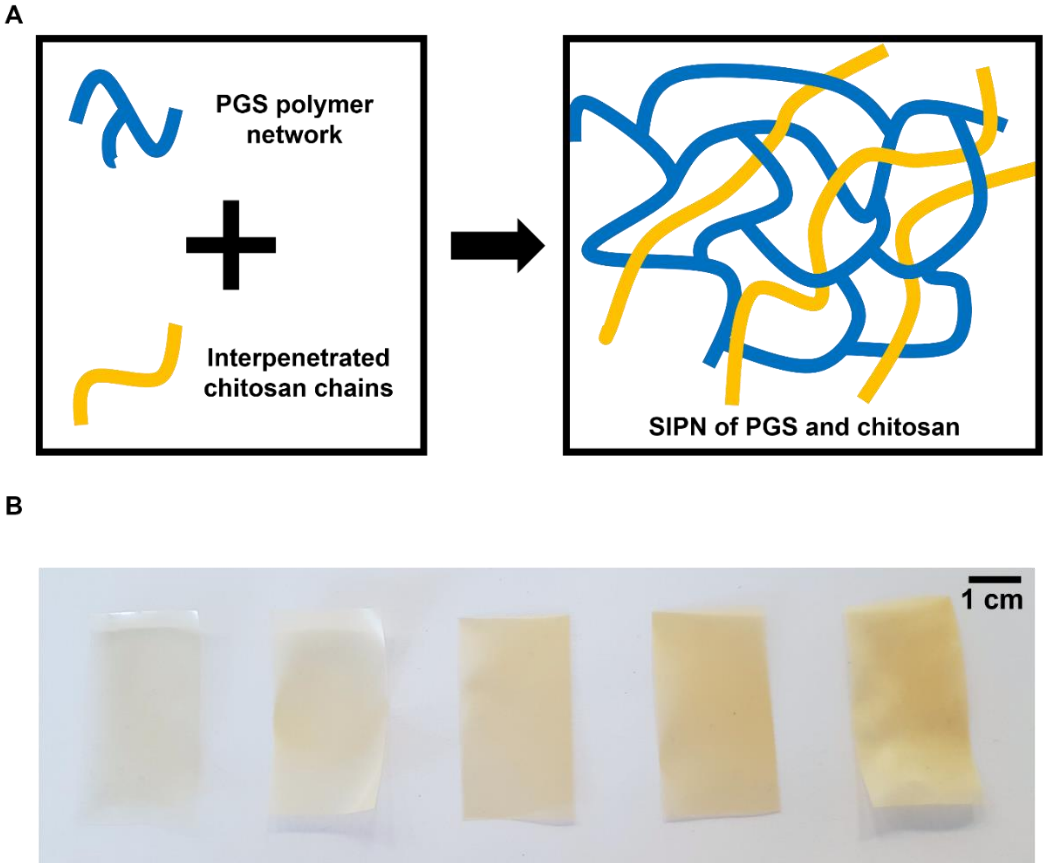

Figure 6.3 (A) The planned SIPN structure made of the PGS polymer network and interpenetrated chitosan chains. (B) Photos showing the samples by a solvent method with 2 g of chitosan and 0, 0.1, 0.2, 0.4, and 0.8 g of the PGS pre-polymer

not performed. Future work can include introduction of biocompatible chain extender such as PEG for development of PGS-based stretchable SIPNs.[326]

6.3 PGS microspheres by a "deep frying" approach

PGS has its advantage in developing a degradation-controlled drug delivery device as it exhibits a surface erosion degradation behaviour with a linear degradation rate unlike the other conventional thermoplastic polymers in biomedical applications such as PLA, PGA, and PLGA which show bulk degradation behaviours.[11] Therefore, drug carriers built based on PGS would have more linear and constant drug release rate with its linear degradation rate compare to the other conventional degradable polymers.

PGS is usually synthesised in a two-step approach. The first step is preparation of the pre-polymer in a reactor set-up as we have discussed in the previous chapters. The second step is the casting and curing of the pre-polymer in a vacuum oven, well above 100 °C (usually the curing temperature of 110 to 150 °C is used), to promote the formation of ester bonds by removal of the water vapour generated from the polycondensation reaction.[9,22] The intrinsic drawback in architecture with PGS comes from this conventional preparation technique. The PGS pre-polymer is a solid at room temperature, but melts and flows like a fluid at an elevated temperature of its typical curing condition, destroying any pre-built structures.[26] There are various material architectures which are particularly beneficial in biomedical applications, such as porous foams for tissue engineering and wound healing, films for wound healing and surgical devices. One of them is a microsphere, which can be injected or indigested to be administrated *in vivo*.

Due to this difficulty in architecture, the PGS-based microspheres have been very sparsely studied. As far as I know, there is only one example of this which is a PGS-based PU microspheres prepared with isocyanate crosslinkers and surfactants in a chemical solvent.[44] However this microsphere is not a purely PGS and contains PEG, thus show a bulk degradation kinetics due to the hydration effects from PEG. With this type of microsphere, we cannot expect to utilise the surface erosion behaviour of PGS. Furthermore, the use of toxic chemicals makes a concern of sample purification, which will also dissolve and wash-out any pre-loaded drugs. This work aimed to develop a method to prepare a pure PGS microsphere without any additives. When we cook deep-fried foods, the starch and protein polymers in the foods chemically react at an elevated oil temperature to build new chemical bonds.[327] Inspired by this, an experimental set-up was designed as follows to make PGS microspheres in a hot silicone oil.

Molten resin of the PGS pre-polymer (synthesised in the same method as chapter 4) was put into the hot silicone oil bath in a drop-by-drop manner to minimise the coagulation of the pre-polymer resins, whilst the oil was vigorously stirred. The oil temperature was set to a typical curing temperature of 120 °C and the curing time of 24 h was used. The use of surfactants would reduce the size of PGS microspheres by modulating the surface tension of the PGS pre-polymer before its curing in the oil bath. However, that can yield a PGS microsphere coated by surfactant molecules, requiring a further purification. Another way to control the size of PGS microspheres can be the use of different viscosity in the silicone oils as viscosity of liquid is corelated with the surface tension.[328] Total three different silicone oils were used; 5, 100, and 500 cst, to evaluate the possibility in controlling sizes in PGS microspheres.

The prepared PGS microspheres were not dissolved but rather swollen in a variety of solvents (1,4-dioxane, acetone, chloroform, dimethylformamide, ethanol, isopropanol methanol, and tetrahydrofuran), which indicates the PGS pre-polymer was chemically cured in a hot oil bath. Figure 6.4A shows the microscopic image of the prepared PGS microspheres

(Nikon SMZ800 stereoscopic zoom microscope). The measured diameter of PGS microspheres (n = 50) from three different silicone oils is shown in Figure 6.4B. A decreasing trend in the size of PGS microspheres was observed with increasing viscosity of silicone oils. The measured diameter of microspheres from three different silicone oils were 977 ± 332 μm (from 5 cst), 421 ± 165 μm (from 100 cst), and 399 ± 144 μm (from 500 cst). As we can see the size distribution was far too wide for uses in medical applications. A further study is required on the way to produce microspheres with much narrower size distributions for more predictable and uniform performance. Further research on this project has not been performed due to the lack of time.

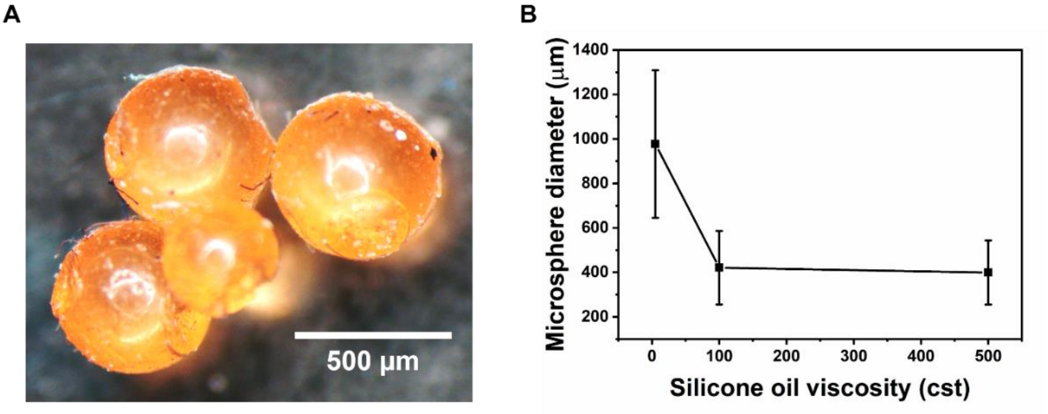

Figure 6.4 (A) A micrograph shows synthesised PGS microspheres by a "deep-frying" approach synthesised in a silicone oil bath with 100 cst. (B) The measure sizes of PGS microspheres by three different silicone oils used in the study.

6.4 Poly(glycerol sebacate)-*co*-β-cyclodextrin PU elastomer hydrogels

Cyclodextrin (CD) is a cyclic oligosaccharide, which is consisted of macrocyclic ring of glucose units linked by α-1,4 glycosidic bonds. It has been widely studied in drug delivery systems, with its ability to make host-guest supramolecular inclusion complexes due to its hydrophobic cavity as shown in Figure 6.5A.[329–331] This project was aimed to develop a new PGS-*co*-CD-based PU elastomer system, having the advantages of elastomeric properties in PGS and the drug loading ability of CD. As CD and the PGS pre-polymer have abundant hydroxyl groups, HDI was used to form the urethane bonds between them with its wide applications in biocompatible elastomers.[44]

Amongst α-, β-, and γ-, CD (consisted of 6, 7, and 8 glucose units, respectively), β-CD was chosen for its superior ability to make inclusion complexes with cholesterol molecules than other types of CDs, as the goal was to develop a sustainable drug delivery system for E2, which is a pro-angiogenic compound for regenerative medicine applications.[332] β-CD is also the most readily available form with the most various derivatives such as hydroxyalkyl-β-CD, dimethyl-β-CD, trimethyl-β-CD, glycosyl-β-CD, diglycosyl-β-CD, maltosyl-β-CD, and dimaltosyl-β-CD, with a range of solubility and ability to make the inclusion complexes.[331] These derivatives with different drug solubility and loading capacity properties can be studied in the future to fine-tune the drug loading and releasing behaviours in the PGS-*co*-CD PU elastomer system.

For the synthesis, 1 g of each the PGS pre-polymer and β-CD were used, which gives a theoretical amount of the hydroxyl groups of 19.8 mmol. To fully react all the hydroxyl groups, 1.583 mL of HDI would be required. However, we assumed that too high crosslinking density in this system would be detrimental in terms of the elastomeric property and drug loading capacity in the final product by reducing the free spaces in the polymer matrix. Based on this assumption, three different amounts of HDI were used; 0.396 mL, 0.792 mL, and 1.583 mL, aiming 25%, 50%, and 100% of HDI-grafting on the total hydroxyl groups from the PGS pre-polymer and β-CD. The sample from 0.396 mL of HDI yielded an extremely fragile and weak

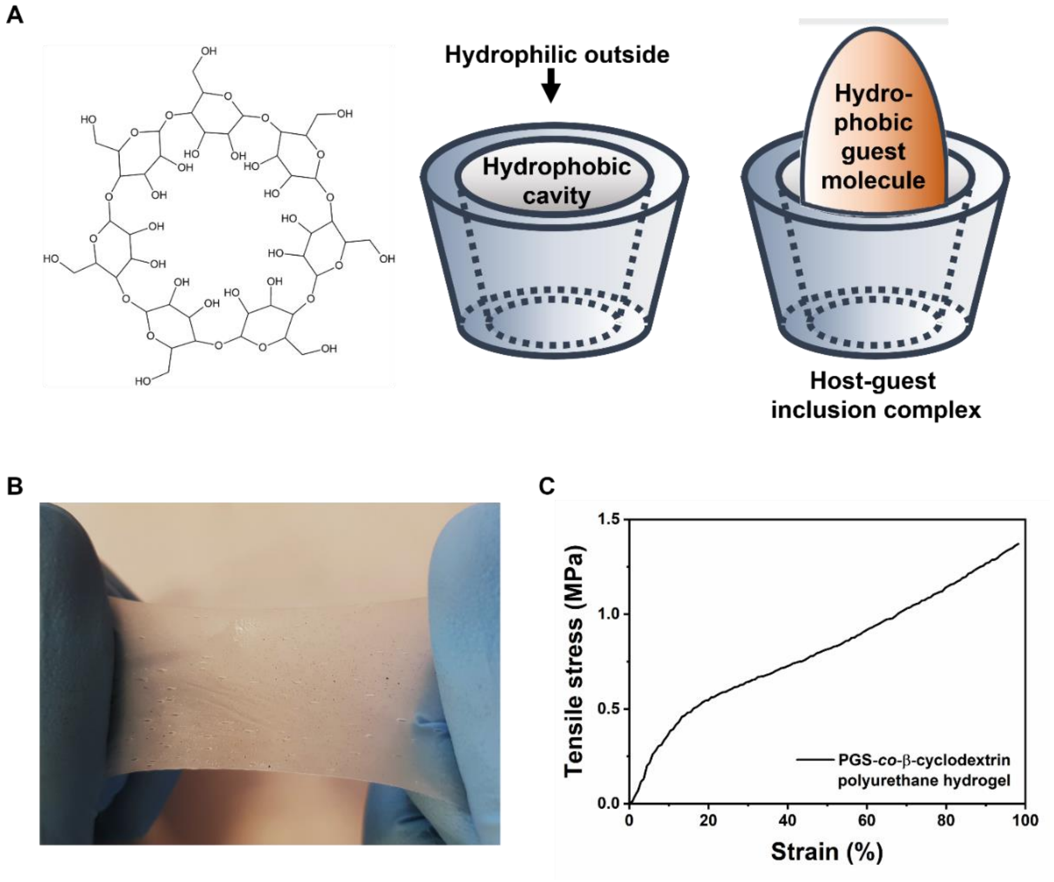

Figure 6.5 (A) The molecular structure and inclusion complex of CD. (From left to right) the molecular structure of β-CD, the hydrophilic edge and hydrophobic cavity of CDs, and the host-guest inclusion complex based on CDs. (B) Photographs demonstrating the flexibility and stretchability of the hydrated PGS-*co*-β-CD PU elastomer. (C) A representative tensile stress-strain curve of the water-swollen PGS-*co*-β-CD PU elastomer with 0.792 mL of HDI.

sample, possibly due to the incomplete crosslinking of polymers and subsequent crystallisation of CD. The samples from 0.792 mL of HDI was flexible and stretchable. The swelling ratio at equilibrium of this PGS-*co*-β-CD PU elastomer with 0.792 mL of HDI was 147.4 ± 5.2% (n = 3). Even at the fully hydrated state, the PGS-*co*-β-CD PU elastomer exhibited flexibility and stretchability as demonstrated in Figure 6.5B. The representative tensile stress-strain curve is shown in Figure 6.5C. The measured tensile Young's modulus, ultimate strength, and elongation at break values were 2.30 ± 0.44 MPa, 1.26 ± 0.28 MPa, and 88 ± 24%, respectively. The samples from 1.583 mL of HDI was too hard and brittle due to the too high crosslinking density, which is not suitable to use as an elastomer.

Further studies on this material was ceased here mainly due to the lack of time. Future study can include the drug loading and releasing tests as well as the use of CD derivatives for different drug types to optimise the drug delivery property. As β-CD is a polyol containing 21 hydroxyl groups per molecule (as shown in Fig 6.4A), intermolecular bonds across the centre of β-CD by HDI are possible. This can block the opening of β-CD, limiting its ability to form the host-guest inclusion complex. However, cyclodextrins are, in general, have rigid molecular structure, which will make the intermolecular bonds difficult.[329] Nevertheless, one solution is pre-formation of the inclusion complex between β-CD and the desired drug species before the crosslinking by HDI.[119] Introduction of a protecting group for the hydroxyl groups by the formation of esters, ethers, and acetals to minimise the inter molecular bonding of β-CD can be also considered in the future.[333]

Chapter 7 Overall conclusions and future work

7.1 Overall conclusions

This thesis has been focused on the development and characterisation of new PGS-based multifunctional bioelastomers for advanced healthcare such as soft tissue engineering, drug delivery, and wound healing. Various material designs including copolymers, nanocomposites, hydrogels, and porous scaffolds have been studied. Some of the bioelastomers studied here also have stimuli-responsive, controllable drug release, biomimetic mechanical properties, and pro-angiogenic activity. The key findings of each chapter can be discussed as below.

First, a new copolymer structure based on PGS and gelatin was studied. The synthesis strategy included the usage of the PGS pre-polymer with a relatively low molecular weight, which enabled accommodation of the further chemical reaction with gelatin utilising their innate chemical functional groups. This new copolymer system offered a set of new abilities which is valuable of soft tissue healthcare. The pH-responsive properties were studied for stimuli-controlled drug delivery applications. The improved hydration properties together with the biomimetic mechanical properties demonstrated a great potential in soft tissue engineering, together with the architecture of a porous scaffold.

Secondly, a PU-clay nanocomposite elastomer system was investigated. The polymer network structure with the covalently bonded PGS and PEG segments with the well-dispersed clay was achieved with an isocyanate crosslinked to from the urethane linkages between the polymer segments, and an organically modified clay for better compatibility with polymers. The effect of the organoclay on the modulation of the hydration, mechanical, diffusional, and degradation behaviours were evaluated for the potential applications in developing medical devices for the soft tissue engineering and controlled drug delivery.

Thirdly, polyester-clay nanocomposite elastomer hydrogels were designed and characterised. No additional chemical crosslinkers were used. Instead, PGS with excessive carboxyl functional groups and a relatively small molecular weight enabled the formation of the covalently bonded network structure PEG, whilst natural MMT clay was intercalated. Mechanical properties were modulated by the loading of MMT with the addition physical crosslinking effect. The loading of MMT also created interesting bioactive properties which cannot be found in PGS alone, such as pro-angiogenic ability and malodourous diamine-controlling. Together with the proven biocompatibility and biodegradability as well as improved hydration properties and porous structural architecture illustrated the potential applications of this new hydrogel in soft tissue engineering and wound healing.

Overall, this thesis has been an exploration to develop new elastomers. A new set of attractive properties have been introduced into the PGS-based elastomers. A set of existing properties have been engineered in the PGS-based elastomers. A number of material structures have been fabricated with the PGS-based elastomers. In conclusion, the elastomers developed in this thesis, presented great potentials in soft tissue healthcare applications.

7.2 Future work

The future applications of the new PGS-based elastomers can be vast. Before the actual applications, the interaction with the cells other than fibroblasts can be further investigated *in vitro* depending on the target tissue. For instance, if the application is targeting the skin regeneration, a test with keratinocytes needs to be done to fully address the potential in the tissue regeneration. The tests with stem cells can also be done for the potential use in stem cell-based therapy. After the studies in vitro, a critical examination *in vivo* needs to be performed on the elastomers to establish the biocompatibility and biodegradability in a more clinically relevant way.

Future research work can also include the development of injectable medical devices. Injectable microspheres or nanoparticles consisted of the elastomers in this thesis can be attractive in drug delivery and soft tissue engineering. A top-down approach involving grinding can be performed, however the grinding was not ideal as the size distribution was large and the shape is extremely irregular (tested with pure PGS by a cryo-milling approach). A biocompatible bottom-up method can be studied in the future including enzymatic crosslinking method with esterase enzymes.

Architecture of other structures which can benefit soft tissue healthcare include the tubes and conduits for vascular and nerve applications. To do this, the meltable resins of elastomers in this thesis can be cast into a casting mould with a desired shape, and cured subsequently to achieve the shape. For this plan, the casting moulds from a 3D printing technique with a computer-aided design method can be used. However, it will be even interesting if we can directly 3D print the elastomers into a desired shape. Unfortunately, the elastomer resins melt at the curing temperature and destroy the pre-built structures. In this case, we can utilise a structure supporting polymers with the higher melting points than the curing temperature of the elastomer resins in this thesis. For this purpose, biocompatible structure supporting polymers can be used and left in the final product. Otherwise, they can be washed out, as the elastomers in this thesis are consisted of covalently crosslinked network structure.

With respect to the nanocomposite elastomers in this thesis, the nanofillers have been MMT-based clays. Other types of clays with different specific surface area and charge can be used to engineer the properties, or other types of nanofillers such as carbon-based nanofillers of CNT, graphene, and graphene oxide can be explored. For instance, elastomeric cell simulators, soft robotics or implantable bioelectronics can be designed with electronically conductive nanofillers for bio-sensing or minimaly-invasive surgery applications.

For the nanocomposite elastomers with pro-angiogenic ability, the effect of MMT on the angiogenesis can be further studied. For this purpose, the adsorption properties of MMT with growth factors can be investigated for a better use of the pro-angiogenic ability of MMT.

Concerning the copolymer elastomer involving gelatin, other types of gelatin with different molecular weights and electrostatic charges can be studied. To understand if an engineering of hydration, pH-responsiveness, and mechanical properties is possible.

Bibliography

1 C. J. Bettinger, J. P. Bruggeman, J. T. Borenstein and R. S. Langer, *Biomaterials*, 2008, **29**, 2315–2325.

2 Q. T. Nguyen, Y. Hwang, A. C. Chen, S. Varghese and R. L. Sah, *Biomaterials*, 2012, **33**, 6682–6690.

3 P. Gupta, K. Vermani and S. Garg, *Drug Discov. Today*, 2002, **7**, 569–579.

4 K. Y. Lee and D. J. Mooney, *Chem. Rev.*, 2001, **101**, 1869–1879.

5 M. Kokabi, M. Sirousazar and Z. M. Hassan, *Eur. Polym. J.*, 2007, **43**, 773–781.

6 F. Ganji, S. Vasheghani-Farahani and E. Vasheghani-Farahani, *Iran. Polym. J.*, 2010, **19**, 375–398.

7 T. Garg, O. Singh, S. Arora and R. S. R. Murthy, *Crit. Rev. Ther. Drug Carrier Syst.*, 2012, **29**, 1–63.

8 H. Davis and J. Leach, *Top. Multifunct. Biomater. devices*, 2008, 1–26.

9 Y. Wang, G. A. Ameer, B. J. Sheppard and R. Langer, *Nat. Biotechnol.*, 2002, **20**, 602–606.

10 Y. Wang, Y. M. Kim and R. Langer, *J. Biomed. Mater. Res. A*, 2003, **66**, 192–197.

11 I. Pomerantseva, N. Krebs, A. Hart, C. M. Neville, A. Y. Huang and C. A. Sundback, *J. Biomed. Mater. Res. - Part A*, 2009, **91**, 1038–1047.

12 R. Rai, M. Tallawi, N. Barbani, C. Frati, D. Madeddu, S. Cavalli, G. Graiani, F. Quaini, J. A. Roether, D. W. Schubert, E. Rosellini and A. R. Boccaccini, *Mater. Sci. Eng. C*,

2013, **33**, 3677–3687.

13 R. A. Allen, W. Wu, M. Yao, D. Dutta, X. Duan, T. N. Bachman, H. C. Champion, D. B. Stolz, A. M. Robertson, K. Kim, J. S. Isenberg and Y. Wang, *Biomaterials*, 2014, **35**, 165–173.

14 C. A. Sundback, J. Y. Shyu, Y. Wang, W. C. Faquin, R. S. Langer, J. P. Vacanti and T. A. Hadlock, *Biomaterials*, 2005, **26**, 5454–5464.

15 C. D. Pritchard, K. M. Arnér, R. A. Neal, W. L. Neeley, P. Bojo, E. Bachelder, J. Holz, N. Watson, E. A. Botchwey, R. S. Langer and F. K. Ghosh, *Biomaterials*, 2010, **31**, 2153–2162.

16 D. Motlagh, J. Yang, K. Y. Lui, A. R. Webb and G. A. Ameer, *Biomaterials*, 2006, **27**, 4315–4324.

17 G. Jin, A. E. Ensley, R. M. Nerem and W. Yadong, *J. Biomed. Mater. Res. - Part A*, 2007, **83**, 1070–1075.

18 J. M. Kemppainen and S. J. Hollister, *J. Biomed. Mater. Res. - Part A*, 2010, **94**, 9–18.

19 M. Frydrych, S. Román, S. Macneil and B. Chen, *Acta Biomater.*, 2015, **18**, 40–49.

20 Z. You, H. Cao, J. Gao, P. H. Shin, B. W. Day and Y. Wang, *Biomaterials*, 2010, **31**, 3129–3138.

21 R. Maliger, P. J. Halley and J. J. Cooper-White, *J. Appl. Polym. Sci.*, 2013, **127**, 3980–3986.

22 D. Kafouris, F. Kossivas, C. Constantinides, N. Q. Nguyen, C. Wesdemiotis and C. S. Patrickios, *Macromolecules*, 2013, **46**, 622–630.

23 Q. Z. Chen, A. Bismarck, U. Hansen, S. Junaid, M. Q. Tran, S. E. Harding, N. N. Ali and A. R. Boccaccini, *Biomaterials*, 2008, **29**, 47–57.

24 X. Li, A. T. L. Hong, N. Naskar and H. J. Chung, *Biomacromolecules*, 2015, **16**, 1525–1533.

25 Y. Li, W. D. Cook, C. Moorhoff, W. C. Huang and Q. Z. Chen, *Polym. Int.*, 2013, **62**, 534–547.

26 M. Frydrych and B. Chen, *J. Mater. Chem. B*, 2013, **1**, 6650–6661.

27 E. S. Place, N. D. Evans and M. M. Stevens, *Eff. Br. mindfulness Interv. acute pain Exp. An Exam. Individ. Differ.*, 2009, **8**, 457–470.

28 E. N. Marieb, *Essentials of Human Anatomy & Physiology. (8th Edition)*, San Francisco, CA: Pearson Benjamin Cummings, 2006.

29 Anatomy and Physiology of soft tissues.

30 B. R. Krause and A. D. Hartman, *J. Lipid Res.*, 1984, **25**, 97–110.

31 M. KJAeR, *Physiol. Rev.*, 2004, **84**, 649–698.

32 G. A. Holzapfel, *Biomechanics of soft tissue*, Academic Press, 2000.

33 B. Hamilton and R. Schwartz, *J. Biol. Chem.*, 1935, **109**, 745–754.

34 E. C. M. Mariman and P. Wang, *Cell. Mol. Life Sci.*, 2010, **67**, 1277–1292.

35 Q. Chen, S. Liang and G. A. Thouas, *Prog. Polym. Sci.*, 2013, **38**, 584–671.

36 Y. C. Fung, *Biorheology*, 1973, **10**, 139–155.

37 R. J. Minns and P. D. Soden, *J. Biomech.*, 1973, **6**, 153–165.

38 R. Langer and J. P. Vacanti, *Science (80-.).*, 1993, **260**, 920–926.

39 P. X. Ma, *Mater. Today*, 2004, **7**, 30–40.

40 R. Balint, N. J. Cassidy and S. H. Cartmell, *Tissue Eng. Part B Rev.*, 2013, **19**, 48–57.

41 D. F. Williams, *Biomaterials*, 2008, **29**, 2941–2953.

42 F. J. O'Brien, *Mater. Today*, 2011, **14**, 88–95.

43 Q. Liu, L. Jiang, R. Shi and L. Zhang, *Prog. Polym. Sci.*, 2012, **37**, 715–765.

44 M. Frydrych, S. Román, N. H. Green, S. MacNeil and B. Chen, *Polym. Chem.*, 2015, **6**, 7974–7987.

45 M. J. N. Pereira, B. Ouyang, C. A. Sundback, N. Lang, I. Friehs, S. Mureli, I. Pomerantseva, J. McFadden, M. C. Mochel, O. Mwizerwa, P. Del Nido, D. Sarkar, P. T. Masiakos, R. Langer, L. S. Ferreira and J. M. Karp, *Adv. Mater.*, 2013, **25**, 1209–1215.

46 T. Wu, M. Frydrych, K. O. Kelly and B. Chen, *Biomacromolecules*, 2014, **15**, 2663–2671.

47 Y. Li, G. A. Thouas and Q.-Z. Chen, *RSC Adv.*, 2012, **2**, 8229.

48 R. Shi, D. Chen, Q. Liu, Y. Wu, X. Xu, L. Zhang and W. Tian, *Int. J. Mol. Sci.*, 2009, **10**, 4223–4256.

49 I. Vroman and L. Tighzert, *Materials (Basel).*, 2009, **2**, 307–344.

50 Y. L. Chung, S. Ansari, L. Estevez, S. Hayrapetyan, E. P. Giannelis and H. M. Lai, *Carbohydr. Polym.*, 2010, **79**, 391–396.

51 P. X. Ma, *Adv. Drug Deliv. Rev.*, 2008, **60**, 184–198.

52 E. Yuksel, *Semin. Plast. Surg.*, 2005, **19**, 261.

53 P. A. Gunatillake, R. Adhikari and N. Gadegaard, *Eur. Cells Mater.*, 2003, **5**, 1–16.

54 J. Patterson, M. M. Martino and J. A. Hubbell, *Mater. Today*, 2010, **13**, 14–22.

55 J. Gao, P. Crapo, R. Nerem and Y. Wang, *J. Biomed. Mater. Res. - Part A*, 2008, **85**, 1120–1128.

56 B. Dhandayuthapani, Y. Yoshida, T. Maekawa and D. S. Kumar, *Int. J. Polym. Sci.*, , DOI:10.1155/2011/290602.

57 C. Liu, Z. Xia and J. T. Czernuszka, *Chem. Eng. Res. Des.*, 2007, **85**, 1051–1064.

58 S. L. Liang, W. D. Cook, G. A. Thouas and Q. Z. Chen, *Biomaterials*, 2010, **31**, 8516–8529.

59 L. Zhou, H. He, C. Jiang and S. He, *J. Appl. Polym. Sci.*, 2015, **132**, 42196.

60 Q. Z. Chen, S. L. Liang, J. Wang and G. P. Simon, *J. Mech. Behav. Biomed. Mater.*, 2011, **4**, 1805–1818.

61 R. Ravichandran, J. R. Venugopal, S. Sundarrajan, S. Mukherjee and S. Ramakrishna, *Tissue Eng. Part A*, 2011, **17**, 1363–1373.

62 Y. Shen, G. Wang, X. Huang, Q. Zhang, J. Wu, C. Tang, Q. Yu and X. Liu, *J. R. Soc. Interface*, 2012, **9**, 313–327.

63 S. Ber, G. Torun K??se and V. Hasirci, *Biomaterials*, 2005, **26**, 1977–1986.

64 J. D. Kretlow, L. Klouda and A. G. Mikos, *Adv. Drug Deliv. Rev.*, 2007, **59**, 263–273.

65 H. J. Chung and T. G. Park, *Adv. Drug Deliv. Rev.*, 2007, **59**, 249–262.

66 H. A. Klok, *Macromolecules*, 2009, **42**, 7990–8000.

67 V. L. Sales, G. C. Engelmayr, J. A. Johnson, J. Gao, Y. Wang, M. S. Sacks and J. E. Mayer, *Circulation*, 2007, **116**, 55–63.

68 C. J. Bettinger, B. Orrick, A. Misra, R. Langer and J. T. Borenstein, *Biomaterials*, 2006, **27**, 2558–2565.

69 M. Lee, University of California Los Angeles, 2007.

70 S. MacNeil, *Mater. Today*, 2008, **11**, 26–35.

71 C. J. Bettinger, *Macromol. Biosci.*, 2011, **11**, 467–482.

72 R. K. Singh, D. Seliktar and A. J. Putnam, *Biomaterials*, 2013, **34**, 9331–9340.

73 S. G. Kumbar, S. P. Nukavarapu, R. James, L. S. Nair and C. T. Laurencin, *Biomaterials*, 2008, **29**, 4100–4107.

74 H. J. Chung and T. G. Park, *Tissue Eng. Part A*, 2009, **15**, 1391–1400.

75 V. Guarino, M. A. Alvarez-Perez, A. Borriello, T. Napolitano and L. Ambrosio, *Adv. Healthc. Mater.*, 2013, **2**, 218–227.

76 S. Dhivya, V. V. Padma and E. Santhini, *Biomedicine*, 2015, **5**, 24–28.

77 C. Lindholm and R. Searle, *Int. Wound J.*, 2016, **13**, 5–15.

78 A. Demir and E. Cevher, *Biomater. Appl. Nanomedicine*, , DOI:10.5772/25177.

79 K. Woo, V. L. C. de G. Santos and T. Alam, *Wounds Int.*, 2018, **9**, 6–14.

80 V. Jones, J. Grey and K. Harding, *Br. Med. J.*, 2006, **332**, 777–780.

81 J. S. Boateng, K. H. Matthews, H. N. E. Stevens and G. M. Eccleston, *J. Pharm. Sci.*,

2008, **97**, 2892–2923.

82 Z. Lu, J. Gao, Q. He, J. Wu, D. Liang, H. Yang and R. Chen, *Carbohydr. Polym.*, 2017, **156**, 460–469.

83 S. Patan, *J. Neurooncol.*, 2000, **50**, 1–15.

84 M. Lovett, K. Lee, A. Edwards and D. L. Kaplan, *Tissue Eng. Part B. Rev.*, 2009, **15**, 353–70.

85 G. Gigliobianco, C. K. Chong and S. MacNeil, *J. Biomater. Appl.*, 2015, **30**, 50–60.

86 D. L. Trump and C. S. Johnson, *Vitamin D and cancer*, 2011.

87 T. A. Winning and G. C. Townsend, *Clin. Dermatol.*, 2000, **18**, 499–511.

88 A. J. Sophia Fox, A. Bedi and S. A. Rodeo, *Sports Health*, 2009, **1**, 461–468.

89 K. Wittmann, S. Dietl, N. Ludwig, O. Berberich, C. Hoefner, K. Storck, T. Blunk and P. Bauer-Kreisel, *Tissue Eng. Part A*, 2015, **21**, 1343–1353.

90 G. M. Rubanyi, A. Johns and K. Kauser, *Vascul. Pharmacol.*, 2002, **38**, 89–98.

91 E. H. Judah, *Soc. Thought*, 2002, **21**, 107.

92 E. D. Albrecht, J. S. Babischkin, Y. Lidor, L. D. Anderson, L. C. Udoff and G. J. Pepe, *Hum. Reprod.*, 2003, **18**, 2039–2047.

93 B. Naik, P. Karunakar, M. Jayadev and V. R. Marshal, *J. Conserv. Dent.*, 2013, **16**, 284–93.

94 S. Singh, B. M. Wu and J. C. Y. Dunn, *Biomaterials*, 2011, **32**, 2059–2069.

95 A. Lesman, L. Gepstein and S. Levenberg, *Ann. N. Y. Acad. Sci.*, 2010, **1188**, 46–51.

96 C. Fidkowski, M. R. Kaazempur-Mofrad, J. Borenstein, J. P. Vacanti, R. Langer and Y. Wang, *Tissue Eng.*, 2005, **11**, 302–309.

97 T. G. Kim, S. H. Park, H. J. Chung, D. Y. Yang and T. G. Park, *Adv. Funct. Mater.*, 2010, **20**, 2303–2309.

98 T. Yeung, P. C. Georges, L. A. Flanagan, B. Marg, M. Ortiz, M. Funaki, N. Zahir, W. Ming, V. Weaver and P. A. Janmey, *Cell Motil. Cytoskeleton*, 2005, **60**, 24–34.

99 D. P. Dowling, I. S. Miller, M. Ardhaoui and W. M. Gallagher, *J. Biomater. Appl.*, 2011, **26**, 327–347.

100 R. González-Pinzón, R. Haggerty and D. D. Myrold, *J. Geophys. Res. Biogeosciences*, 2012, **117**, 1–10.

101 R. Parenteau-Bareil, R. Gauvin and F. Berthod, *Materials (Basel).*, 2010, **3**, 1863–1887.

102 T. H. Barker, *Biomaterials*, 2011, **32**, 4211–4214.

103 A. O. Elzoghby, *J. Control. Release*, 2013, **172**, 1075–1091.

104 H. Tan and K. G. Marra, *Materials (Basel).*, 2010, **3**, 1746–1767.

105 J. G. Rouse and M. E. Van Dyke, *Materials (Basel).*, 2010, **3**, 999–1014.

106 W. Liu, C. R. Carlisle, E. A. Sparks and M. Guthold, *J. Thromb. Haemost.*, 2010, **8**, 1030–1036.

107 B. Wang, W. Yang, J. McKittrick and M. A. Meyers, *Prog. Mater. Sci.*, 2016, **76**, 229–318.

108 X. Lou and T. V. Chirila, *J. Biomater. Appl.*, 1999, **14**, 184–191.

109 W. Zhao, X. Jin, Y. Cong, Y. Liu and J. Fu, *J. Chem. Technol. Biotechnol.*, 2013, **88**,

327–339.

110 S. V. Madihally and H. W. T. Matthew, *Biomaterials*, 1999, **20**, 1133–1142.

111 E. A. Soliman and M. Furuta, *Food Nutr. Sci.*, 2014, **05**, 1040–1055.

112 R. Yao, R. Zhang, F. Lin and J. Luan, *Biotechnol. Bioeng.*, 2013, **110**, 1430–1443.

113 I. Armentano, M. Dottori, E. Fortunati, S. Mattioli and J. M. Kenny, *Polym. Degrad. Stab.*, 2010, **95**, 2126–2146.

114 B. Guo and P. X. Ma, *Sci. China Chem.*, 2014, **57**, 490–500.

115 C. W. Patrick, *Anat. Rec.*, 2001, **263**, 361–366.

116 S. A. Soule and K. V. Cashman, *J. Volcanol. Geotherm. Res.*, 2004, **129**, 139–153.

117 D. G. Barrett and M. N. Yousaf, *Molecules*, 2009, **14**, 4022–4050.

118 A. Patel, A. K. Gaharwar, G. Iviglia, H. Zhang, S. Mukundan, S. M. Mihaila, D. Demarchi and A. Khademhosseini, *Biomaterials*, 2013, **34**, 3970–3983.

119 H. Ye, C. Owh and X. J. Loh, *RSC Adv.*, 2015, **5**, 48720–48728.

120 W. F. Daamen, J. H. Veerkamp, J. C. M. van Hest and T. H. van Kuppevelt, *Biomaterials*, 2007, **28**, 4378–4398.

121 S. Sartori, V. Chiono, C. Tonda-Turo, C. Mattu and C. Gianluca, *J. Mater. Chem. B*, 2014, **2**, 5128–5144.

122 J. F. Mano, G. A. Silva, H. S. Azevedo, P. B. Malafaya, R. A. Sousa, S. S. Silva, L. F. Boesel, J. M. Oliveira, T. C. Santos, A. P. Marques, N. M. Neves and R. L. Reis, *J. R. Soc. Interface*, 2007, **4**, 999–1030.

123 M. F. Maitz, *Biosurf. Biotribol.*, 2015, **1**, 161–176.

124 E. Bugnicourt, P. Cinelli, A. Lazzeri and V. Alvarez, *Express Polym. Lett.*, 2014, **8**, 791–808.

125 E. G. Roberts, N. G. Rim, W. Huang, A. Tarakanova, J. Yeo, M. J. Buehler, D. L. Kaplan and J. Y. Wong, *Macromol. Biosci.*, 2018, **18**, 1–10.

126 N. Annabi, S. M. Mithieux, G. Camci-Unal, M. R. Dokmeci, A. S. Weiss and A. Khademhosseini, *Biochem. Engneering J.*, 2013, **15**, 110–118.

127 D. H. T. Le and A. Sugawara-Narutaki, *Mol. Syst. Des. Eng.*, 2019, **4**, 545–565.

128 Q. Liu, M. Tian, R. Shi, L. Zhang, D. Chen and W. Tian, *J. app*, 2007, **104**, 1131–1137.

129 S. Bodakhe, S. Verma, S. K. Samal, S. S. Sharma and N. Kumar, *Nanomedicine*, 2012, **8**, 1777–1796.

130 S. Gerecht, S. A. Townsend, H. Pressler, H. Zhu, C. L. E. Nijst, J. P. Bruggeman, J. W. Nichol and R. Langer, *Biomaterials*, 2007, **28**, 4826–4835.

131 J. L. Ifkovits, J. J. Devlin, G. Eng, T. P. Martens, G. Vunjak-Novakovic and J. A. Burdick, *ACS Appl. Mater. Interfaces*, 2009, **1**, 1878–1886.

132 C. L. E. Nijst, J. P. Bruggeman, J. M. Karp, L. Ferreira, A. Zumbuehl, C. J. Bettinger and R. Langer, *Biomacromolecules*, 2007, **8**, 3067–3073.

133 Y. Wu, L. Wang, B. Guo and P. X Ma, *J. Mater. Chem. B*, 2014, **2**, 3674–3685.

134 C. Zhu, S. R. Kustra and C. J. Bettinger, *Acta Biomater.*, 2013, **9**, 7362–70.

135 C. Zhu, S. R. Kustra and C. J. Bettinger, *Acta Biomater.*, 2013, **9**, 7362–7370.

136 H. M. Aydin, K. Salimi, Z. M. O. Rzayev and E. Pişkin, *Biomater. Sci.*, 2013, **1**, 503–

509.

137 W. Cai and L. Liu, *Mater. Lett.*, 2008, **62**, 2175–2177.

138 G. C. Engelmayr, M. Cheng, C. J. Bettinger, J. T. Borenstein, R. Langer and L. E. Freed, *Nat. Mater.*, 2008, **7**, 1003–1010.

139 R. Rai, M. Tallawi, A. Grigore and A. R. Boccaccini, *Prog. Polym. Sci.*, 2012, **37**, 1051–1078.

140 D. Manzanedo, Boston: Department of Materials Science and Engineering, Massachusetts Institute of Technology, 2006.

141 X. J. Loh, A. Abdul Karim and C. Owh, *J. Mater. Chem. B*, 2015, **3**, 7641–7652.

142 Z. Wang, J. Zhuge, H. Fang and B. A. Prior, *Biotechnol. Adv.*, 2001, **19**, 201–223.

143 G. Liu, B. Hinch and A. D. Beavis, *J. Biol. Chem.*, 1996, **271**, 25338–25344.

144 S. Kobayashi and K. Manabe, *Acc. Chem. Res.*, 2002, **35**, 209–217.

145 Q. Chen, X. Yang and Y. Li, *RSC Adv.*, 2012, **2**, 4125–4134.

146 S. Sant, D. Iyer, A. K. Gaharwar, A. Patel and A. Khademhosseini, *Acta Biomater.*, 2013, **9**, 5963–5973.

147 Y. Li, G. A. Thouas, H. Shi and Q. Chen, *J. Biomater. Appl.*, 2014, **28**, 1138–1150.

148 S. L. Liang, X. Y. Yang, X. Y. Fang, W. D. Cook, G. A. Thouas and Q. Z. Chen, *Biomaterials*, 2011, **32**, 8486–8496.

149 Q. Chen, L. Jin, W. D. Cook, D. Mohn, E. L. Lagerqvist, D. A. Elliott, J. M. Haynes, N. Boyd, W. J. Stark, C. W. Pouton, E. G. Stanley and A. G. Elefanty, *Soft Matter*, 2010, **6**, 4715–4726.

150 D. Dippold, M. Tallawi, S. Tansaz, J. A. Roether and A. R. Boccaccini, *Eur. Polym. J.*, 2016, **75**, 504–513.

151 M. Kharaziha, M. Nikkhah, S. R. Shin, N. Annabi, N. Masoumi, A. K. Gaharwar, G. Camci-Unal and A. Khademhosseini, *Biomaterials*, 2013, **34**, 6355–6366.

152 H. Park, B. L. Larson, M. D. Guillemette, S. R. Jain, C. Hua, G. C. Engelmayr and L. E. Freed, *Biomaterials*, 2011, **32**, 1856–1864.

153 R. Ravichandran, J. R. Venugopal, S. Sundarrajan, S. Mukherjee and S. Ramakrishna, *World J. Cardiol.*, 2013, **5**, 28–41.

154 R. Ravichandran, J. R. Venugopal, S. Sundarrajan, S. Mukherjee, R. Sridhar and S. Ramakrishna, *Int. J. Cardiol.*, 2013, **167**, 1461–1468.

155 R. Ravichandran, J. R. Venugopal, S. Sundarrajan, S. Mukherjee, R. Sridhar and S. Ramakrishna, *Nanotechnology*, 2012, **23**, 385102.

156 M. Tallawi, R. Rai, M. R-Gleixner, O. Roerick, M. Weyand, J. A. Roether, D. W. Schubert, A. Kozlowska, M. El Fray, B. Merle, M. Göken, K. Aifantis and A. R. Boccaccini, *Macromol. Symp.*, 2013, **334**, 57–67.

157 M. Tallawi, D. C. Zebrowski, R. Rai, J. A. Roether, D. W. Schubert, M. El Fray, F. B. Engel, K. E. Aifantis and A. R. Boccaccini, *Tissue Eng. Part C Methods*, 2015, **21**, 585–596.

158 Z. J. Sun, B. Sun, R. Bin Tao, X. Xie, X. L. Lu and D. L. Dong, *J. Biomed. Mater. Res. - Part A*, 2013, **101 A**, 253–260.

159 W. L. Neeley, S. Redenti, H. Klassen, S. Tao, T. Desai, M. J. Young and R. Langer, *Biomaterials*, 2008, **29**, 418–426.

160 S. Redenti, W. L. Neeley, S. Rompani, S. Saigal, J. Yang, H. Klassen, R. Langer and M. J. Young, *Biomaterials*, 2009, **30**, 3405–3414.

161 P. M. Crapo, J. Gao and Y. Wang, *J. Biomed. Mater. Res. - Part A*, 2008, **86**, 354–363.

162 A. K. Gaharwar, M. Nikkhah, S. Sant and A. Khademhosseini, *Biofabrication*, 2014, **7**, 015001.

163 M. J. Kim, M. Y. Hwang, J. Kim and D. J. Chung, *Biomed Res. Int.*, , DOI:10.1155/2014/956952.

164 C. G. Jeong and S. J. Hollister Scott J., *Biomaterials*, 2010, **31**, 4304–4312.

165 Z. J. Sun, C. Chen, M. Z. Sun, C. H. Ai, X. L. Lu, Y. F. Zheng, B. F. Yang and D. L. Dong, *Biomaterials*, 2009, **30**, 5209–5214.

166 I. S. Tobias, H. Lee, G. C. Engelmayr, D. Macaya, C. J. Bettinger and M. J. Cima, *J. Control. Release*, 2010, **146**, 356–362.

167 Q. Chen, S. Liang and G. A. Thouas, *Soft Matter*, 2011, **7**, 6484.

168 H. I. Pryor, E. O'Doherty, A. Hart, G. Owens, D. Hoganson, J. P. Vacanti, P. T. Masiakos and C. A. Sundback, *Surgery*, 2009, **146**, 490–497.

169 Q. Z. Chen, J. M. W. Quinn, G. A. Thouas, X. Zhou and P. A. Komesaroff, *Adv. Eng. Mater.*, 2010, **12**, 642–648.

170 H. Shi, Q. Gan, X. Liu, Y. Ma, J. Hu, Y. Yuan and C. Liu, *RSC Adv.*, 2015, **5**, 79703–79714.

171 D. Hull and T. W. Clyne, *An Introduction to Composite Materials*, Cambridge University Press, 1981.

172 F. Hussain, *J. Compos. Mater.*, 2006, **40**, 1511–1575.

173 B. Chen, J. R. G. Evans, H. C. Greenwell, P. Boulet, P. V. Coveney, A. A. Bowden and A. Whiting, *Chem. Soc. Rev.*, 2008, **37**, 568–594.

174 D. G. B. QUANG T. NGUYEN, *Adv. Polym. Technol.*, 2006, **25**, 270–285.

175 K. Wang, L. Chen, J. Wu, M. L. Toh, C. He and A. F. Yee, *Macromolecules*, 2005, **38**, 788–800.

176 S. Thomas, A. P. Meera and H. J. Maria, *Plast. Res. Online*, 2012, 7–9.

177 Y. Cui, S. Kumar, B. Rao Kona and D. van Houcke, *RSC Adv.*, 2015, **5**, 63669–63690.

178 P. Kiliaris and C. D. Papaspyrides, *Prog. Polym. Sci.*, 2010, **35**, 902–958.

179 H. F. Mark, *Encyclopedia of Polymer Science and Technology, Concise*, John Wiley & Sons, 2013.

180 J. D. Sudha, S. Sivakala, C. K. Chandrakanth, K. S. Neethu, K. N. Rohini and R. Ramakrishnan, *Express Polym. Lett.*, 2014, **8**, 107–115.

181 S. Guggenheim, 1995, 371–388.

182 F. Uddin, *Metall. Mater. Trans. A Phys. Metall. Mater. Sci.*, 2008, **39**, 2804–2814.

183 Amethyst Galleries, The clay group.

184 J. F. Burst, *Appl. Clay Sci.*, 1991, **5**, 421–443.

185 S. a. Solin, *Annu. Rev. Mater. Sci.*, 1997, **27**, 89–115.

186 Lhoist UK Ltd., Clay Manufacturing.

187 L. B. de Paiva, A. R. Morales and F. R. Valenzuela Díaz, *Appl. Clay Sci.*, 2008, **42**, 8–

24.

188 G. W. Beall and M. Goss, *Appl. Clay Sci.*, 2004, **27**, 179–186.

189 M. Ogawa, T. Handa, K. Kuroda and C. Kato, *Chem. Lett.*, 1990, **1**, 71–74.

190 J. J. Luo and I. M. Daniel, *Compos. Sci. Technol.*, 2003, **63**, 1607–1616.

191 P. Taylor, J. Liu, W. Boo, A. Clearfield and H. Sue, *Mater. Manuf. Process.*, 2017, **6914**, 37–41.

192 F. C. H. Pinto, A. Silva-Cunha, G. A. Pianetti, E. Ayres, R. L. Oréfice and G. R. Da Silva, *J. Nanomater.*, , DOI:10.1155/2011/528628.

193 J. U. Ha and M. Xanthos, *Int. J. Pharm.*, 2011, **414**, 321–331.

194 S. Barua, P. Chattopadhyay, L. Aidew, A. K. Buragohain and N. Karak, *Polym. Int.*, 2015, **64**, 303–311.

195 E. A. Naumenko, I. D. Guryanov, R. Yendluri, Y. M. Lvov and R. F. Fakhrullin, *Nanoscale*, 2016, **8**, 7257–7271.

196 H. Bai, A. Polini, B. Delattre and A. P. Tomsia, *Chem. Mater.*, 2013, **25**, 4551–4556.

197 M. C. Koetting, J. T. Peters, S. D. Steichen and N. A. Peppas, *Mater. Sci. Eng. R Reports*, 2015, **93**, 1–49.

198 J. Zhu and R. E. Marchant, *Expert Rev. Med. Devices*, 2011, **8**, 607–626.

199 I. El-Sherbiny and M. Yacoub, *Glob. Cardiol. Sci. Pract.*, 2013, **2013**, 316–42.

200 M. Ebara, Y. Kotsuchibashi, R. Narain, N. Idota, Y.-J. Kim, J. M. Hoffman, K. Uto and T. Aoyagi, in *Smart Biomaterials*, Springer Japan, 2014, p. 9.

201 Y. Wang, Y. M. Kim and R. Langer, *J. Biomed. Mater. Res.*, 2003, **66**, 192–197.

202 Q.-Y. Liu, S.-Z. Wu, T.-W. Tan, J.-Y. Weng, L.-Q. Zhang, L. Liu, W. Tian and D.-F. Chen, *J. Biomater. Sci. Polym. Ed.*, 2009, **20**, 1567–1578.

203 P. Aramwit, N. Jaichawa, J. Ratanavaraporn and T. Srichana, *Mater. Express*, 2015, **5**, 241–248.

204 A. P. Kishan, R. M. Nezarati, C. M. Radzicki, A. L. Renfro, J. L. Robinson, M. E. Whitely and E. M. Cosgriff-Hernandez, *J. Mater. Chem. B*, 2015, **3**, 7930–7938.

205 A. Sharma, S. Bhat, T. Vishnoi, V. Nayak and A. Kumar, *Biomed Res. Int.*, 2013, **2013**, 478279.

206 M. Tamura, F. Yanagawa, S. Sugiura, T. Takagi, K. Sumaru and T. Kanamori, *Sci. Rep.*, 2015, **5**, 15060.

207 M. E. Hoque, T. Nuge, T. K. Yeow, N. Nordin and R. G. S. V Prasad, *Polym. Res. J.*, 2015, **9**, 15–32.

208 K. Yue, G. Trujillo-de Santiago, M. M. Alvarez, A. Tamayol, N. Annabi and A. Khademhosseini, *Biomaterials*, 2015, **73**, 254–271.

209 J. Ma, H. Cao, Y. Li and Y. Li, *J. Biomater. Sci. Polym. Ed.*, 2002, **13**, 67–80.

210 S. Sornkamnerd, M. K. Okajima and T. Kaneko, *ACS Omega*, 2017, **2**, 5304–5314.

211 J. S. Barbieri, D. J. Margolis and B. A. Brod, *J. Invest. Dermatol.*, 2017, **137**, 2491–2496.

212 T. Hattori, R. Hallberg and P. L. Dubin, *Langmuir*, 2000, **16**, 9738–9743.

213 T. R. Anderson, M. E. Marquart and A. V. Janorkar, *J. Biomed. Mater. Res. - Part A*,

2015, **103**, 782–790.

214 Y. Murawaki, H. Kawasaki and H. Burkhardt, *Pathol. Res. Pract.*, 1994, **190**, 929–33.

215 J. S. Chawla and M. M. Amiji, *Int. J. Pharm.*, 2002, **249**, 127–138.

216 A. Rodriguez-Galan, L. Franco and J. Puiggali, *Polymers (Basel).*, 2011, **3**, 65–99.

217 T.-H. Nguyen and B.-T. Lee, *J. Biomed. Sci. Eng.*, 2010, **03**, 1117–1124.

218 O. Dragostin, S. Samal, F. Lupascu, A. Pânzariu, P. Dubruel, D. Lupascu, C. Tuchilus, C. Vasile and L. Profire, *Int. J. Mol. Sci.*, 2015, **16**, 29843–29855.

219 E. A. Kamoun, X. Chen, M. S. Mohy Eldin and E. R. S. Kenawy, *Arab. J. Chem.*, 2015, **8**, 1–14.

220 J. T. Bamgbose, A. A. Bamigbade, S. Adewuyi, E. O. Dare, A. A. Lasisi and A. N. Njah, *J. Chem. Chem. Eng.*, 2012, **6**, 272–283.

221 E. M. Davis, M. Minelli, M. G. Baschetti and Y. A. Elabd, *Ind. Eng. Chem. Res.*, 2013, **52**, 8664–8673.

222 S. B. Tiwari and A. R. Rajabi-Siahboomi, in *Drug Delivery Systems*, eds. K. K. Jain and J. M. Walker, Springer Science & Business Media, Totowa, NJ, 2008, p. 224.

223 E. P. Holowka and S. K. Bhatia, in *Drug Delivery: Materials Design and Clinical Perspective*, Springer Science & Business Media, New York, NY, 2014, p. 8.

224 G. Aguirre-Alvarez, D. J. Pimentel-Gonzalez, R. G. Campos-Montiel, T. Foster and S. E. Hill, *CyTA--J. Food*, 2011, **9**, 243–249.

225 G. Ninan, J. Joseph and Z. Abubacker, *J. Food Sci.*, 2010, **75**, 620–626.

226 Y. Tsuda, in *Polyimides and Other High Temperature Polymers: Synthesis,*

Characterization and Applications, Volume 5, ed. K. L. Mittal, CRC Press, Boca Raton, FL, 2009, p. 26.

227 J. A. Moore and W. W. Bunting, in *Advances in Polymer Synthesis, Volume 31*, eds. B. M. Culbertson and J. E. McGrath, Plenum Press, New York, NY, 1985, p. 69.

228 K. Pal, A. K. Banthia and D. K. Majumdar, *AAPS PharmSciTech*, 2007, **8**, E142–E146.

229 R. S. H. Wong, M. Ashton and K. Dodou, *Pharmaceutics*, 2015, **7**, 305–319.

230 A. D. Lantada, E. C. Mayola, S. Deschamps, B. P. Sánchez, J. P. G. Ruíz and H. A. Iniesta, in *Microsystems for Enhanced Control of Cell Behavior: Fundamentals, Design and Manufacturing Strategies, Applications and Challenges*, ed. A. D. Lantada, Springer, Cham, 2016, p. 306.

231 S. J. Hollister, *Nat. Mater.*, 2006, **4**, 518–524.

232 V. V. Khutoryanskiy, *Nat. Mater.*, 2015, **14**, 963–964.

233 D. F. Evans, G. Pye, R. Bramley, A. G. Clark, T. J. Dyson and J. D. Hardcastle, *Gut*, 1988, **29**, 1035–41.

234 E. Osti, *Ann. Burns Fire Disasters*, 2008, **21**, 73–7.

235 J. P. D. Garcia, M. F. Hsieh, B. T. Doma, D. C. Peruelo, I. H. Chen and H. M. Lee, *Polymers (Basel).*, 2014, **6**, 39–58.

236 S. Riedel, B. Heyart, K. S. Apel and S. G. Mayr, *Sci. Rep.*, 2017, **7**, 2–7.

237 Azizullah, Nisar-ur-Rehman, W. Liu, A. Haider, U. Kortz, M. Sohail, S. A. Joshi and J. Iqbal, *Des. Monomers Polym.*, 2016, **19**, 697–705.

238 Y. Liu, X. Fan, B. Wei, Q. Si, W. Chen and L. Sun, *Int. J. Pharm.*, 2006, **308**, 205–209.

239 L. Liu, W. Yao, Y. Rao, X. Lu and J. Gao, *drug Deliv.*, 2017, **24**, 569–581.

240 M. Biondi, F. Ungaro, F. Quaglia and P. A. Netti, *Adv. Drug Deliv. Rev.*, 2008, **60**, 229–242.

241 N. A. Liechty, W. B., Kryscio, D.R., Slaughter, B. V. and Peppas, *Annu. Rev. Chem. Biomol. Eng.*, 2010, **1**, 149–173.

242 N. V. Gama, A. Ferreira and A. Barros-Timmons, *Materials (Basel).*, , DOI:10.3390/ma11101841.

243 Y. Tamer and B. Chen, *Soft Matter*, 2018, **14**, 1195–1209.

244 C. Prisacariu and E. Scortanu, *High Perform. Polym.*, 2011, **23**, 308–313.

245 F. Ji, W. Lin, Z. Wang, L. Wang, J. Zhang, G. Ma and S. Chen, *ACS Appl. Mater. Interfaces*, 2013, **5**, 10489–10494.

246 X. Zhang, C. Jia, X. Qiao, T. Liu and K. Sun, *Polym. Test.*, 2016, **54**, 118–125.

247 B. Louage, L. Tack, Y. Wang and B. G. De Geest, *Polym. Chem.*, 2017, 5033–5038.

248 H. Y. Ren, M. Zhu and K. Haraguchi, *Macromolecules*, 2011, **44**, 8516–8526.

249 K. Miller, *Med. Sci. Monit.*, 2000, **6**, 158–67.

250 S. Yoon and B. Chen, *Polym. Chem.*, 2018, **9**, 3727–3740.

251 B. Chen and J. R. G. Evans, *Scr. Mater.*, 2006, **54**, 1581–1585.

252 S. S. Ray, K. Okamoto and M. Okamoto, *Macromolecules*, 2003, **36**, 2355–2367.

253 S. S. Ray, K. Yamada, M. Okamoto, Y. Fujimoto, A. Ogami and K. Ueda, *Polymer (Guildf).*, 2003, **44**, 6633–6646.

254 S. Sinha Ray, K. Yamada, M. Okamoto, A. Ogami and K. Ueda, *Chem. Mater.*, 2003, **15**, 1456–1465.

255 S. S. Babu, S. Mathew, N. Kalarikkal, S. Thomas and E. K. Radhakrishnan, *3 Biotech*, 2016, **6**, 1–9.

256 P. Cirri and P. Chiarugi, *Am. J. Cancer Res.*, 2011, **1**, 482–497.

257 J.-W. Rhim, S.-I. Hong, H.-M. Park and P. K. W. Ng, *J. Agric. Food Chem.*, 2016, **54**, 5814–5822.

258 D. Burgentzlé, J. Duchet, J. F. Gérard, A. Jupin and B. Fillon, *J. Colloid Interface Sci.*, 2004, **278**, 26–39.

259 R. N. Darie, E. Pâslaru, A. Sdrobis, G. M. Pricope, G. E. Hitruc, A. Poiată, A. Baklavaridis and C. Vasile, *Ind. Eng. Chem. Res.*, 2014, **53**, 7877–7890.

260 A. K. Gaharwar, A. Patel, A. Dolatshahi-Pirouz, H. Zhang, K. Rangarajan, G. Iviglia, S.-R. Shin, M. A. Hussain and A. Khademhosseini, *Biomater. Sci.*, 2015, **3**, 46–58.

261 W. Dang, V. Vinciguerra, L. Lorenzelli, M. U. Ocheje, B. P. Charron, A. Nyayachavadi and S. Rondeau-Gagné, *Flex. Print. Electron*, 2017, **2**, 43002.

262 S. Lampman, *Characterization and Failure Analysis of Plastics*, ASM International, Materials Park, 2003.

263 K. L. Harrison and M. J. Jenkins, *Polym. Int.*, 2004, **53**, 1298–1304.

264 H. Assaedi, F. U. A. Shaikh and I. M. Low, *J. Asian Ceram. Soc.*, 2016, **4**, 19–28.

265 K. Y. Law, *J. Phys. Chem. Lett.*, 2014, **5**, 686–688.

266 K. J. Kubiak, M. C. T. Wilson, T. G. Mathia and P. Carval, *Wear*, 2011, **271**, 523–528.

267 Hideo Nakae, Ryuichi Inui, Yosuke Hirata and Hiroyuki Saito, *Acta Mater.*, 2003, **46**, 2313–2318.

268 M. C. Wang, J. J. Lin, H. J. Tseng and S. H. Hsu, *ACS Appl. Mater. Interfaces*, 2012, **4**, 338–350.

269 M. M. Cherif, M. Amal and B. Ramdane, *MATEC Web Conf.*, 2018, **149**, 1–6.

270 S. Abdurrahmanoglu, V. Can and O. Okay, *J. Appl. Polym. Sci.*, 2008, **109**, 3714–3724.

271 O. Oguz and O. Wilhelm, *Macromolecules*, 2007, **40**, 3378–3387.

272 E. Caló and V. V. Khutoryanskiy, *Eur. Polym. J.*, 2015, **65**, 252–267.

273 D. Suhag, R. Bhatia, S. Das, A. Shakeel, A. Ghosh, A. Singh, O. P. Sinha, S. Chakrabarti and M. Mukherjee, *RSC Adv.*, 2015, **5**, 53963–53972.

274 L. Fan and S. K. Singh, *Controlled Release: A Quantitative Treatment*, Springer-Verlag, Berlin Heidelberg, 2012.

275 C.-W. Chang, A. van Spreeuwel, C. Zhang and S. Varghese, *Soft Matter*, 2010, **6**, 5157.

276 M. Kato, A. Usuki, N. Hasegawa, H. Okamoto and M. Kawasumi, *Polym. J.*, 2011, **43**, 583–593.

277 S. L. Liang, W. D. Cook, G. A. Thouas and Q. Z. Chen, *Biomaterials*, 2010, **31**, 8516–8529.

278 A. P. Ebrahimi, *J. Vasc. Interv. Neurol.*, 2009, **2**, 155–62.

279 M. Lepoitevin, M. Jaber, R. Guégan, J. M. Janot, P. Dejardin, F. Henn and S. Balme, *Appl. Clay Sci.*, 2014, **95**, 396–402.

280 G. Sposito, N. T. Skipper, R. Sutton, S. Park, A. K. Soper and J. A. Greathouse, *Proc.*

Natl. Acad. Sci. U. S. A., 1999, **96**, 3358–64.

281 A. A. Adeyemo, I. O. Adeoye and O. S. Bello, *Appl. Water Sci.*, 2017, **7**, 543–568.

282 K. Akazawa, K. Iwasaki, M. Nagata, N. Yokoyama, H. Ayame, K. Yamaki, Y. Tanaka, I. Honda, C. Morioka, T. Kimura, M. Komaki, A. Kishida, Y. Izumi and I. Morita, *Inflamm. Regen.*, 2017, **37**, 1–6.

283 S. Maisanaba, S. Pichardo, M. Puerto, D. Gutiérrez-praena and A. M. Cameán, *Environ. Res.*, 2015, **138**, 233–254.

284 F. B. Barlas, D. Ag Seleci, M. Ozkan, B. Demir, M. Seleci, M. Aydin, M. A. Tasdelen, H. M. Zareie, S. Timur, S. Ozcelik and Y. Yagci, *J. Mater. Chem. B*, 2014, **2**, 6412.

285 K. Fukushima, A. Rasyida and M. C. Yang, *J. Polym. Res.*, , DOI:10.1007/s10965-013-0302-6.

286 K. Majdzadeh-Ardakani, S. Zekriardehani, M. R. Coleman and S. A. Jabarin, *Int. J. Polym. Sci.*, 2017, **2017**, 1–10.

287 G. E. Zaikov, L. I. Bazylak and A. K. Haghi, Eds., *Functional Polymer Blends and Nanocomposites: A Practical Engineering Approach*, Apple Academic Press, Oakville, 2014.

288 E. Dickinson, R. Ettelaie, T. Kostakis and B. S. Murray, *Langmuir*, 2004, **20**, 8517–8525.

289 B. P. Binks and T. S. Horozov, *Angew. Chemie - Int. Ed.*, 2005, **44**, 3722–3725.

290 Q. L. Loh and C. Choong, *Tissue Eng. Part B Rev.*, 2013, **19**, 485–502.

291 R. Bongartz, D. Ag, M. Seleci, J.-G. Walter, E. E. Yalcinkaya, D. O. Demirkol, F. Stahl, S. Timur and T. Scheper, *J. Mater. Chem. B*, 2013, **1**, 522–528.

292 W. H. Yu, N. Li, D. S. Tong, C. H. Zhou, C. X. Lin and C. Y. Xu, *Appl. Clay Sci.*, 2013, **80**–**81**, 443–452.

293 R. Parfitt and D. Greenland, *Clay Miner.*, 1970, **8**, 305–315.

294 S.-I. Hong and J.-W. Rhim, *J. Nanosci. Nanotechnol.*, 2008, **8**, 5818–5824.

295 R. Xu, H. Xia, W. He, Z. Li, J. Zhao, B. Liu, Y. Wang, Q. Lei, Y. Kong, Y. Bai, Z. Yao, R. Yan, H. Li, R. Zhan, S. Yang, G. Luo and J. Wu, *Sci. Rep.*, 2016, **6**, 1–12.

296 S. Dikici, N. Mangir, F. Claeyssens, M. Yar and S. Macneil, *Regen. Med.*, 2019, **14**, 179–197.

297 N. Mangir, S. Dikici, F. Claeyssens and S. Macneil, *ACS Biomater. Sci. Eng.*, 2019, **5**, 3190–3200.

298 B. A. Dikici, S. Dikici, G. C. Reilly, S. MacNeil and F. Claeyssens, *Mater. 2019, Vol. 12, Page 2643*, 2019, **12**, 2643.

299 S. Dikici, F. Claeyssens and S. MacNeil, *J. Biomater. Appl.*, 2019, **34**, 546–559.

300 D. Ribatti, B. Nico, A. Vacca and M. Presta, *Nat. Protoc.*, 2006, **1**, 85–91.

301 X. Qi, W. F. Wang, J. Wang, J. L. Yang and Y. P. Shi, *Food Chem.*, 2018, **259**, 245–250.

302 S. Liu, X. Rong, G. Fan, Q. Li and Y. Wei, *Chinese J. Burn.*, 2013, **29**, 526–530.

303 A. Esposito, O. Raccurt, J. Y. Charmeau and J. Duchet-Rumeau, *Appl. Clay Sci.*, 2010, **50**, 525–532.

304 C. Ghobril and M. W. Grinstaff, *Chem. Soc. Rev.*, 2015, **44**, 1820–1835.

305 X. Landreau, B. Lanfant, T. Merle, C. Dublanche-Tixier and P. Tristant, *Eur. Phys. J. D*, 2012, **66**, 1–8.

306 A. Sood, M. S. Granick and N. L. Tomaselli, *Adv. Wound Care*, 2014, **3**, 511–529.

307 A. Faghihnejad and H. Zeng, *Langmuir*, 2013, **29**, 12443–12451.

308 K. T. Campbell, D. Q. M. Craig and T. McNally, *J. Appl. Polym. Sci.*, 2014, **131**, 1–7.

309 I. Stefanov, S. Pérez-Rafael, J. Hoyo, J. Cailloux, O. O. Santana Perez, D. Hinojosa-Caballero and T. Tzanov, *Biomacromolecules*, 2017, acs.biomac.7b00111.

310 J. W. Rhim, *Carbohydr. Polym.*, 2011, **86**, 691–699.

311 C. Teng, J. Qiao, J. Wang, L. Jiang and Y. Zhu, *ACS Nano*, 2016, **10**, 413–420.

312 G. W. Brindley, *Clay Miner.*, 1966, **6**, 237–259.

313 M. C. Corobea, D. Donescu, C. Petcu, C. Radovici, S. Serban, E. Constantinescu and M. Miculesclt, *J. Optoelectron. Adv. Mater.*, 2007, **9**, 3358–3360.

314 S. Mane, *Can. Chem. Trans.*, 2016, **4**, 210–225.

315 M. Sokolsky-Papkov, K. Agashi, A. Olaye, K. Shakesheff and A. J. Domb, *Adv. Drug Deliv. Rev.*, 2007, **59**, 187–206.

316 N. Mangır, C. J. Hillary, C. R. Chapple and S. MacNeil, *Eur. Urol. Focus*, 2019, **5**, 280–289.

317 D. Wang, Y. Liu, J. Han, D. Zai, M. Ji, W. Cheng, L. Xu, L. Yang, M. He, J. Ni, Z. Cai and C. Yu, *PLoS One*, 2011, **6**, 1–6.

318 K. Nikhil, S. Sharan, R. Wishard, S. R. Palla, R. Krishna Peddinti and P. Roy, *Steroids*, 2016, **108**, 17–30.

319 C. A. Vaiana, M. K. Leonard, L. F. Drummy, K. M. Singh, A. Bubulya, R. A. Vaia, R. R. Naik and M. P. Kadakia, 2011, 3139–3146.

320 H. K. Lim, A. B. Rahim, V. I. Leo, S. Das, T. C. Lim, T. Uemura, K. Igarashi, J. Common and L. A. Vardy, *J. Invest. Dermatol.*, 2018, **138**, 2653–2665.

321 N. An, C. H. Zhou, X. Y. Zhuang, D. S. Tong and W. H. Yu, *Appl. Clay Sci.*, 2015, **114**, 283–296.

322 M. L. Auad, S. R. Nutt, V. Pettarin and P. M. Frontini, *Express Polym. Lett.*, 2007, **1**, 629–639.

323 Q. H. Zeng, A. B. Yu, G. Q. (Max) Lu and D. R. Paul, *J. Nanosci. Nanotechnol.*, 2005, **5**, 1574–1592.

324 A. Montembault, C. Viton and A. Domard, *Biomaterials*, 2005, **26**, 1633–1643.

325 E. S. Dragan, *Chem. Eng. J.*, 2014, **243**, 572–590.

326 L. J. Macdougall, M. M. Pérez-Madrigal, J. E. Shaw, M. Inam, J. A. Hoyland, R. O'Reilly, S. M. Richardson and A. P. Dove, *Biomater. Sci.*, 2018, **6**, 2932–2937.

327 E. Choe and D. B. Min, *J. Food Sci.*, , DOI:10.1111/j.1750-3841.2007.00352.x.

328 H. Schonhorn, *J. Chem. Eng. Data*, 1967, **12**, 524–525.

329 J. C. de Miranda, T. E. A. Martins, F. Veiga and H. G. Ferraz, *Brazilian J. Pharm. Sci.*, 2011, **47**, 665–681.

330 Y. Yu, J. Li, Y. Sun, Q. Liang, X. Peng, Y. Liu and Y. Hu, *Pet. Sci.*, 2008, **5**, 263–268.

331 P. Saokham, C. Muankaew, P. Jansook and T. Loftsson, *Molecules*, 2018, **23**, 1–15.

332 C. Coisne, D. Hallier-Vanuxeem, M. C. Boucau, J. Hachani, S. Tilloy, H. Bricout, E. Monflier, D. Wils, M. Serpelloni, X. Parissaux, L. Fenart and F. Gosselet, *Front. Physiol.*, 2016, **7**, 1–14.

333 J. E. McMurry, *Organic Chemistry*, Brooks/Cole, 8th ed., 2008.

334 B. Hoyer, A. Bernhardt, A. Lode, S. Heinemann, J. Sewing, M. Klinger, H. Notbohm and M. Gelinsky, *Acta Biomater.*, 2014, **10**, 883–892.

335 B. Huber, K. Borchers, G. E. Tovar and P. J. Kluger, *J. Biomater. Appl.*, 2016, **30**, 699–710.

336 R. Safaeijavan, M. Soleimani, A. Divsalar, A. Eidi and A. Ardeshirylajimi, *Iran. J. Basic Med. Sci.*, 2014, **17**, 903–911.

337 J. J. Mao, *Biol. Cell*, 2005, **97**, 289–301.

338 F. Hussin, M. K. Aroua and W. M. A. W. Daud, *Chem. Eng. J.*, 2011, **170**, 90–106.

339 M. Hetzer and D. De Kee, *Chem. Eng. Res. Des.*, 2008, **86**, 1083–1093.

340 V. Mittal, *Materials (Basel).*, 2009, **2**, 992–1057.

341 R. Hafidz and C. Yaakob, *Int. Food Res. J.*, 2011, **817**, 813–817.

342 A. Babu, J. Periasamy, A. Gunasekaran, G. Kumaresan, S. Naicker, P. Gunasekaran and R. Murugesan, *J. Biomed. Nanotechnol.*, 2013, **9**, 177–192.